DE-AC21-94MC31167--1
(5891)

Advanced Hot-Gas Filter Development

Topical Report
September 30, 1994 - May 31, 1996

By
J. E. Lane
J. F. LeCostaouec
C. J. Painter
W. A. Sue
K. C. Radford

Work Performed Under Contract No.: DE-AC21-94MC31167

For
U.S. Department of Energy
Office of Fossil Energy
Federal Energy Technology Center
P.O. Box 880
Morgantown, West Virginia 26507-0880

By
Westinghouse Electric Corporation
Science and Technology Center
1310 Beulah Road
Pittsburgh, Pennsylvania 15235-5098

Disclaimer

TABLE OF CONTENTS

LIST OF FIGURES

LIST OF TABLES

1. EXECUTIVE SUMMARY

Westinghouse, with Techniweave, Inc. as a major subcontractor, has undertaken a 20 month Phase I program, under DOE Contract DE-AC-94MC31167, in order to develop a next generation ceramic composite hot gas filter material. The program goal is to develop and demonstrate the suitability of the Westinghouse/Techniweave composite filter material for candle filter use in Pressurized Fluidized Bed Combustion (PFBC) and/or Integrated Gasification Combined Cycle (IGCC) power generation systems. The principle objective of Phase I is to develop and qualify an advanced 3D fiber-reinforced ceramic composite filter material for full-scale filter testing in Phase II.

Phase I, Filter Material Development and Evaluation, activities included Task 3, Subtask 3.1, the development, characterization and testing, to meet filter material requirements, of the oxide-based 3D reinforced ceramic composite filter material. Development activities included the

- identification and selection of a low cost 3D fiber architecture
- weaving methods to fabricate 3D preforms for filter use
- optimization of the matrix processing method

Characterization and testing activities included

- microstructural characterization
- filtration properties evaluation
- mechanical property testing
- thermal aging
- flow-through corrosion testing

Also included was an assessment of potential non-destructive evaluation (NDE) methods.

This filter development program incorporates a three phase route to transition the filter fabrication technical approach to the pilot scale demonstration and commercialization maturity level. Phase II, Prototype Filter Fabrication and Evaluation, of this program is intended to fabricate two prototype filters, using the material developed in Phase I, and conduct filter qualification testing in a simulated pressurized fluidized-bed combustion environment in the Westinghouse High-

Temperature High-Pressure (HTHP) filter test facility (Task 3, Subtask 3.2 activities). This phase also would include an assessment of Phase I and II filter manufacturing-related data and the preparation of filter manufacturing plans, along with the development of a plan to identify and evaluate filter degradation mechanisms (Task 4 activities).

Phase III, Optional Pilot-Scale Filter Manufacturing, (Optional Task 5) would conduct manufacturing activities to produce 50 full-size candle filters for field testing and evaluation at Southern Company Service's Wilsonville PSD Facility. Manufacturing quality assurance/quality control and non-destructive evaluation procedures developed during Phases I and II would be implemented in this phase.

The results and recommendations form Phase I are briefly summarized in the following paragraphs.

Phase I activities resulted in a low cost, three-dimensional (3D) fiber architecture, for hot gas candle filter applications, that was both easy to manufacture and automate. Weaving trials produced a list of candidate warp interlock fiber architectures for candle filters and demonstrated the feasibility of using the warp interlock architecture to fabricate seamless tubes, closed end tubes, and flange sections for candle filters. A thick wall, low fiber volume fraction, warp interlock architecture, identified as Architecture #9, was selected for candle filter applications because adequate strength and toughness were obtained in both the warp (axial direction of the filter) and fill (circumferential direction of the filter) directions.

The ceramic composite filter material based on the initial candidate fiber architectures had low breaking loads < 1 lb which were expected to cause resulting filters to be susceptible to breakage during handling and installation in filter systems. The use of stuffers to modify the downselected architecture #9 was successful and resulted in higher strengths and significantly higher breaking loads as compared to the architecture #9-based composites and was also able to easily meet the filter permeability requirements. These fiber architecture improvements and replacement of the Nextel 550 fiber with either Nextel 610 or 720 resulted in a higher strength filter material with significantly higher load carrying capability; and a material which would be expected to have improved resistance to alkali species in the hot gas filter environment.

High temperature (870°C), flow-through tests for 400 h with cyclic backpulsing showed that the Nextel 550 fiber reinforced ceramic composite material degraded, embrittle and failed in test environments containing 20 ppm NaCl/5-7% steam/air and were unaffected in steam/air only environments. The above degradation was attributed to the alkali species reacting with the

amorphous silica phase in the Nextel 550 fiber causing devitrification of this phase, embrittlement of the fiber, and subsequent failure of the composite material. SEM showed crystallization along the fibers and platelet, and possibly whisker, growth within the matrix for those specimens exposed to the alkali containing environment.

Mechanical property testing showed that the use of either the N610 or N720 fiber greatly increases strengths and breaking loads and significantly improves the handleability of the composite filter material. The N720 CMCs were 50% and 94% stronger in the warp and fill directions, respectively, than the best N550 CMCs. The greatest improvement was in the breaking load which for the N720 CMCs was 165% and 152% stronger in the warp and fill directions, respectively, than the best N550 CMC shown. The N610 CMCs, in the fill direction, were 42% stronger and had a 42% higher breaking load than the best N550 CMC in the table.

Screening tests assessed the permeability and room temperature mechanical properties of ceramic composites made from each candidate fiber architecture. These tests determined that permeability was not a discriminator for selecting a fiber architecture and that the major criteria was the mechanical properties test results. The in-situ deposition of a membrane layer was demonstrated during the fabrication of these composite samples for the screening tests; this capability simplifies and reduces the cost of filter manufacturing.

A composite processing study determined that the processing method for matrix infiltration, the mullite filler particle size and the source of the mullite sol were the major processing variables affecting the performance and cost of the filter material. A one-sided matrix infiltration process, using vacuum to pull the matrix from the outside through to the inside of the filter, was determined to be the lowest cost approach to producing candle filters; this process also facilitates the in-situ deposition of the membrane layer. Pressure applied during the infiltration process showed the feasiblity of increasing composite strength without compromising permeability.

The processing study also identified a low cost source of mullite filler powder and through an evaluation of particle size distribution effects on composite processing determining that this powder could be used in the as-received condition, without classifying, for filter manufacturing, and further reduces filter costs. During this study, for the Nextel 550 filter CMCs, the Techniweave mullite sol was selected for use as the matrix material. The Techniweave sol has a long shelf-life, is easy to use and handle during composite fabrication, is environmentally-friendly and recyclable, has a low crystallization temperature of 1000°C, is expected to provide a more

stable matrix, and is expected have less fiber degradation during processing than the Westinghouse mullite sol, which has a higher crystallization temperature of 1150°C.

Ceramic composite filter material specimens thermally aged for up to 5000 hours in static air at 870°C did not show any change in strength as a function of time at temperature and had essentially identical x-ray diffraction spectra independent of aging time.

Non-destructive evaluation methods for ceramic matrix composite filter materials have not been developed and the development of these methods were beyond the capabilities of this program. At this time, the best approach is to monitor existing development efforts for CMC NDE methods and try to tailor the results of these efforts to meet the needs of a CMC filter material.

The low cost approach to develop oxide/oxide composite filters should be continued under Phase II and Phase III of this DOE project. Continuing activities in Phase II should verify that improved fibers Nextel 610 and Nextel 720 will deliver improved ceramic filter materials. Implementation of fibers Nextel 610 or Nextel 720 in improved filters should employ the optimized architecture and matrix processing already developed under this current phase of the program. Thermal aging and high temperature flow through testing should be conducted with ceramic composite filter materials made with Nextel 610 and Nextel 720 to determine the effect of temperature, time at temperature, and hot gas filter environments on the properties of these fibers.

The use of a zirconia interface appears to have increased the strength and load carrying capability of the Nextel 550 fiber filter CMCs made with Techniweave sol sample and fired at 1050°C, as compared to a similar sample made without the zirconia interface. Additional testing and analyses are recommended to characterize the interface coating, to understand what role the interface coating is providing in this filter composite material, and to determine if these improvements would also be seen if the fiber was changed to Nextel 610 or 720. The Westinghouse sol should be reconsidered for use with the hot gas filter CMCs which use Nextel 610 and 720 fibers. The W-sol is currently a lower cost sol than the Techniweave sol, which may also be subject to future supplier problems.

The planned activities for Phase III (fabrication of fifty full sized filters and prepilot field testing at Wilsonville) should be pursued immediately after the completion of the Phase II activities.

2. INTRODUCTION

The application of high-performance, high-temperature particulate control devices is considered to be beneficial to advanced fossil fuel processing technology, to selected high-temperature industrial processes, and to waste incineration concepts. Ceramic rigid filters represent the most attractive technology for these applications due to their capability to withstand high-temperature corrosive environments. However, current generation monolithic filters have demonstrated poor resistance to crack propagation and can experience catastrophic failure during use.

Past Westinghouse field experience in Advanced Particulate Filtration systems has shown that failures of these monolithic ceramic filter elements result from a variety of causes, e.g., creep/fatigue fractures, catastrophic thermal shock fracture, chemical attack leading to loss in strength, and back-pulsing induced cracking. However, the basic problem leading to these failures is that the monolithic ceramic filter material has very low resistance to crack propagation, i.e., the material is not damage-tolerant.

To address this problem, ceramic fiber-reinforced ceramic matrix composite (CMC) filter materials are needed for reliable damage tolerant candle filters. Other than the subject of this report, there are three other CMC filters under development. Two are nonoxide based, they are chemical vapor infiltration (CVI) SiC matrix-based CMC filter materials with oxide and nonoxide fiber reinforcement. These nonoxide filter materials have been shown to be susceptible to high temperature oxidation in air/steam conditions and to phase changes in sodium-containing environments.[1] Previous efforts at Westinghouse have also indicated the potential susceptibility of nonoxide filter matrices to oxidize and/or experience corrosive attack during operation at high temperature, particularly in a steam and/or steam/alkali-containing environment.[2-4] These results do not indicate that nonoxide filters would not necessarily work in a hot gas filter system, however, these results do indicate that these materials are subject to a degradative reaction which could lead to brittle failure of the filters, similar in nature to that of a monolithic filter.

There is one oxide CMC filter under development. This is a filament wound alumina fiber-reinforced alumina matrix composite material. This material should provide good corrosion resistance, and being an oxide, it is not subject to oxidation. Filament wound structures provide in-plane reinforcement but do not have reinforcing fibers in the through thickness direction. Thus, these structures can be susceptible to delamination-type failures.

This program is focused on the development of an oxide-fiber reinforced oxide matrix composite filter material that is cost competitive with prototype next generation filters. This goal would be achieved through the development of a low cost sol-gel fabrication process and a three-dimensional (3D) fiber architecture optimized for high volume filter manufacturing. The 3D continuous fiber reinforcement provides a damage tolerant structure which is not subject to delamination-type failures.

This report documents the Phase I, Filter Material Development and Evaluation, results. Section 2 provides a program summary. Technical results, including experimental procedures, are presented and discussed in Section 3. Sections 4 and 5 provide the Phase I conclusions and recommendations, respectively. The remaining sections cover acknowledgments and references.

3. TECHNICAL RESULTS AND DISCUSSION

The results of Subtask 3.1, Coupon development, fabrication, and testing (which was the focus of this Phase I program), are covered in this section. The objective of this subtask was to develop and qualify an oxide-based 3D fiber-reinforced ceramic composite filter material for subsequent full-scale candle filter fabrication and testing in Phase II. This subtask included the development of the 3D fiber architecture and the composite fabrication process, which are discussed in Sections 3.1 and 3.2, respectively. The results of thermal aging tests, high temperature flow-through corrosion tests, and the assessment of NDE methods are presented in Section 3.3. Based on the results from Sections 3.1 - 3.3, improvements were made to the fiber architecture, and the initial fiber used during architecture development was replaced with two other candidate fibers. The improvements that resulted from these modifications are detailed in Section 3.4.

The baseline filter material manufacturing process used throughout the Phase I program is shown schematically in Figure 3.1. The process is simple and uses low cost commonly available manufacturing equipment. Basically, a fiber preform of the desired shape is woven then vacuum infiltrated with a matrix solution (sol + powder) and cured at low temperature, typically less than 800°C, to form the filter composite material. After curing, two-to-four sol-only infiltration and low temperature curing cycles are performed in order to increase the strength of the material. During the infiltration process, a membrane layer is typically formed on the filtering surface.The sol used during these infiltrations is recycled. The final step is a high temperature cure typically between 1000 and 1200°C.

3.1 Fiber Architecture Development

A low cost, three-dimensional (3D) fiber architecture, that is both easy-to-manufacture and automatable, is required to produce an economical 3D fiber preform suitable for candle filter use. Toughness in all directions, good mechanical properties, homogeneously distributed porosity, and surface smoothness are desirable features for selecting a preform for fabricating a ceramic matrix composite (CMC) candle filter fiber preform. A 3D fiber architecture has been designed to fulfill

these requirements. The program's fiber architecture design philosophy has been guided by the selection of automatic net shape weaving techniques, the generation of thin wall structures, the achievement of fiber continuity through highly stressed regions and the tailoring of the preform to the mode of matrix introduction.

The fiber architecture, or weave design, which can be thought of as the unit cell for the fiber preform, can take on any shape, simple or complex, that the fiber is capable of being woven into. For this program, the preform target shape is a candle filter. Selection of the candle filter fiber architecture and preform manufacturing approach were driven by both technical and commercialization requirements.

Over the past five years, Techniweave has developed equipment and process technology for economically weaving ceramic fibers, using multilayer fabric designs, as seamless, tubular filter preforms. During a joint Westinghouse/Techniweave IRAD program, the use of a multilayer fabric was demonstrated for fabricating a porous mullite/mullite CMC. This experience provided the basis for selecting a multi-layer fabric design known as a warp interlock, Figure 3-2, as the

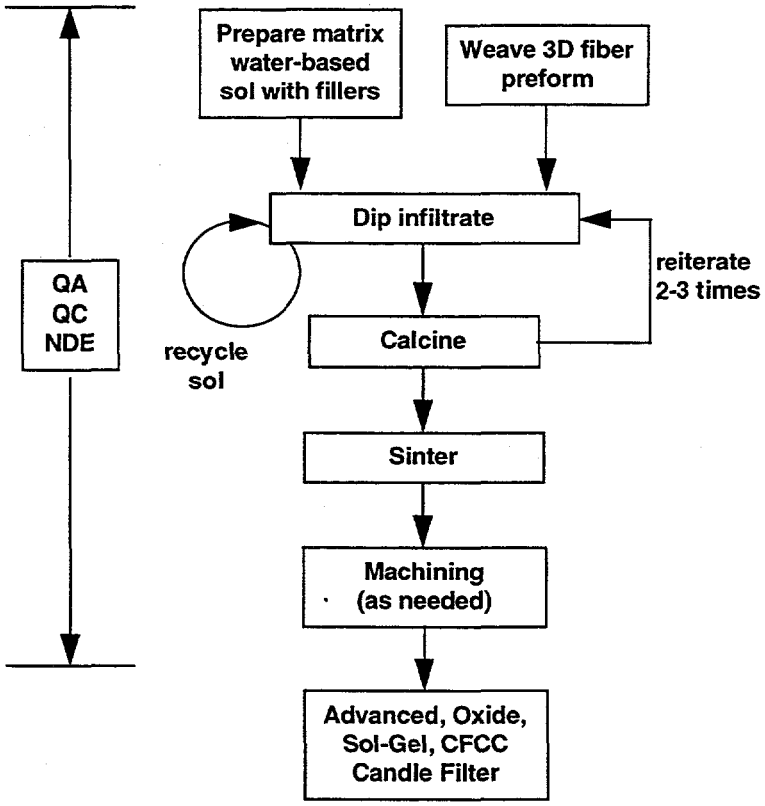

Figure 3.1-- Schematic of sol-gel manufacturing of ceramic matrix composite oxide/oxide hot gas filter.

baseline weave architecture for this program.

The baseline warp interlock architecture of Fig. 3-2 was the starting point for the weaving trials which were used to select the candidate fiber architectures, as discussed in Section 3.1.1. These candidate architectures were used to make filter composite samples, which were evaluated by a set of screening tests for their applicability to filter applications, detailed in Section 3.1.2. The screening test results were used to make an initial fiber architecture downselect, which is discussed in Section 3.1.3. Based on additional requirements for the filter material, which were not known or realized until later in this program, modifications to this architecture were required. The rationale and the modifications are discussed later in this report in Section 3.4.

3.1.1 Weaving Trials

A major portion of the preform cost has been associated with the high price of the fiber. To address this issue, an architecture design and weaving method were pursued that would use the least amount of fiber while providing suitable mechanical strength, fracture toughness and filtration characteristics. First, to minimize cost, the weave design, or fiber architecture, had to be able to be woven on a loom. Loom fabrication provided a simple low cost and automatable production method for continuous manufacture of candle filter fiber preforms.

Secondly, filter composite material properties, mechanical and filtration, are affected by the fiber architecture design and the preform construction. Although a baseline architecture has

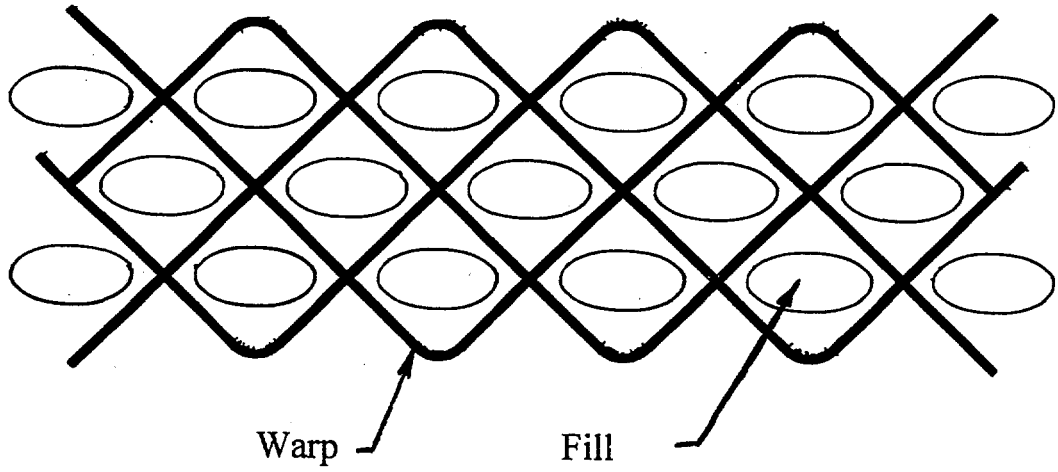

Figure 3.2 -- Three layer warp interlock weave, baseline fiber architecture, where the warp yarns provide axial and radial, or through-thickness, reinforcement and the fill yarns provide hoop, or circumferential, reinforcement for a candle filter shape.

been selected, there are several architecture and preform parameters which can be varied to change the mechanical and filtration properties of the preform, these include:

- Yarn parameters
  - Denier: in this case, the number of filaments per yarn (e.g., 2000)
  - Construction: number of yarns per bundle (i.e. 1/2 = 2 yarns per bundle)
  - Twist: number of turns per inch for the yarns in a bundle (e.g., think of a rope made of twisted strands)
- Fiber distribution by direction (warp and fill)
- Total fiber volume
- Wall thickness
- Number of warp fibers

Table 3-1 summarizes the twelve weave candidates selected for the weaving trials; the rationale for the selection of each candidate is discussed in Table 3-2. Preliminary weaving trials were conducted to establish what maximum level of fiber volume could be achieved in the warp (axial direction along the length of the filter) and fill (circumferential direction) directions without damaging the fibers. It was determined that a balanced weave could be woven with a maximum total fiber volume of 35%. The axial and circumferential loading on a candle filter in use are expected to be different. In order to be able to optimize the fiber volume in both directions, some preforms were woven with different amounts of fiber volume in the warp and fill directions.

The yarn parameters were varied to modify the sizes and distributions of porosity in the

Table 3.1 -- Selected Weave Candidates and Target Parameters

CANDIDATE NO.	WEAVE CHARACTERISTICS						COMMENTS
	Style	Thick (in)	V_{fw}	V_{ff}	VF_{tot}	Yarn	
Prelim Trials	W/I	0.06	~50	~50	35	2000 1/2, 1.5	Trials to determine V_{fw};V_{ff}
1	W/I	0.06	50	50	35	2000 1/2, 1.5	Baseline
2	W/I	0.06	50	50	25	2000 1/2, 1.5	Min VF_{tot}
3	W/I	0.06	50	50	40	2000 1/2, 1.5	Min VF_{tot}
4	MOD W/I	0.06	50	50	35	2000 1/2, 1.5	Surface floats
5	API	0.06	50	50	35	2000 1/2, 1.5	Vary interlocks API vs W/I
6	API MODIFIED	0.06	50	50	35	1000 1/2, 1.5; 2000 1/2, 1.5	Fine surface layer
7	W/I	0.3	50	50	35	2000 1/2, 1.5	Thinnest
8	W/I	0.09	50	50	35	2000 1/2, 1.5	Thickest
9	W/I	0.09	50	50	25	2000 1/2, 1.5	Thick, low VF_{tot}
10	W/I	0.06	75	25	35	2000 1/2, 1.5	V_{fw} V_{ff} variation
11	W/I	0.06	50	50	35	2000 1/2, 2.7	Higher twist yarn
12	*YARN SERVING EXPERIMENTS FOR #13*						
13	W/I	0.06	50	50	35	2000, roving	Served roving yarn

V_{fw}: fiber volume in warp direction; V_{ff}: fiber volume in fill direction; VF_{tot}: total fiber volume
W/I: warp interlock; Mod W/I: modified warp interlock (increase length of fibers running at the preform surface to increase smoothness); API: adjacent ply interlock

preform. The amount of fiber, or number of floats, at the preform surface was modified to control the filtering surface smoothness and porosity.

A low cost woven preform is required. The best solution was one that would provide adequate filtration and mechanical performance while using the least amount of fiber. Thus, the preform wall thickness was limited to 0.1 in. thick to control fiber cost and permit ease of manufacture and automation.

Nextel 440 fiber was used to conduct these trials since it was significantly lower in price than Nextel 550. Nextel 440, 70 wt% Al_2O_3-28 wt% SiO_2-2 wt% B_2O_3, is a 10-12 μm fiber with aluminum borate and amorphous silica phases. Nextel 550, 73 wt%/Al_2O_3-27 wt% SiO_2, is a 10-12 μm fiber with aluminum oxide and amorphous silica phases. The weaving characteristics of these two fibers are virtually identical.

The primary objective of the initial weaving trials was to determine how closely the targeted weave parameters (thickness, fiber volume fraction in warp and fill directions, total fiber volume fraction) could be achieved with the selected yarns and preform architectures. One particular item of interest was to determine what maximum fiber volume could be attained without damaging the fibers.

Table 3.2 -- Rationale for the Selection of Weaving Trial Candidates

Trial	Rationale
1	baseline architecture, conservative starting point.
2	same as #1 except determined minimum practical fiber volume, estimated to be 25 vol %.
3	same as #1 except determined maximum practical fiber volume, estimated to be 40 vol %.
4	same as #1 except warp yarn floats are used to yield a smoother fabric surface (see Figure 3-3).
5	demonstrated a different weave architecture, known as adjacent ply interlock (see Figure 3-5). It has groups of interlocking yarns that join adjacent fabric layers eliminating the need for through-the-thickness yarns which traverse completely though the thickness between the two outer surfaces. This design would allow the development of layered structures where, for example, a fine weave outer surface could be backed up by a lower density coarser weave. This is analogous to the Schumacher filter with its fine porosity membrane outer layer on a coarser porosity supporting layer. The interlocking yarns in this design will provide through-the-thickness integrity.
6	demonstrated the fine weave surface with the coarse weave supporting layer as discussed in #5.
7	same as #1 except that fewer unit cells were woven through the thickness yielding a thinner 3D fabric.
8	same as #1 except that additional unit cells were woven through the thickness yielding a thicker 3D fabric (see Figure 3-4).
9	combined the maximum possible thickness and minimum possible total fiber volume.
10	evaluated the effect of offsetting the fiber distribution in the warp and fill directions from the baseline conditions of #1. This will affect the structural properties and possibly the pore structure.
11	same as #1 except uses a yarn with higher twist level in order to evaluate the effect of twist on the fabric structural properties.
12	differed from #1 in that rovings, or yarns without twist, were evaluated. Rovings, or untwisted yarns, are more difficult to weave. Techniweave has adopted the practice of overwrapping (serving) rovings with small diameter sacrificial yarn, in this case rayon, to facilitate the weaving of rovings.
13	best candidate roving fabric based on results from #12.

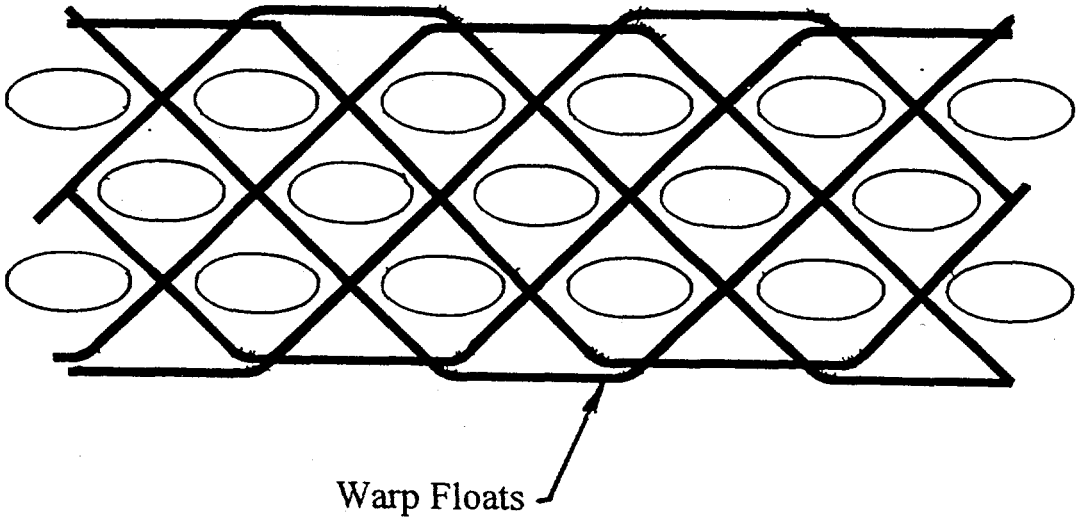

Figure 3.3-- Three layer warp interlock weave, baseline fiber architecture, with surface floats. A double surface float, illustrated above, has warp yarns which float over two surface yarns to increase surface smoothness.

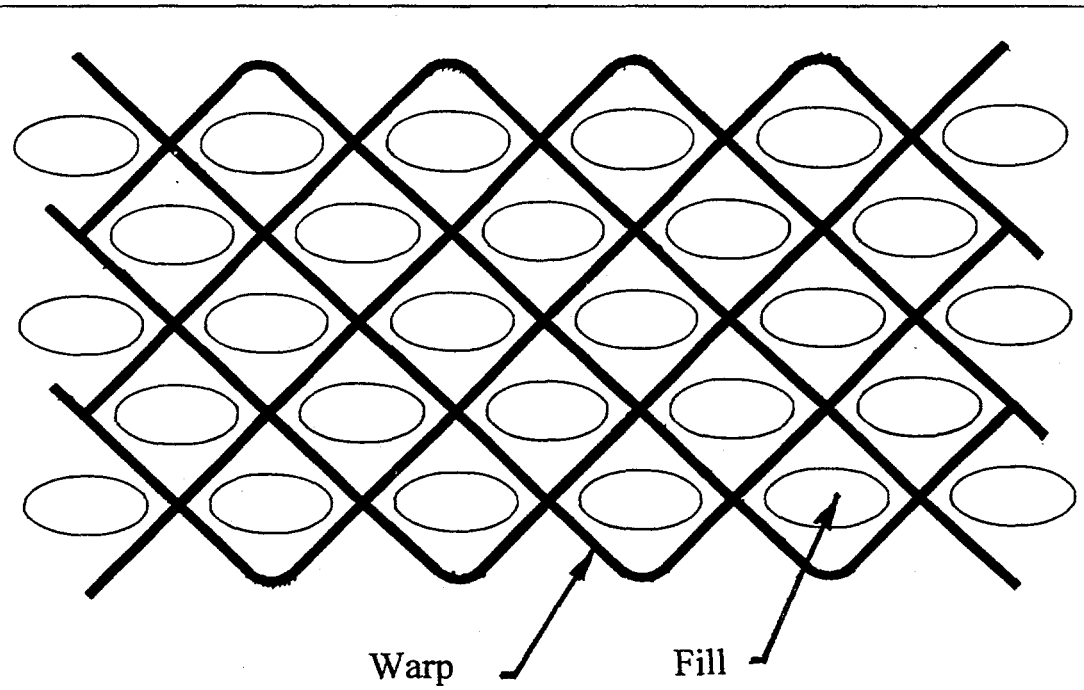

Figure 3.4 -- Five layer warp interlock weave.

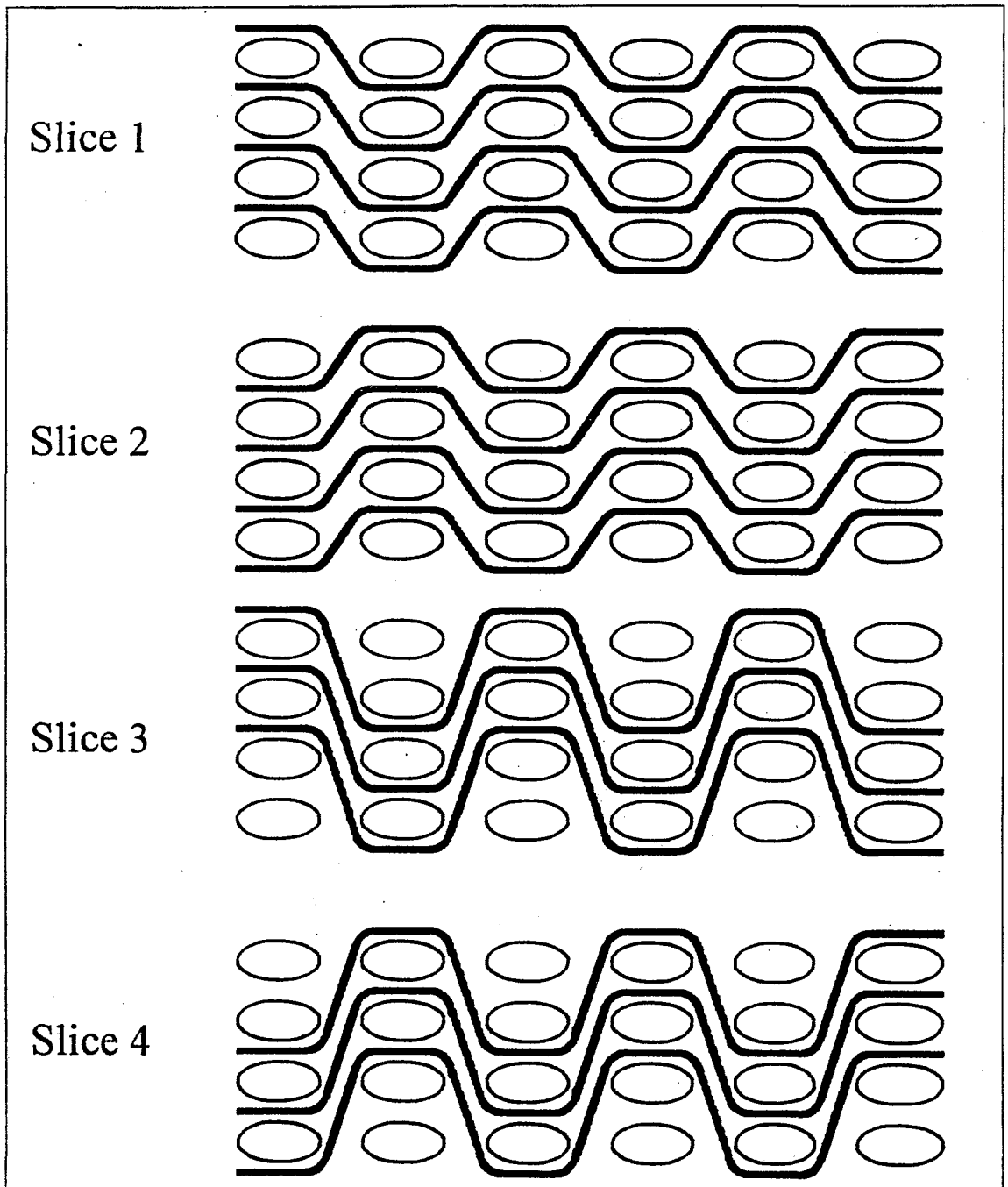

Figure 3.5-- Adjacent ply interlock weave architectures consist of four repeating slices across the fabric width. In effect, slices 1 and 2 combine to yield four plain weave fabrics that are not interconnected. Slices 3 and 4 combine to connect the top fabric layer to the second, the second to the third and the third to the fourth.

Samples of Architecture No. 1, 4, 8, 11 and 13 were woven. Fabrics were examined for fiber damage and fiber volume was calculated by measuring the weight and dimensions of a fabric preform. Fiber volume in a given direction (warp and fill) was measured by taking apart a fabric sample of known dimensions and weighing the amount of fiber for each specific direction.Results are presented in Table 3-3. With the exception of Architecture No. 4 (surface floats), the total fiber volume for each sample was lower than the 35% targeted value. The number of picks in the fill direction, which contributes to the fiber volume, had to be decreased during weaving because damage to the yarn was observed at higher pick counts. Fiber volume of Architectures No. 1 and 8 were measured in both the fill and warp directions. The results presented in Table 3-2 indicate that a reasonably balanced architecture could be achieved. The best surface smoothness was achieved with Architecture No. 4 (surface float).

Trials 14-17, shown in Table 3-3, were added in order to evaluate the manufacturing issues of the warp interlock fiber architecture for making tubular, closed-end, and flange sections of the candle filter. The surface float architecture, similar to Architectures 1 and 2 in Table 3-2, was selected for these trials. These trials demonstrated the feasiblity of using the warp interlock architecture to make seamless tubes, closed end tubes and flange sections, as seen from Fig. 3-6, which shows a woven closed end seamless tube section for a candle filter.

Table 3.3 -- Experimental Weaving Trials

Cand. No.	Style	Thick (in)	V_{fw}	V_{ff}	VF_{tot}	Yarn	Comments
1	W/I	0.066	52	48	29	N-440, 2000 1/2, 2.7	3 Layer
8	W/I	0.101	46	54	33	N-440, 2000 1/2, 2.7	5 Layer
13	W/I	0.105			32	N-440, 2000 1/2, 2.7	Same as #8 except fill = 3-1000 de roving + (4+2) 100 de rayon (fugitive fiber)
11	W/I	0.101			31	N-440, 2000 1/2, 2.7	Same as #8 except fill = 2000 1/2, 4.0
4	W/I	0.075			36	N-440, 2000 1/2, 2.7	Same as #1 except surface floats
14	Circular W/I	0.06				N-312, 2000 1/2, 2.7	Straight tube
15	Circular W/I	0.3				N-312, 2000 1/2, 2.7	Same as #14 with end closure trials
16	Circular W/I	0.09				N-312, 2000 1/2, 2.7	Same as #14 but API vs W/I to split wall for creating flange
17	Circular W/I	0.09				N-312, 2000 1/2, 2.7	Same as #14 but larger fill yarns locally to create thickness for forming flange

V_{fw}: fiber volume in warp direction; V_{ff}: fiber volume in fill direction; VF_{tot}: total fiber volume
W/I: warp interlock; API: adjacent ply interlock

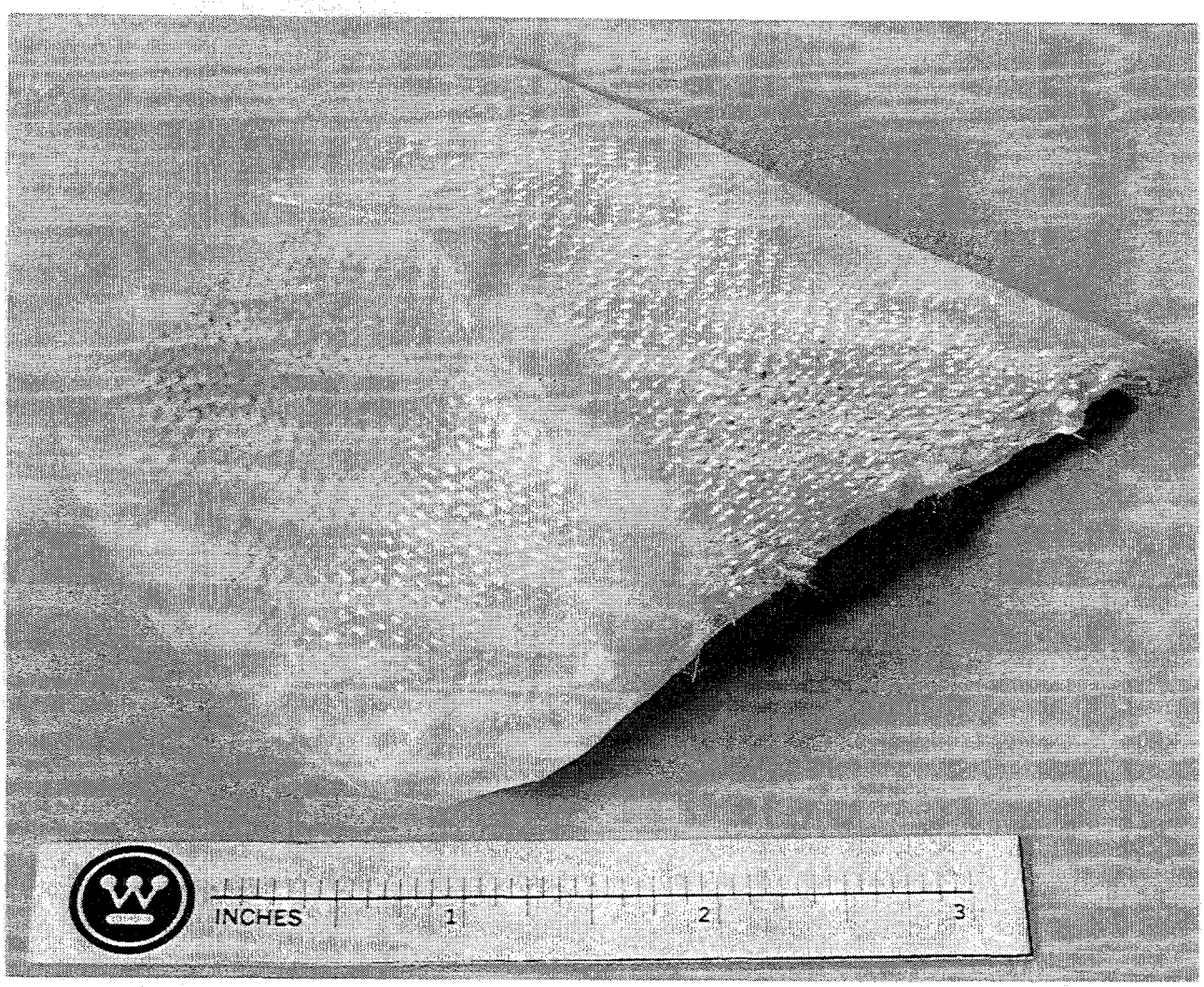

Figure 3.6 -- Integrally woven closed end for candle filter demonstrates capability to fabricate preform using low cost weaving techniques.

Based on the preliminary weaving trials and the results shown earlier in Table 3-3, a finalized list of preform candidate architectures, Table 3-4, was selected for composite fabrication, testing, and evaluation. The rationale for these selections is shown in Table 3-5. From this table, candidate architectures 1-9 were evaluated in this program; architectures 10 and 11 were not evaluated.

As the program progressed it became apparent that it would not be necessary to evaluate architectures 10 and 11. The original intent of these architectures was to form a preform with a fine porosity in order to generate a smooth candle surface for easy cleanability during back pulsing. During the course of the architecture screening tests, success was achieved at the in-situ deposition of a membrane layer on all the fiber architectures. This membrane layer met the need for making a smooth cleanable surface during back pulsing and eliminated the need to evaluate architectures 10 and 11.

Table 3.4 -- Finalized List of Weave Candidates

CANDIDATE ARCH.	WEAVE CHARACTERISTICS - TARGET VALUES						COMMENTS
	Style	Thick (in)	V_{fw} (%)	V_{ff} (%)	Vf_{tot} (%)	Yarn	
1	W/I TF	0.08	50	50	35	2000 1/2, 1.5	TF: Three surface float
2	W/I DF	0.08	50	50	35	2000 1/2, 1.5	DF: Double surface float
3	W/I DFR	0.08	50	50	35	2000 1/2, 1.5	DFR: Double surface float, random design
4	W/I DF(U)	0.065	60	40	35	2000 1/2, 1.5 (W) / 1000 1/2, 1.5 (F)	DF(U): Double surface float, higher fiber volume in warp direction
5	W/I R	0.10	50	50	35	2000 1/2, 2.7 (W) / 1000 1/2, 2.7 (F)	R: Basic angle interlock, random design
6	W/I DFR (F)	0.08	50	50	35	2000 1/2, 1.5	DFR (F): Double surface float with fugitive yarn
7	W/I DFR (HF)	0.08	60	40	40	2000 1/2, 2.7	DFR (HF): Double surface float with higher fiber volume
8	W/I DFR (LF)	0.08	60	40	30	2000 1/2, 2.7 (W) / 2000 1/2, 4.0 (F)	DFR (LF): Double surface float with lower fiber volume
9	W/I DFR (T)	0.06	60	40	35	2000 1/2, 2.7 (W) / 1000 1/2, 2.7 (F)	DFR (T): Double surface float, low thickness
10	API	0.10			35		Alternate adjacent ply interlock
11	API MODIFIED	0.10			35		Alternate interlock with fine surface layer
Others	To Be Defined						Evaluate effect of higher twist yam

V_{fw}: fiber volume in warp direction; V_{ff}: fiber volume in fill direction; VF_{tot}: total fiber volume
W/I: warp interlock; Mod W/I: modified warp interlock (increase length of fibers running at the preform surface to increase smoothness); API: adjacent ply interlock; W: warp direction,: F: fill direction

Table 3.5-- Preform Architecture Selection Rationale

CANDIDATE ARCHITECTURES	RATIONALE
1	This candidate has floats on one surface that are three unit cells long and on the opposite surface that are one unit cell long (see Figures 3-1 and 3-2 for an explanation of floats where Fig. 3-1 shows one unit cell float on both surfaces and Fig. 3-2 shows two unit cell float on both surfaces.) Floats are used to create a smoother surface.
2	The warp yarn floats are used to yield a smoother fabric surface (see Fig. 3-2) Floats are placed in an organized pattern.
3	Similar to #2, but the floats are placed in a random pattern to minimize the creation of aligned ridges.
4	Same as #3, except evaluated unbalanced fiber volumes in warp and fill directions. The warp direction (which would be the longitudinal axis of a candle filter) has much greater fiber volume than the fill direction (hoop direction of the candle filter). This will affect the structural properties, increased bend strengths, and possibly the pore structure. Stresses due to a longitudinal bending moment are the highest expected stresses for a filter.
5	Base line warp interlock architecture (1-4 and 6-9 are modifications of this architecture).
6	Same as #3, except evaluated use of fugitive yarn in warp direction to modify porosity shape.
7	Same as #3, except evaluated higher fiber volume.
8	Same as #3, except evaluated lower fiber volume.
9	Same as #3, except evaluated thinner wall achieved through greater spread of warp yarn.
10	Adjacent ply interlock (API) fiber architecture, see Figure 3-3, which has groups of interlocking yarns that join adjacent fabric layers. There are no through-the-thickness yarns which traverse entirely from one surface to the other. The interlocking yarns provide through-the-thickness integrity.
11	Same as #10, except creates a finer weave on one surface with the balance of the weave (subsurface) being a coarser weave. This facilitates creating a finer surface porosity.
others	Additional architectures woven with higher twist yarn. These yarns maintain the circularity of the yarn during weaving and is expected to generate preforms with larger pores.

3.1.2 Screening Test

The screening test objective was to determine the best fiber architecture from Table 3-4 for the filter application. For this test, Nextel 550 (N550) fiber was used to weave preforms from architectures 1-9. Each preform was then characterized to determine how well it met the target parameters shown earlier in Table 3-4. These results are discussed in Section 3.1.2.1.

The preforms were then infiltrated with the matrix solution to make filter material composite plates as described as the introduction to Section 3, see Fig. 3.1, for testing and evaluation. Two test panel sizes were prepared for each architecture:

1) 101.6 mm x 152.4 mm CMC test panels were made using Techniweave's baseline matrix fabrication process combining water-based mullite sol and mullite powder infiltration. These test panels were fabricated with an in-situ formed membrane layer. Fabricated composites were sent to Westinghouse for evaluation. The 152.4 mm length of these panels was parallel to the fill direction. The warp direction, which was the 101.6 mm length, generally had a higher strength than the fill direction. This was of importance for those candidate architectures which had unequal fiber volume fractions in the fill and warp directions, e.g., architectures 1 and 4 in Table 3-4.

2) 50.8 mm x 50.8 mm CMC test plates were made with just the mullite sol. The mullite powder was not used for the composite matrix in these samples. These samples were used to determine the permeability of the fiber architecture without the additional influence of the powder.

Test specimens were machined from each CMC plate for evaluating permeability, density, and room temperature 4-pt bend strength. Figure 3.7, photographs of permeability disk specimens, shows the general appearance of architectures 1-6. Cross-sections of the typical CMC filter material , regardless of fiber architecture, showed a graded density structure, see Figure 3.8 (a), with the filtering membrane at the outer surface of the fiber preform. The permeability property results are presented in Section 3.1.2.2.

The matrix, mullite powder + mullite sol, concentration was highest at the membrane layer, see Figure 3.8 (b) for representative microstructure, and was lowest at what would be the internal surface of a candle filter, as seen in Figure 3.8 (a). The typical membrane layer, Fig. 3.8 (b), was composed of coarse mullite particles bonded together with the mullite sol. The mechanical properties, presented in Section 3.1.2.3, of these CMC filter materials were expected to be dominated by the fibers due to the inhomogeneous distribution and low concentration of matrix material.

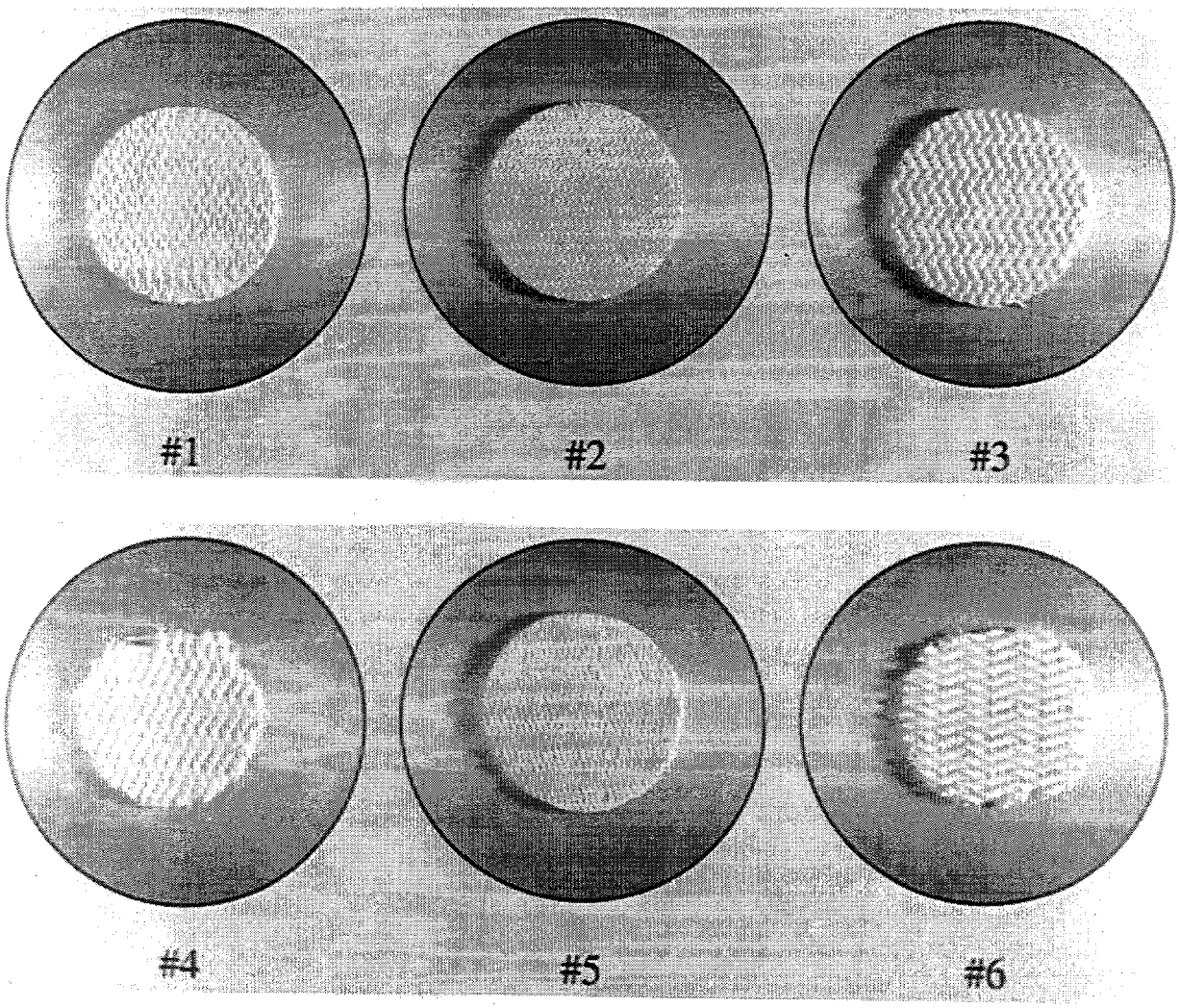

Figure 3.7 -- Optical micrographs of permeability disk specimens for architectures 1-6 which shows the appearance of these architectures. The surface showing is what would be the internal surface of a candle filter (the clean gas side). The membrance, or actual filtering surface, is the down side of the disks and is not shown in this figure.

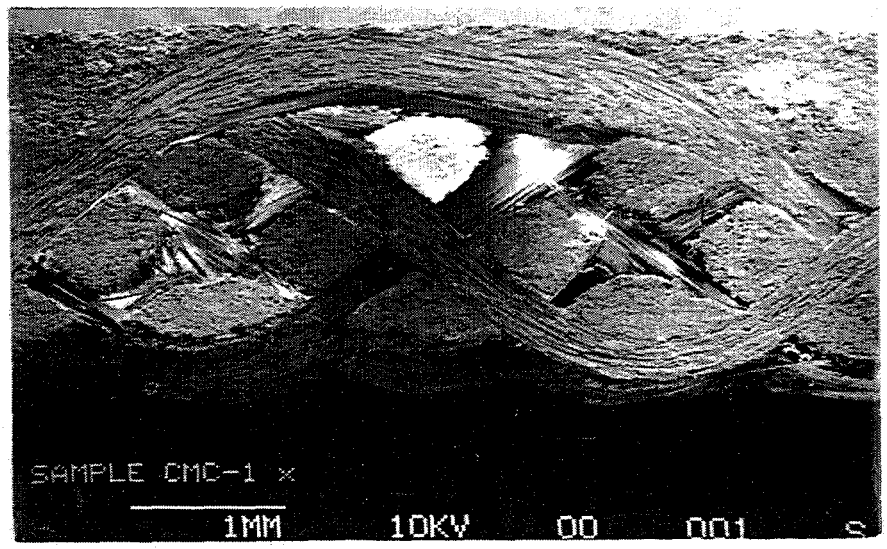

(a)

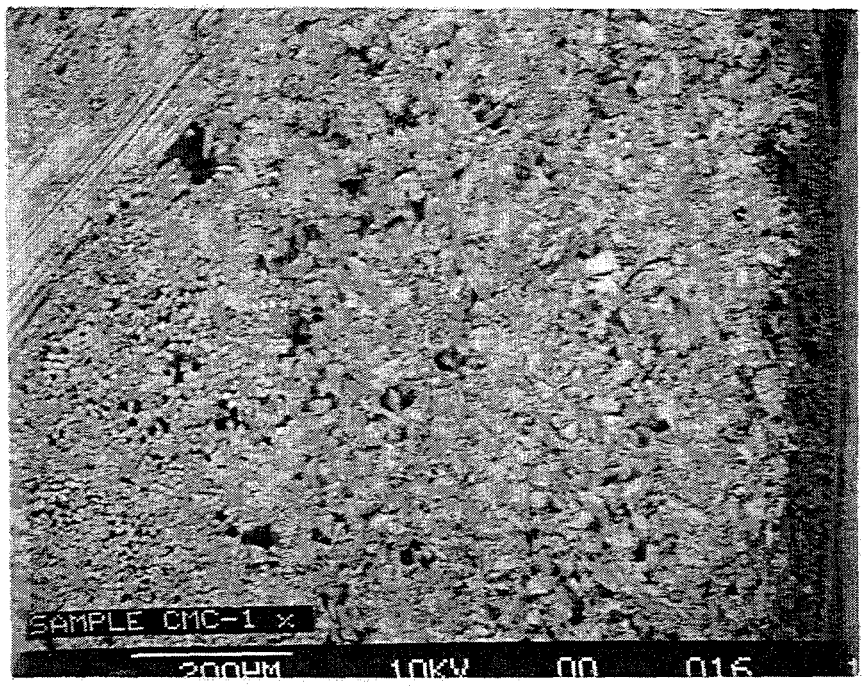

(b)

Figure 3.8 -- (a) Low magnification SEM micrograph of a typical filter CMC cross-section of the filter wall. The membrance or filtering surface is at the top of the photo. (b) Higher magnification backscattered SEM micrograph showing the typical microstructure of the membrance layer. This image is rotated 90° clockwise of (a) so that the membrane is to the right of the figure and parallel to the long edge of the page.

3.1.2.1 Preform Characterization

Table 3-6 shows the measured and targeted weave parameters for the selected weave, or architecture, candidates. Candidates 1, 2 and 3 met their targeted parameters. Architectures 4, 5 and 6 were thinner then expected, otherwise, they were close to meeting their targeted values. The use of the smaller denier (number of grams of fiber per 9000 meters) yarn, 1000 as opposed to 2000 previously, in the fill direction is believed to be the reason for the thinner preform.

For candidates 5 - 9 higher yarn twist (2.7 instead of 1.5) was used to increase the handleability of the fiber. However, fiber yarns with a higher twist (2.7) retain their rounded shape during weaving as opposed to a yarn with a lower twist (1.5) which would flatten during weaving. Accordingly, it is believed that architectures 7-9 had preform thicknesses which were higher than their targeted values due to the higher twist yarns.

Although architectures 5 and 6 used higher twist yarns, their thicknesses were lower than their targeted values. For 5, this is believed to be due to the use of lower denier fiber in the fill direction. For 6, the use of a fugitive fiber during weaving is believed to have caused the lower thickness value.

Architecture 9 had the highest fiber volume in the warp direction, 72% as opposed to its targeted value of 60%. This may have been due to the use of lower denier fiber (1000) in the fill direction. Architectures 7 and 8 used a higher denier fiber (2000) in the fill direction and both had warp and fill fibers volumes close to the targeted values of 60% and 40%, respectively.

Table 3.6 -- Measured Weave Parameters of Candidate Architectures as Compared to Targeted Values

CANDIDATE ARCHITECTURES		WEAVE PARAMETERS								
		Thickness (in)		V_{fw} (%)		V_{ff} (%)		V_{ftot} (%)		Yarn
No.	Description	Target	Actual	Target	Actual	Target	Actual	Target	Actual	Parameters
1	3 surface float	0.08	0.08	50	53.8	50	46.2	35	33	2000 1/2, 1.5
2	2 surface float	0.08	0.08	50	50	50	50	35	34.8	2000 1/2, 1.5
3	2 surface float random	0.08	0.08	50	50	50	50	35	34	2000 1/2, 1.5
4	2 surface float random	0.08	0.065	60	63.6	40	36.4	35	32.5	2000 1/2, 1.5 (W) 1000 1/2, 1.5 (F)
5	baseline warp interlock	0.10	0.069	40	41	60	59	35	32	2000 1/2, 2.7 (W) 1000 1/2, 2.7 (F)
6	2 surface float fugitive yarn random	0.08	0.064	60	56	40	44	35	25	2000 1/2, 2.7
7	2 surface float random	0.08	.097	60	64	40	36	40	29	2000 1/2, 2.7
8	2 surface float random	0.08	.092	60	57.7	40	42.3	30	28	2000 1/2, 2.7 (W) 2000 1/2, 4.0 (F)
9	2 surface float random	0.06	.07	60	72	40	28	35	28	2000 1/2, 2.7 (W) 1000 1/2, 2.7 (F)

V_{fw}: fiber volume in warp direction; V_{ff}: fiber volume in fill direction; VF_{tot}: total fiber volume

The measured overall fiber volume of preform 7 was 29%, less than the targeted value of 40%. In this thin wall construction, the definition, or roughness, of the preform surface has a significant impact on the measured wall thickness which also directly affects the calculated fiber volume. The higher twist yarn used to weave 7 would contribute to a rougher surface because, as noted above, higher twist yarns stay round, whereas, lower twist yarns flatten out which would create a smoother surface.

3.1.2.2 Permeability

The permeability test is a simple low cost accept/reject test. The Westinghouse permeability test rig measures the pressure drop through a 41 mm dia. disk, up to 6 mm thick, at face velocities ranging from 0.76-to-15.24 cm/s (1.5-to-30 fpm). The test results are reported as a gas flow resistance ratio, R, of the pressure drop (measured in inches of water, in-wg) to the face velocity (feet per minute fpm), are compared with data from known hot gas filter materials. Empirically determined acceptable permeability results are R $<$ 1 in-wg/fpm at room temperature.

The candidate architecture CMC samples were evaluated in this rig in two positions: a) "up" position, this is the normal expected filter material orientation where the expected external surface of the filter material is the face exposed directly to the flowing gas stream, as it would be in use, and b) "down" position, this refers to directly exposing the face of the filter material that would normally be the internal surface of the candle filter to the flowing gas stream. The intent of this evaluation was to assess if there were significant differences in the flow resistance through the material based on its orientation in the test rig: no differences were expected.

During initial testing, it was noted that some of the test specimens had leaks at the edges or were poor fits in the test rig. These problems were corrected by acquiring improved tooling, diamond core drills, for machining permeability test specimens. Additionally, the data measured in the "up" and "down" positions did not always correlate; this was determined to be due to the heterogeneous nature of the filter material which prevented acceptable sealing of the specimens in the test rig in the "down" position. Thus, only the "up" position data was considered in the evaluation.

The data for the nine architecture samples is shown in Table 3.7. All measured architectures met the gas flow resistance requirement of $<$ 1 in-wg/fpm at room temperature.

Table 3.7 -- Gas Flow Resistance as a Function of Fiber Architecture

Architecture	Gas Flow Resistance (in-wg/fpm at 70 °F)
1	0.434
2	0.129
3	0.193
4	0.332
5	0.425
6	0.264
7	0.594
8	0.534
9	0.524

As noted at the beginning of Section 3.1.2, 50.8 mm x 50.8 mm plates were made with just the mullite sol; mullite powder was not used for matrix fabrication in these samples. The purpose of this experiment was to determine the effect of the fiber architecture on gas flow resistance without the influence of the filler powder. During the first test five of the initial CMC samples of architectures 1 to 6 had poor edge fits and there was poor sealing with the sample holder. Attempts to improve the fit and the seal with a ceramic adhesive were not successful. Thus, a second set of 50.8 mm x 50.8 mm samples were fabricated from fiber architectures 1 to 9 for further testing. Test specimens were then machined with improved tooling (diamond core drill) which yielded good test specimens.

Test results for the these samples showed very low gas flow resistance, R values ranging from 0.043 to 0.056 iwg/fpm, for all architectures indicating that there was significant gas flow through and around the test specimens. Because of these very low permeability values for all test specimens, this test was unable to be used to distinguish significant flow resistance differences between the individual architectures. These tests demonstrated the need for the powder filler material for creating the tortuous pore path necessary for good filtering behavior.

3.1.2.3 Mechanical Properties

Room temperature 4-point bend test results are shown in Table 3.8 for each candidate architecture CMC sample. Initially, bend test specimens were machined from each direction, warp and fill, of the CMC plates made from the first six architectures. These first bend specimens were 3 mm wide x 45 mm long. After machining and testing of these specimens, Techniweave expressed concern that the specimens were too narrow and might not completely encompass the cell size of the fiber architecture and would provide misleading bend test results.

Due to this concern, additional test specimens were machined from CMC plates of architectures 1-6. Because there was limited material, these specimens were machined from the "stronger" direction, based on the '3 mm' test specimen results, for each architecture (for architecture #4, suitable material remained to permit re-testing in both directions.). The samples were 6 mm wide by 45 mm long or twice as wide as the initial 4-pt bend test specimens. These additional specimens were tested to verify the original '3 mm' data, specifically to ensure the suitability of "thin" test samples, and to acquire load vs. deflection curve data which was mistakenly not done the first time these materials were tested. The mean strengths in each direction (original data and data for new samples) are shown in the table.

Test results showed that the strength for architecture 4 (warp direction) was significantly higher for the wider test specimens. In general, for the remaining architectures, there was a trend towards higher mean strengths with the wider test specimens. However, the large spreads in most of the test results do not allow for absolutely concluding that the wider specimens gave higher strengths. For architectures 4 and 6, tested in the fill direction, the mean strengths were lower for the wider specimens.

The data indicated that sample width may have had an affect on bend strength results for these composite filter materials and that this affect appeared to be both architecture and test

Table 3.8 -- Room Temperature 4-Point Bend Strength Results

CANDIDATE ARCHITECTURES		PREFORM DATA				CMC	CMC BEND STRENGTH			
		Thick	V_{fw}	V_{ff}	V_{ftot}	Density	Warp Direction (psi)		Fill Direction (psi)	
No.	Description	(in.)	(%)	(%)	(%)	(g/cm^3)	3 mm	6 mm	3 mm	6 mm
1	3 surface float	0.080	18	15	33	1.40	1058 ± 224 (5)	NT	1577 ± 455 (6)	2339 ± 456 (7)
2	2 surface float	0.080	17	17	35	1.43	1100 ± 80 (5)		1731 ± 214 (6)	1825 ± 696 (7)
3	2 surface float random	0.080	17	17	34	1.42	1322 ± 289 (5)		1931 ± 328 (5)	2097 ± 253 (7)
4	2 surface float random	0.065	21	12	33	1.25	1104 ± 119 (6)	1908 ± 102 (7)	917 ± 429 (6)	853 ± 172 (7)
5	baseline warp interlock	0.069	~13	~19	32	1.39	1888 ± 367 (6)	2340 ± 224 (7)	921 ± 122 (6)	
6	2 surface float fugitive yarn random	0.064	~14	~11	25	1.79	2076 ± 563 (6)		2061 ± 973 (6)	1690 ± 501 (7)
7	2 surface float random	.0970	19	10	29	1.18		843 ± 255 (12)		625 ± 148 (6)
8	2 surface float random	.0920	16	12	28	1.68		929 ± 148 (10)		1427 ± 328 (6)
9	2 surface float random	.070	20	8	28	1.36		2144 ± 522 (10)		1201 ± 522 (9)

V_{fw}: fiber volume in warp direction; V_{ff}: fiber volume in fill direction; VF_{tot}: total fiber volume; NT: not tested; value in parentheses represents number of specimens tested

direction dependent. Based on these results, future testing of filter composite materials should conservatively use wider test specimen widths, a minimum of 6 mm.

Density values, as shown above in Table 3.8, ranged from 1.18 to 1.76 g/cm^3 which corresponds to 38 and 57 % of theoretical density (3.11 g/cm^3), respectively. The density and strength results in Table 3.8 are discussed in detail in the next section on the architecture downselect.

3.1.3 Architecture Downselect

The downselect process quickly narrowed in on strength and toughness as the primary discriminators between the various architectures. Permeability and cost of fabrication were non-issues as all architectures met the permeability requirements and initial preform weaving trials showed that fabrication costs were expected to be similar. The remainder of this discussion focuses on the differences in strength and toughness as related to the different architectures and is based on data presented in prior sections. The effects of fiber volume, fiber architecture, and matrix content on strength are discussed, as is a qualitative analysis of toughness.

3.1.3.1 Effect of Fiber Volume on Strength

The nine architectures were woven into preforms with total fiber volume ranging from 25 to 35%. Fiber volume in the warp and fill directions was nomalized to compare the various architectures. Preforms 5 and 6 were excluded from this analysis as insufficient material was available to measure the fiber volume in the fill (circumferential direction of a filter) and warp (axial or along the length of a filter) directions.

The fiber volume in the fill direction consists of straight fiber tows completely aligned in what would be the circumferential direction of a candle filter. Thus, 100% of the fill fibers are contributing to the strength in the fill direction.

In contrast, the fiber volume in the warp direction, although running in the axial direction of a filter, is not straight but is interwoven around the fill fibers. Thus, the warp fibers have a large proportion of the fiber going through the preform thickness and a lesser quantity of fiber directly aligned in the warp or axial direction. The warp fiber strength is divided to give through thickness strength and integrity to the preform and to give axial strength along the candle filter.

The length of the float (fibers running parallel to the surface in the warp direction) directly contributes to the axial reinforcement with basic angle interlock (#5), no fiber parallel at the

surface, and the three surface float (#1), most fiber parallel at the surface, being the two extremes. The contribution of the warp fibers to the axial reinforcement is, however, more directly dependent on the preform thickness. Thinner wall architectures exhibit through thickness fibers having a smaller angle with the axial direction (i.e., the degree of misalignment with the axial direction is smaller with thinner preforms than thicker ones) which increases their contribution to strength in the axial direction.

Fill Direction Effects. A direct correlation could not be established between strength and the amount of fiber volume in the fill direction. However, composites with fiber volume greater than 15% in the fill direction, #1, #2, and #3, exhibited greater strength than those with 8-12 % fiber volume. Other potential relationships which would be interesting to evaluate for potential correlations include first micro-cracking strength vs fiber volume, bending modulus vs density, and bending modulus vs fiber volume. These will be evaluated if time and funding permit.

Examination of the ultimate strength for candidates #4, #7, #8, and #9 indicate that other factors besides fiber volume contribute to the composite strength. Comparison of the #4 to #9 and #8 to #9 would suggest that composite density is also affecting strength, see Table 1. The density of the composite is strongly related to the amount of mullite matrix (from sol + filler powder) in the preform. The penetration of the mullite powder within the preform is affected by the preform architecture (geometrical thickness and yarn construction, or the yarn denier and twist) and the degree of repeatability of the infiltration process. The latter issue will be evaluated in final testing of the best filter material where several identical panels will be made for more in-depth testing.

The partial conclusions that were drawn from the review of data in the fill direction are:

- It is possible to achieve reasonable strength level (1200 psi) with only a small amount of fiber in the fill direction (8%).
- Higher strength level (up to 2300 psi) can be achieved with 15% fiber volume.
- The amount of matrix affects the strength level. The respective contributions of the fiber and matrix to the composite strength are not known and their determination is not a trivial issue.

Warp Direction Effects. Direct comparison of the composite mechanical strength in the warp direction for the different CMCs was only conducted for preforms with equivalent thicknesses (see prior discussion on fiber volume effects). This comparison was further narrowed to the preforms exhibiting the same double float architecture with the random design: #3, #4, #7, #8, and #9. Normalized fiber volume in the warp direction varied between 16 - 20%. Preform

thicknesses ranged from 0.064 in. to 0.097 in. Given the above constraints, only two sets of architectures were available for direct comparison: #7 to #8 and #4 to #9.

The lowest strengths in the warp direction are observed for #'s 7 and 8, which have thicker preforms, 0.097 in. and 0.092 in., respectively, and intermediate fiber volumes, 18% and 16%, respectively. The strength of these two composites, 843 psi and 929 psi, respectively, is essentially the same.

The other two composites exhibiting similar thicknesses are #4 and #9, 0.065 in. and 0.070 in., respectively. The normalized warp fiber volume is the same for both composites, about 20%. Analysis of the strength results is complicated because for #4 changes in bend specimen width affected the magnitude of the bend strength; wider specimens were stronger than narrow specimens. The narrow specimen data is given less weight because the wider specimens provide a more uniform and representative cross-section of this architecture for bend testing. Composite #9 was tested using wider specimens. The strengths of #4 and #9 are 1908 and 2144, respectively. These strengths are comparative and could be considered relatively the same given the wide standard variations associated with these samples.

The partial conclusions that were drawn from the review of data in the warp direction are:

- Width of the flexure bar specimens can affect the strength data. It is recommended that all future testing be conducted with specimens at least 6 mm (0.24 in.) in width.
- An average bend strength of 2100 psi in the warp direction can be achieved with double float architectures which have low fiber volumes (~11% for #6) and high densities (1.79 g/cc) or matrix content and which have high fiber volumes (20% for #9) and lower densities (1.36 g/cc) or less matrix content.
- Introduction of stuffer fibers in the warp, or axial, direction could advantageously be used to minimize the effect of preform thickness on the contribution of the fiber in the warp direction. Stuffers in this case would be fibers woven in the warp direction where the stuffer fibers are straight in-plane fibers aligned in the warp or axial direction but which do not weave around the fill fibers like the warp fibers typically do. The stuffers are not additional fibers but are warp fibers which are straigthened out in the warp direction. The use of stuffer fibers would increase the axial, or warp direction, strength at the expense of decreasing the through-thickness strength.

3.1.3.2 Effect of Fiber Architecture on Strength

Recognizing the complexities in interpreting the test results (limited characterization, sample size effects, etc.) two items, length of the surface float and design repetition, related to the preform architecture were however isolated and are discussed below.

Effect of the Length of Surface Float. Comparison of #1 (3 surface float) and #2 (2 surface float) indicates that the two surface float architecture design provides a narrower spread of strength values than does the three surface float design. The three float design was examined in an attempt to achieve a smoother surface. This approach however does not provide as rigid a preform as does the two surface float. Thus, additional manipulation of the surface float preform can cause variations in the preform which result in composites with widely varying properties. As noted previously, the use of stuffer in this case is expected to greatly increase the stability of the preform and result in composite filter material with more uniform and repeatable properties.

Effect of Design Repetition. Composites #2 and #3 were prepared from preforms exhibiting similar characteristics except for the repetitiveness of the pattern. The #2 architecture has a more oriented fiber pattern than does #3. This preferred orientation of #2 resulted in a rougher surface with aligned ridges and valleys. The random pattern of #3 showed a more uniform surface. Providing a random orientation of the pattern seems to also have a beneficial effect on the mechanical properties of the material; a smoother more uniform surface has less stress concentrations than would the surface of #2. The strength of #3 was slightly higher than that of #2.

3.1.3.3 Effect of Matrix on Composite Strength

Architecture #6 was designed with a fugitive yarn to yield a more open composite for improved permeability characteristics. The composite made from #6 had a low fiber volume and a high strength in both directions. The high strength was due to the high density which resulted from a large amount of matrix in the composite, see Figure 3.9. This composite had more matrix because of the fugitive fiber which provided additional surface area to deposit the matrix on during infiltration processing. Because of this high matrix content, this composite exhibited fracture behavior more like that of a monolithic. This issue is considered in the following section.

3.1.3.4 Qualitative Evaluation of Toughness

An appropriate test for toughness was difficult to determine for these composites due to their low thicknesses and heterogeneous microstructures. A qualitative approach was used to compare the shapes of the load-deflection curves (deflection was measured during bend testing with a three probe extensometer) for the various architectures, load-deflection curves for the various architectures are shown in Appendix 1.

A material exhibiting a higher strength at the point where the composite loses linearity, i.e. "yields", (defined in dense composites as the first micro-cracking stress/load) and showing a significant load carrying ability beyond that point can intuitively be qualified as a tougher composite. This point in essence also takes into account the area under the curve. Using this criteria, #4 (warp direction data only available) would be the least suitable and #9 would be the most desirable. Composite #9 exhibits a "yield stress" of 1280 psi in the warp direction and subsequently carried a load to a 2100 psi level and continued to exhibit good strain carrying capability beyond the ultimate load point thus demonstrating a noncatastrophic failure mode.

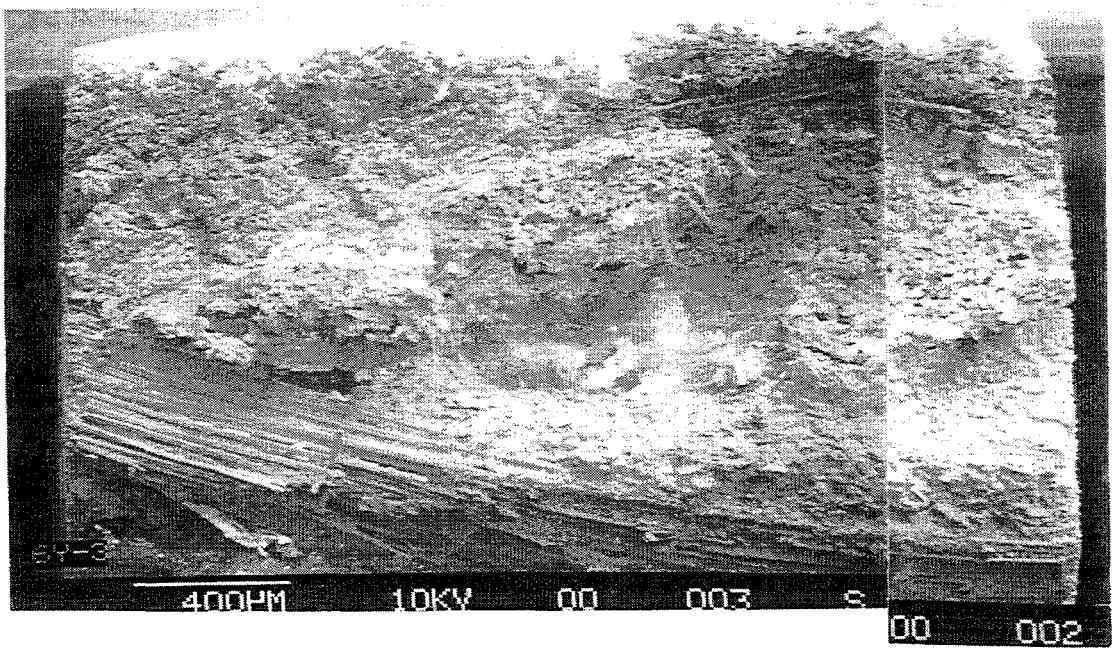

Figure 3.9 -- SEM Micrographs of CMC #6 showing the fracture cross-section of a bend bar; the membrance layer is at the top surface. Note the high concentration of matrix material throughout this specimen, as compared to Figure 3.8(a).

3.1.3.5 Architecture Downselect Conclusions

The architecture downselect process picked #9. The downselect was conducted by direction as follows:

Warp.

- The axial (warp) direction of the candle filter is subjected to bending loads. Candidates with warp strengths less than 1000 psi were first rejected -- #7 and #8.
- Architectures with a nonrandom (oriented design) were rejected (for reasons discussed previously). This left architectures #3, #4, #5, #6, and #9.
- The composites exhibiting the highest warp strengths were then selected. These were #3, #6 and #9.
- Toughness then was considered and #9 had the best qualitatively determined toughness. Architecture #3 might have been further considered if there was additional strength data with wider bend bar specimens for evaluation. Architecture #6 did not have load-deflection data for the warp direction. However, a #6P, the P represents the use of pressure during matrix processing, did have load-deflection curves. From these curves, is was determined that #6 had a low degree of toughness, most likely due to its high matrix content which made it act more like a monolithic.

Fill.

- Using the first two criteria above, minimum strength and randomness of design, the list was narrowed to #3, #6, #8, and #9.
- In general, load-deflection curves in the fill direction showed less load carrying ability after the initial "yield" than those of the warp direction. Again, #6 exhibited poor toughness. This left #3, #8 and #9.

Combining the results above, #8 was rejected due to its low warp strength. Given the available data, #9 was chosen over #3 due to its higher warp strength and because it had the best qualitative toughness characteristics.

In summary, fiber architecture #9 was selected because adequate flexure strength was obtained in both the warp and fill directions. The load-deflection curves exhibited the best toughness.

3.2 Composite Processing

The objective of this task was to optimize the matrix processing conditions to minimize fabrication cost while maintaining acceptable filter performance. Several processing variables can influence the density/porosity, mechanical properties, performance, and cost of the hot gas filter:

- Processing method
- Mullite filler powder
    - Particle size distribution
    - Concentration of mullite filler powder added to sol
- Mullite sol

    - Viscosity
    - Source
    - Concentration
- Calcining temperature and time
- Sintering temperature and time

Because this effort was conducted concurrently with the fiber architecture development task, the 3D fiber architecture developed during the contractor's internal filter development program was used as the baseline architecture for most of the composite processing study.

A Taguchi design of experiments approach was initially considered in order to provide a systematic analysis of the effects of the processing variables. The intent of using the Taguchi process was to identify the major effects (variables) and the most optimum values for these effects in order to meet the permeability requirements. However, during the course of the matrix processing study, use of the Taguchi process was determined not to be necessary for evaluating the above list of processing variables.

For this composite processing study, permeability was the primary response to be measured because it is the most important filter parameter. Regardless of strength, surface condition, etc., if a candidate filter material does not meet the permeability requirement, it cannot be considered for filter applications. The second most important factor considered was the capability for a set of processing conditions to form a filtering surface membrane *in-situ*, which is directly related to permeability.

From the processing variables listed above, the major effects determined during the composite processing study were the processing method (Section 3.2.1), the mullite filler particle (Section 3.2.2) and the mullite sol (Section 3.2.3). These factors are discussed in more detail in the following sections. Calcining temperature and time were not major factors; for cost reasons both temperature and time would be kept as low as possible. Sintering temperature effects are briefly discussed in Section 3.2.3 on the mullite sol; time was not evaluated.

3.2.1 Processing Method

The objective was to develop a low cost method with only two matrix processing steps:

1. Infiltration of the ceramic preform with a water-based mullite sol (no mullite filler powder) to rigidize the ceramic preform and provide a protective coating on the fibers.

2. Infiltration of the ceramic preform with a water-based mullite sol with mullite filler powder added. The purpose of the filler is to create a tortuous porosity network.

These two steps are discussed in the following sections.

3.2.1.1 Sol-Only Infiltration Step

As noted above, the objective was to fabricate filter materials using only two matrix processing steps. The first step is a sol-only infiltration to rigidize the preform and to provide a protective coating on the fibers.

Past experience indicates that if the initial infiltration yields a coating which is too thick, the resulting preform will be stiff and difficult to process in subsequent steps. Furthermore, to optimize the mechanical properties of the composite filter material, it is desirable to have a thin, uniform crack-free coating with minimal bridging between the fibers.

The suitability of the water-based mullite sol for forming a uniform, thin coating was evaluated by dip coating woven Nextel 550 fabric in three sol concentrations: 10, 5, and 2.5 wt%. The fabrics were then air dried, calcined at 800 °C for 1 hour and then examined using a scanning electron microscope.

The 10 wt% mullite sol resulted in a very thick and cracked coating; significant fiber bridging was observed, Fig 3.10 (a). The 5 wt% sol also yielded a thick cracked coating, Fig 3.10 (b). The 2.5 wt% mullite sol was found to give the most uniform crack-free mullite coating with minimal bridging, Fig 3.10 (c). The 2.5 wt% sol was selected for use in all subsequent CMC fabrication.

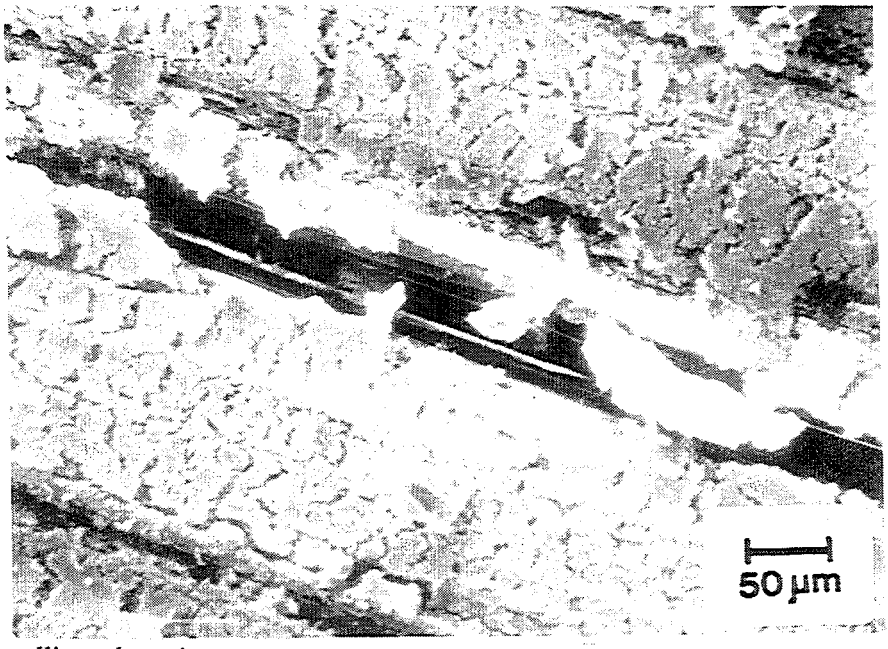

(a) 10 wt% mullite sol coating

Figure 3.10 - SEM photomicrographs of Nextel 550 coated with (a) 10 wt% mullite sol, (b) 5 wt% mullite sol, and (c) 2.5 wt% mullite sol.

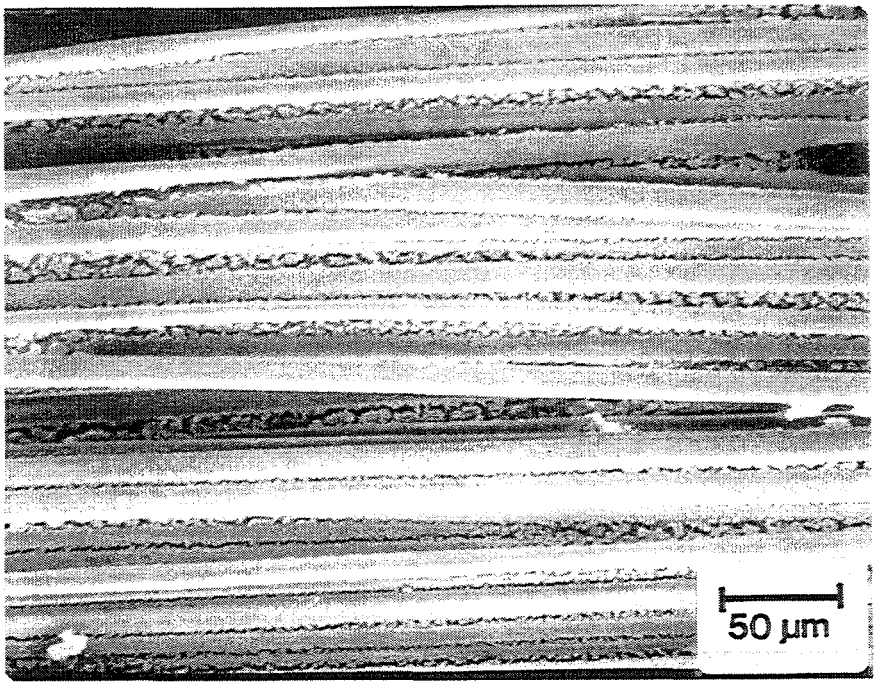

b) 5.0 wt% mullite sol coated

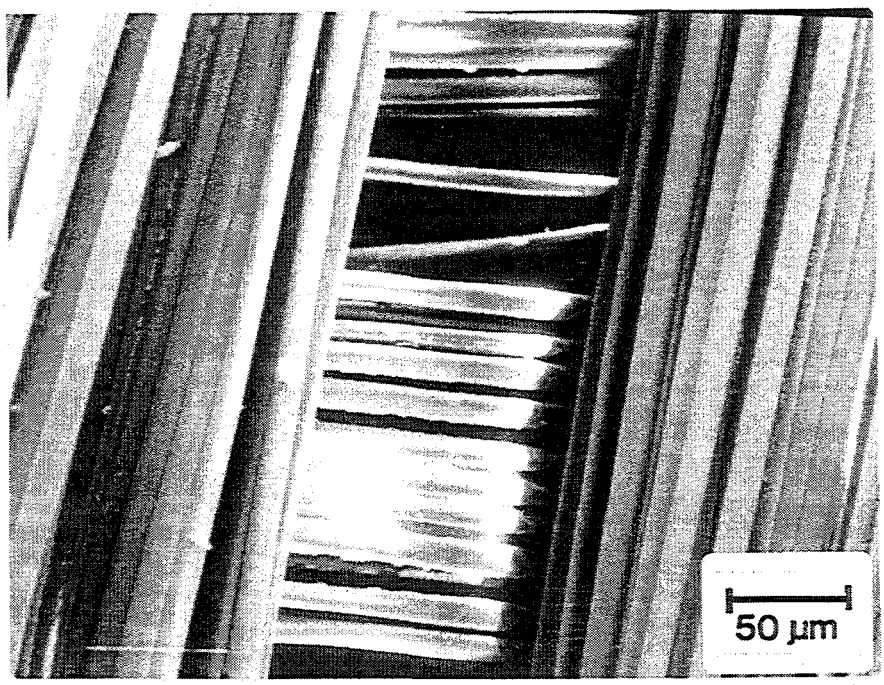

c) 2.5 wt % mullite sol coated

Figure 3.10 - (continued)

3.2.1.2 *Matrix Infiltration Method*

The intent of this effort was to develop a method which could infiltrate the matrix into the fiber preform in one step and that would also form a membrane layer on the fiber preform surface. The permeability ratio was compared for a conventional vacuum infiltration approach and for a one-sided flow-through vacuum infiltration method. In the conventional method, the infiltrant enters the composite preform from all exposed surfaces. In the one-sided approach, vacuum was used to pull the infiltrant from one exposed surface through the composite, see Figure 3.11.

For each method, a fiber preform was infiltrated with an aqueous 10 wt% mullite sol

Table 3.9 -- Gas Flow Resistance as a Function of Infiltration Method

Vacuum Infiltration Method	Gas Flow Resistance (in-wg/fpm at 70 °F)	
	Up	Down
Conventional	2.160	2.637
One-Sided Flow-Through	0.283	0.332

containing 10 wt% mullite powder. The particle size of the mullite powder was 10-44 microns. After 5 infiltration cycles, the immersion densities of the samples were 1.80 g/cm^3 and 1.68 g/cm^3 for the conventional and one-sided infiltrated samples, respectively. These values correspond to 58 % and 54 % of theoretical density (3.11 g/cm^3), respectively.

The gas flow resistance was measured for each sample. As shown in Table 3.9, the sample infiltrated from one-side only was within the filter specification for gas flow resistance (i.e., R < 1 in-wg/fpm), while the conventionally infiltrated sample had a gas flow resistance exceeding the target specification.

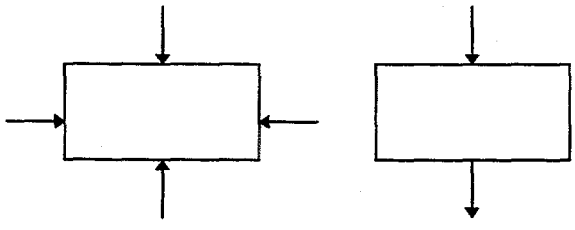

Figure 3.11 -- Schematic of conventional vacuum infiltration and one-sided flow-through vacuum infiltration techniques

The one-sided infiltration approach was selected for all CMC fabrication. This approach was also expected to give the lowest manufacturing cost. During filter manufacturing the filter matrix would be vacuum infiltrated from only one side into the preform; this would be from the outside to the inside. Unless otherwise noted, filter composite processing development work and test sample fabrication at Westinghouse and Techniweave used the one-sided flow-through vacuum infiltration method with similar sample fabrication setups.

3.2.1.3 Pressure-Assisted Infiltration

Pressure was applied during the matrix infiltration process in an effort to increase the amount of matrix infiltrated into the preform and thus increase the composite strength without compromising permeability. Four-point bend tests were conducted on CMC specimens fabricated from architectures 3, 5 and 6 with pressure assisted matrix infiltration. The strength data obtained for the pressure infiltrated samples was compared to the data measured on the conventionally processed samples of architectures 3, 5 and 6, see Table 3.10. Except for architecture 5, the mean flexure strengths obtained for the pressure infiltrated samples were generally higher than for the conventionally processed samples. As shown in the table, acceptable permeability results were obtained for the pressure assist samples.

Table 3.10- Permeability and Strength Data for Pressure-Assist Samples as Compared to Conventional Infiltration Samples

Sample ID or Fiber Arch.	Permeability	Mean 4-Pt Bend Strength (psi)					
		Warp Direction			Fill Direction		
	Pressure Assist	Standard Infiltration		Pressure Assist	Standard Infiltration		Pressure Assist
	(iwg/fpm)	3 mm wide	6 mm wide	6 mm wide	3 mm wide	6 mm wide	6 mm wide
CMC 3-P	0.612	1322	N. M.	1499	1931	2097	2954
CMC 5-P	0.1	1888	2340	2190	921	N. M.	1479
CMC 6-P	Poor sample*	2076	N. M.	2899	2061	1690	2331

*Sample for 6-P had edge defects which prevented good sealing in the permeability test rig; additional material was not available for machining a second sample.

3.2.2 Mullite Filler Particle

The objective of this effort was to identify a low cost source of mullite powder and to determine the appropriate particle size distribution for composite filter fabrication. The mullite filler particle size distribution affects filter permeability (tortuosity of the pore channels), density

(amount of porosity), and cost (powder cost; number of infiltration cycles). Based on prior Westinghouse and Techniweave internal research, three particle size distribution ranges were selected for development and evaluation:

1. narrow and fine, ~1-10 microns;
2. moderate and medium, ~5-20 microns; and,
3. coarse and broad, baseline.

For distributions 1 and 3, commercial sources were available, but distribution 2 was not available commercially. Particle size classification was used to obtain distribution 2.

For distribution 1, Keith Ceramics (England) manufactures a 1-10 micron dense fused mullite powder that is distributed by Refractory Minerals Company Incorporated (RMCI) in the United States for about $1.00/lb. This powder, along with the baseline powder, were considered but were not used for reasons noted below.

Particle size classification requires a coarse starting powder which is then classified into various size fractions. Powder samples of the baseline material at $26.00/lb, and from Keith Ceramics (RMCI in U.S.), -200 mesh at < $1.00/lb, were supplied to Powder Technology, Inc. for analysis. Based on particle size analyses of these two materials, Powder Technology indicated that both materials could be used as feedstock for providing not just distribution 2 but all three size distributions needed for testing. Approximately 100 pounds of the baseline powder would be required to generate 10 pounds for each of the three size ranges.

Similarly, about two hundred pounds of the Keith -200 mesh, dense fused mullite powder would be required. Since the Keith powder costs less than $1.00/lb, it was the more economical choice for feedstock material, see Figure 3.12 for particle size distribution. All three distributions were obtained from the Keith powder; this eliminated variability due to obtaining materials from different sources. Even with classification the Keith powder, at pennies per pound, provides a cost effective approach for high volume filter production. As shown in Figure 3.13, the actual particle size distributions were very close to the targeted particle size distributions. Testing and evaluation of these three particle size distributions is discussed in the following paragraphs.

Processing experiments, Table 3.11, were conducted to determine the influence of mullite powder size distribution and of powder concentration in the matrix slurry on filter gas flow resistance. Nextel 550 preforms, with a 3D angle interlock architecture, were used for these experiments. Preform sections, 100 mm x 100 mm, were dip coated with a 2.5 wt% mullite sol. The coated preforms were air dried and then calcined at either 600°C or 800°C for 2 hours. Disk

specimens, suitable for permeability testing, were machined from the coated preforms for matrix processing.

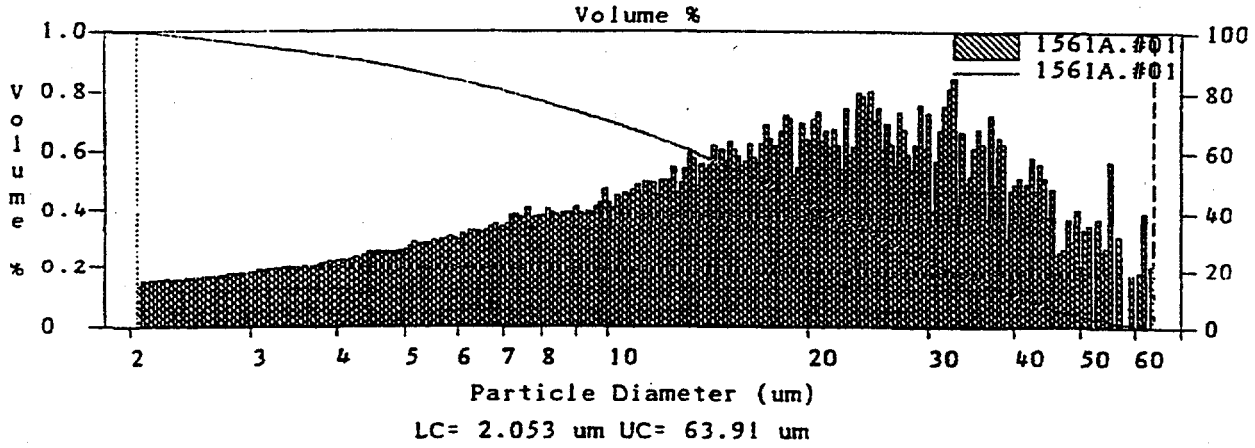

Volume Statistics (Geometric) 1561A.#01

Calculations from	2.05 um to 63.91 um			
Volume	$62.14*10^6$	um^3		
Mean:	14.88	um	Std. Dev.:	0.822
Median:	16.87	um	Variance:	0.675
Mean/Median Ratio:	0.882			
Mode:	32.63	um		

% >	10.00	25.00	50.00	75.00	90.00
Size um	40.41	28.52	16.87	8.383	4.353

Mean particle diameter: 14.88 microns

Figure 3.12 -- Typical particle size distribution for Keith Ceramics, -200 mesh at < $1.00/lb, as measured by Powder Technology, Inc.

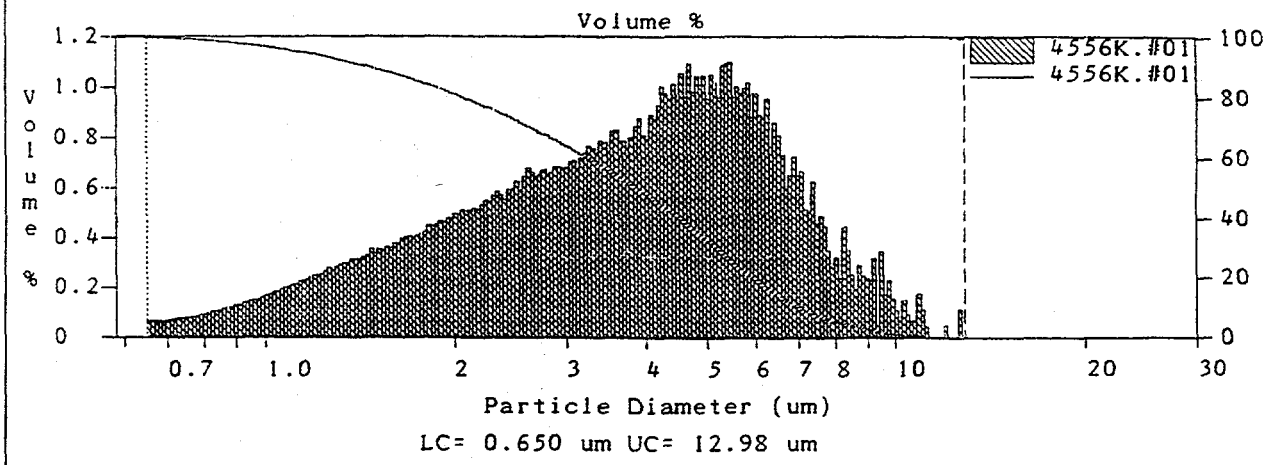

(a) mean particle size: 3.489 microns

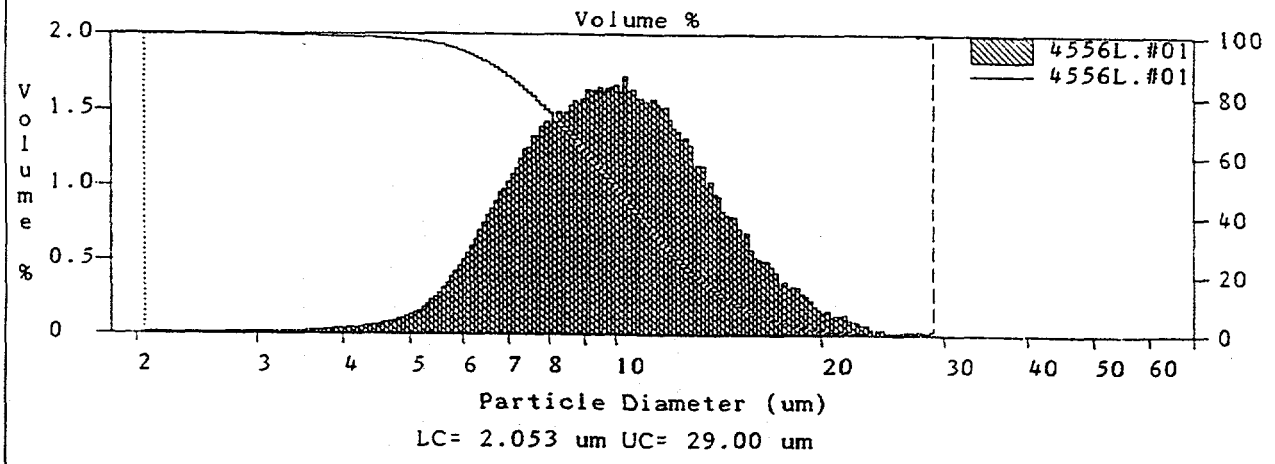

(b) mean particle size: 9.88 microns

Figure 3.13-- Classified mullite powder particle size distribution data for the (a) narrow and fine distribution with a target distribution of 1-10 μms and (b) the moderate and medium distribution with a target of 5-20 μms.

The one-sided infiltration method was used to infiltrate each disk with a matrix slurry composition (mullite sol + mullite powder). The goal was to infiltrate until a thin, uniform membrane layer was formed on the disk surface. The infiltration efficiency of the various slurries was monitored. Upon completion of the infiltration processing, samples were either sintered or set aside (if processing results were unacceptable). After sintering, selected samples were evaluated for gas flow resistance.

The major and minor processing variables and their selected values for evaluation are shown below:

Major

- Mullite Powder Particle Size Distributions: The initially targeted distributions of 1 - 10 μm, 5 - 20 μm, and baseline were utilized. Additionally, the -200 mesh mullite feedstock was also evaluated due to the potential cost savings.
- Concentration of Mullite Filler Powder: A low, 10 wt%, and a high, 30 wt%, concentration were selected for evaluation.

Minor

- Concentration of Mullite in Aqueous Base Sol: A low, 5 wt%, and a high, 10 wt%, concentration were selected for evaluation.
- Calcining Temperature: Temperatures of 600 and 800 °C were selected.
- Sintering Temperature: Temperatures of 1050 and 1150 °C were selected.

Both the calcining and sintering times were held constant at 2 and 4 hours, respectively. The calcining and sintering temperatures were varied because temperature has a more significant

Table 3.11 -- Baseline Filter CMC Processing Experiments

Spec. ID	Processing Variables			Experimental Results			
	Mullite Powder Particle Size Distribution	Mullite Sol Conc. (wt %)	Mullite Powder Conc. in Sol (wt %)	Perm. (iwg/ fpm)	Membrane Formation	Cycles	Bulk Density (g/cm^3)
FD-1	1-10 μm	5	10	1.201	N	15	1.12
FD-2	1-10 μm	10	30	-0.007	N	13	1.16
FD-3	5-20 μm	5	10	1.306	N	15	1.21
FD-4	5-20 μm	10	30	1.080	N	2	1.42
FD-5	baseline	5	30	0.486	Y	6	1.24
FD-6	baseline	10	10	-0.021	N	na	1.13
FD-7	5-20 μm	5	30	1.898	Y	1	1.21
FD-8	5-20 μm	10	10	0.154	Y	7	1.34
FD-9	-200 mesh	5	10	0.818	Y	2	1.27
FD-10	-200 mesh	10	30	0.062	Y	1	1.22
FD-11	-200 mesh	5	30	0.603	Y	3	1.23
FD-12	-200 mesh	10	10	0.231	Y	2	1.24
FD-13	-200 mesh	5	30	0.295	Y	2	1.20
FD-14	-200 mesh	10	10	0.263	Y	1	1.22

impact on microstructure development than does time at temperature. The times were chosen conservatively to provide sufficient time for all significant reactions to occur.

For each experiment, the results and the values of the major processing variables are shown above in Table 3.11. The following observations were noted for these experiments:

- The finest particle size distribution, 1-10 microns, was easily pulled through the coarse porosity network of the standard angle interlock fiber architecture. A membrane layer on the surface of the composite was unable to be formed after several infiltration cycles.
- The medium particle size distribution, 5 - 20 microns, at a loading of 10 wt%, formed a membrane layer after several infiltration cycles (7-15). The number of cycles required to form this layer was not practical. At an increased powder loading of 30 wt% in the sol, this particle size distribution was used to form a membrane layer within one to two cycles.
- The broad and coarse baseline and -200 mesh (< 70 microns) powder distributions readily formed a membrane in one cycle.
- Pinholes were often observed in the membranes. This pinhole formation was not a processing issue but was observed to correspond to the filling of the coarse surface porosity of the angle interlock fiber architecture. It was not a characteristic of any of the particle size distributions. These pinholes did not necessarily imply a potential leak as the angle interlock architecture in its own right has quite tortuous porosity and would stop any penetration of the ash. The disadvantage of pinholes is that they would be more likely to plug up with ash. Thus, a large number of pinholes, if plugged with ash, could reduce the available filtering surface area. It was possible to eliminate these pinholes by a secondary infiltration step prior to the final firing step. However, with the alternative architectures developed by Techniweave, pinholing was not been observed nor is it expected to be an issue.

  In Section 3.1.2, Screening Test, pinholing was not observed during fabrication of the screening test samples for evaluating the new candidate fiber architectures. These architectures have finer surface porosity and are not prone to pinholing, as is the above angle interlock architecture.
- The minor processing variables, mullite sol concentration, calcining temperature and sintering temperature, did not appear to have any influence on permeability or the formation of the membrance layer.
- Nine of the fourteen specimens met the gas flow resistance criteria (R < 1 in-wg/fpm).
- Based on performance and expected cost (powder cost and processing costs, i.e. # of processing cycles required to infiltrate the preform and generate a membrane layer), the use of the baseline powder or -200 mesh mullite powders provided good gas flow resistance properties and required fewer processing cycles when compared to the 1 - 10 micron and 5 - 20 micron powder distributions.

Because of the low cost of the Keith Ceramics -200 mesh mullite powder, < $1.00/lb, preliminary tests were conducted with the new architectures to determine if this powder could be

used in the as received condition (without classifying) for filter manufacturing. Techniweave fabricated 50.8 mm x 50.8 mm composite panels from architectures 3 and 4 with the Keith -200 mesh and classified 5-20 micron mullite powders for permeability measurement. Sample descriptions and permeability test results are shown in Table 3.12. These samples met the gas flow resistance requirements and demonstrated the potential feasiblity of using the -200 mesh RCMI powder.

Table 3.12 -- Gas Flow Resistance Measurements

Fiber Architecture	Sample Number	Sample Description	Gas Flow Resistance (in-wg/fpm)
3	3	infiltrated with T-sol and -200 mesh mullite powder	0.600
4	4	infiltrated with T-sol and 5-20 micron mullite powder	0.237
4	4A	infiltrated with T-sol and -200 mesh mullite powder	0.397
4	4B	infiltrated with T-sol and -200 mesh mullite powder	0.248

3.2.3 Mullite Sol

The objectives of this effort were: (1) to evaluate the feasiblity of increasing the aqueous mullite sol viscosity in order to simplify fabrication and to reduce cost, and (2) to compare the Westinghouse aqueous mullite sol to the Techniweave aqueous mullite sol. Commercial suppliers of aqueous mullite sols were not available at the time of this work.

3.2.3.1 Sol Viscosity

The objective of this effort was to increase the mullite sol viscosity in order to simplify fabrication and reduce production and capital equipment costs. Generally, a higher viscosity solution aids in keeping ceramic filler powders in suspension, provides for a more homogeneous infiltration of the fiber preform, and eliminates the need for mechanical agitation to keep the powder dispersed in solution. The Westinghouse sol was used for this study; the Techniweave sol being similar in nature was expected to behave in the same manner as the Westinghouse sol.

Several water-soluble polymers were evaluated in terms of their effectiveness for increasing the viscosity of the water-based mullite sol. These additives include: Carbopol by Goodyear (cross-linked polyacrylic acid polymer), Surfynol CT-324 by Air Products (pigment grind additive of proprietary composition), and Elvanol by Dupont (Polyvinyl Alcohol).

Unfortunately, these products were found to be either incompatible with the water-based mullite sol or were ineffective for increasing the sol viscosity.

Carbopol and Elvanol were incompatible with the sol; they were not able to be dissolved in the water-based mullite sol. Surfynol CT-324, did not completely dissolve in the water-based mullite sol, but was found to significantly improve the dispersability of the mullite powder in the sol. Concentrations in the range of 5 - 10% by mullite powder weight were found to be beneficial. The viscosity of the sol increased from 20 cp to 400-800 cp, depending on the mullite powder concentration in the sol. Unfortunately, the undissolved portions of Surfynol were in the form of large, fat-like globules. During preform infiltration, these Surfynol globules clogged the pores of the composite preform and formed a coating on the preform surface which inhibited infiltration of the mullite sol and mullite filler powder.

Technical personnel at BF Goodrich, Air Products and Rohm & Haas were contacted to discuss the compatibility difficulties that were encountered. The vendors indicated that such water-soluble additives are targeted for use in systems having a pH in excess of 3. The two water-based mullite sols under evaluation have a pH less than 2. This pH difference causes a chemical incompatibility between the additives and the sol.

The vendors did suggest polyethylene imine and polyvinylpyrrolidone as possible compatible additives for low pH solutions. Polyethylene immine retains its charge in acidic conditions and hence may work in conjunction with a low pH sol. Polyvinylpyrrolidone has good solubility and chemical stability in both water and many organic solvents.

Other methods evaluated for either improving powder dispersion or increasing sol viscosity included: 1) The application of an "ionic" polyvinyl alcohol (PVA) coating to the surface of the mullite filler powder, prior to dispersion in the sol, as a means to improve the dispersability of the mullite powder, and 2) the use of a thermal treatment of the water-based sol to increase sol viscosity. Neither approach was successful.

3.2.3.2 Sol Evaluation

The objective of this effort was to evaluate the two mullite sols being used in this program. Westinghouse was using their own internally developed sol which has a mullite crystallization temperature of 1150°C and Techniweave was using a mullite sol (from another source) which has a mullite crystallization temperature of 1000°C. Both sols are water-based with a low pH. For the Techniweave sol (T-sol), the major issues are its continued availability and its present high cost

Table 3.13 -- Sol Evaluation Test Matrix and Tensile Test Results

Sample ID	Sol Source		Firing Temperature (°C)		No. Specs. Tested	Room Temp. Tensile Strength (psi)	
	Westinghouse	Techniweave	1050	1150		Mean	Std. Dev.
7A		X	X		5	955	289
7B		X		X	6	877	308
7C		X	X		6	1532	203
7D	X		X		5	2394	355
7E	X			X	6	1670	397

Note: sample 7C had a zirconia interface coating

(~$625.00/liter). For the Westinghouse sol (W-sol), the major issue was the effect of the 1150°C crystallization temperature on the Nextel 550 fibers.

A test matrix, Table 3.13, was developed to evaluate these two sols along with the effect of firing temperature on the fiber properties. In parallel, a single test plate with an appropriate interface coating (selected by Westinghouse) was fabricated to allow comparison of a composite with an interface coating with composites without an interface coating. Samples were fabricated by Techniweave. Westinghouse machined 152.4 mm x 12.7 mm test specimens and conducted room temperature tensile testing. Tensile testing was selected over bend testing because of the higher volume of material, i.e. fibers, subjected to tensile loads. Additionally, tensile testing is the preferred test method to demonstrate the damage tolerance , or resistance to crack propagation, of a ceramic composite material.

In general, the strength results shown in Table 3.13 were low, however, this was expected because the warp direction, which is the low strength direction, was parallel to the applied tensile load. The following observations were noted from the data:

- The Westinghouse sol samples were higher in strength than the Techniweave sol samples.
- The interface coating improved the strength of the Techniweave sol samples.
- For the same sol, specimens fired at 1050°C had higher strengths than those fired at 1150°C. These results indicate that fiber degradation may be occurring at the 1150°C firing temperature, which was near the maximum recommended (by 3M) use temperature of N550.

The stress-strain curves for all test specimens exhibited noncatastrophic failure characteristics which demonstrated the capability of this composite to resist crack propagation, see Figure 3.14.

The stress-strain curves for the W-sol samples show a decrease in both strength and strain carrying capability with the increased firing temperature. The 1150°C sample is expected to have a

more crystalline matrix than that of the 1050°C sample (fired below the complete mullite crystallization temperature of 1150°C for the W-sol) which is expected to be comprised of an amorphous phase along with crystalline mullite and alumina. This amorphous phase contributes to the increased strength of the W-sol samples. However, amorphous phases in hot gas filter environments will crystallize and will also act as sinks for alkali species; these events as they happen would be expected to reduce the strength of the W-sol samples.

The immersion densities of each sample ranged between 50 and 65% of theoretical density (3.11 g/cm^3). The tensile strength correlated with density within samples but not across samples, i.e., the W-sol samples had low densities and the highest strengths, whereas, the T-sol samples had generally the same or higher densities but lower strengths, see Figure 3.15. Generally, for most materials, strength increases with increasing density.

Although, from the table and above figures, the T-sol samples have lower strengths than the W-sol samples, the T-sol samples are expected to have a more stable matrix material in a hot gas filtering environment. The use of the zirconia interface appears to have increased the strength and load carrying capability of the T-sol sample fired at 1050°C. Additional testing and analyses

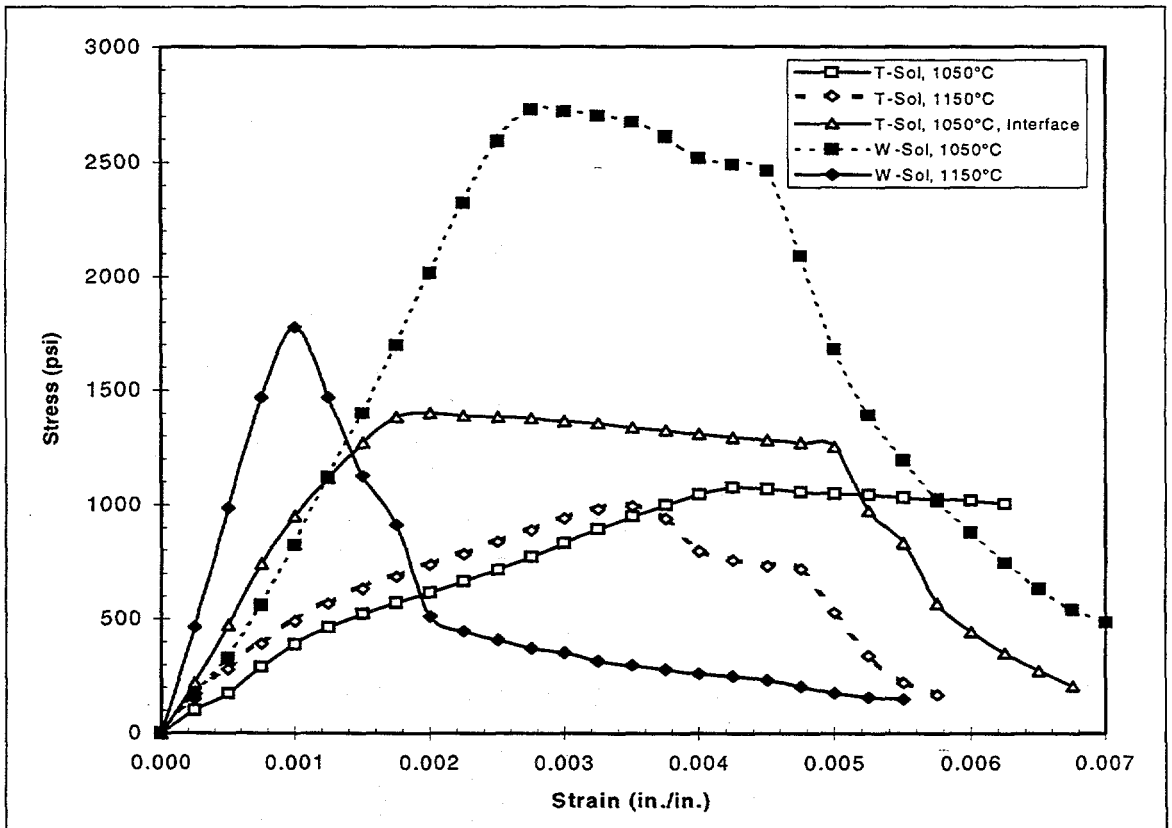

Figure 3.14 -- Representative stress vs strain curves for each sample listed in Table 3.12.

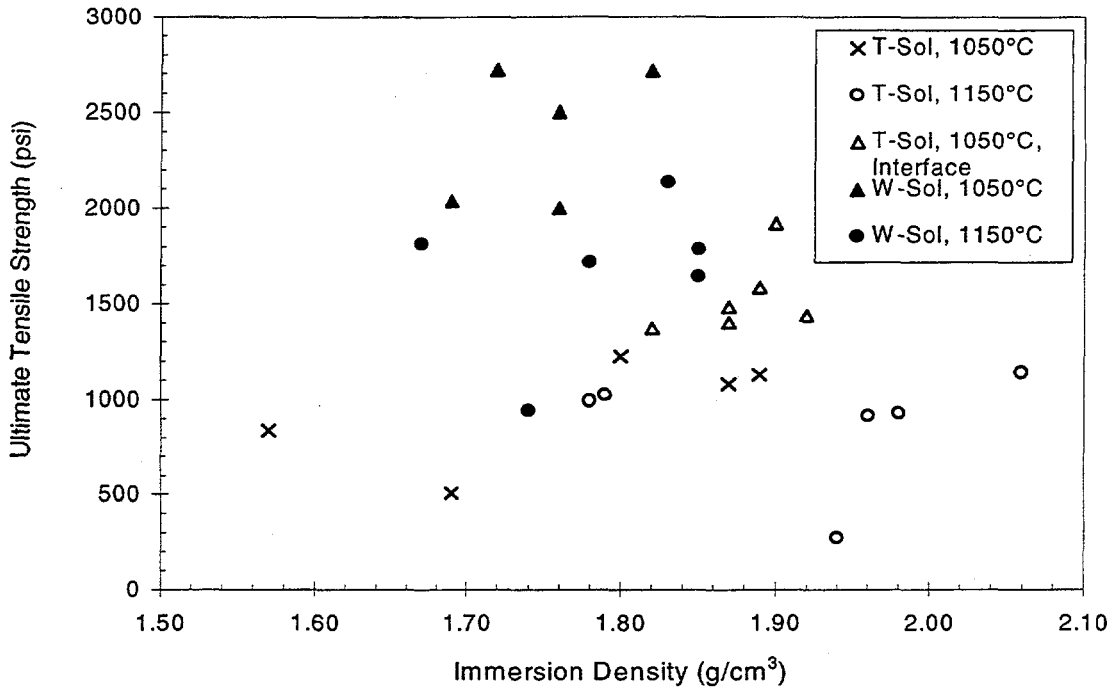

Figure 3.15 -- Plot of ultimate tensile strength vs immersion density for all the tensile test specimens of each sample in Table 3.12.

would need to be done to confirm these results and to understand what role the interface coating is providing in this filter composite material.

X-ray diffraction patterns of the test specimens in Table 3.13 are shown in Figure 3.16. A semi-qunatitative analysis of these patterns was conducted as described below. This method was used all analyses in this report.

Semi-quantitative analyses of multi-phase XRD diffraction patterns can be conducted since the intensity of a pattern for a particular phase in a mixture is dependent on the concentration of that particular phase in the mixture. The analysis performed here relied on the External Standard Method (a reference line for each individual phase was obtained from the JCPDS, Joint Committee on Powder Diffraction Standards, pattern for each phase) as described in "Elements of X-Ray Diffraction, 2nd Edition" by B. D. Cullity, p. 407-411.

A sensitivity factor was first calculated for the mixture using the following equation:

$$SF_{mixture}=\sum(I_{exp})_{i=1\ to\ n}/(I_{JCPDS})_{i=1\ to\ n}$$

where:

I_{exp} = experimental intensity for largest un-interfered $peak_{i=1\ to\ n}$

I_{JCDPS} = JCPDS intensity for same $peak_{i=1\ to\ n}$

where n represents the number of phases in the mixture. The experimental peak chosen for each phase in the above calculation was the highest intensity line for each phase present in the mixture that did not overlap/interfere with lines associated with other phases in the pattern. The experimental intensity, I_{exp}, for the peak was obtained directly from the diffraction peak file software. The JCPDS peak intensity, I_{JCDPS}, was the known intensity for the pure phase as taken from the JCPDS library for the same peak measured experimentally.

The concentration for an individual phase was then determined using the following calculation:

$$\text{Concentration in wt.\%}_{\text{phase a}} = (I_{exp})_a/(I_{JCPDS})_a/SF \times 100$$

The results of the semi-quantitative analysis, Table 3.14, showed that the T-sol samples had a higher mullite content than that of the W-sol samples. The amorphous content in the T-sol samples was due to the Nextel 550 fibers (composed of amorphous silica, γ- and δ-alumina); the T-sol fully crystallizes into mullite at 1000°C. The W-sol 1050°C had a higher level of amorphous silica, Figure 3.16, which was due to the fiber and the incomplete crystallization of the W-sol;. the W-sol, as noted earlier, crystallizes at 1150°C. The increased mullite content at 1150°C for both sols was believed to be due to the initiation of devitrification of the fiber, and for the W-sol, additional crystallization of the sol. This supposition was supported by the tensile strength results, Fig. 3.14, which shows decreased strength and damage tolerance (decreased strain carrying capability) for the 1150°C samples. This mechanical property degradation was associated with a degradation in mechanical properties of the fiber.

Table 3.14 -- X-Ray Diffraction Results for Nextel 550/Mullite Matrix Composite Samples

Sample Number	Description	$Al_6Si_2O_{13}$ Mullite JCPDS 15-776	γ-Al_2O_3 JCPDS 10-425 (a)	δ-Al_2O_3 JCPDS 16-394 (a)	Al_2O_3 JCPDS 11-517 (a)	Al_2O_3 (b) Corundum JCPDS 42-1468 (or 43-1484)	Comments
7A	T-Sol, 1050°C	47	14	19	20	possible trace	greater amorphous content than 7B
7B	T-Sol, 1150°C	59	11	16	14	0	preferentially oriented along [110]; greater amorphous content than 7C
7C	T-Sol, 1050°C, ZrO_2 Coating	55	11	13	13	8	best pattern produced; no ZrO_2 observed
7D	W-Sol, 1050°C	26	20	28	26	possible (c)	very poor pattern; high amorphous content
7E	W-Sol, 1150°C	39	16	22	23	possible trace	poor pattern with high amorphous content

General Notes:

1. Phase composition results highly qualitative due to poor overall quality of XRD spectra.
2. γ and δ Al_2O_3 phases have similar XRD patterns and it is believed that both forms are present.
3. No crystalline form(s) of SiO_2 can be identified in any of the samples.

Specific Notes:

(a) Patterns for Al_2O_3 (JCPDS 11-517, 10-425, and 16-394) are very similar (e.g., dominant peaks overlap), therefore, it is difficult to positively differentiate between these phases.

(b) Possible identification based on presence of very small 100% intensity peak for Corundum.

(c) May be present but poor quality of XRD pattern precludes positive identification.

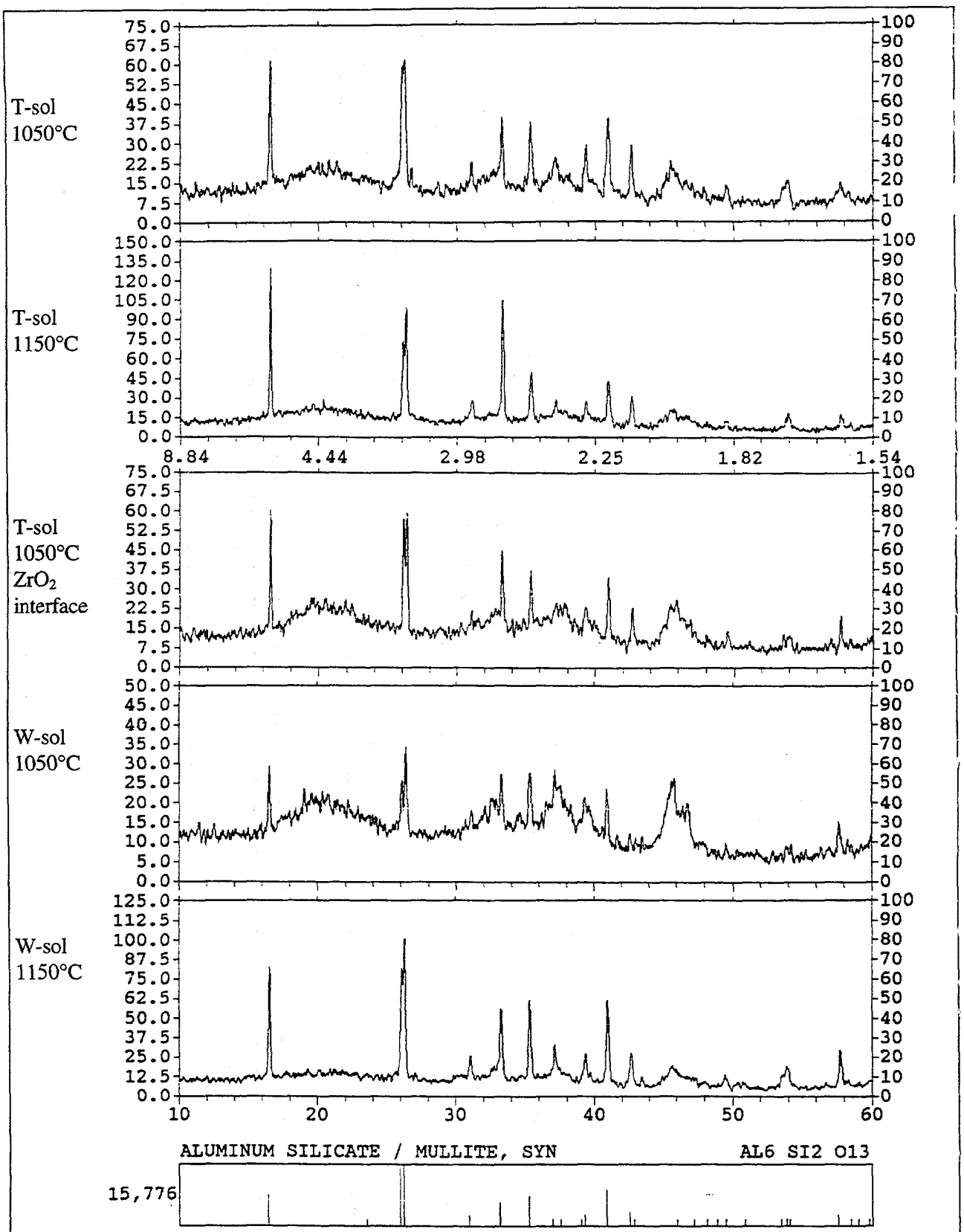

Figure 3.16 -- XRD diffraction patterns for the various T-sol and W-sol samples described in Table 3.13 where the x- and y-axes are intensity (counts per second) and 2Θ (degrees), respectively.

3.3 Composite Material Evaluation

Two types of tests were conducted to determine the combined effects of temperature, time, and the environment on the Nextel 550-based filter composite material's mechanical properties and failure characteristics. First, thermal aging tests were conducted in which bend specimens were exposed to 150, 300, 800, 2000, and 5000 h at 870°C in static air and then bend tested at room temperature.

Second, four high-temperature, flow-through corrosion tests were conducted in which specimens were exposed for 400 h at 870°C with simulated pulse cycling in flow-through steam/air with and without alkali. Post-test characterization included high temperature bend testing and microstructural evaluation.

3.3.1 Thermal Aging

Thermal aging experiments at 870°C (1600°F) were conducted in order to evaluate potential interactions between the fiber and the matrix which could embrittle the composite filter material. Thermal aging times were 150, 300, 800, 2000, and 5000 h. After aging specimens were tested in 4-pt bending at room temperature and evaluated via x-ray diffraction in order to determine if phase changes occurred. Because there was insufficient material from any one architecture to conduct these tests, specimens were used from the first five architectures for the thermal aging experiments. These specimens all had the same matrix composition and were processed identically. The resulting thermal aging bend data was then normalized with respect to the as-received bend data in order to eliminate architecture effects.

3.3.1.1 Bend Strength Results

CMC plates 1-5, which were fabricated from architectures 1-5, respectively, were used to provide the thermal aging test specimens. The test specimens for the aging test were taken from the same plate as the as-received baseline unaged specimens. Specifically, as the bend specimens were machined, every other one was chosen for thermal aging in order to eliminate local differences in the plate.

The 4-pt bend strength data for the aged and unaged specimens is shown in Table 3.15. In general, there was not any change in strength as a function of time at 870°C. However, there were two exceptions, and these are more clearly seen in Figure 3.17. The two exceptions were the warp direction specimens of CMC #4 and the fill direction specimens of CMC #5.

Table 3.15 -- Room Temperature 4-Pt Bend Strength of As-Received and Thermally Aged Nextel 550 CMC Filter Material

CMC Arch. Spec. No.	Aging Time	Room Temperature 4-Pt Bend Strength (psi)			
		As-Received		After Aging	
	h	Warp or 'x'	Fill or 'y'	Warp or 'x'	Fill or 'y'
1	150	1058 ± 224 (5)	1577 ± 455 (6)	1084 ± 210 (5)	1827 ± 353 (6)
2	300	1100 ± 80 (5)	1731 ± 214 (6)	930 ± 185 (5)	1829 ± 305 (5)
3	800	1322 ± 289 (5)	1931 ± 328 (5)	1146 ± 128 (5)	1821 ± 223 (4)
4	2000	1104 ± 119 (6)	917 ± 429 (6)	2144 ± 278 (5)	1152 ± 396 (6)
4W	2000	1888 ± 367 (6)	921 ± 122 (6)	n/a	n/a
5	5000	2076 ± 563 (6)	2061 ± 973 (6)	2136 ± 222 (6)	936 ± 347(6)

Note: numbers in parentheses represent the number of specimens tested.

In Figure 3.17, the data was normalized to eliminate effects on strength due to differences in weave pattern and fiber volume. All samples evaluated in the thermal aging test program were chemically the same, i.e., Nextel 550 fiber reinforced mullite matrix, and were processed in exactly the same manner. Strength differences from sample-to-sample (e.g., #1 vs. #2, #2 vs. #4, etc.) were due to differences in the specific weave pattern and in the fiber volume in the warp and fill directions. Normalization of the data allowed direct comparison of the bend strength results without confounding due to the weave and fiber volume differences.

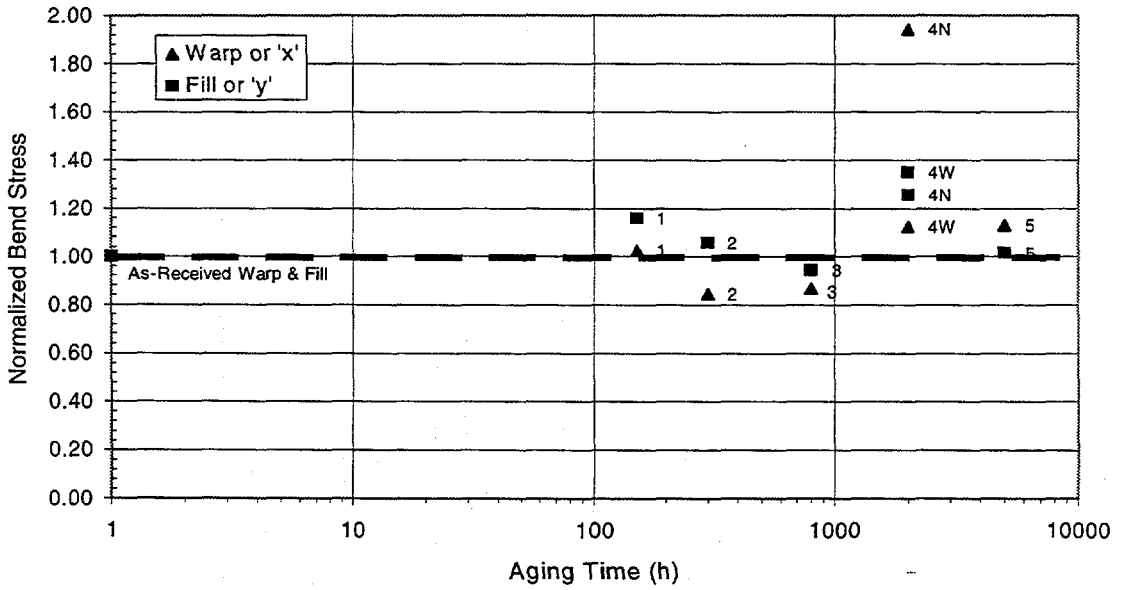

Figure 3.17 -- Plot of room temperature 4-pt bend vs. time which has been normalized with respect to the fiber architecture.

For CMC #4, the aged strength in the warp direction was almost twice that of the as-received specimens while the strength in the fill direction appeared unaffected by the thermal aging. For CMC #5, the aged strength in the fill direction was about half that of the as-received specimens while the strength in the warp direction appears unaffected by the thermal aging. These differences were believed to be a test specimen size effect. The data shown in this table, except for CMC #4W, was measured from bend specimens which were 3 mm in width, which was believed to be too narrow for these fiber architectures, as discussed previously in the Section 3.1.2.3 Mechanical Properties.

If there was a change in strength due to thermal exposure, that change would be expected to have occurred independent of test direction. Note that in Table 3.15, the strength data for the wider test specimens of CMC #4W is shown; this data was comparable to that of the thermally aged specimens. The difference between CMC #4 and CMC #4W was the width of the 4-pt bend test specimens, 3 mm vs 6 mm, respectively. The CMC #4W specimens were machined from the same plate as the CMC #4 as-received and thermally-aged specimens. For CMC #5, there was insufficient material to machine wider specimens from the fill direction for comparison to the aged data.

3.3.1.2 XRD Results

X-ray diffraction was conducted for both the as-received and thermally aged CMC filter material specimens. The x-ray diffraction spectra for these Nextel 550 fiber/mullite matrix filter composite samples were essentially identical; a typical XRD pattern, 2000 h aged sample, is shown in Figure 3.18 (a). Only slight variations in extremely small peaks, which may be attributable to "noise" in the patterns, were observed. Furthermore, discrimination between these very minor peaks was difficult because of the high background and poor peak intensity/sharpness (due to the presence of some amorphous material), as shown in Figure 3.18 (b), in which the XRD pattern for the as-received unaged Nextel 550/mullite CMC is overlaid with the pattern from the 2000 h aged CMC. A qualitative analysis of the spectra, Table 3.16, shows very little change in the phase composition of these specimens, irregardless, of aging time.

X-ray diffraction spectra were also obtained on as-received Nextel 550 fabric and samples aged at 870°C for 150, 300 and 800 hours. All Nextel 550 fabric produced essentially identical x-ray diffraction spectra, see Figure 3.19. These spectra showed characteristics associated with highly amorphous materials: broad peaks and high background noise. These characteristics

interfered with both phase identification. Additionally, qualitative analyses were not conducted because of the poor quality of the x-ray diffraction pattern (which was a result of the large concentration of amorphous phase present in the as-produced fiber), as noted in the results presented in Table 3.16.

The amorphous characteristics observed in the Nextel 550 fibers, as-received and thermally aged, and to a lesser extent in the composite samples, were due to amorphous silica. Since this phase is considered to be amorphous, no JCPDS card number is given in the Table 3.16 for silica.

Microstructural analyses, via scanning electron microscopy, were planned but not conducted for two reasons: (1) bend strength data and XRD data did not indicate that any significant changes had occurred due to thermal aging at 870°C up to 5000 h in static air, and (2) development of the Nextel 550 fiber-based filter CMCs was stopped due to the need for higher strength filter CMCs, which were being developed using Nextel 610 and 720 fibers. The thermally aged N550 samples have been retained and microstructural analyses can be done if warranted.

Table 3.16 -- X-Ray Diffraction Analyses of As-Received and Thermally Aged Nextel 550 Fiber and Nextel 550/Mullite Matrix Filter Material CMCs

(all *qualitative* results given in wt.%, JCPDS card numbers given in square brackets)

Sample	Condition	$Al_6Si_2O_{13}$ Aluminum Silicate Mullite [15-776]	γ-Al_2O_3 Aluminum Oxide [10-425]	δ-Al_2O_3 Aluminum Oxide [16-394]	SiO_2 Silicon Oxide (b)	Unknown(s)
N550 fiber (a)	As-received	0	present	present	possible	0
N550 fiber (a)	Aged @ 870°C - 150 hrs.	0	present	present	possible	0
N550 fiber (a)	Aged @ 870°C - 300 hrs.	0	present	present	possible	0
N 550 fiber (a)	Aged @ 870°C - 800 hrs.	0	present	present	possible	0
CMC #1	As-Received	52	23	25	"	trace amounts possible (d)
CMC #1	Aged @ 870°C - 150 hrs.	56	19	25	"	" (d)
CMC #2	Aged @ 870°C - 300 hrs.	54	20	26	"	" (d)
CMC #3	Aged @ 870°C - 800 hrs.	52	25	23	"	" (d)
CMC #4	Aged @ 870°C - 2000 hrs.	58	19	23	"	" (d)
CMC #5	Aged @ 870°C - 5000 hrs.	53	21	26	"	" (d)

3.3.2 High Temperature Flow-Through Corrosion Testing

Four high-temperature, flow-through corrosion tests, see Table 3.17, were conducted in which specimens were exposed to 400 h at 870°C with simulated pulse cycling in flow-through steam/air with and without alkali. Post-test characterization included high temperature bend testing and microstructural evaluation. Samples 1 and 2 did not have an interface coating; samples 4 and 5 had a zirconia interface coating, as-deposited by Techniweave, on the fibers. Except for the

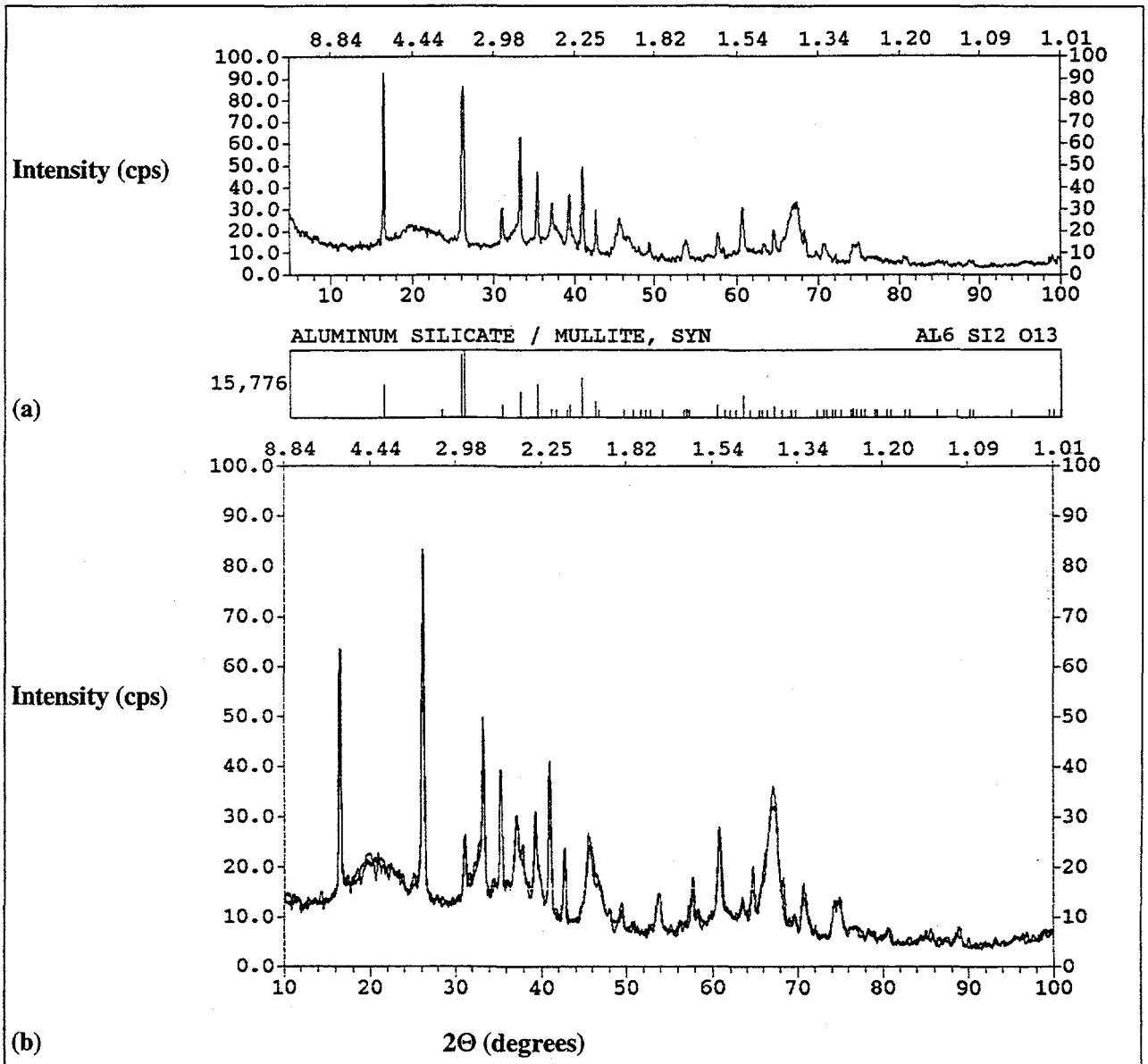

Figure 3.18 -- (a) X-ray diffraction spectrum for CMC #4 thermally aged at 870°C for 2000 h and a computer generated line plot of the x-ray lines for mullite, and (b) x-ray diffraction spectra for the thermally aged Nextel 550/mullite CMC #4 and for the as-received unaged Nextel 550/mullite CMC #1 overlaid on top of each other.

interface coating, these samples were all processed the same. The intent of these tests was to determine the effect of steam and steam+alkali environments on samples with and without the interface coating.

Table 3.17 - Flow Through Test Samples and Test Conditions

CMC Test Panel ID	Sol Source	ZrO_2 Interface	Test Conditions
CMC 9 BIS-1	Techniweave	No	400 h, 870°C, steam/20 ppm NaCl
CMC 9 BIS-2	Techniweave	No	400 h, 870°C, steam
CMC 9 BIS-4	Techniweave	Yes	400 h, 870°C, steam/20 ppm NaCl
CMC 9 BIS-5	Techniweave	Yes	400 h, 870°C, steam

For these tests composite plates were made from the downselected architecture #9 using the standard matrix processing conditions, which have been used throughout the fiber architecture development effort. Disc specimens, 69 mm diameter, were machined from the plates with a diamond core drill. These specimens were then subjected to flow-through corrosion testing in the Westinghouse Flow-Through Filter Test Facility under the experimental test conditions shown in Table 3.17.

As noted above, the original objective of these tests was to determine whether an interface coating was needed to protect the fibers. Disks 2 (no interface) and 5 (zirconia interface), after being exposed for 400 h at 870°C in the 5-7% steam/air flow-through environment, retained their

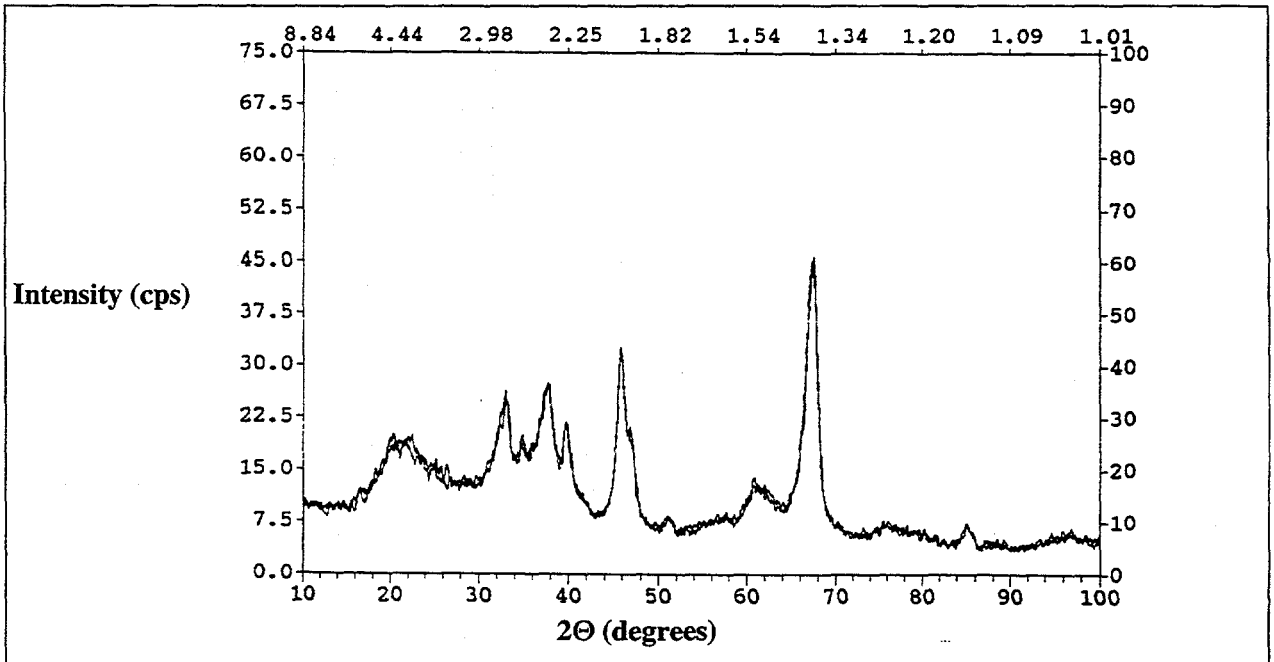

Figure 3.19 -- X-ray diffraction spectra of the 300 h and 800 h thermally aged Nextel 550 fiber overlaid on top of each other. Spectra for the as-received and 150 h aged N550 fiber were identical to these.

original flatness and white color, see disks 2 and 5 shown on the left halves of Figures 3.20 and 3.21, respectively. For all four discs, there was some discoloration of the woven fabric surface which resulted from the delivery of a 0.5 second back pulse cycle to the disc at every 20 minute interval during the course of testing.

In contrast to disks 2 and 5, disks 1 and 4 shown on the right halves of Figures 3.20 and 3.21, respectively, when subjected to 400 h of flow-through testing at 870°C in a 20 ppm NaCl/5-7% steam/air flow-through environment, puckered in the direction of the pulse cycle gas flow and failed. These failures occurred along a common central axis and were associated with the centers of the disks which were the areas most directly contacted by the pulse cycle gas. As shown in Figure 3.22, failure occurred across the fill yarns, or parallel to the warp direction. These failures correlated with the room temperature 4-point bend strength data for Architecture 9, which showed that the fill direction, 1201 psi, was the weaker direction as compared to the warp direction, 2144 psi, as shown earlier in Table 3.8.

Bend testing was conducted at 870°C for as-received and exposed samples, see Table 3.18. Testing was not conducted for the alkali exposed samples as they were damaged during the flow-through exposure testing. The results for Samples 1, as-received, and 2, flow-through tested, (these samples should be identical to each other) indicate there was a strength increase in the fill direction as a result of the flow-through test exposure. This was a result of the devitrification of the amorphous phase which was primarily in the Nextel 550 fiber. This crystallization of the amorphous phase in the flow through test environment has been observed previously for the Coors monolithic filter, which is a mullite-based material with an amorphous phase.

Samples 4, as received, and 5, flow-through tested, with the fiber-interface coating, showed statistically no difference in strength in the fill direction at 870°C and both were equivalent in strength to Sample 2, and stronger than Sample 1. The interface coating may have beneficially affected the strength results, but further testing and evaluation would be needed to confirm this observation. Figures 3.20 and 3.21 clearly showed the results of the flow-through testing, where samples exposed to the steam/air only survived the test, whereas, the disks exposed steam/air with sodium cracked and failed. Subsequent SEM examinations of the sodium/steam/air exposed samples, Figures 3.23 and 3.24, showed crystallization had occurred along the outer surfaces of the Nextel 550 fibers and within the sol-gel matrix material where platelets, and or needle-like,

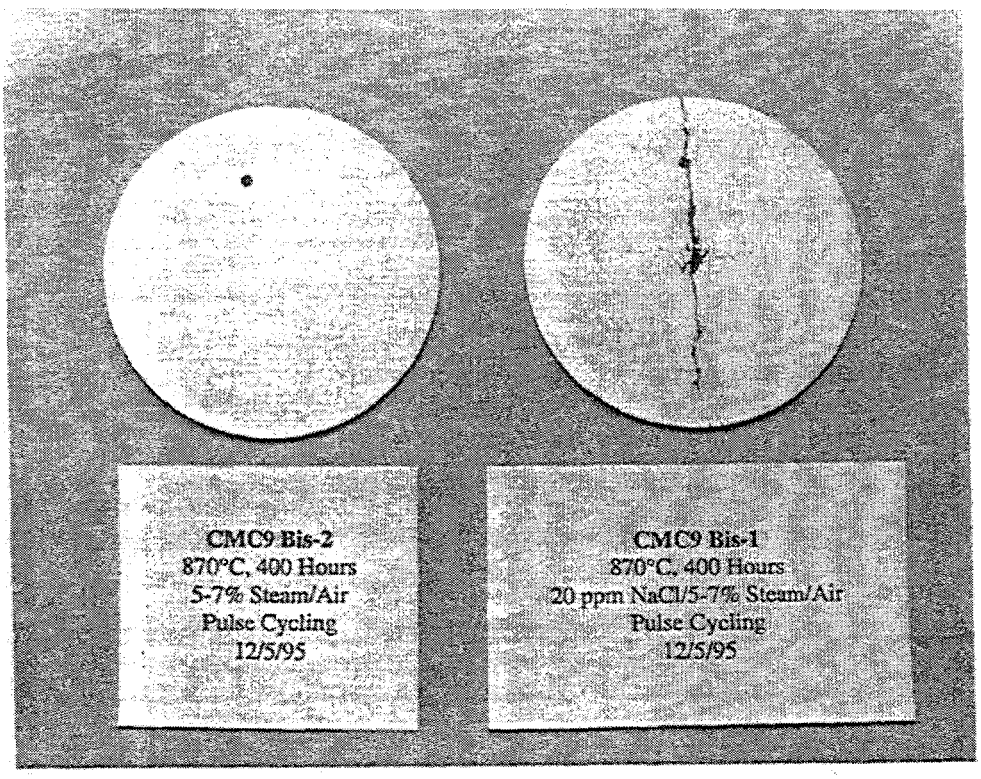

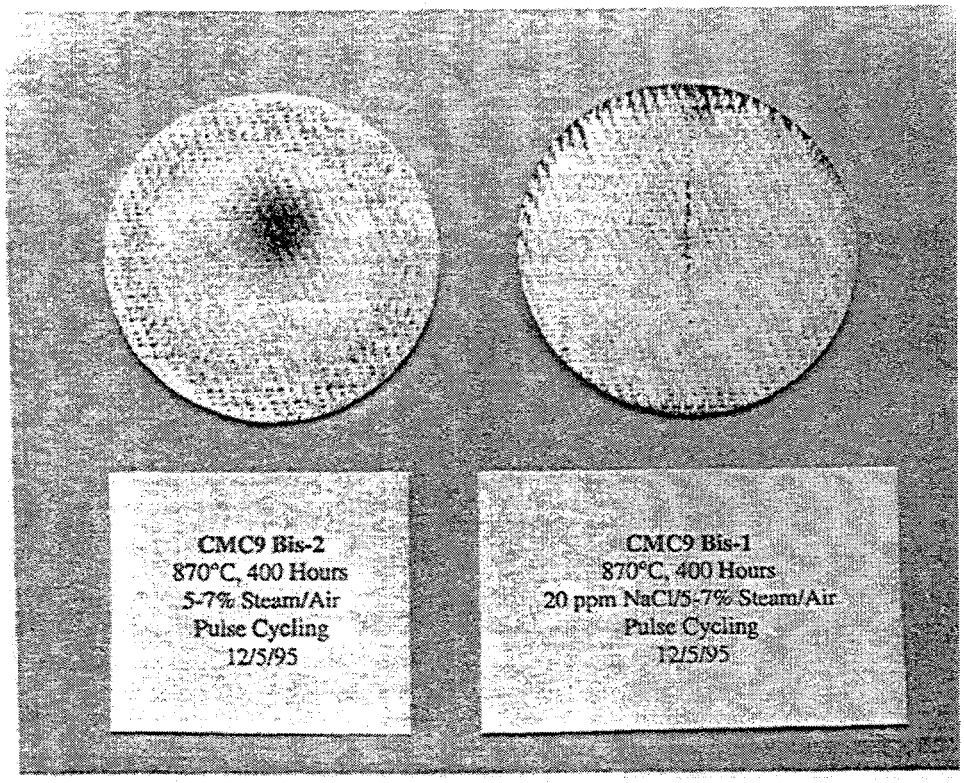

Figure 3.20 -- Photographs of filter disks 1 and 2 (disks without an interface coating) after 400 h exposure at 870°C to the steam/air and alkali/steam/air Flow-Through Test environment. The top and bottom photographs illustrate the integrity of the membrane-coated surfaces and the pulse-cycled surfaces after testing.

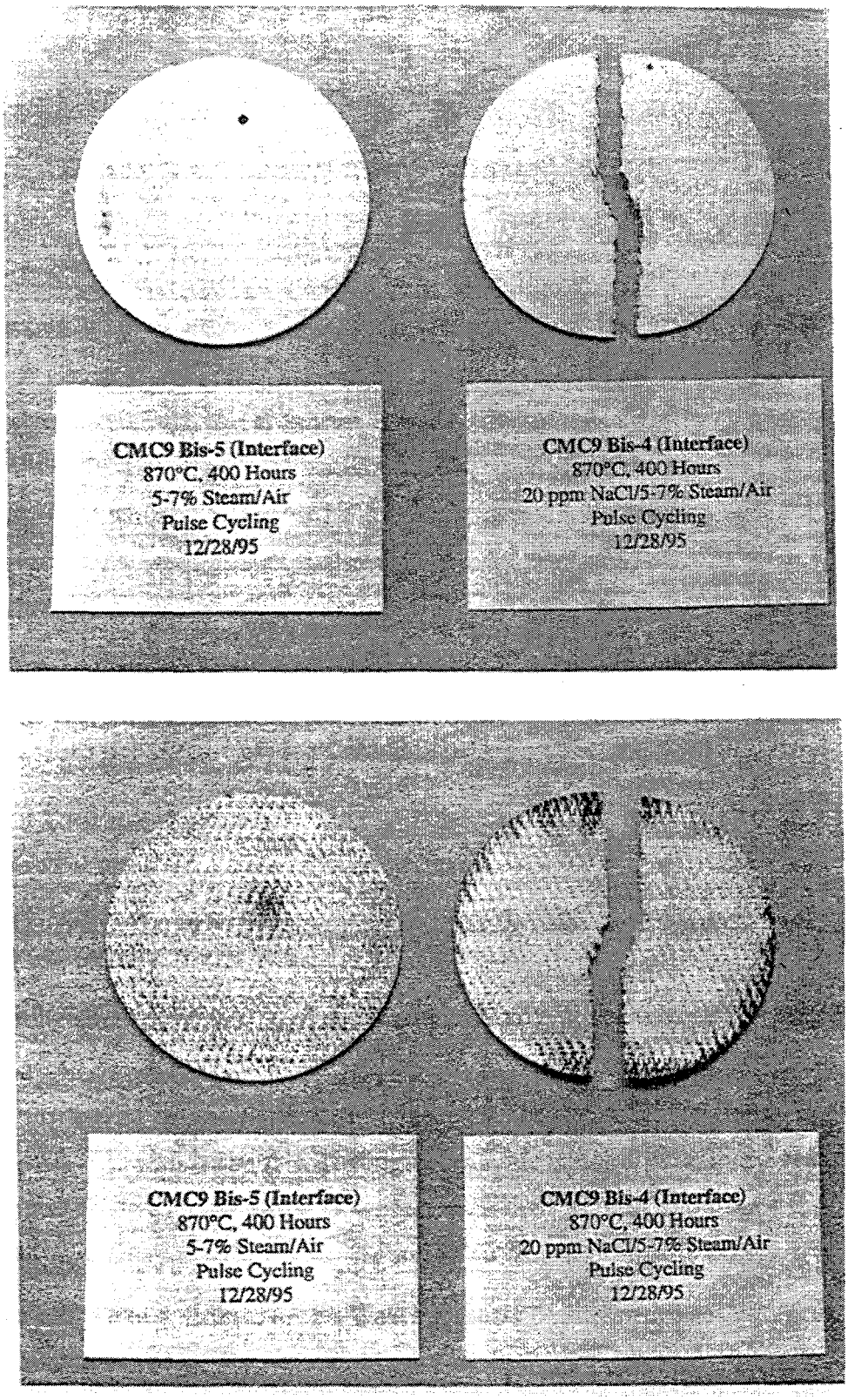

Figure 3.21 -- Photographs of filter disks 4 and 5 (disks with a zirconia interface coating) after 400 h exposure at 870°C to the steam/air and alkali/steam/air Flow-Through Test environment. The top and bottom photographs illustrate the integrity of the membrane-coated surfaces and the pulse-cycled surfaces after testing.

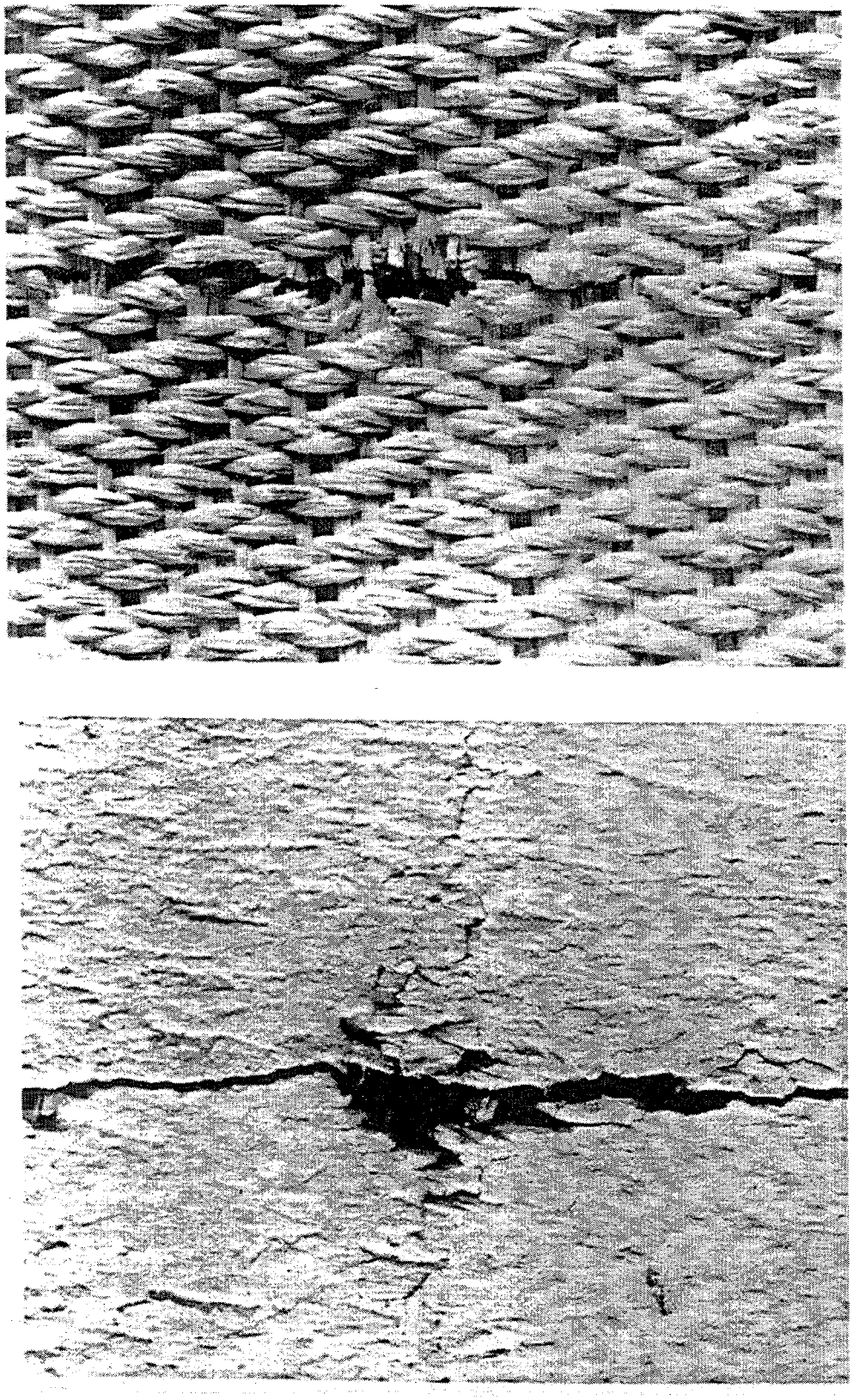

Figure 3.22 -- Low magnification photographs showing the fracture characteristics of disks 1 and 5, which were subjected to the alkali/steam/air Flow-Though Test. The top photograph shows that the failure occurred through the fill yarns parallel to the warp direction. The bottom photograph shows the crack formation in the membrane layer.

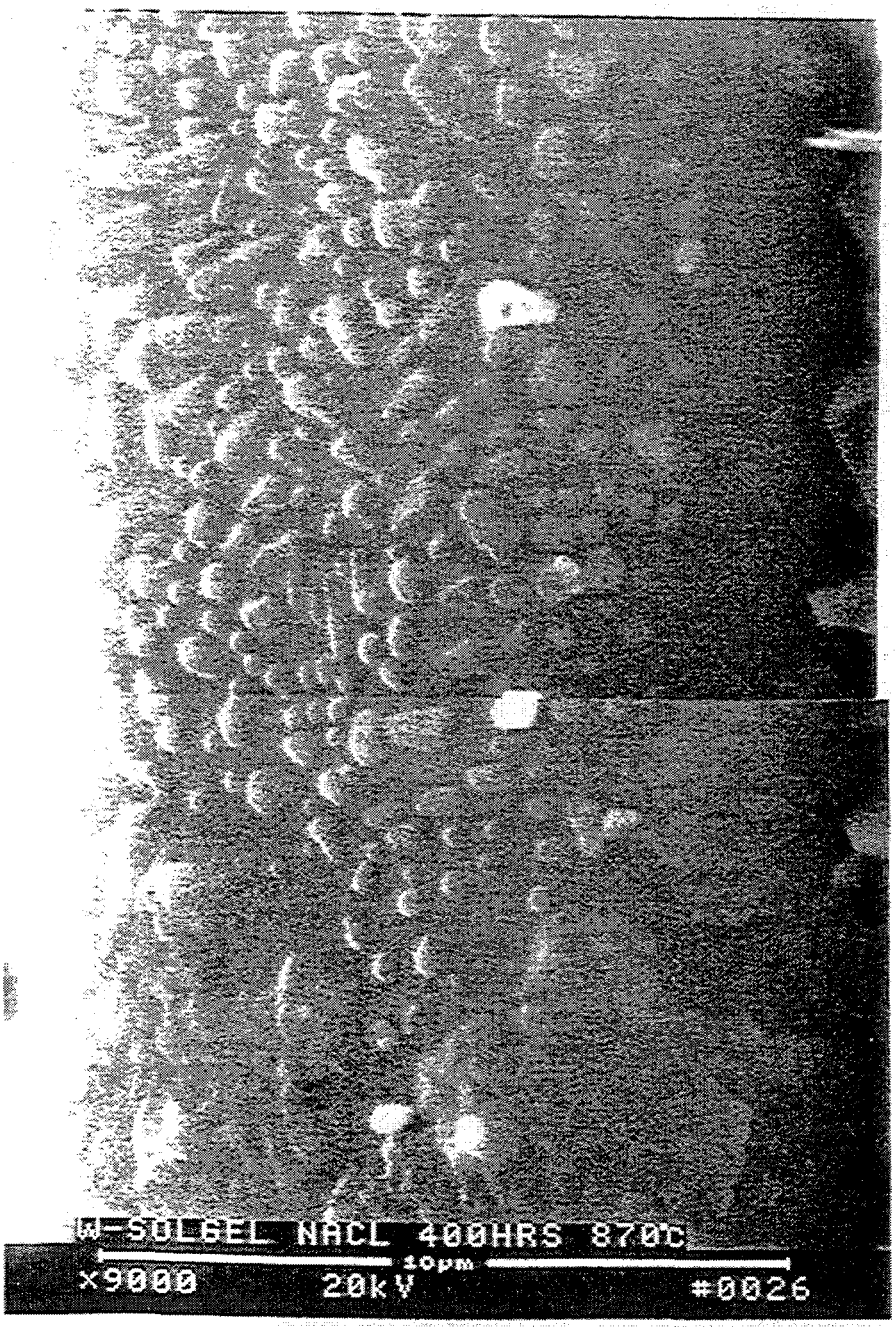

Figure 3.23 -- SEM photomicrograph showing crystallization on the surface of the Nextel 550 fiber after 400 h of exposure at 870°C in the 20 ppm NaCl/5-7% Steam/Air Flow-Through Test environment.

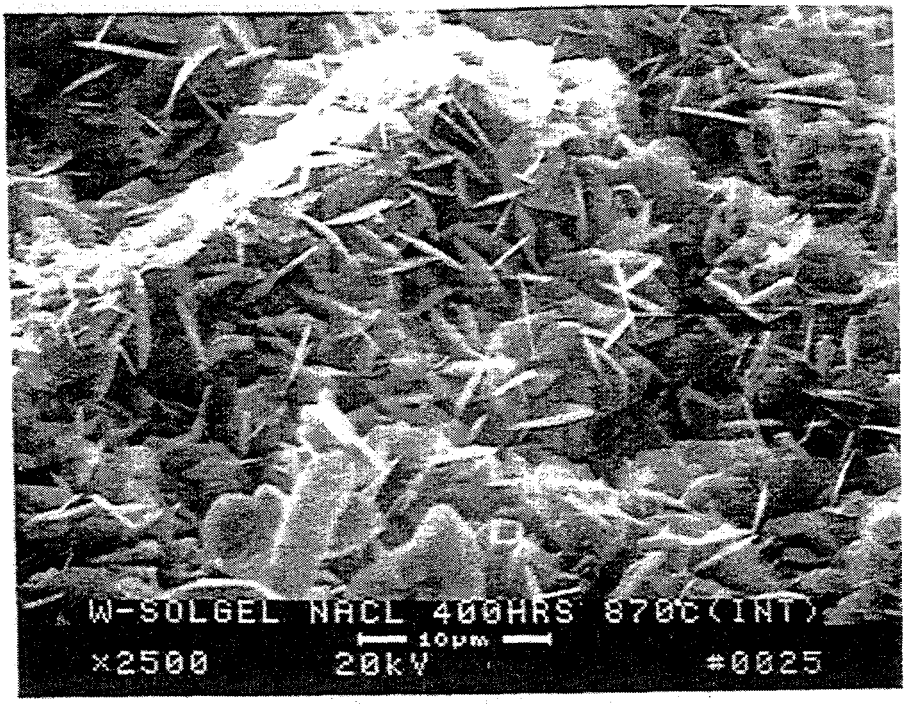

Figure 3.24 -- SEM photomicrograph showing the platelet/needlelike growth which occurred in the matrix material during the 400 h of exposure at 870°C in the 20 ppm NaCl/5-7% Steam/Air Flow-Through Test environment.

structures had formed, respectively. EDAX, energy dispersive x-ray showed the presence of sodium and silicon with a lower concentration of aluminum than expected at the fiber surfaces. It did not matter whether an interface coating was present or not, however, both these non-interface and fiber interface coated samples embrittled and failed in the presence of sodium. The embrittlement was attributed to the alkali (Na) gas phase which caused the devitrification, or crystallization, of the amorphous phase in the Nextel 550 fiber.

These high-temperature, flow-through tests conducted with Nextel 550 reinforced ceramic composite filter materials showed that this material was susceptible to alkali (Na) attack. The as-produced Nextel 550 fiber is composed of δ- and γ-alumina and amorphous silica. SEM and EDAX analyses indicated that the Nextel 550 fiber, with this amorphous silica phase, was probably attacked by the sodium resulting in devitrification of the amorphous silica which caused embrittlement of the fiber. The test coupons used for the high temperature steam/air/alkali test (870°C, 400 h) broke in two either during testing or immediately upon removal from the test rig; these coupons were highly embrittled. The test coupons subject to steam/air-only were not embrittled and were intact, and remained intact, after removal from the test rig.

Degradation of the Nextel 550 fiber (alumina with an amorphous silica phase) in the presence of alkali at 870°C was not unexpected; the zirconia fiber coating was also unable to offer sufficient protection to the fiber to enable it to be used in this environment. Other fibers, Nextel 312 and 440, along with other materials which have a glassy phase, the Coors filter material in its early developmental phase and SiC or Si_3N_4 materials (with their inherent silica surface layer) also degrade in this environment.

Table 3.18 - 4-Point Bend Testing at 870°C

Sample ID	ZrO_2 Interface	Test Conditions	Warp Direction		Fill Direction	
			Breaking Load (lbs)	Strength (psi)	Breaking Load (lbs)	Strength (psi)
Membrane surface tested in tension						
CMC 9 BIS-1	N	As-received	1.03 ± 0.07 (4)*	767 ± 27 (4)	1.15 ± 0.11 (6)	853 ± 96 (6)
CMC 9 BIS-2	N	Steam/air exposed	not tested	not tested	1.54 ± 0.15 (7)	1141 ± 94 (7)
CMC 9 BIS-4	Y	As-received	1.59 ± 0.15 (4)	1169 ± 142 (4)	1.56 ± 0.20 (6)	1191 ± 167 (6)
CMC 9 BIS-5	Y	Steam/air exposed	not tested	not tested	1.28 ± 0.17 (7)	1014 ± 118 (7)
Membrane surface tested in compression						
CMC 9 BIS-1	N	As-received	1.99 ± 0.29 (4)	1474 ± 177 (4)	1.34 ± 0.09 (6)	1022 ± 67 (6)
CMC 9 BIS-4	Y	As-received	3.77 ± 0.37 (4)	2835 ± 0.37 (4)	1.95 ± 0.22 (5)	1447 ± 124 (5)

*numbers in parentheses indicates number of bend bars tested

3.3.3 Potential of Non-Destructive Evaluation

The development effort and resources needed for NDE development for CMC filter materials are beyond the current capabilities of this program. Such an effort would be complicated by the following issues, as applied to a ceramic composite filter:

1) composite filters are heterogeneous, multi-phase structures
2) filters have high porosity
3) there is a lack of information about what features to look for
4) currently, a well-defined material and established manufacturing process do not exist
5) the need for a very low cost technique
6) the need to be able to evaluate a large structure.

Currently, the recommended approach is to monitor existing development efforts for CMC NDE methods and try to tailor the results of these efforts to meet the needs of a CMC filter material.

Non-destructive evaluation (NDE) methods have not been developed for ceramic composite materials and considerable research will be needed to develop and verify acceptable techniques for structural and porous CMCs, i.e., filter materials[5]. The DOE Continuous Fiber Ceramic Composite (CFCC) Initiative managed by the Office of Industrial Technology is supporting initial development of NDE methods for ceramic composite materials at Argonne National Laboratory[6]. The techniques under evaluation include infrared, x-ray, and acoustics. These methods are intended to be used for (a) "go, no-go" component selection; (b) development of improved material processing; and (c) lifetime prediction models. The NDE methods under evaluation are being studied to detect and characterize: (1) delaminations, (2) thermal shock damage, (3) fiber-matrix interface degradation, (e.g., due to oxidation), (4) density variations (e.g., incomplete infiltration, and (5) fiber damage caused by processing of composite materials.

3.4 Filter Material Improvements

Modifying the fiber architecture and replacing the Nextel 550 fiber with either Nextel 610 or 720 resulted in a higher strength filter material with significantly higher load carrying capability and a material which would be expected to have better resistance to alkali species in the hot gas filter operating environment. These improvements were made because of the results of the room temperature bend strength testing and the high temperature, flow-through testing. These results are discussed in the following paragraphs and the improvements used to resolve them are discussed in the following subsections.

First, even though the material had sufficient strength, 1000-2000 psi (see Table 3.8), for filter use the breaking loads < 1 lb were considered to be too low. Potential filters made from a material with low load capability were considered to be susceptible to breakage during handling and installation. These low breaking loads were primarily due to thin wall structures, ≤ 0.100 in., and low fiber volume fractions, < 30 %, which were initially targeted early on in the program in order to reduce cost.

Second, the filter composite material was embrittled during flow-through testing in an alkali environment as discussed previously in Section 3.3.2. Although this test was relatively harsh, it was considered an accelerated environmental test which could be indicative of long-term material behavior. The degradation, and subsequent failure of the filter material in this environment, due to the devitrification, or crystallization, of the amorphous phase in the Nextel 550 fiber.

3.4.1 Architecture Modifications

The use of stuffers to modify architecture #9 was successful and resulted in higher strengths and significantly higher breaking loads as compared to the original downselected architecture #9 and was also able to easily meet the filter material permeability requirements. The stuffers were added in the warp direction of architecture #9 which was expected to increase preform thickness and stiffness with minimal effect on cost. The stuffer architectures and their respective CMCs are described below; the permeability and bend strength evaluations of these CMCs are discussed in the following paragraphs:

- CMC 10 -- (1) 101.6 mm x 152.4 mm plate, Techniweave sol, standard process; architecture would simulate #9 but have axial stuffers with same fill fiber volume as 9 and with distribution of remaining fiber between through thickness and stuffer directions
- CMC 11 -- (1) 101.6 mm x 152.4 mm plate, Techniweave sol, standard process; architecture same as 10 but double amount of stuffer and decrease through thickness fiber volume
- CMC 12 -- (1) 101.6 mm x 152.4 mm plate, Techniweave sol, standard process; architecture same as 11 but increase fiber volume in fill direction
- CMC 13 -- (1) 101.6 mm x 152.4 mm plate, Techniweave sol, standard process; architecture same as 11 but with overwrapped fiber in the different directions in an attempt to locally increase the bundles' fiber volume
- CMC 14 -- (1) 101.6 mm x 152.4 mm plate, Techniweave sol, standard process; architecture same as 11 but with modified yarn to decrease cost
- CMC 14-P -- (1) 101.6 mm x 152.4 mm plate, Techniweave sol, standard process; architecture same as 14 but fabricated using pressure
- CMC 15 -- (1) 101.6 mm x 152.4 mm plate, Techniweave sol, standard process; architecture same as 11 but with modified yarn introduced in the fill direction

The permeability, or gas flow resistance, results are shown in Table 3.19; based on this data CMCs 10-13 and 14P offered the most promise for use as a hot gas candle filter material. CMCs 10 and 11 were within the Westinghouse gas flow resistance requirement, i.e. < 1 in-wg/fpm. CMC 12 met the requirement in the membrane up orientation but was slightly high in the membrane down orientation.

Unlike the prior three samples, CMCs 13-15 had a high gas flow resistance in the membrane down position. CMCs 13, 14P and 15 met the gas flow resistance requirement when tested in the "membrane up" position, i.e. the normal expected orientation during use. CMC 14 exceeded the Westinghouse gas flow resistance requirement (permeability ratio $\leq$ 1 in-wg/fpm at 70 °F) in both directions and CMC 15 had an unacceptably high value in the "membrane down" position.

Table 3.19 -- Gas Flow Resistance Results for the Suffer-Modified Architectures

Fiber Architecture	Thick. (in.)	Membrane Up* (in-wg/fpm)	Membrane Down (in-wg/fpm)
10	0.073	0.241	0.692
11	0.064	0.186	0.186
12	0.097	0.524	1.253
13	0.125	0.345	1.710
14	0.125	1.822	3.777
14P	0.125	0.441	1.548
15	0.150	0.540	3.350

*Membrane Up: normal expected orientation during use

From the bend test results, Table 3.20, the use of stuffers increased the warp strength and load carrying capability, as compared to the conventional Architecture 9-based CMCs. The highest breaking loads, warp - 6.6 lb and fill 8.2 lb, were achieved by CMC 13 with a 0.15 in. wall thickness. Based on a qualitative evaluation of the load-deflection curves (shown in the Appendix), toughness for the stuffer modified composites appeared to be better than for CMCs based on the originally downselected Architecture 9.

For 14 and 15, which used a modified stuffer yarn made from low cost short fibers, the breaking load results were encouraging; they were comparable to the stuffer architectures which use only continuous fiber and were significantly better than the conventional architecture (#9). The strength needs improving, particularly for #15. These lower strengths may have also been because it was realized after machining that the cell sizes for these hybrid architectures were larger than for

the other architectures, thus wider bend bars should have been prepared for these samples. In particular, many fill tows and warp fiber loops were missing in CMC 15. Optimization of the modified yarn approach would be required to increase strength (use of other types of short fiber) and decrease permeability (use of fugitive yarn).

CMC 13, which had the highest breaking loads, also used the most fiber and would result in the highest cost filter of the various stuffer architectures, as shown in Table 3.20. This table shows the effect of wall thickness on the fiber cost per filter based on the current fiber cost of $330.00/lb for Nextel 550 and a surface area of 0.28 m^2 per candle filter. CMCs 14, 14P and 15 were not considered in this evaluation as they were made from the modified yarn which would be expected to further lower cost but world require additional development for use in filter applications.

Table 3.20 -- Summary of Mechanical Testing Results for CMCs 10-15

Sample ID	Mean Thick (in.)	Warp Direction (X)		Fill Direction (Y)	
		Mean Strength* (psi)	Breaking Load (lb)	Mean Strength* (psi)	Breaking Load (lb)
9 conventional	0.059	2144 ± 522 (10)	0.64	1201 ± 522 (9)	0.45
10	0.073	3731 ± 160 (4)	3.0	1652 ± 223 (5)	1.6
11	0.069	3745 ± 284 (5)	2.8	2525 ± 245 (3)	2.1
12	0.105	3745 ± 165 (4)	3.3	3044 ± 300 (4)	6.2
13	0.149	2334 ± 280 (5)	6.4	1958 ± 440 (5)	8.2
14	0.126	1516 ± 160 (5)	5.0	1351 ± 230 (5)	4.2
14P	0.130	1697 ± 290 (4)	5.0	1389 ± 225 (4)	4.6
15	0.186	430 ± 70 (5)	3.2	689 ± 190 (5)	4.4

*number of samples tested is shown in parentheses

Table 3.21 -- Fiber Cost per Filter - Architectures 11, 12 and 13

Preform ID	Fiber Volume (%)	Wall Thickness (in.)	Fiber Weight per Filter (lb)	Fiber Cost per Filter ($)
11	29	.071	0.98	324
12	28	.110	1.46	482
13	21	.150	1.58	522

Field Test Specimens: A total of 24 Nextel 550 fiber/mullite matrix CMC plates (3 in. x 3 in.) were fabricated from preforms 11½ and 14 for surveillance testing at field sites. Preform 11½ is a compromise between architectures 11 and 12. Architecture 12 had a very high fiber volume in the fill direction which resulted in more fiber fracture during weaving, whereas, 11 had a low fiber volume in the fill direction. Architecture 11½ has an intermediate fiber count in the fill direction. Architecture 14, containing short length fibers, was also selected to evaluate the effect of the power plant environment on the short length fibers.

3.4.2 Improved Fibers

Based on the flow-through corrosion test results, Nextel 610 (alumina) and Nextel 720 (polycrystalline mullite) were evaluated as replacements for the Nextel 550 fiber. As discussed earlier in Section 3.3.2, N550 test specimens in the steam/NaCl flow through test environment embrittled, whether an interface coating was present or not. The embrittlement has been attributed to the alkali (Na) gas phase which causes the devitrification, or crystallization, of the amorphous phase in the Nextel 550 fiber.

The backup position to Nextel 550, developed at a Westinghouse/Techniweave program review at Techniweave in May 1995, was to replace N550, if necessary, with either Nextel 610, polycrystalline alumina, or Nextel 720, polycrystalline mullite. These fibers were not chosen for the initial Phase I development work because of their higher cost; at the time of the start of this program these fibers were approximately 5-6 times higher in cost (~$1800/lb vs. $350/lb for Nextel 550). At this time, the cost of N610 and N720 has decreased to $500/lb and $460/lb, respectively. Additionally, replacement of the N550 with the N720 or N610 was always considered to be a simple change in the fabrication of the oxide/oxide filter CMC. The matrix fabrication process is generic and can be used for any of the above oxide fibers.

Due to the lower elastic modulus, i.e., reduced stiffness, precrystallized N610 is much easier to weave than crystallized N610. After weaving, the precrystallized N610 preform is subjected to a heat treatment cycle which converts the fiber to normal fully crystalline N610.

The preform architecture used for the N720 (CMC 15) and for the N610 (CMC 16) samples was most similar to N550 architectures 11 and 12, which were stuffer modified versions of architecture 9. Table 3.22 provides the relevant measured characteristics of the two preforms.

Table 3.22 -- Characteristics of N720 and N610 3D Fiber Preforms

Characteristic	Preform 15	Preform 16
Fiber Type	N720 polycrystalline: ~50% mullite and 50% alumina	N610 polycrystalline alumina
Thickness (in.)	0.120	0.120
Fiber Volume (%)	30	26.5
Fill (%)	13.9	11.5
Warp Stuffer (%)	6.8	6.0
Warp Interlock (%)	9.3	9.0

Two 101.6 mm x 152.4 mm CMC plates were fabricated from these preforms, N610 and N720, using Techniweave's baseline fabrication process. Plates were not subjected to the normal final heat treatment, in order to examine the effect of different sintering temperatures on the strength and toughness of the composites. This evaluation was possible due to the better thermochemical stability of the N610 and N720 as compared to the N550.

Several 50.8 mm x 50.8 mm coupons were cut from the N610 and N720 preform material. These coupons were used to fabricate filter material CMCs from which the following processing variables were evaluated:

1. Sintering temperature: baseline (<1100°C, Techniweave proprietary), 1100°C, 1150°C, and 1200°C. Higher sintering temperatures, which affect the densification of the matrix, may provide a more refractory and stronger matrix component capable of increased load carrying capability. However, higher sintering temperatures can also result in increased fiber-matrix interaction which can cause fiber degradation and ultimately lower strength and less tough CMCs.
2. Matrix composition: mullite filler powder + mullite sol or mullite filler powder + alumina sol. The alumina sol has a higher viscosity than the mullite sol and, based on Techniweave IRAD, does not penetrate the fiber tows as well as the mullite sol, thus, minimizing the potential matrix-fiber interaction. Additionally, water-based alumina sols are low cost and are more readily available than water-based mullite sols. However, minimal fiber-matrix contact can result in poor load transfer between the matrix and the fiber resulting in less sharing of the load and lower CMC strengths.
3. Interface coating: none or fugitive carbon. The use of the C interface was to minimize fiber-matrix interaction during composite processing. Downside of the C interface is the same as above for the matrix composition.

The objective was to evaluate the effect of these different parameters on room temperature strength, breaking load, and toughness.

The processing conditions and observations for each sample are shown in Table 3.23, N720 CMCs, and Table 3.24, N610 CMCs. Flexure specimens were machined from the N720 and N610 CMC samples shown in these tables. The N720 and N610 test results are summarized in Tables 3.25. These results show that all the Nextel 720 and Nextel 610 CMCs have much higher strengths and breaking loads, regardless of processing conditions, than filter CMCs made with Nextel 550, as shown more specifically in Table 3.26.

Table 3.26 compares the mean strength and breaking load results of Nextel 550 CMCs 9 and 10-13 (stuffer-modified) to that of Nextel 720 CMCs 15-3 (warp, or candle axial, direction) and 15-4 (fill, or candle circumferential, direction) and Nextel 610 CMC 16-3 (fill direction). These CMCs were selected for this comparison because they were all processed using the same standard baseline Techniweave process including the sintering temperature. From the table, the

N720 CMCs were 50% and 94% stronger in the warp and fill directions, respectively, than the best N550 CMCs shown. The greatest improvement was in the breaking load which for the N720 CMCs is 165% and 152% stronger in the warp and fill directions, respectively, than the best N550 CMC shown. The N610 CMCs, in the fill direction, were 42% stronger and had a 42% higher breaking load than the best N550 CMC in the table. Because of the improved breaking loads, the use of either the N610 or N720 fiber greatly increases the handleability of this filter material.

Table 3.23 -- Description of Nextel 720 Reinforced CMC Samples

Sample ID	Interface	Matrix	Sintering Temperature (°C)	Observations
CMC 15-C1	fugitive carbon	mullite	baseline	matrix through the thickness
CMC 15-C2	fugitive carbon	mullite	1100	matrix through the thickness but less than that of CMC 15-C1
CMC 15-C3	fugitive carbon	mullite	1150	same as CMC 15-C2
CMC 15-C4	fugitive carbon	mullite	1200	same as CMC 15-C1
CMC 15-C5	fugitive carbon	mullite + alumina	1100	none
CMC 15-3	none	mullite	baseline	matrix through the thickness
CMC 15-4	none	mullite	baseline	matrix through the thickness
CMC 15-5	none	mullite	1100	lesser amount of matrix through the thickness
CMC 15-6	none	mullite	1150	matrix through the thickness
CMC 15-7	none	mullite	1200	matrix through the thickness

Table 3.24 -- Description of Nextel 610 Reinforced CMC Samples

Sample ID	Interface	Matrix	Sintering Temperature (°C)	Observations
CMC 16-C1	fugitive carbon	mullite	1100	
CMC 16-C2	fugitive carbon	mullite + alumina	1100	coupons were cut at angle with fill direction
CMC 16-3	none	mullite	baseline	
CMC 16-4	none	mullite	1100	
CMC 16-5	none	mullite + alumina	1100	
CMC 16-6	none	mullite	1150	coupons were cut at angle with fill direction

Table 3.25 -- Flexure Strength Results* for Nextel 610 and 720 CMCs

Sample ID	Test Direction	Sintering Temperature (°C)	Mean 4-pt Bend Strength (psi)	Mean Breaking Load (lb)
Nextel 610				
CMC 16-C1	Fill	1100	4585 ± 346 (3)	11.69
CMC 16-C2	Fill	1100	3609 ± 197 (3)	9.92
CMC 16-3	Fill	baseline	4334 ± 1168 (3)	13.68
CMC 16-4	Fill	1100	4232 ± 331 (3)	13.22
CMC 16-5	Fill	1100	3863 ± 521 (3)	11.03
CMC 16-6	Fill	1150	4532 ± 557 (3)	13.76
Nextel 720				
CMC 15-C1	Warp	baseline	4186 ± 735 (3)	10.31
CMC 15-C2	Warp	1100	4477 ± 1128 (3)	13.99
CMC 15-C3	Warp	1150	5887 ± 334 (3)	13.7
CMC 15-C4	Warp	1200	6446 ± 833 (3)	15.14
CMC 15-C5	Warp	1100	3375 ± 605 (3)	8.98
CMC 15-3	Warp	baseline	5507 ± 408 (3)	17.0
CMC 15-4	Fill	baseline	5910 ± 628 (3)	20.7
CMC 15-5	Warp	1100	5828 ± 372 (3)	15.33
CMC 15-6	Warp	1150	5788 ± 1074 (3)	14.43
CMC 15-7	Warp	1200	5444 ± 640 (3)	15.14

*number of samples tested is shown in parentheses

Table 3.26 -- Bend Strength and Breaking Load Comparison of Filter CMCs made with Nextel 550, 720 and 610 Fibers

(All CMCs were processed the same and fired at the standard baseline processing temperature)

Sample ID	Warp Direction (X)		Fill Direction (Y)	
	Mean Strength* (psi)	Breaking Load (lb)	Mean Strength* (psi)	Breaking Load (lb)
Nextel 550 CMCs				
9 - conventional	2144 ± 522 (10)	0.64	1201 ± 522 (9)	0.45
10 - stuffer	3731 ± 160 (4)	3.0	1652 ± 223 (5)	1.6
11 - stuffer	3745 ± 284 (5)	2.8	2525 ± 245 (3)	2.1
12 - stuffer	3745 ± 165 (4)	3.3	3044 ± 300 (4)	6.2
13 - stuffer	2334 ± 280 (5)	6.4	1958 ± 440 (5)	8.2
Nextel 720 CMCs with preform architecture similar to 11 & 12				
15-3 (warp) and 15-4 (fill)	5507 ± 408 (3)	17.0	5910 ± 628 (3)	20.7
Nextel 610 CMCs with preform architecture similar to 11 & 12				
16-3	not measured	not measured	4334 ± 1168 (3)	11.69

*number of samples tested is shown in parentheses

The following observations were noted about the effect of processing temperature, matrix material, and interface on N720 and N610 CMC strength, breaking load and toughness:

Nextel 720 CMCs

- The processing temperature does not affect the strength of the CMCs (3-7) without the carbon interface coating, however, there does appear to be a decrease in the toughness, on a qualitative basis, at temperatures of 1100°C and above.
- For the CMCs (C1-C5) with the carbon interface coating, strength appears to increase with increasing processing temperature without any affects on toughness.
- The highest breaking loads resulted from CMCs 15-3 and 15-4 without the C coating and which were processed at the baseline firing temperature. Good toughness was also evident for these specimens.
- Mullite matrix CMCs had higher strength and breaking loads than the alumina-mullite matrix CMCs. However, the fracture toughness characteristics appeared to be better for the alumina-matrix CMCs.

Nextel 610 CMCs

- For CMCs 16-3, -4 and -6, there is a trend upwards in the mean breaking strength with increasing processing temperature, however, this is not conclusive given the large standard deviations about the mean.
- CMC 16-C1, with the carbon interface, had the highest mean strength of all the N610 CMCs tested.
- Mullite matrix CMCs had higher strength and breaking loads than the alumina-mullite matrix CMCs.
- The fracture toughness characteristics were good all the N610 CMCs.

A more systematic study would have to be conducted to draw any final conclusion. However, the observations noted above point in the direction of a possible fiber-matrix interaction during processing with the mullite sol. This was not unexpected given that the fiber and matrix are the same chemistry. The alumina sol, being a single phase sol, without the presence of a silica component, was less likely to react with the mullite fibers. For filter applications, the best fiber matrix combinations for long term high temperature chemical stability may be N720 fiber/alumina matrix or N610 fiber/mullite matrix.

4. CONCLUSIONS

1. A low cost, three-dimensional (3D) fiber architecture, that was both easy to manufacture and automate, was developed for hot gas candle filter applications.

2. Weaving trials produced a list of candidate warp interlock fiber architectures for candle filters and demonstrated the feasibility of using the warp interlock architecture to fabricate seamless tubes, closed end tubes, and flange sections for candle filters.

3. Screening tests assessed the permeability and room temperature mechanical properties of ceramic composites made from each candidate fiber architecture. These tests determined that permeability was not a discriminator for selecting a fiber architecture and that the major criteria was the mechanical properties test results.

4. The in-situ deposition of a membrane layer was demonstrated during the fabrication of the composite samples for the screening tests; this capability simplifies and reduces the cost of filter manufacturing.

5. A thick wall, low fiber volume fraction, warp interlock architecture, identified as Architecture #9, was selected for candle filter applications because adequate strength and toughness were obtained in both the warp (axial direction of the filter) and fill (circumferential direction of the filter) directions.

6. The ceramic composite filter material based on the initial candidate fiber architectures had low breaking loads < 1 lb which were expected to cause resulting filters to be susceptible to breakage during handling and installation in filter systems.

7. A composite processing study determined that the processing method for matrix infiltration, the mullite filler particle size and the source of the mullite sol were the major processing variables affecting the performance and cost of the filter material.

8. A one-sided matrix infiltration process, using vacuum to pull the matrix from the outside through to the inside of the filter, was determined to be the lowest cost approach to producing

candle filters; this process also facilitates the in-situ deposition of the membrane layer. Pressure applied during the infiltration process showed the feasiblity of increasing composite strength without compromising permeability.

9. A low cost source of mullite filler powder was identified and an evaluation of particle size distribution effects on composite processing determining that this powder could be used in the as-received condition, without classifying, for filter manufacturing, and further reduces filter costs.

10. For the Nextel 550 filter CMCs, the Techniweave mullite sol, should be used for the matrix material. The Techniweave sol has a long shelf-life, is easy to use and handle during composite fabrication, is environmentally-friendly and recyclable, has a low crystallization temperature of 1000°C, is expected to provide a more stable matrix, and is expected have less fiber degradation during processing than the Westinghouse mullite sol, which has a higher crystallization temperature of 1150°C.

11. Ceramic composite filter material specimens thermally aged for up to 5000 hours in static air at 870°C did not show any change in strength as a function of time at temperature and had essentially identical x-ray diffraction spectra independent of aging time.

12. High temperature (870°C), flow-through tests for 400 h with cyclic backpulsing showed that the Nextel 550 fiber reinforced ceramic composite material degraded, embrittle and failed in test environments containing 20 ppm NaCl/5-7% steam/air and were unaffected in steam/air only environments. The above degradation was attributed to the alkali species reacting with the amorphous silica phase in the Nextel 550 fiber causing devitrification of this phase, embrittlement of the fiber, and subsequent failure of the composite material. SEM showed crystallization along the fibers and platelet, and possibly whisker, growth within the matrix for those specimens exposed to the alkali containing environment.

13. Non-destructive evaluation methods for ceramic matrix composite filter materials have not been developed and the development of these methods were beyond the capabilities of this program. At this time, the best approach is to monitor existing development efforts for CMC NDE methods and try to tailor the results of these efforts to meet the needs of a CMC filter material.

14. Fiber architecture improvements and replacement of the Nextel 550 fiber with either Nextel 610 or 720 resulted in a higher strength filter material with significantly higher load carrying capability; and a material which would be expected to have improved resistance to alkali species in the hot gas filter environment.

15. The use of stuffers to modify the downselected architecture (see Conclusion number 5) was successful and resulted in higher strengths and significantly higher breaking loads as compared to the architecture #9-based composites and was also able to easily meet the filter permeability requirements.

16. Mechanical property testing showed that the use of either the N610 or N720 fiber greatly increases strengths and breaking loads and significantly improves the handleability of the composite filter material. The N720 CMCs were 50% and 94% stronger in the warp and fill directions, respectively, than the best N550 CMCs. The greatest improvement was in the breaking load which for the N720 CMCs was 165% and 152% stronger in the warp and fill directions, respectively, than the best N550 CMC shown. The N610 CMCs, in the fill direction, were 42% stronger and had a 42% higher breaking load than the best N550 CMC.

5. RECOMMENDATIONS

1. The low cost approach to develop oxide/oxide composite filters should be continued under Phase II and Phase III of this DOE project.
2. Continuing activities in Phase II should verify that improved fibers Nextel 610 and Nextel 720 will deliver improved ceramic filter materials.
3. The planned activities for Phase III (fabrication of fifty full sized filters and prepilot field testing at Wilsonville) should be pursued immediately after the completion of the Phase II activities.
4. Implementation of fibers Nextel 610 or Nextel 720 in improved filters should employ the optimized architecture and matrix processing already developed under this current phase of the program.
5. Additional testing and analyses should be done to confirm that such tests and analyses should attempt to characterize the interface coating, to understand what role the interface coating is providing in this filter composite material, and to determine if these improvements would also be seen if the fiber was changed to Nextel 610 or 720. The use of a zirconia interface appears to have increased the strength and load carrying capability of the Nextel 550 fiber filter CMCs made with Techniweave sol sample and fired at 1050°C, as compared to a similar sample made without the zirconia interface.
6. The Westinghouse sol should be reevaluated for use with the hot gas filter CMCs which use Nextel 610 and 720 fibers. The W-sol is currently a lower cost sol than the Techniweave sol, which may also be subject to future supplier problems.
7. Further testing should be done to verify that for Nextel 550-based CMCs, the mean flexure strengths obtained for pressure infiltrated filter CMC samples are generally higher than for conventionally processed samples. This testing should be done on the downselected filter material CMC (fiber, matrix, architecture).

8. Thermal aging and high temperature flow through testing should be conducted with ceramic composite filter materials made with Nextel 610 and Nextel 720 to determine the effect of temperature, time at temperature, and hot gas filter environments on the properties of these fibers.

6. ACKNOWLEDGMENTS

The authors wish to acknowledge the program support and technical guidance provided by Ted McMahon, the METC/COR, over the course of Phase I, 9/30/94 - 5/31/96. We would also like to thank Mary Ann Alvin for her technical suggestions, the permeability analyses, and with Rich Kunkle, the conduct of the high temperature flow through corrosion tests; Mike Biondi for his diligent work in the laboratory; Tom Mullin for the SEM support; and, Paula Freyer for the XRD analyses.

7. REFERENCES

1. M. A. Alvin, T. E. Lippert, E. S. Diaz, and E. S. Smeltzer, "Filter Component Assessment," pp. 160-82 in *Proceedings of the Advanced Coal-Fired Power Systems '95 Review Meeting Volume I*, Edited by H. M. McDaniel, D. J. Mollot, and V. K. Venkataraman. DOE/METC-95/1010, Vol. 1 (DE95009732) June 1995.

2. M. A. Alvin, R. E. Tressler, T. E. Lippert, and E. S. Diaz, "Evaluation of Ceramic Filter Material, Selection for Application," *Proceedings of Coal-Fired Power Systems '93 - Advances in IGCC and PFBC Review Meeting*. Edited by D. L. Bonk. DOE/METC-93/6131 (DE93000289) June 1993.

3. M. A. Alvin, D. M. Bachovchin, T. E. Lippert, R. E. Tressler, and K. B. McNerney, "Thermal/Chemical Stability of Ceramic Cross Flow Filter Materials," *Proceedings of Twelfth Annual Gasification and Gas Stream Cleanup Systems Contractors Review Meeting*. Edited by R. A. Johnson and S. C. Jain. DOE/METC-92/6128 (DE93000228), September 1992.

4. M. A. Alvin, T. E. Lippert, D. M. Bachovchin, and R. E. Tressler, "High Temperature Filter Materials," *Proceedings of Coal-Fired Heat Engines, PFBC, and Gas Stream Cleanup Systems Contractors Review Meeting*, October 27-29, 1992, Morgantown, WV.

5. M. Jenkins, p. 23 in *Continuous Fiber Ceramic Composite Program Task 2 Bimonthly Progress Report for December-January 1996*. Compiled by M. Rawlins, R. A. Lowden, and M. A. Karnitz.

6. W. A. Ellingson, J. G. Sun and M. Metcalf, pp. 31-36 in *Continuous Fiber Ceramic Composite Program Task 2 Bimonthly Progress Report for December-January 1996*. Compiled by M. Rawlins, R. A. Lowden, and M. A. Karnitz.

APPENDIX

This appendix contains the room temperature 4-point bend test data and load-deflection curves for candidate ceramic composite filter materials fabricated from architectures 1-9 and from the stuffer-modified architectures 10-15 (based on the down selected architecture 9 from the initial architecture screening study).

WESTINGHOUSE STC. NUCLEAR SERVICES AND MATERIALS TESTING LAB

CUSTOMER: CAROL PAINTER
DATE: 8-31-95
CHARGE NO: 9TC3-HGFIL-33
TESTED BY: R.J.SMYKAL

JOB NO: 68089
TEST SPEED: .050 IN/MIN
TEST MACHINE: 20 KIP INSTRON

FLEXURAL TEST

SPEC. IDENT	TEST TEMP (deg C)	SPAN (in)	WIDTH (in)	THICK (in)	ULTIMATE STRENGTH (lbs)	PSI
*1Y1-2	22	1.57	0.235	0.080	3.10	2427
*1Y2-2	22	1.57	0.233	0.076	3.27	2861
1Y3-2	22	1.57	0.233	0.075	2.62	2354
1Y4-2	22	1.57	0.234	0.079	3.18	2564
1Y5-2	22	1.57	0.233	0.071	2.71	2717
1Y6-2	22	1.57	0.234	0.080	2.30	1808
1Y7-2	22	1.57	0.235	0.075	1.84	1639
2Y1-2	22	1.57	0.237	0.070	2.22	2251
2Y2-2	22	1.57	0.233	0.065	2.06	2464
2Y3-2	22	1.57	0.234	0.067	2.10	2354
2Y4-2	22	1.57	0.234	0.068	2.00	2176
2Y5-2	22	1.57	0.234	0.068	1.62	1763
2Y6-2	22	1.57	0.234	0.066	1.00	1155
2Y7-2	22	1.57	0.233	0.066	0.53	615
3Y1-2	22	1.57	0.234	0.071	1.75	1747
3Y2-2	22	1.57	0.234	0.071	1.99	1986
3Y3-2	22	1.57	0.234	0.071	2.37	2366
3Y4-2	22	1.57	0.235	0.071	1.82	1809
3Y5-2	22	1.57	0.234	0.070	2.28	2341
3Y6-2	22	1.57	0.234	0.070	2.10	2157
3Y7-2	22	1.57	0.235	0.070	2.22	2270

*NOTE: SAMPLE TESTED WITH COARSE WEAVE IN "DOWN" POSITION.

WESTINGHOUSE STC. NUCLEAR SERVICES AND MATERIALS TESTING LAB

CUSTOMER: CAROL PAINTER
DATE: 8-31-95
CHARGE NO: 9TC3-HGFIL-33
TESTED BY: R.J.SMYKAL

JOB NO: 68089-1
TEST SPEED: .050 IN/MIN
TEST MACHINE: 20 KIP INSTRON

FLEXURAL TEST

SPEC. IDENT	TEST TEMP (deg C)	SPAN (in)	WIDTH (in)	THICK (in)	ULTIMATE STRENGTH (lbs)	PSI
4Y1-2	22	1.57	0.234	0.065	0.83	989
4Y2-2	22	1.57	0.234	0.065	0.60	715
4Y3-2	22	1.57	0.233	0.065	0.62	742
4Y4-2	22	1.57	0.234	0.064	0.78	958
4Y5-2	22	1.57	0.234	0.062	0.79	1034
4Y6-2	22	1.57	0.234	0.063	0.75	951
4Y7-2	22	1.57	0.234	0.061	0.43	582
4X1-2	22	1.57	0.233	0.058	1.26	1893
4X2-2	22	1.57	0.233	0.058	1.28	1923
4X3-2	22	1.57	0.233	0.058	1.22	1833
4X4-2	22	1.57	0.233	0.058	1.27	1908
4X5-2	22	1.57	0.234	0.058	1.17	1750
4X6-2	22	1.57	0.233	0.058	1.32	1983
4X7-2	22	1.57	0.233	0.057	1.33	2069
5X1-2	22	1.57	0.235	0.063	1.62	2045
5X2-2	22	1.57	0.235	0.063	1.83	2310
5X3-2	22	1.57	0.235	0.062	1.77	2307
5X4-2	22	1.57	0.235	0.064	1.81	2214
5X5-2	22	1.57	0.235	0.063	1.84	2323
5X7-2	22	1.57	0.234	0.065	2.02	2406
5X8-2	22	1.57	0.235	0.064	2.27	2777
6Y1-2	22	1.57	0.239	0.067	1.54	1690
6Y2-2	22	1.57	0.236	0.065	1.83	2161
6Y3-2	22	1.57	0.235	0.061	1.33	1791
6Y4-2	22	1.57	0.235	0.059	1.25	1799
6Y5-2	22	1.57	0.234	0.057	1.07	1657
6Y6-2	22	1.57	0.233	0.060	1.07	1502
6Y7-2	22	1.57	0.236	0.060	0.40	554

WESTINGHOUSE STC. NUCLEAR SERVICES AND MATERIALS TESTING LAB

CUSTOMER: CAROL PAINTER
DATE: 7-28-95
CHARGE NO: 9TC3-HGFIL-33
TESTED BY: S.WITHROW

JOB NO: 68076
TEST SPEED: .050 IN/MIN
TEST MACHINE: 20 KIP INSTRON

FLEXURAL TEST

SPEC. IDENT	TEST TEMP (deg F)	SPAN (in)	WIDTH (in)	THICK (in)	ULTIMATE STRENGTH (lbs)	PSI
AS RECEIVED						
7X 1	25	1.57	0.150	0.062	0.750	1532
7X 2	25	1.57	0.147	0.084	1.045	1186
7X 3	25	1.57	0.148	0.080	0.610	758
7X 4	25	1.57	0.151	0.084	0.710	785
7X 5	25	1.57	0.149	0.088	0.790	806
7X 6	25	1.57	0.148	0.088	0.700	719
7X 7	25	1.57	0.152	0.085	0.700	751
7X 8	25	1.57	0.150	0.090	0.680	659
7X 9	25	1.57	0.149	0.092	0.770	719
7X 10	25	1.57	0.150	0.090	0.710	688
7X 11	25	1.57	0.150	0.089	0.745	738
7X 12	25	1.57	0.152	0.088	0.770	770
7Y 1	25	1.57	0.283	0.071	0.860	710
7Y 2	25	1.57	0.273	0.084	0.870	532
7Y 3	25	1.57	0.273	0.084	0.830	507
7Y 4	25	1.57	0.275	0.079	0.895	614
7Y 5	25	1.57	0.274	0.085	0.850	506
7Y 6	25	1.57	0.285	0.065	0.900	880

WESTINGHOUSE STC. NUCLEAR SERVICES AND MATERIALS TESTING LAB

CUSTOMER: CAROL PAINTER
DATE: 7-28-95
CHARGE NO: 9TC3-HGFIL-33
TESTED BY: S.WITHROW

JOB NO: 68076
TEST SPEED: .050 IN/MIN
TEST MACHINE: 20 KIP INSTRON

FLEXURAL TEST

SPEC. IDENT	TEST TEMP (deg F)	SPAN (in)	WIDTH (in)	THICK (in)	ULTIMATE (lbs)	STRENGTH PSI
*AS RECEIVED						
8X 1	25	1.57	0.143	0.083	0.670	801
8X 2	25	1.57	0.137	0.075	0.585	894
8X 3	25	1.57	0.136	0.072	0.750	1253
8X 4	25	1.57	0.137	0.078	0.580	819
8X 5	25	1.57	0.139	0.078	0.610	849
8X 6	25	1.57	0.136	0.075	0.560	862
8X 7	25	1.57	0.136	0.077	0.670	978
8X 8	25	1.57	0.138	0.078	0.605	848
8X 9	25	1.57	0.136	0.068	0.600	1123
8X 10	25	1.57	0.144	0.075	0.590	858
8Y 1	25	1.57	0.278	0.075	1.900	1431
8Y 2	25	1.57	0.280	0.064	2.000	2053
8Y 3	25	1.57	0.277	0.072	1.740	1427
8Y 4	25	1.57	0.278	0.072	1.570	1283
8Y 5	25	1.57	0.280	0.073	1.590	1255
8Y 6	25	1.57	0.277	0.072	1.360	1115

WESTINGHOUSE STC. NUCLEAR SERVICES AND MATERIALS TESTING LAB

CUSTOMER: CAROL PAINTER
DATE: 7-28-95
CHARGE NO: 9TC3-HGFIL-33
TESTED BY: S.WITHROW

JOB NO: 68076
TEST SPEED: .050 IN/MIN
TEST MACHINE: 20 KIP INSTRON

FLEXURAL TEST

SPEC. IDENT	TEST TEMP (deg F)	SPAN (in)	WIDTH (in)	THICK (in)	ULTIMATE STRENGTH (lbs)	PSI
AS RECEIVED						
9X 1	25	1.57	0.114	0.061	0.530	1471
9X 2	25	1.57	0.114	0.050	0.610	2520
9X 3	25	1.57	0.114	0.064	0.655	1652
9X 4	25	1.57	0.114	0.045	0.600	3060
9X 5	25	1.57	0.114	0.051	0.675	2681
9X 6	25	1.57	0.114	0.055	0.725	2476
9X 7	25	1.57	0.114	0.057	0.670	2130
9X 8	25	1.57	0.114	0.057	0.625	1987
9X 9	25	1.57	0.114	0.061	0.600	1666
9X 10	25	1.57	0.114	0.063	0.690	1796
9Y 3	25	1.57	0.114	0.063	0.473	1231
9Y 4	25	1.57	0.114	0.063	0.320	833
9Y 5	25	1.57	0.114	0.058	0.390	1197
9Y 6	25	1.57	0.114	0.059	0.380	1128
9Y 7	25	1.57	0.113	0.063	0.740	1943
9Y 8	25	1.57	0.114	0.063	0.420	1093
9Y 9	25	1.57	0.113	0.064	0.790	2010
9Y 10	25	1.57	0.114	0.064	0.425	1072
9Y 11	25	1.57	0.114	0.064	0.120	303

Summary of Mechanical Testing On CMC 10, 11, 12, 13, 14, 15

	Thickness	Width	Strength (psi)	Load (lb)
CMC 10X1	0.073	0.236	3545	2.8
CMC 10X3	0.073	0.236	3650	2.9
CMC 10X4	0.073	0.236	3853	3.1
CMC 10X5	0.073	0.236	3876	3.1
		Average:	**3731 ± 160 psi**	**3 lbs.**
CMC 10Y1	0.073	0.236	1439	1.63
CMC 10Y2	0.073	0.236	1404	1.46
CMC 10Y3	0.073	0.236	1743	1.76
CMC 10Y4	0.073	0.236	1925	1.83
CMC 10Y5	0.073	0.236	1751	1.52
		Average:	**1652 ± 223 psi**	**1.6 lbs.**
CMC 11X1	0.069	0.235	3669	2.2
CMC 11X2	0.069	0.235	3748	2.9
CMC 11X3	0.069	0.235	3338	2.6
CMC 11X4	0.069	0.236	3850	3.1
CMC 11X5	0.069	0.235	4119	3.4
		Average:	**3745 ± 284 psi**	**2.8 lbs.**
CMC 11Y1	0.069	0.235	2431	2.37
CMC 11Y2	0.069	0.235	2343	2.08
CMC 11Y5	0.069	0.235	2803	1.99
		Average:	**2525 ± 245 psi**	**2.1 lbs.**
CMC 12X1	0.103	0.234	3277	3.11
CMC 12X3	0.095	0.234	3478	3.21
CMC 12X4	0.100	0.234	3463	3.2
CMC 12X5	0.105	0.234	3682	3.57
		Average:	**3745 ± 165 psi**	**3.3 lbs.**

	Thickness	Width	Strength (psi)	Load (lb)
CMC 12Y2	0.109	0.234	3060	6.35
CMC 12Y3	0.106	0.234	2627	5.01
CMC 12Y4	0.108	0.234	3336	6.81
CMC 12Y5	0.112	0.234	3156	6.6
		Average:	**3044 ± 300 psi**	**6.2 lbs.**
CMC 13X1	0.142	0.235	2698	9.23
CMC 13X2	0.141	0.235	2534	8.41
CMC 13X3	0.142	0.235	2011	6.91
CMC 13X4	0.142	0.235	2160	7.64
CMC 13X5	0.143	0.235	2270	7.44
		Average:	**2334 ± 280 psi**	**6.4 lbs.**
CMC 13Y1	0.166	0.233	2074	8.81
CMC 13Y2	0.160	0.234	1188	6.52
CMC 13Y3	0.152	0.233	2231	9.3
CMC 13Y4	0.154	0.235	2274	9.1
CMC 13Y5	0.148	0.235	2026	7.42
		Average:	**1958 ± 440 psi**	**8.2 lbs.**
CMC 14 PX2	0.126	0.222	2036	5.86
CMC 14 PX3	0.127	0.232	1842	5.16
CMC 14 PX4	0.126	0.233	1444	4.46
CMC 14 PX5	0.127	0.233	1468	4.32
		Average:	**1697 ± 290 psi**	**5 lbs.**
CMC 14 PX1	0.126	0.230	1098	3.62
CMC 14 PY2	0.126	0.232	1502	4.52
CMC 14 PY3	0.126	0.233	1341	4.06
CMC 14 PY4	0.127	0.234	1617	4.74
		Average:	**1389 ± 225 psi**	**4.2 lbs.**
CMC 14X1	0.130	0.235	1487	5.03
CMC 14X2	0.134	0.235	1284	3.99
CMC 14X3	0.134	0.235	1478	4.88
CMC 14X4	0.134	0.235	1647	5.45
CMC 14X5	0.134	0.235	1684	5.45
		Average:	**1516 ± 160 psi**	**5 lbs.**

	Thickness	Width	Strength (psi)	Load (lb)
CMC 14Y1	0.155	0.234	993	4.81
CMC 14Y2	0.126	0.234	1316	4.19
CMC 14Y3	0.126	0.232	1468	4.73
CMC 14Y4	0.124	0.237	1372	4.17
CMC 14Y5	0.130	0.235	1608	5
		Average:	**1351 ± 230 psi**	**4.6 lbs.**
CMC 15X1	0.193	0.234	474	3.33
CMC 15X2	0.196	0.234	468	3.48
CMC 15X3	0.196	0.233	486	3.61
CMC 15X4	0.197	0.232	316	2.48
CMC 15X5	0.198	0.233	406	3.12
		Average:	**430 ± 70 psi**	**3.2 lbs.**
CMC 15Y1	0.178	0.233	444	3.13
CMC 15Y2	0.170	0.233	879	5.13
CMC 15Y3	0.168	0.233	880	5.45
CMC 15Y4	0.181	0.233	662	4.17
CMC 15Y5	0.179	0.233	581	3.93
		Average:	**689 ± 190 psi**	**4.4 lbs.**

Load-Deflection Curves for CMCs fabricated from Candidate Fiber Architecture #1.

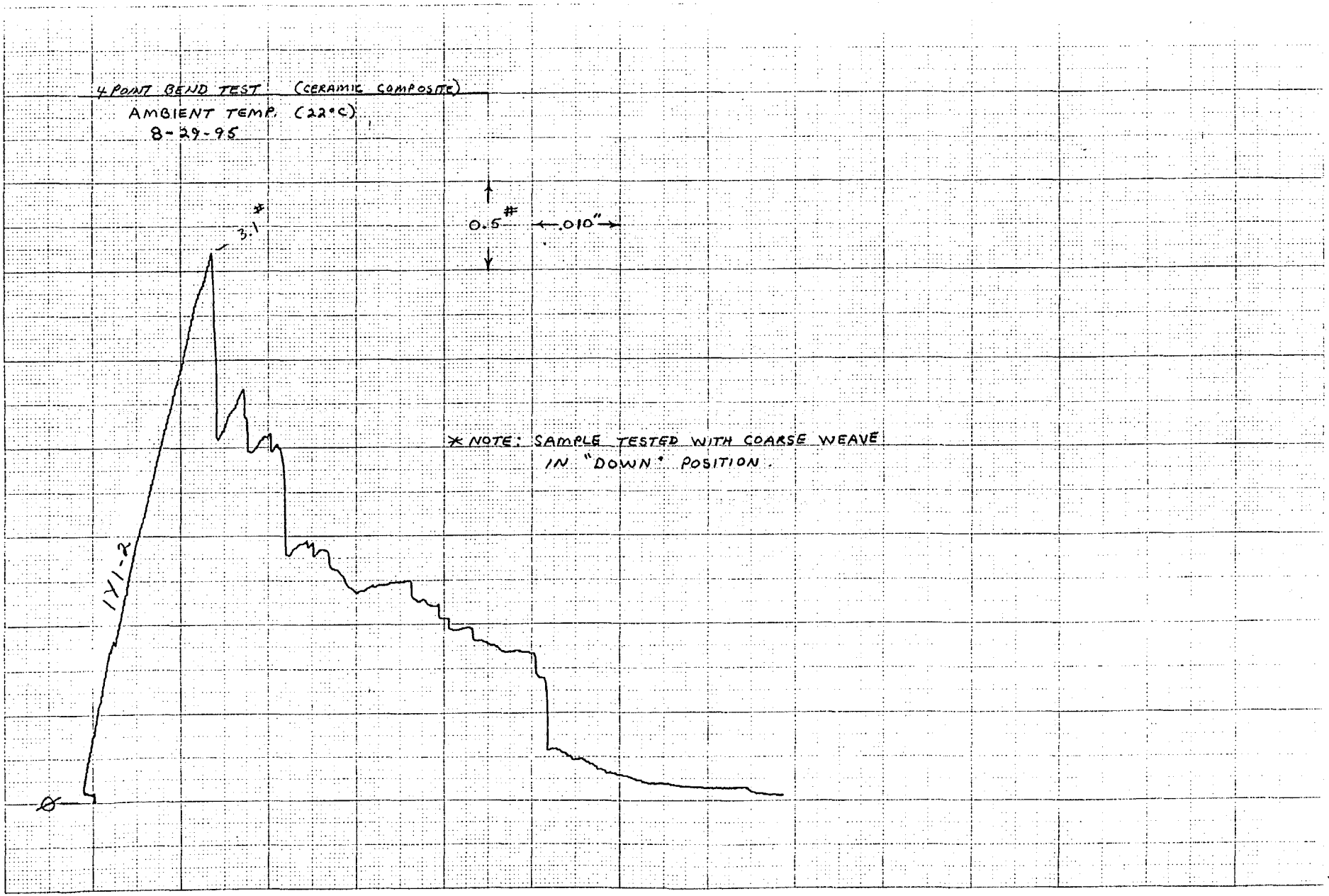
4 POINT BEND TEST (CERAMIC COMPOSITE)
AMBIENT TEMP. (22°C)
8-29-95
0.5 #
.010"
3.1 *
1X1-2
* NOTE: SAMPLE TESTED WITH COARSE WEAVE
IN "DOWN" POSITION.

4 POINT BEND TEST (CERAMIC COMPOSITE)

AMBIENT TEMP. (22°C.)

8-29-95

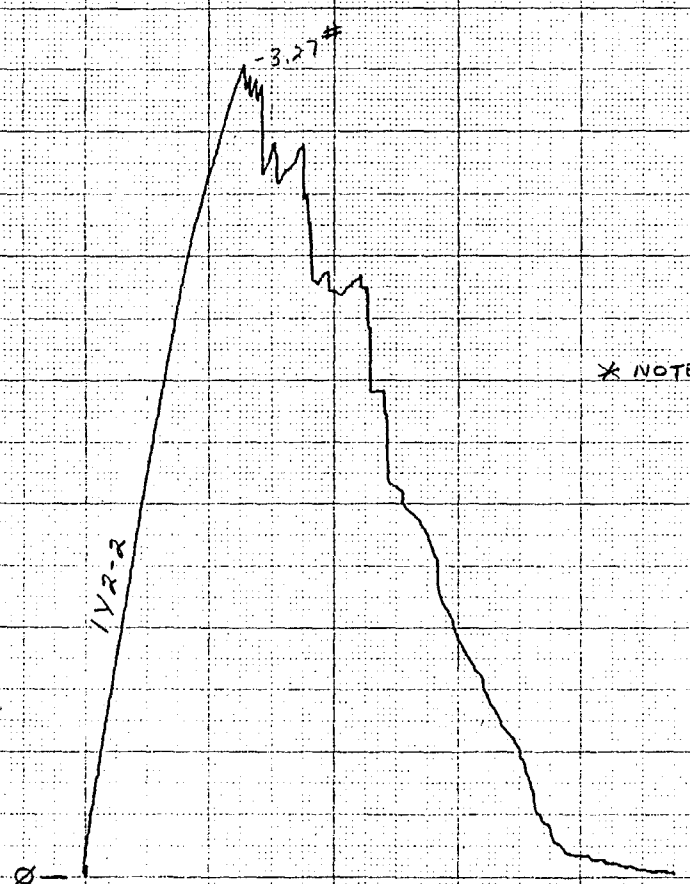

0.5# ← .010" →

* NOTE: SAMPLE TESTED WITH COARSE WEAVE IN "DOWN" POSITION.

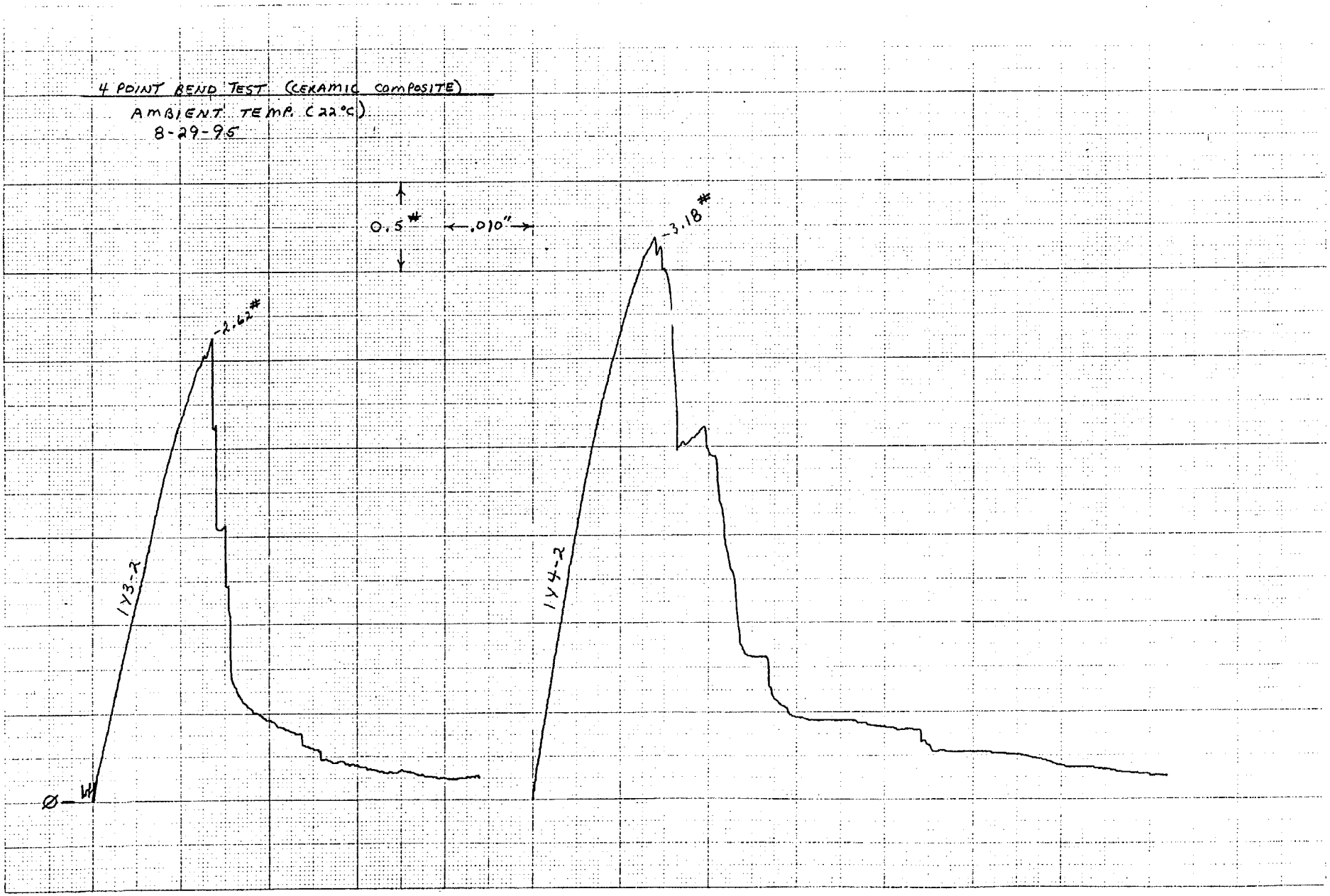
4 POINT BEND TEST (CERAMIC COMPOSITE)
AMBIENT TEMP. (22°C)
8-29-95
0.5#
.010"
2.62#
3.18#
1Y3-2
1Y4-2
Ø

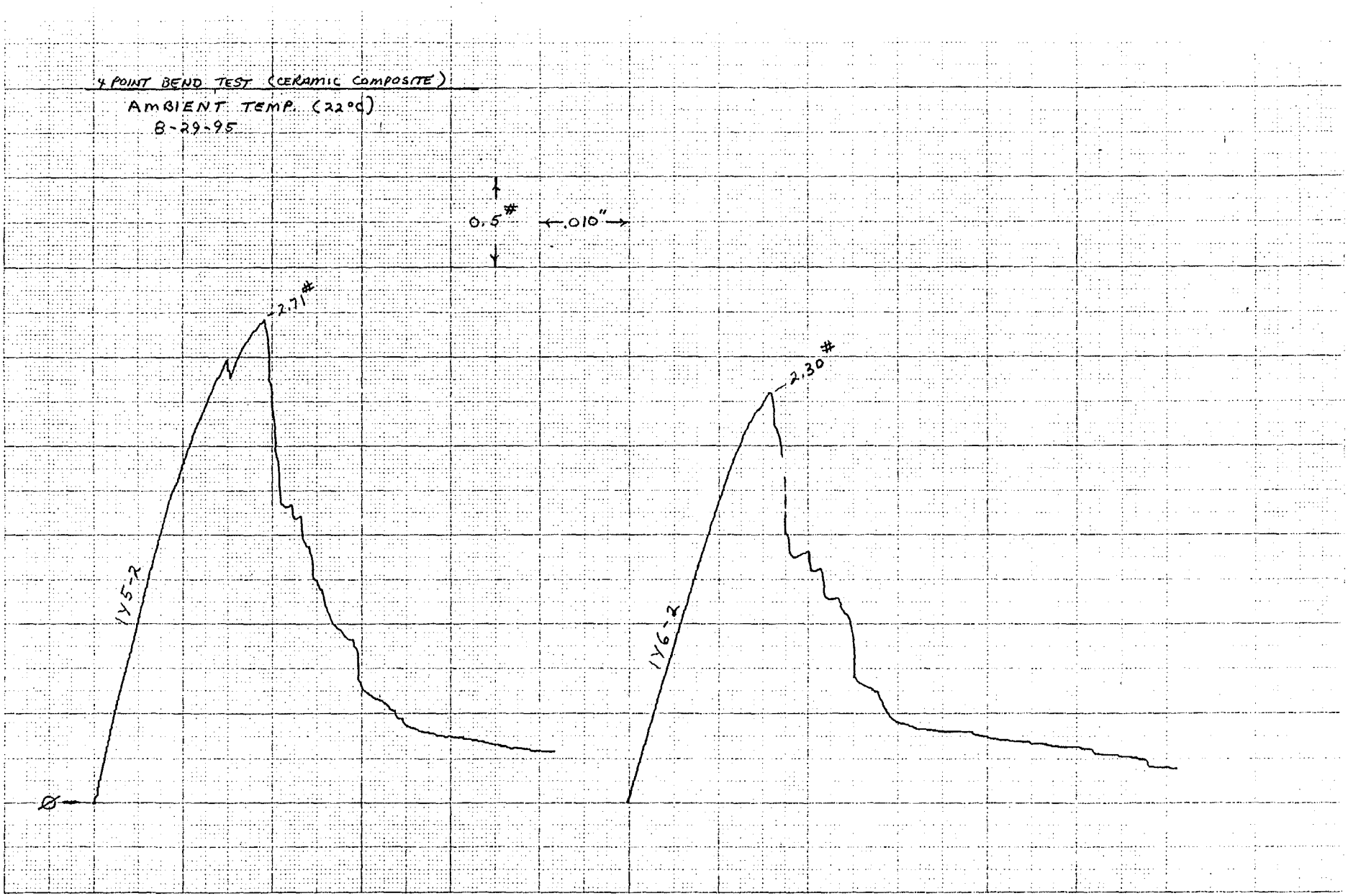
4 POINT BEND TEST (CERAMIC COMPOSITE)
AMBIENT TEMP. (22°C)
8-29-95
0.5#
.010"
2.71#
1Y5-2
2.30#
1Y6-2

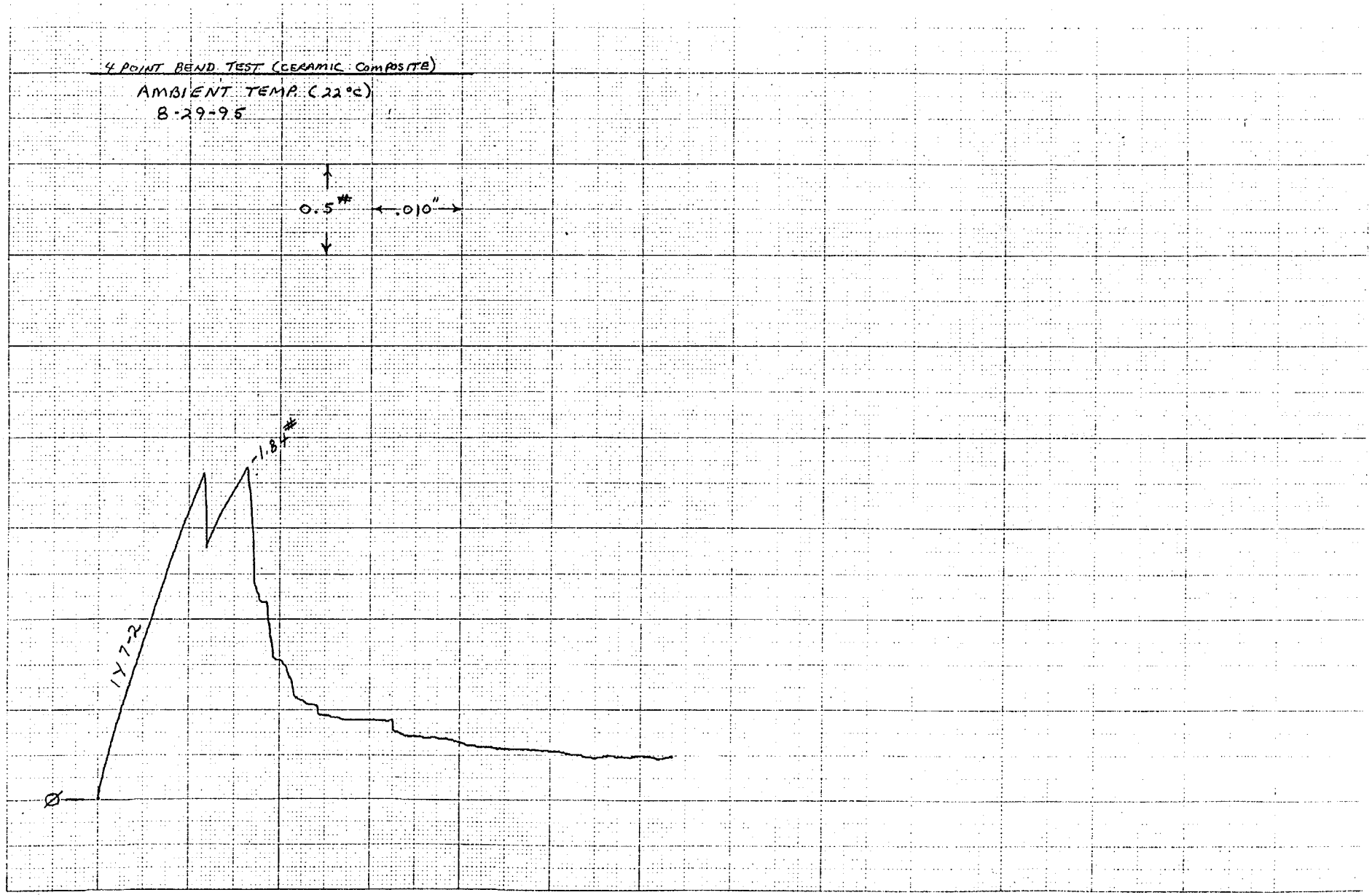
4 POINT BEND TEST (CERAMIC COMPOSITE)
AMBIENT TEMP. (22°C)
8-29-95
0.5#
.010"
1.84#
1Y7-2
Ø

Load-Deflection Curves for CMCs fabricated from Candidate Fiber Architecture #2.

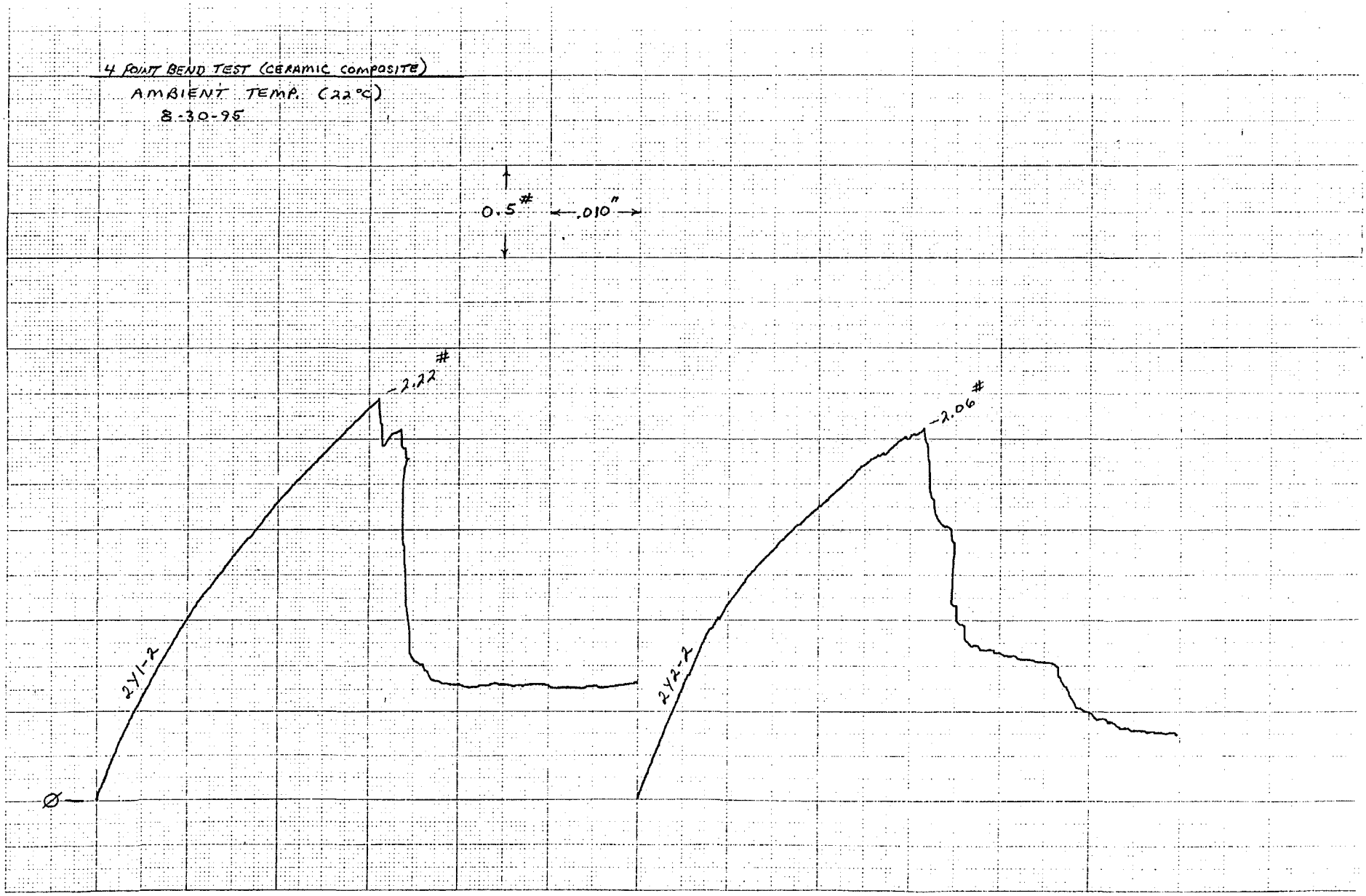
4 POINT BEND TEST (CERAMIC COMPOSITE)
AMBIENT TEMP. (22°C)
8-30-95
0.5#
.010"
2.12#
2.06#
2Y1-2
2Y2-2
Ø

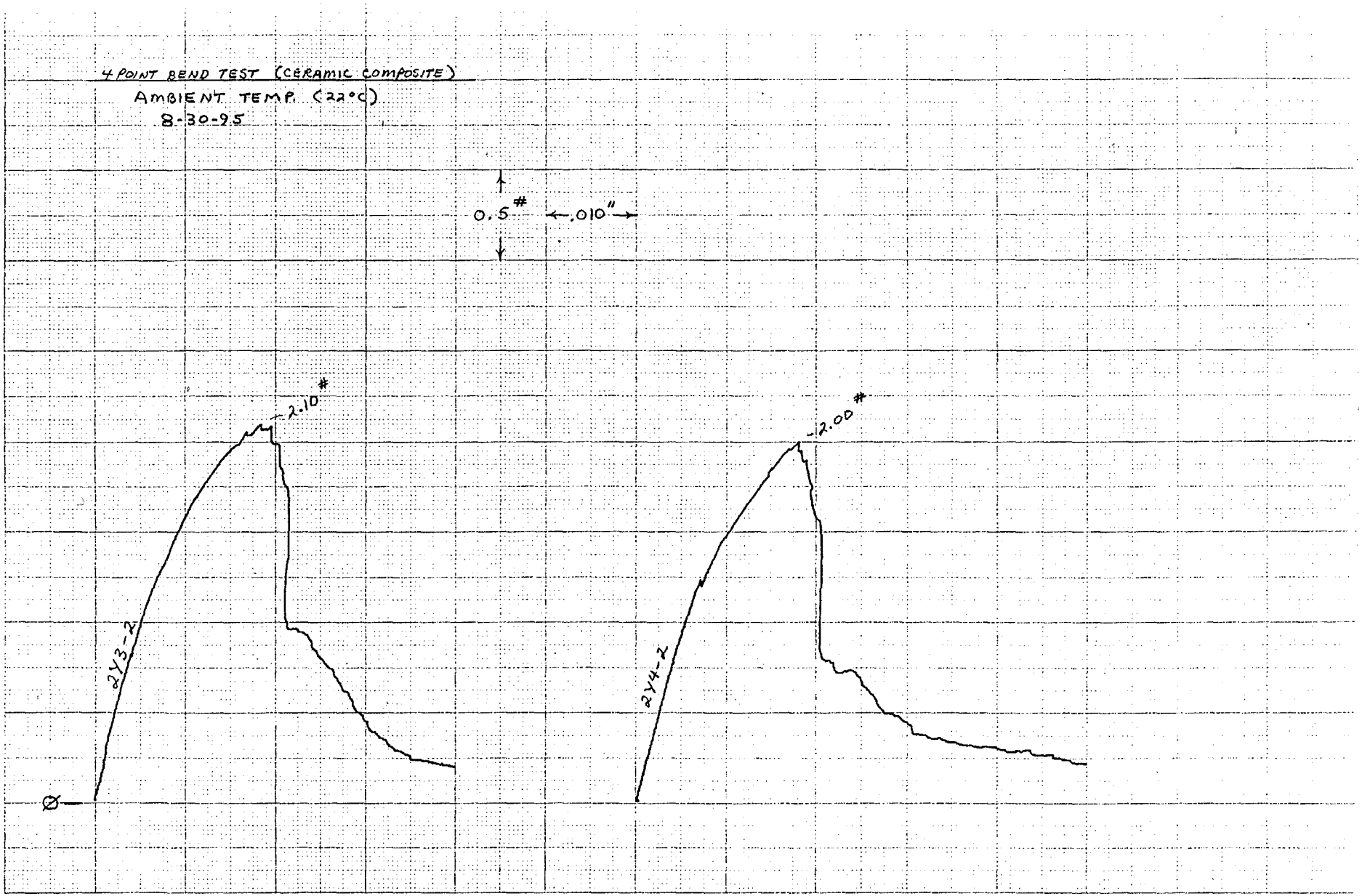
4 POINT BEND TEST (CERAMIC COMPOSITE)
AMBIENT TEMP. (22°C)
8-30-95
0.5 #
.010"
2.10 #
2.00 #
2Y3-2
2Y4-2

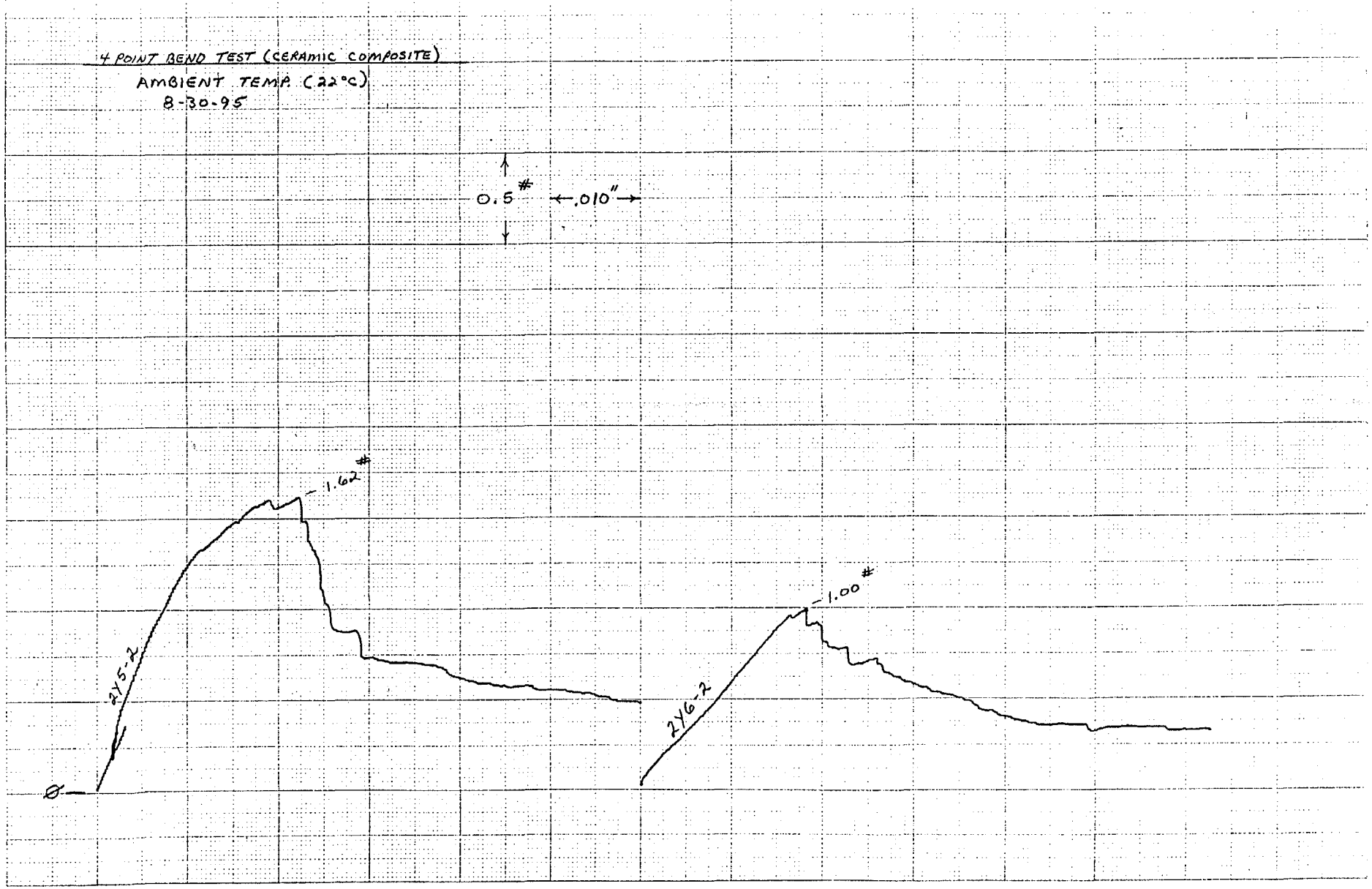
4 POINT BEND TEST (CERAMIC COMPOSITE)
AMBIENT TEMP (22°C)
8-30-95
0.5 #
.010"
1.62 #
2Y5-2
1.00 #
2Y6-2

4 POINT BEND TEST (CERAMIC COMPOSITE)

AMBIENT TEMP. (22°C)

8-30-95

Load-Deflection Curves for CMCs fabricated from Candidate Fiber Architecture #3.

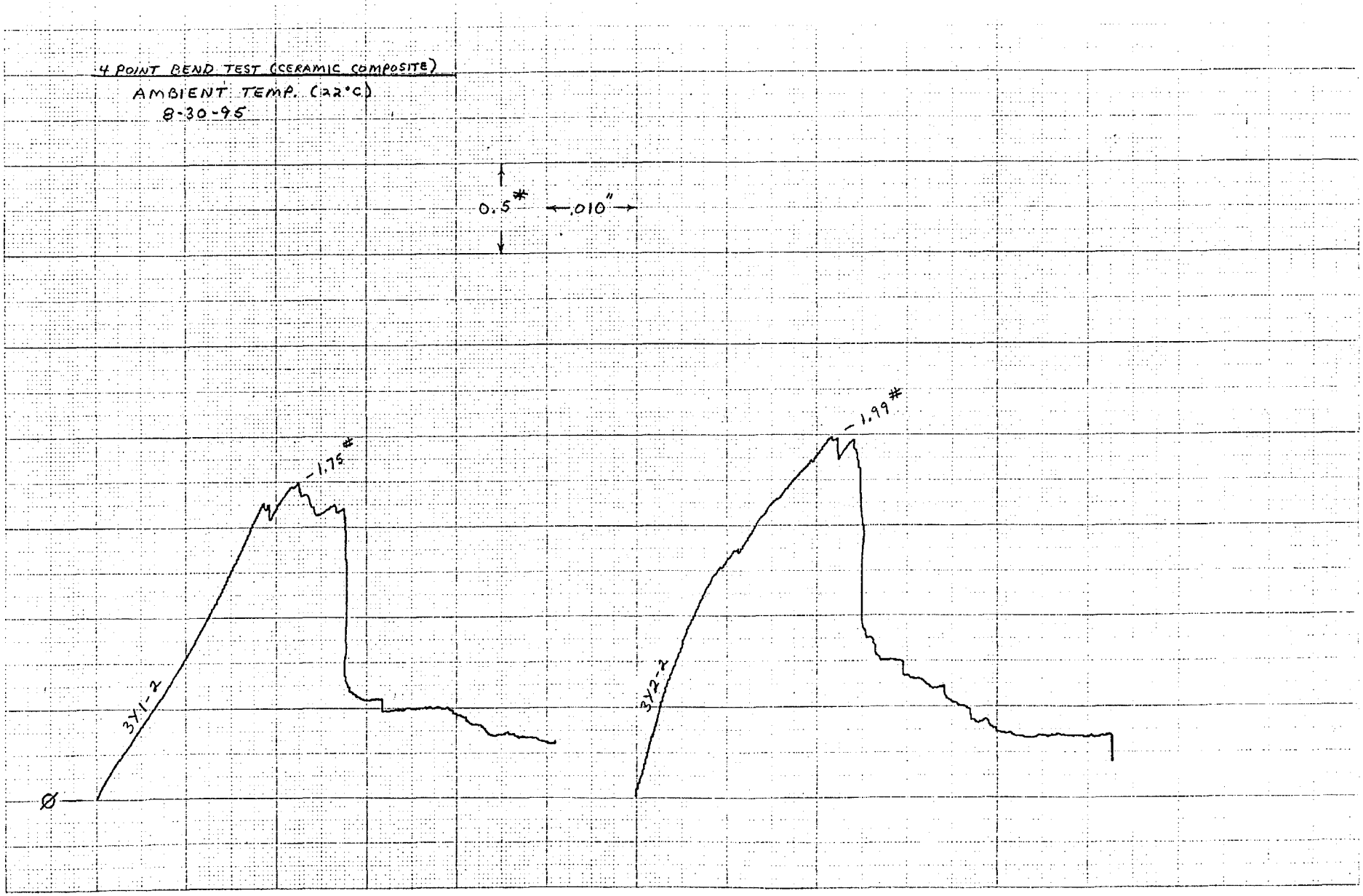
4 POINT BEND TEST (CERAMIC COMPOSITE)
AMBIENT TEMP. (22°C)
8-30-95
0.5#
.010"
1.75#
3Y1-2
1.99#
3Y2-2
Ø

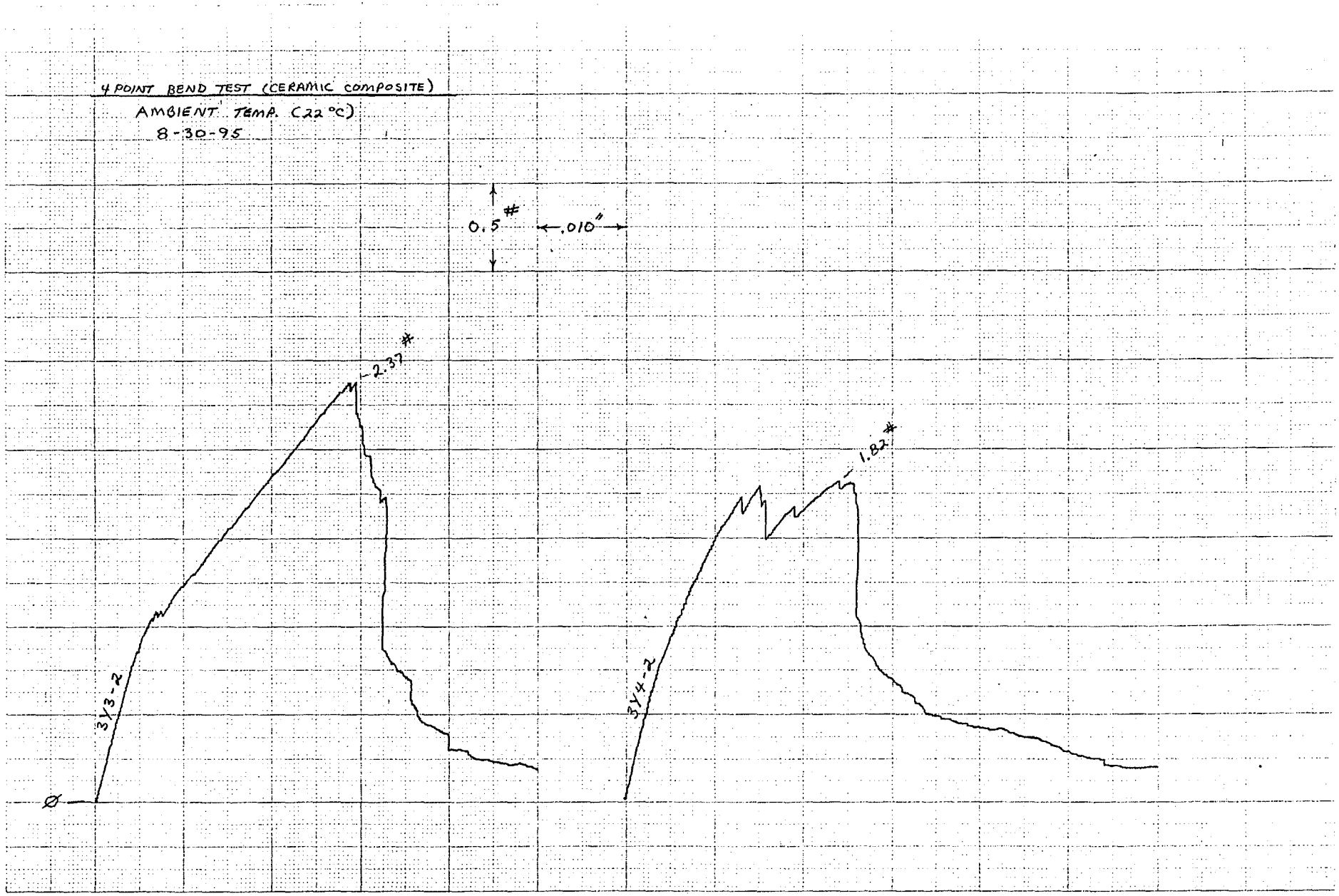
4 POINT BEND TEST (CERAMIC COMPOSITE)
AMBIENT TEMP. (22 °C)
8-30-95
0.5 #
.010"
2.37 #
3Y3-2
1.82 #
3Y4-2
Ø

4 POINT BEND TEST (CERAMIC COMPOSITE)

AMBIENT TEMP. (22°C)

8-30-95

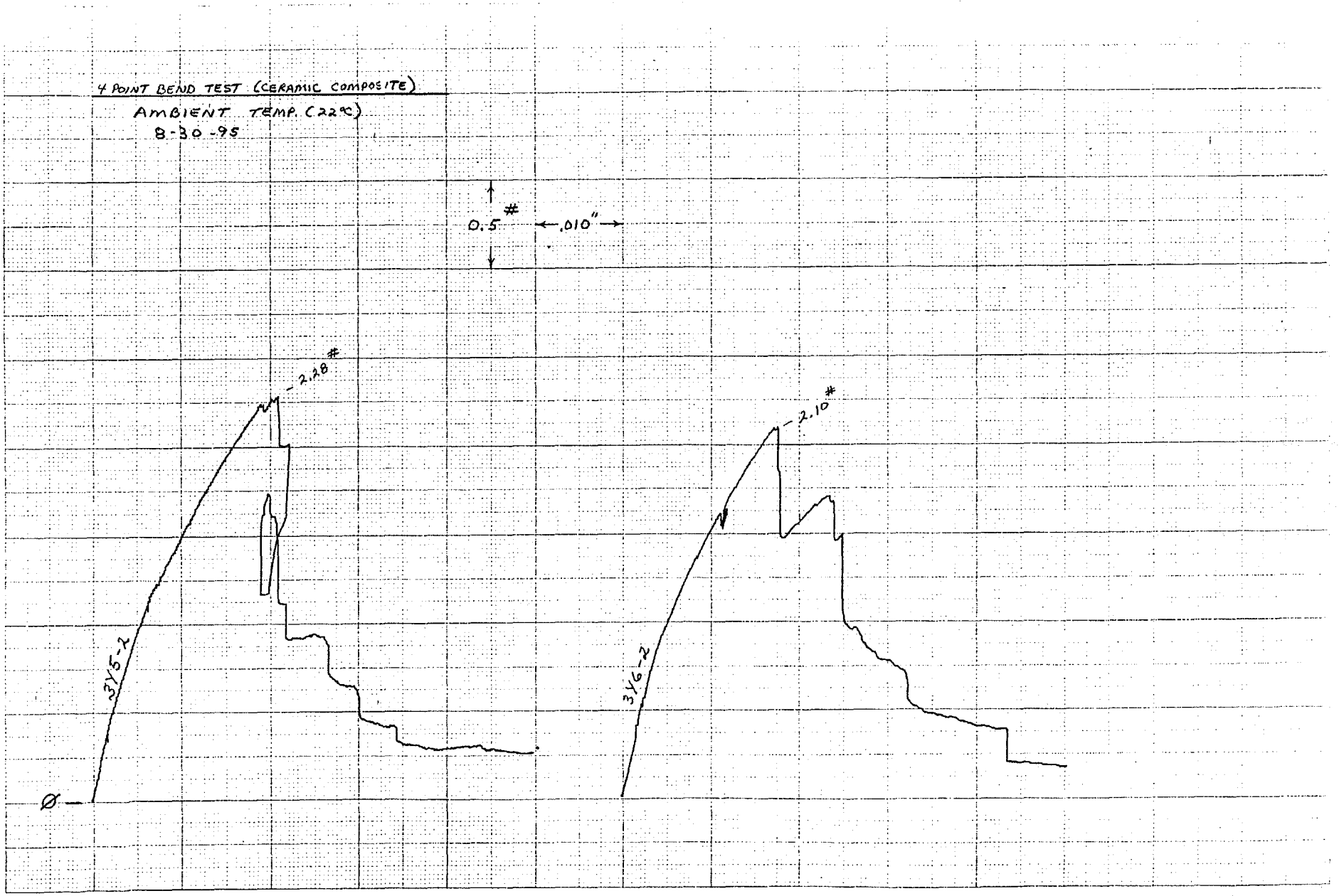

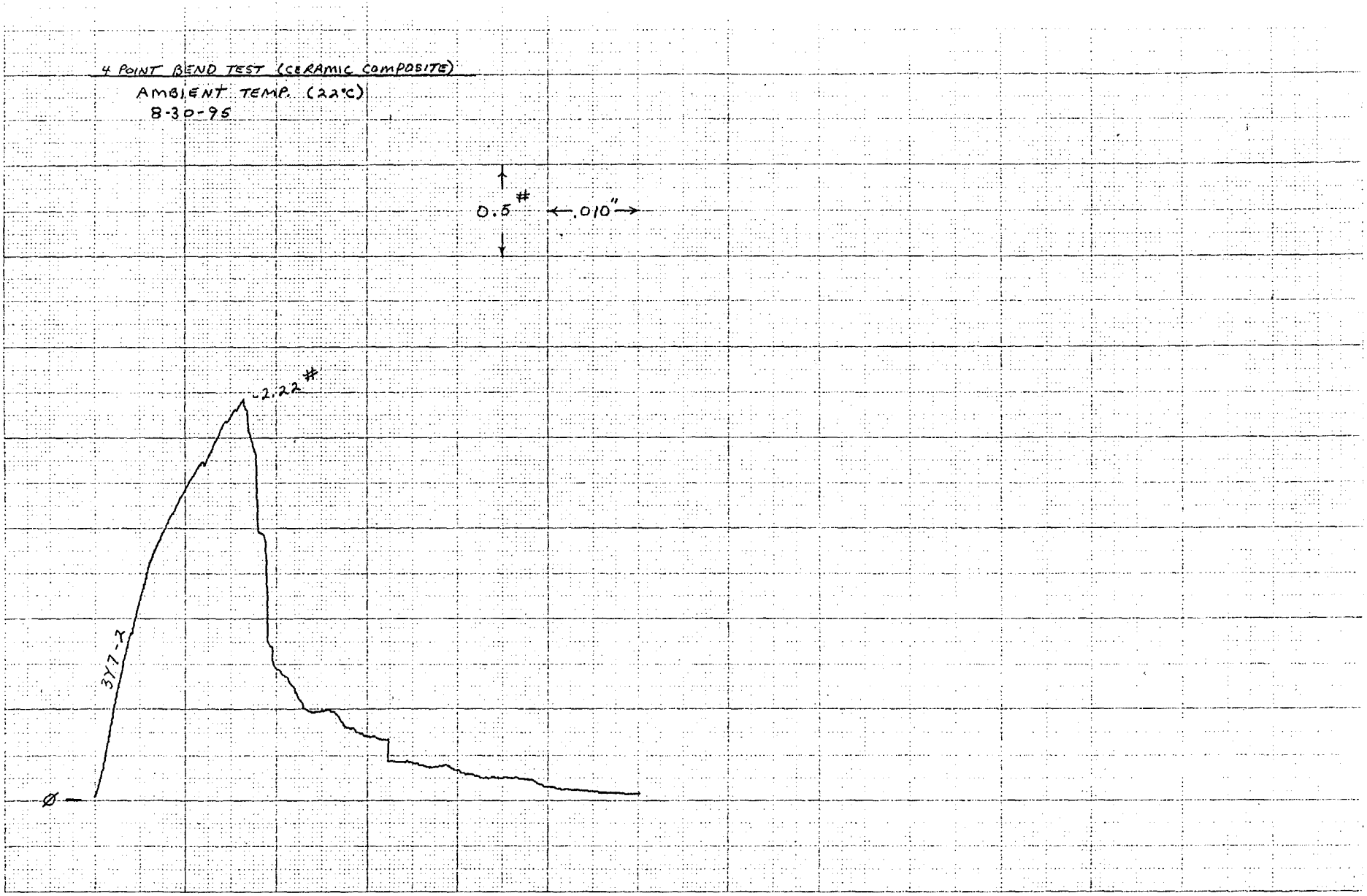
4 POINT BEND TEST (CERAMIC COMPOSITE)
AMBIENT TEMP. (22°C)
8-30-95
0.5 #
.010"
2.22 #
3Y17-2
Ø

Load-Deflection Curves for CMCs fabricated from Candidate Fiber Architecture #4.

4 POINT BEND TEST (CERAMIC COMPOSITE)

AMBIENT TEMP. (22°C)

8-29-95

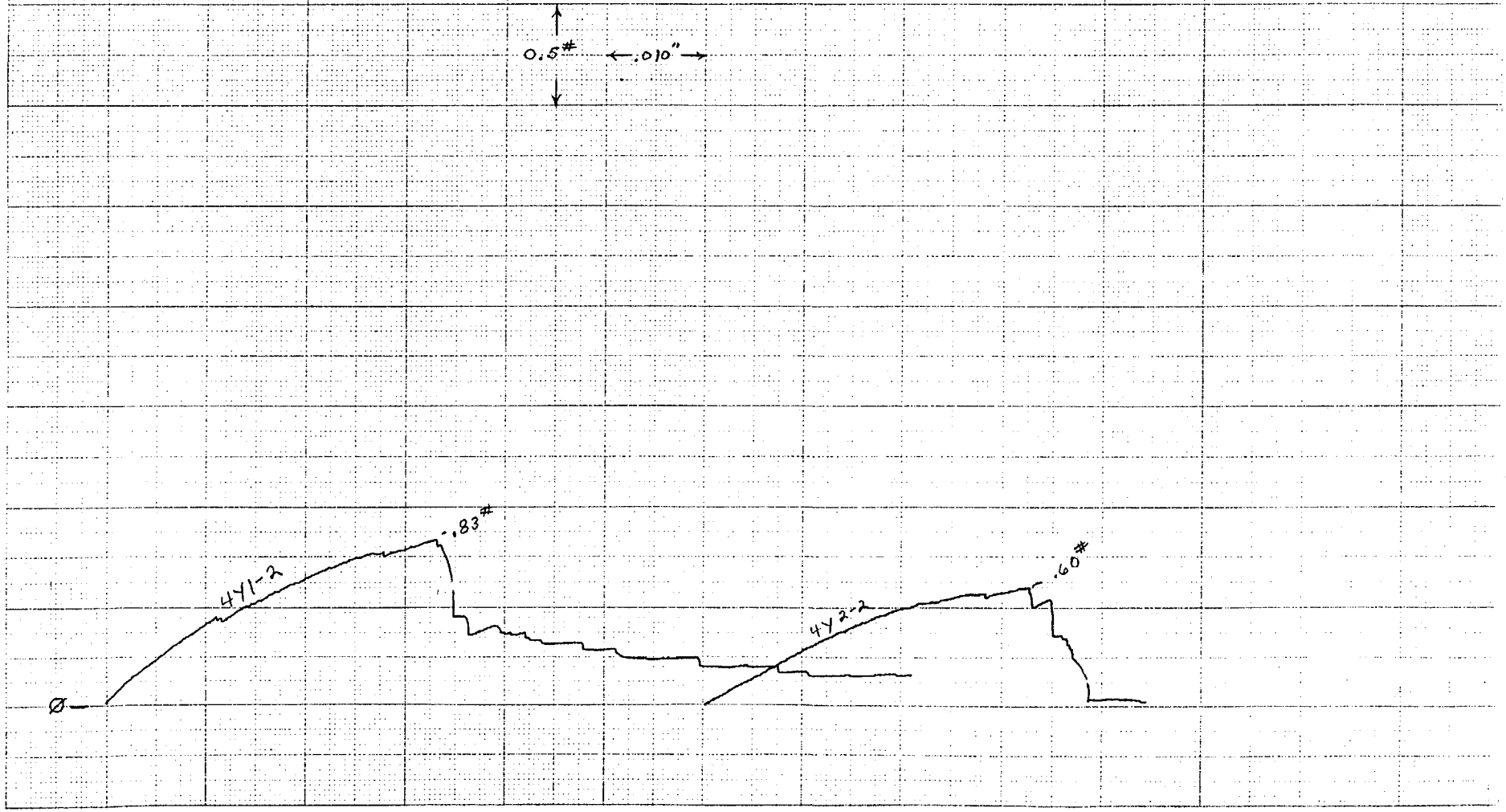

4 POINT BEND TEST (CERAMIC COMPOSITE)

AMBIENT TEMP. (22°C)

8-29-95

4 POINT BEND TEST (CERAMIC COMPOSITE)

AMBIENT TEMP. (22°C)

8-29-95

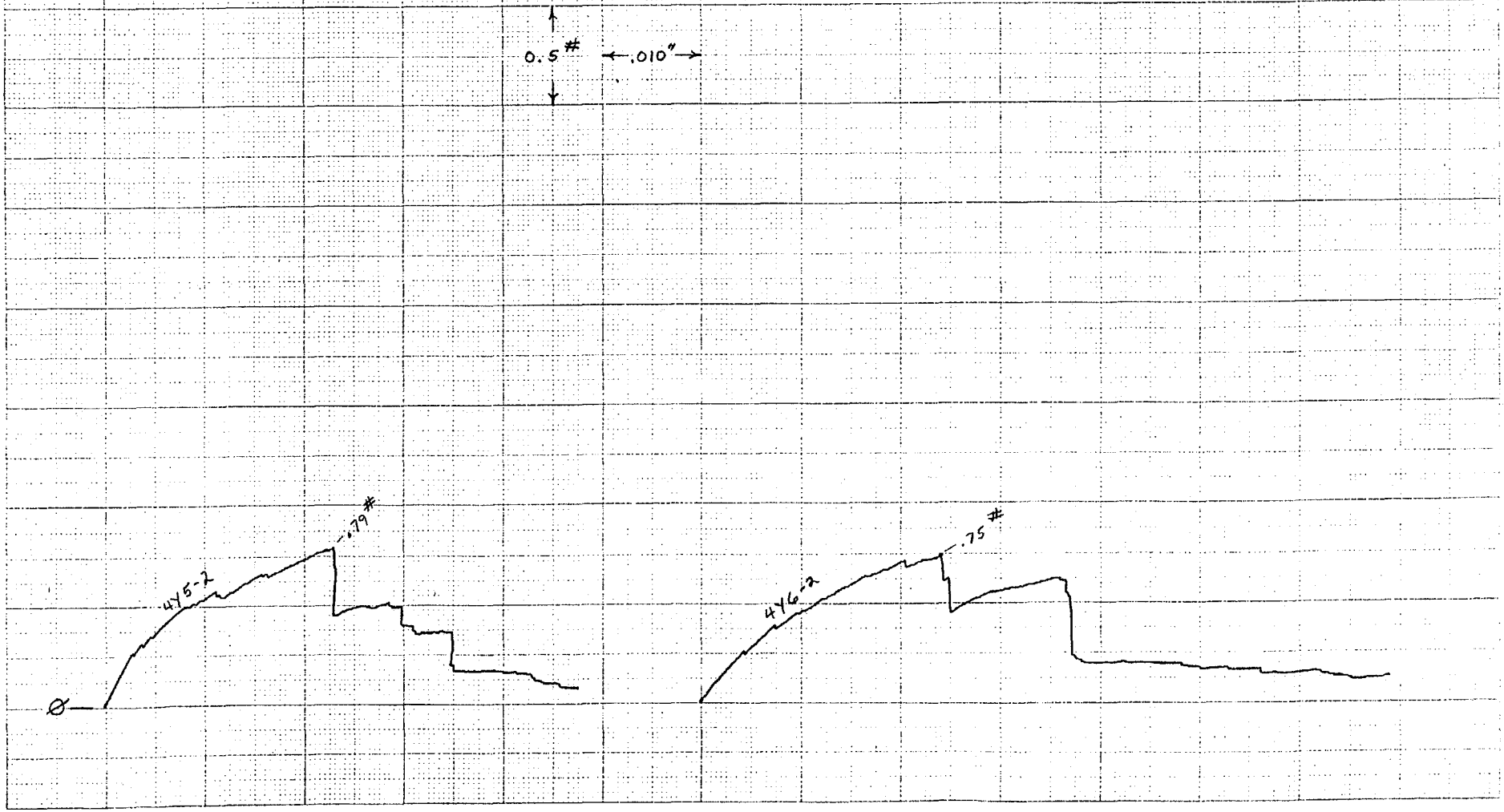

4 POINT BEND TEST (CERAMIC COMPOSITE)

AMBIENT TEMP. (22°C.)

8-29-95

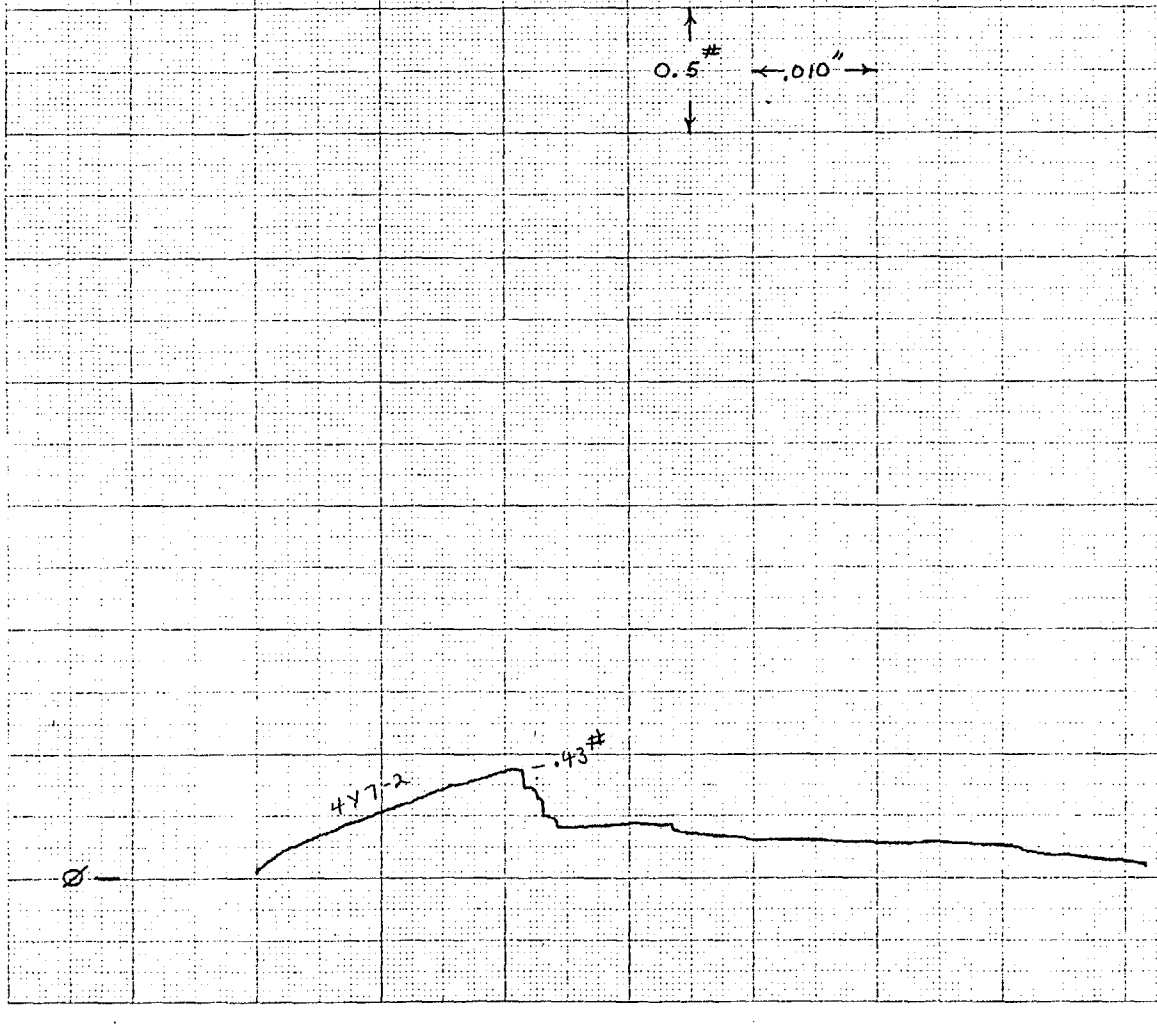

4 POINT BEND TEST (CERAMIC COMPOSITE)

AMBIENT TEMP. (22°C)

8-29-96

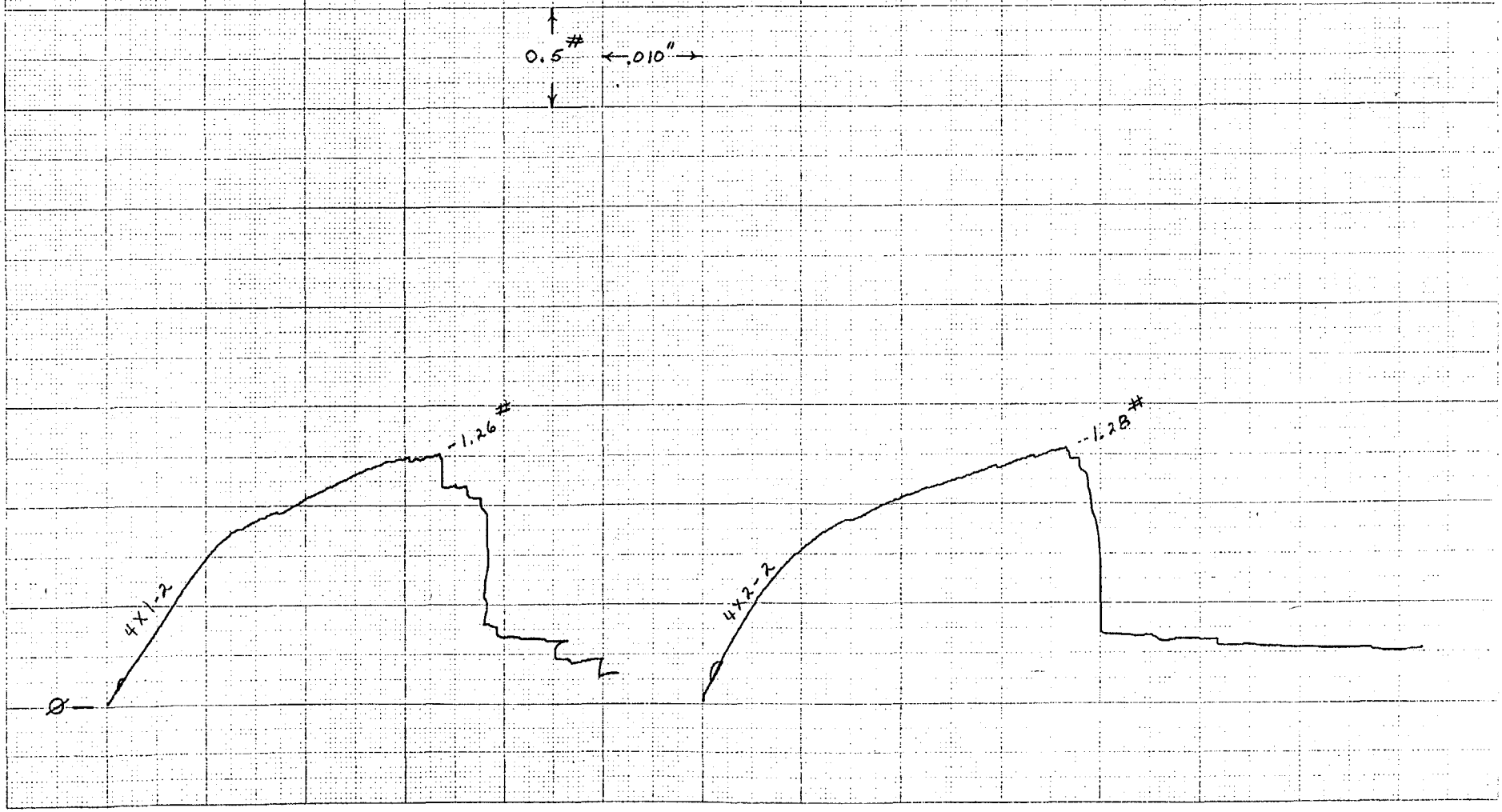

4 POINT BEND TEST (CERAMIC COMPOSITE)

AMBIENT TEMP. (22°C)

8-29-95

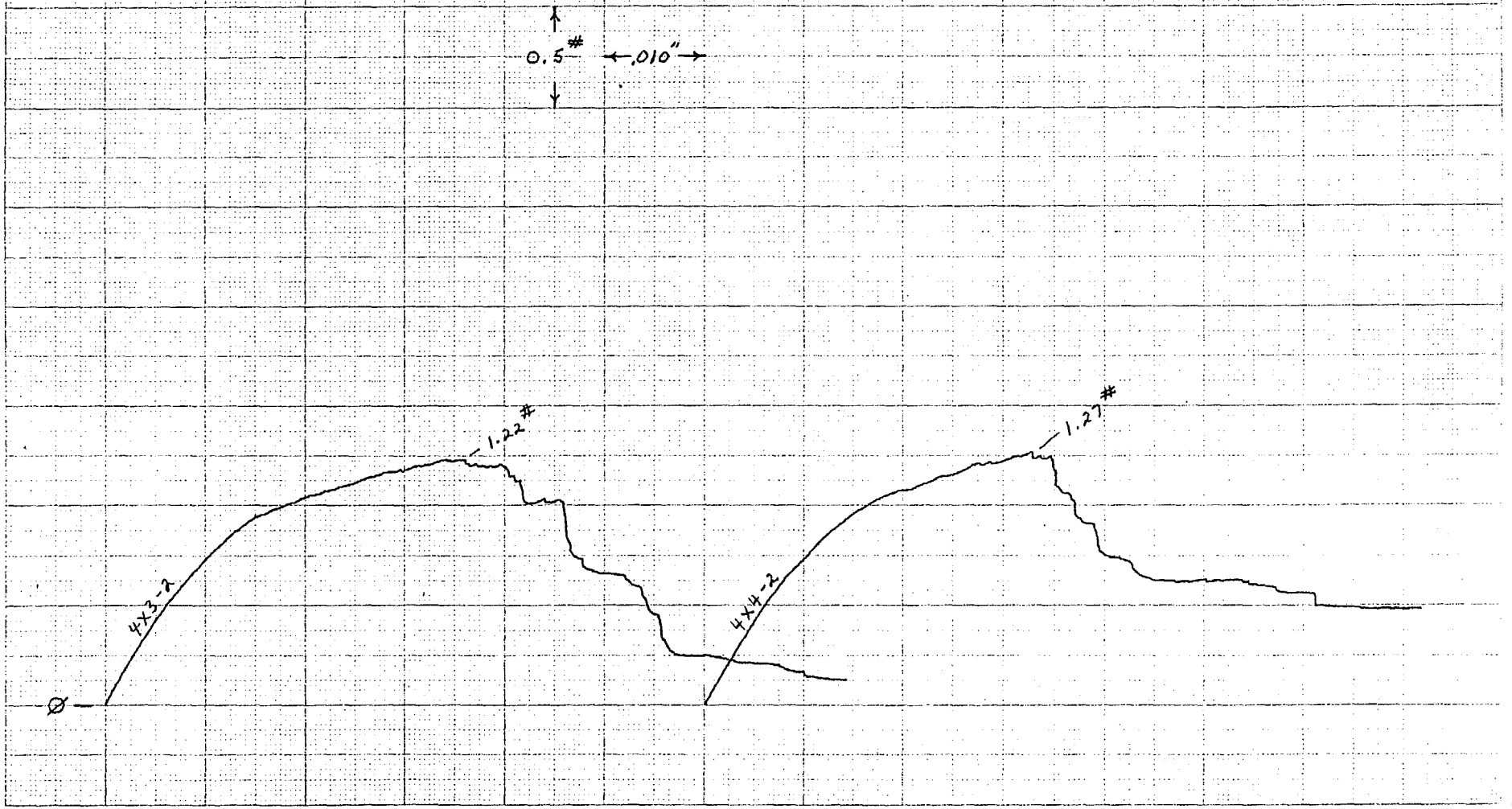

4 POINT BEND TEST (CERAMIC COMPOSITE)

AMBIENT TEMP. (22°C)

8-29-95

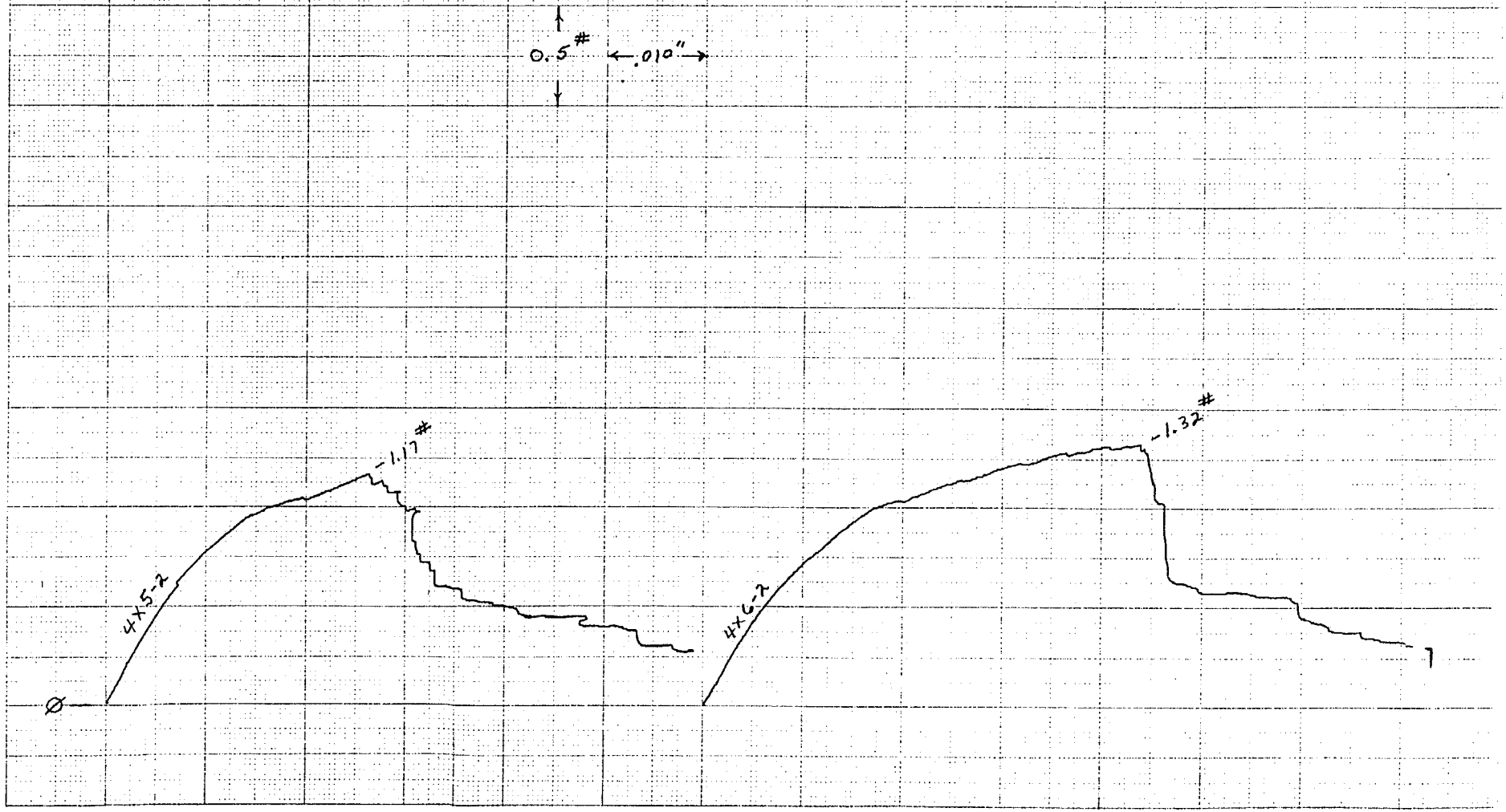

4 POINT BEND TEST (CERAMIC COMPOSITE)

AMBIENT TEMP. (22°C)

8-29-95

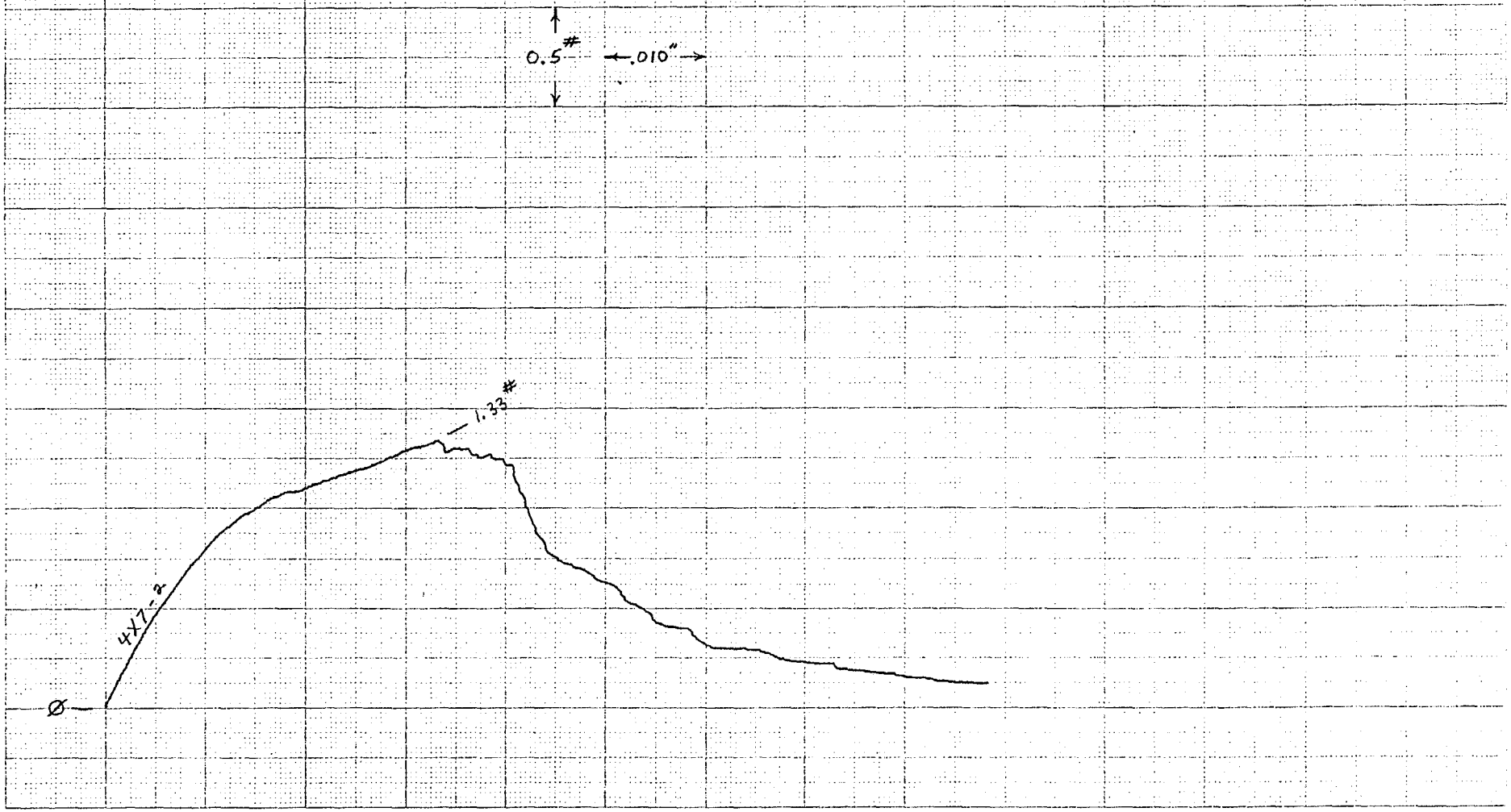

Load-Deflection Curves for CMCs fabricated from Candidate Fiber Architecture #5.

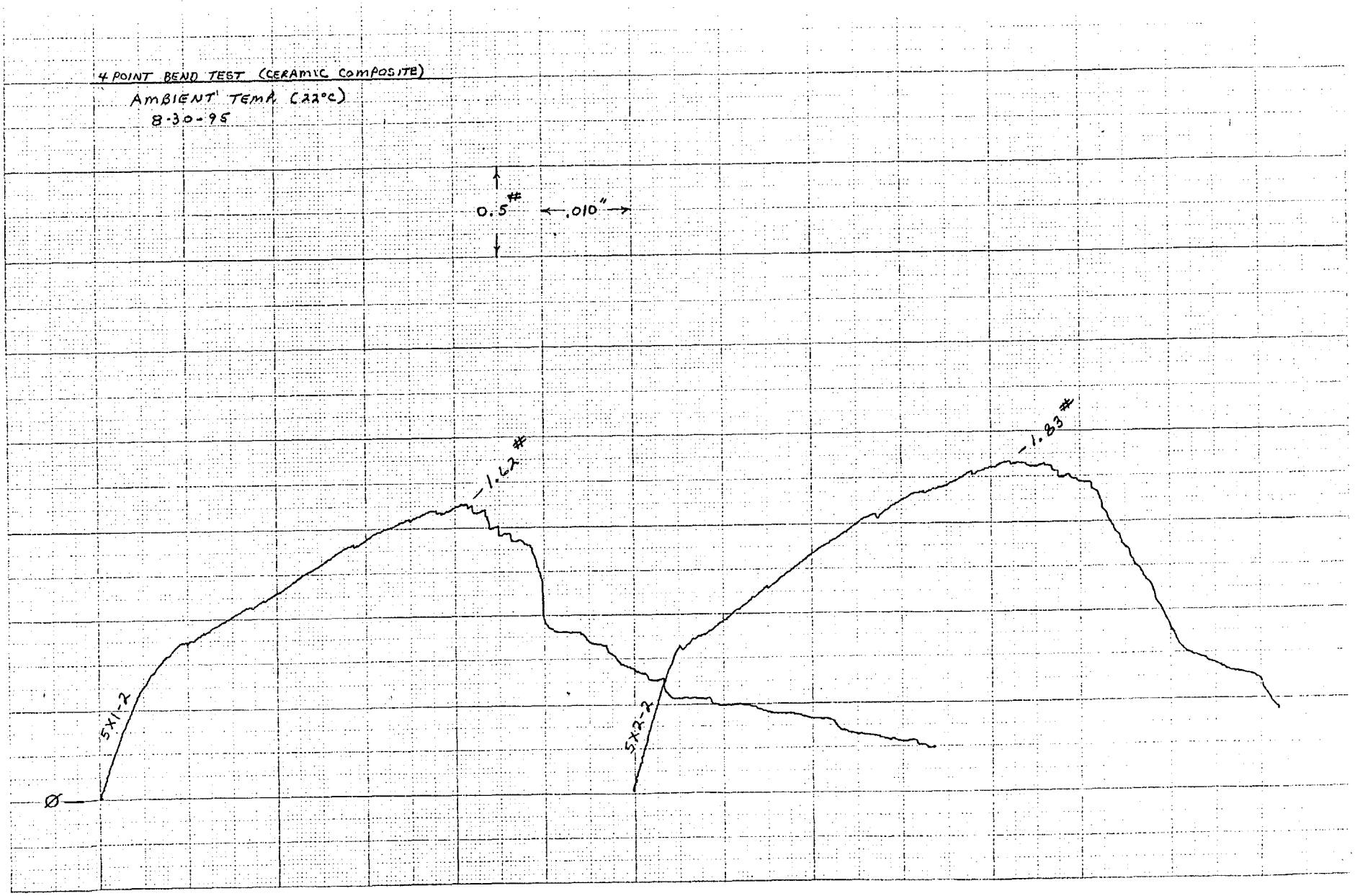
4 POINT BEND TEST (CERAMIC COMPOSITE)
AMBIENT TEMP (22°C)
8-30-95
0.5#
.010"
1.42#
1.83#
5X1-2
5X2-2
Ø

4 POINT BEND TEST (CERAMIC COMPOSITE)

AMBIENT TEMP. (22°C)

8-30-95

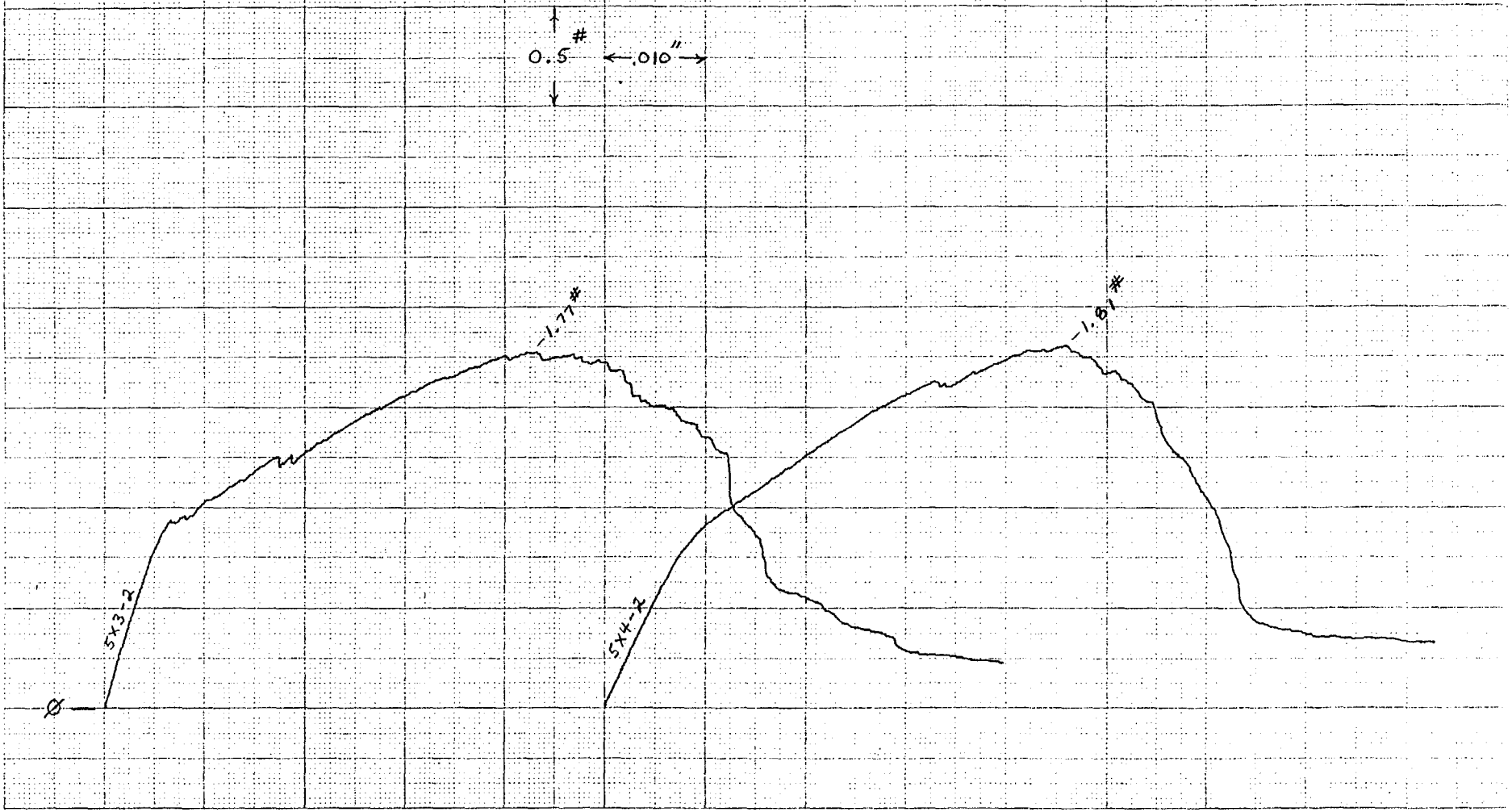

4 POINT BEND TEST (CERAMIC COMPOSITE)

AMBIENT TEMP. (22°C)

8-30-95

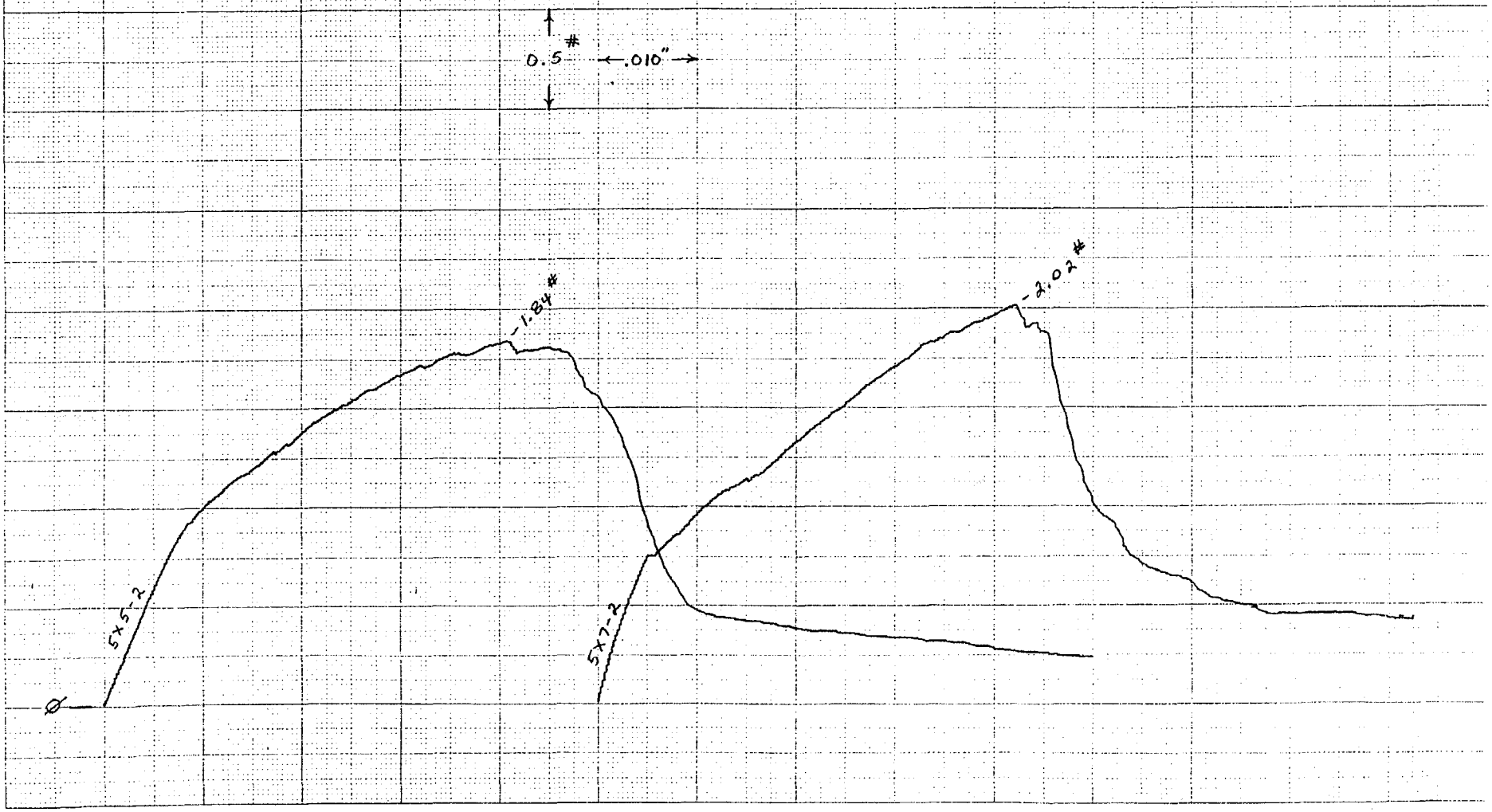

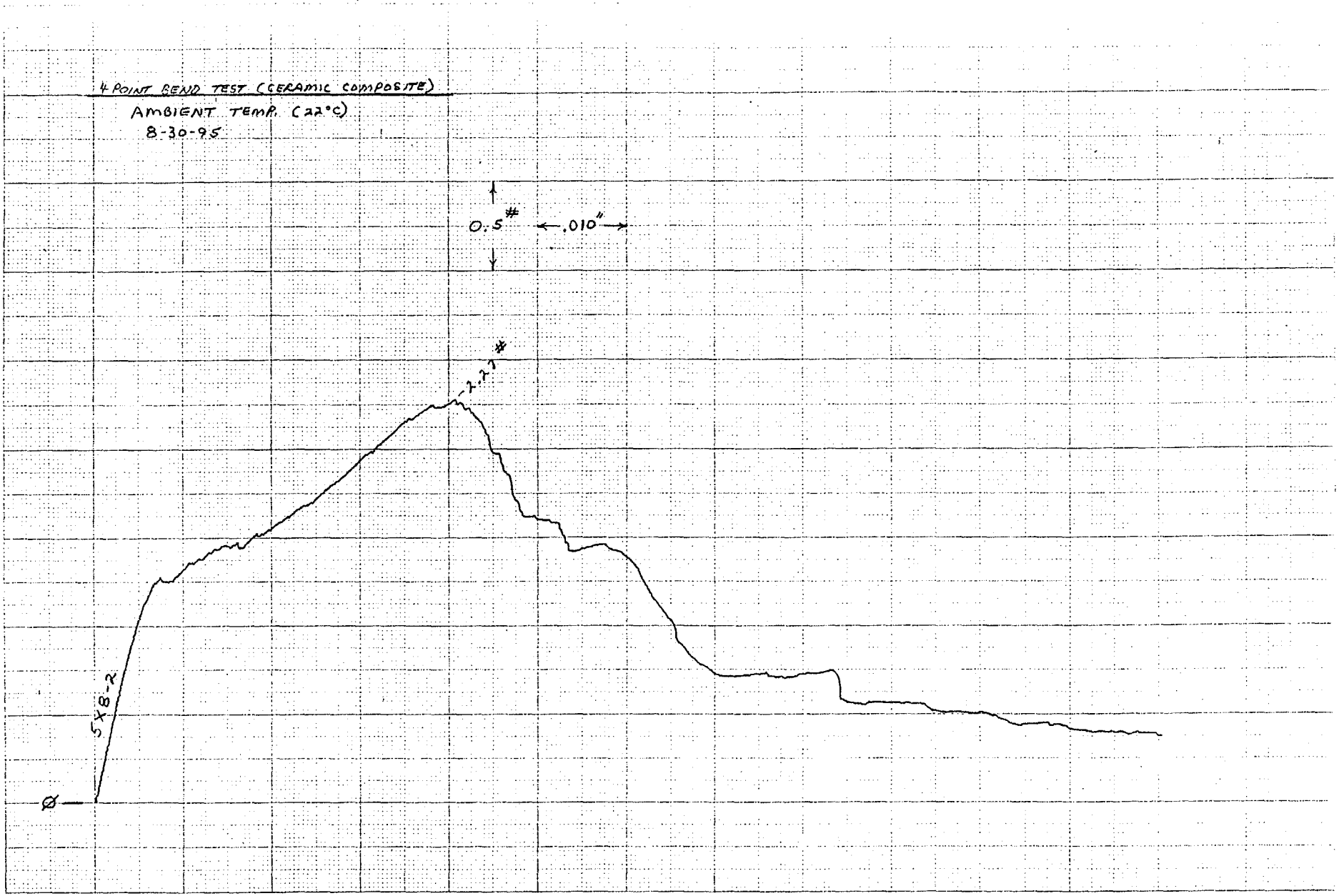
4 POINT BEND TEST (CERAMIC COMPOSITE)
AMBIENT TEMP. (22°C)
8-30-95
0.5 #
.010"
7.7 #
5X8-2
Ø

Load-Deflection Curves for CMCs fabricated from Candidate Fiber Architecture #6.

4 POINT BEND TEST (CERAMIC COMPOSITE)

AMBIENT TEMP. (22°C)

8-30-95

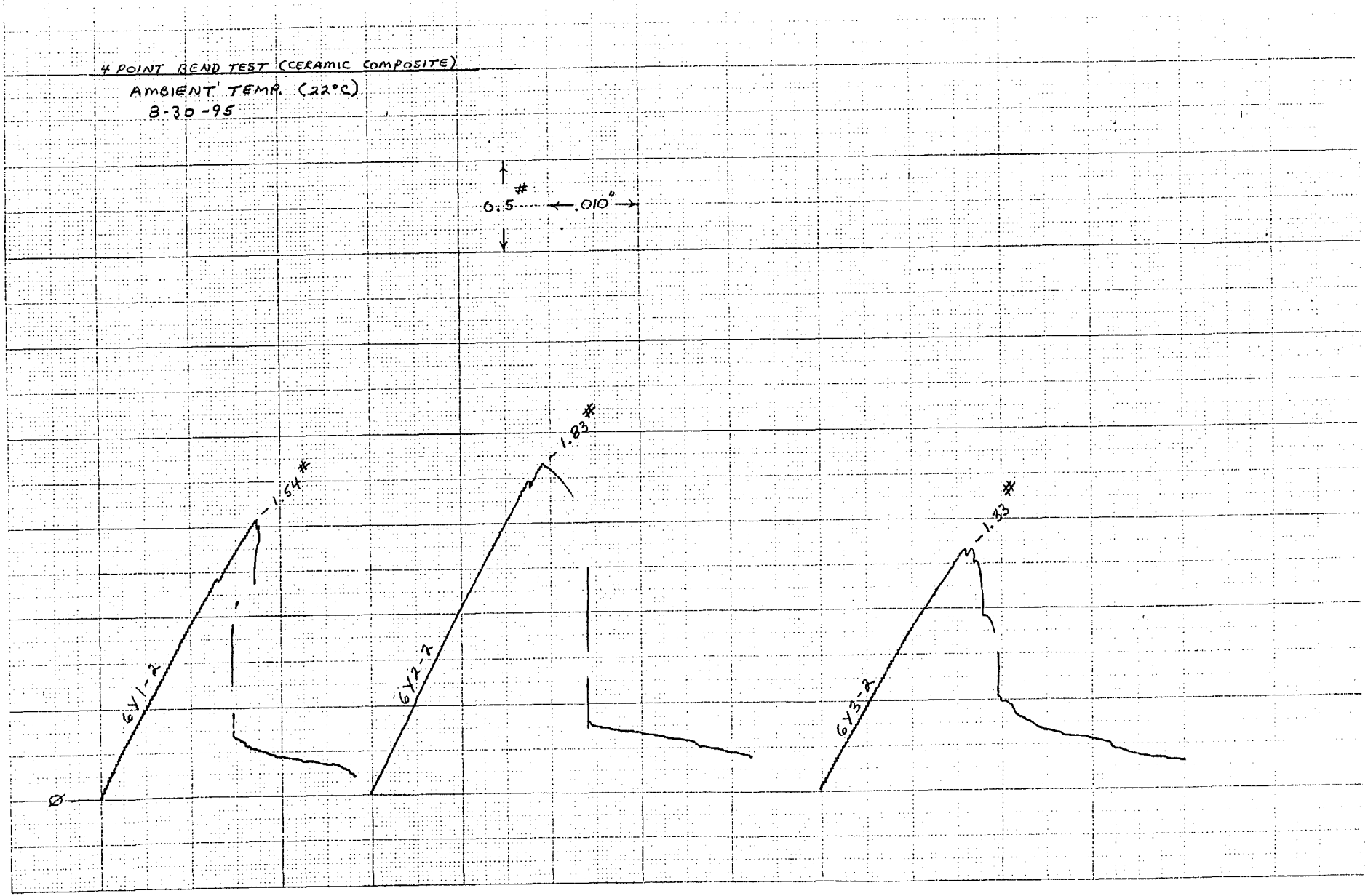

4 POINT BEND TEST (CERAMIC COMPOSITE)

AMBIENT TEMP. (22°C)

8-30-95

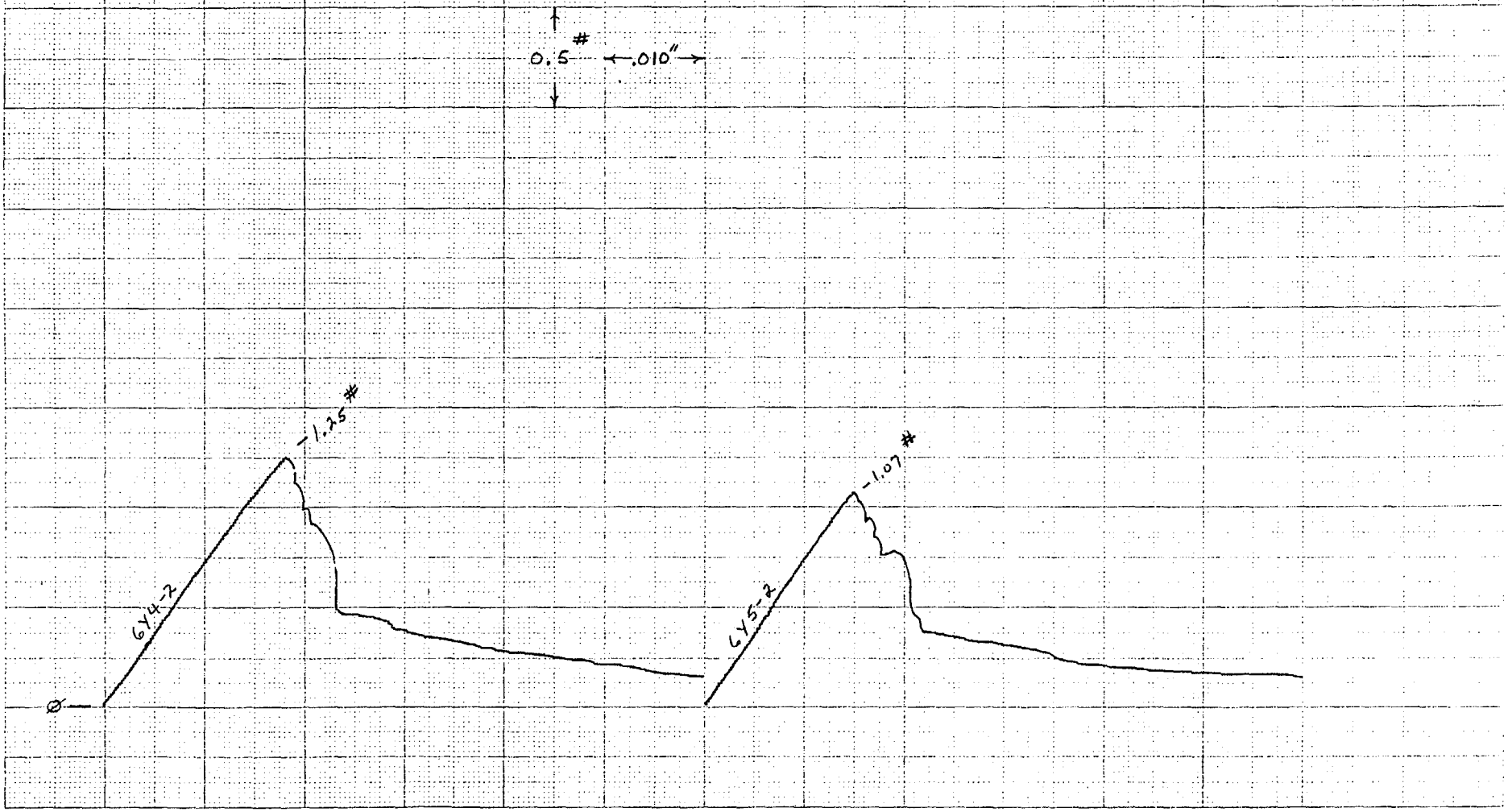

4 POINT BEND TEST (CERAMIC COMPOSITE)

AMBIENT TEMP (22°C)

8-30-95

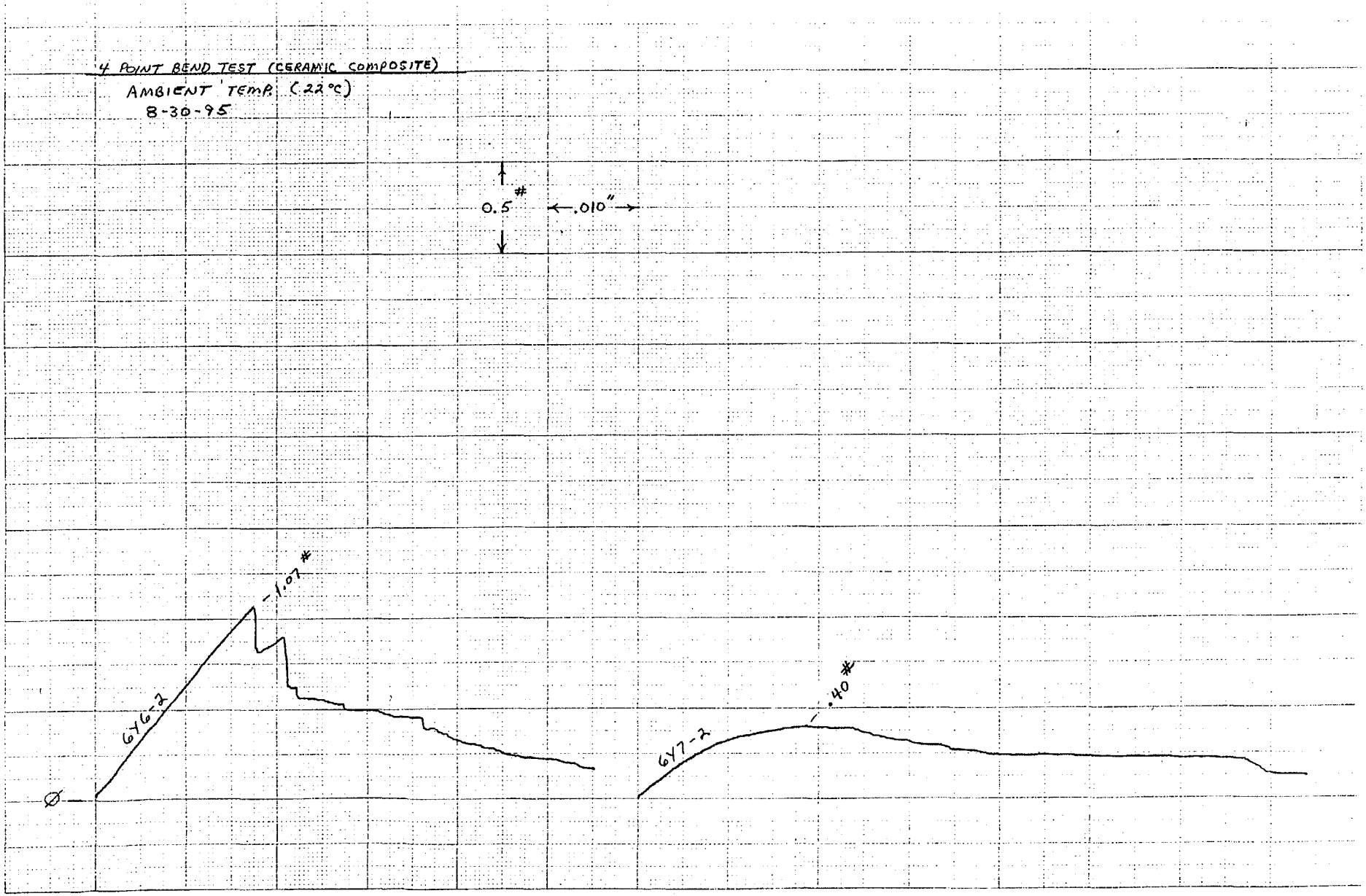

Load-Deflection Curves for CMCs fabricated from Candidate Fiber Architecture #7.

1

7X 97C3 HGFIL-37 WS 68076

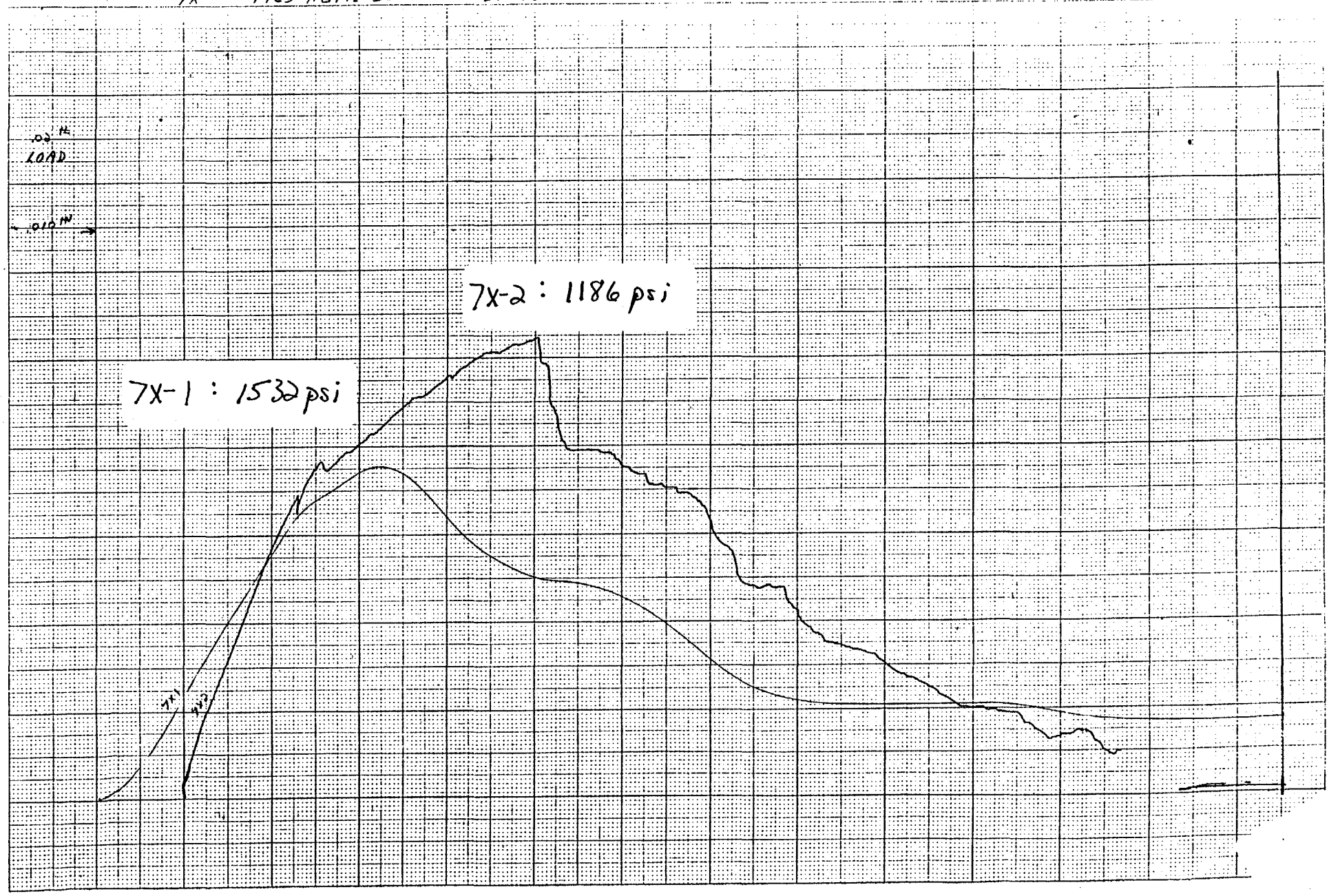

7X-3

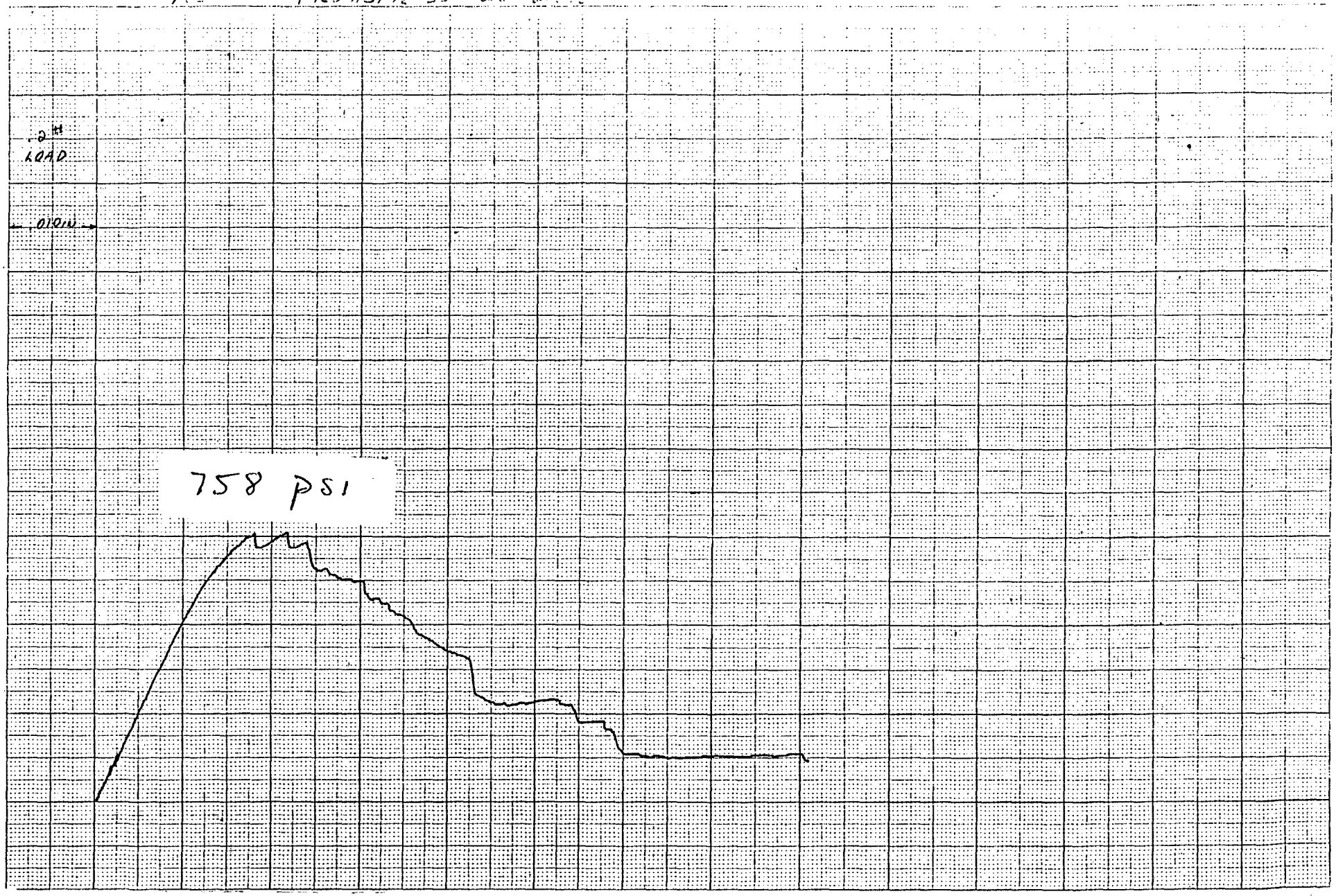

7X-4

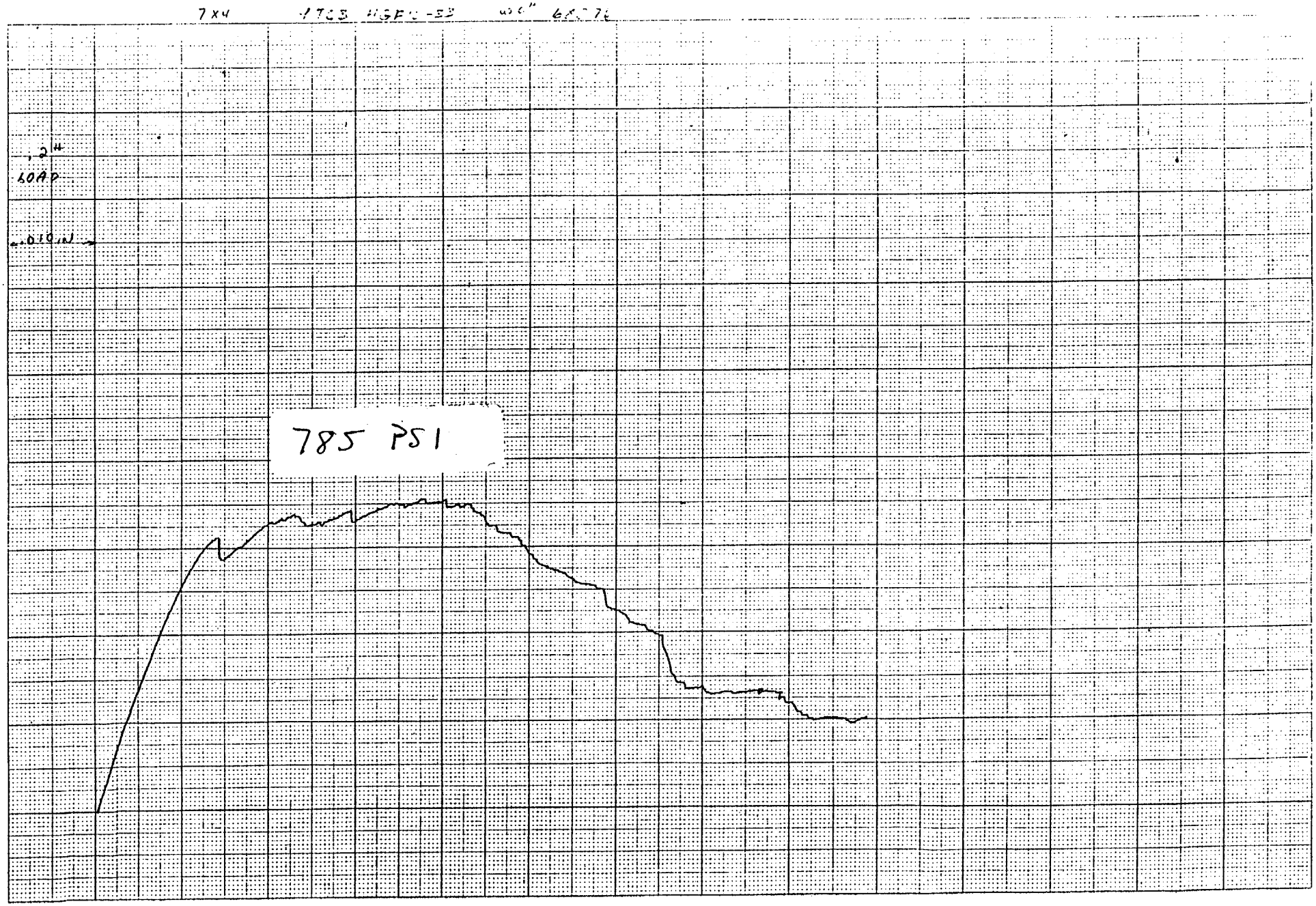

7X-5

7-28-95 7X5 97C NGFIL-33 WO# 6207

.2

.010 IN

806 PSI

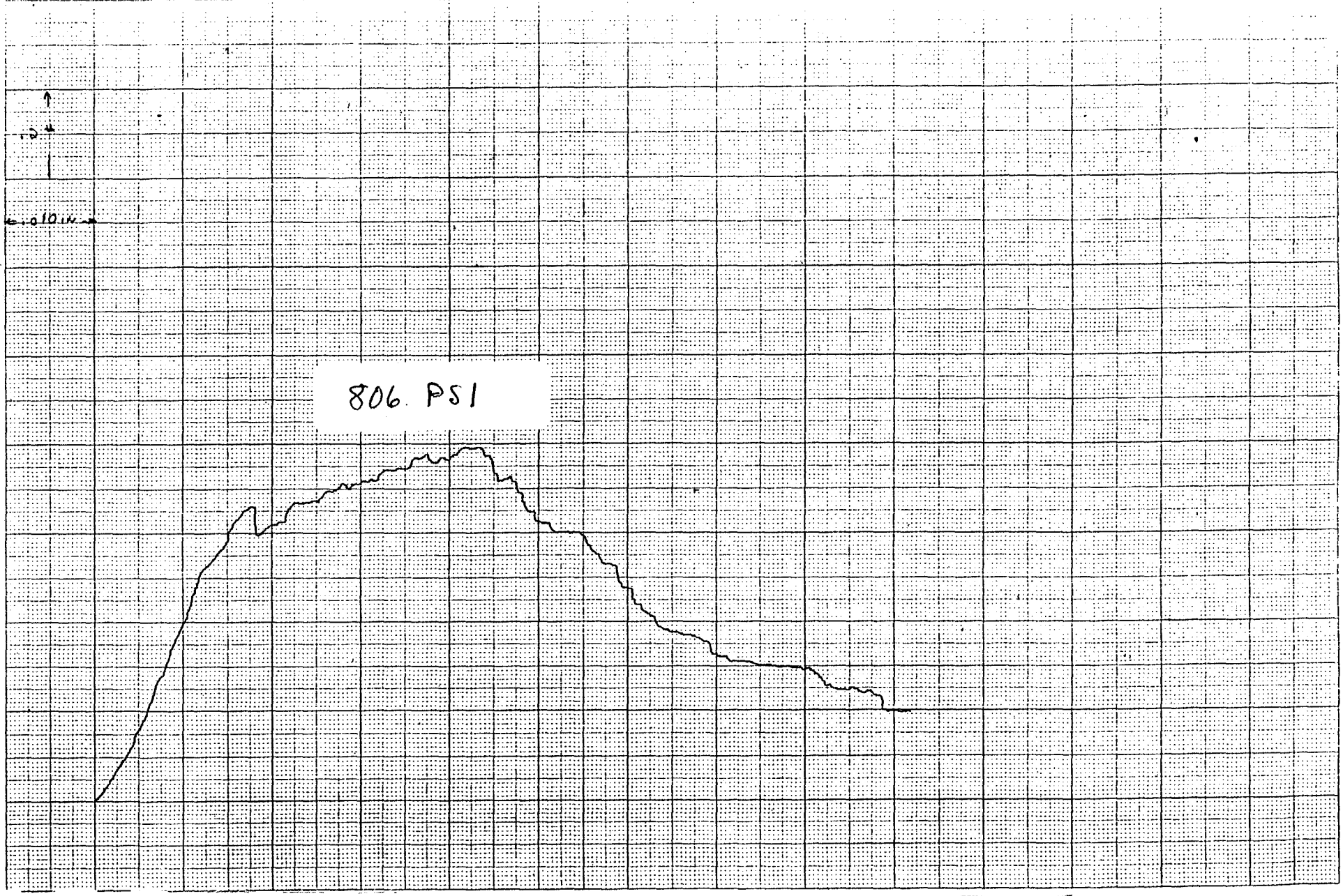

7X-6

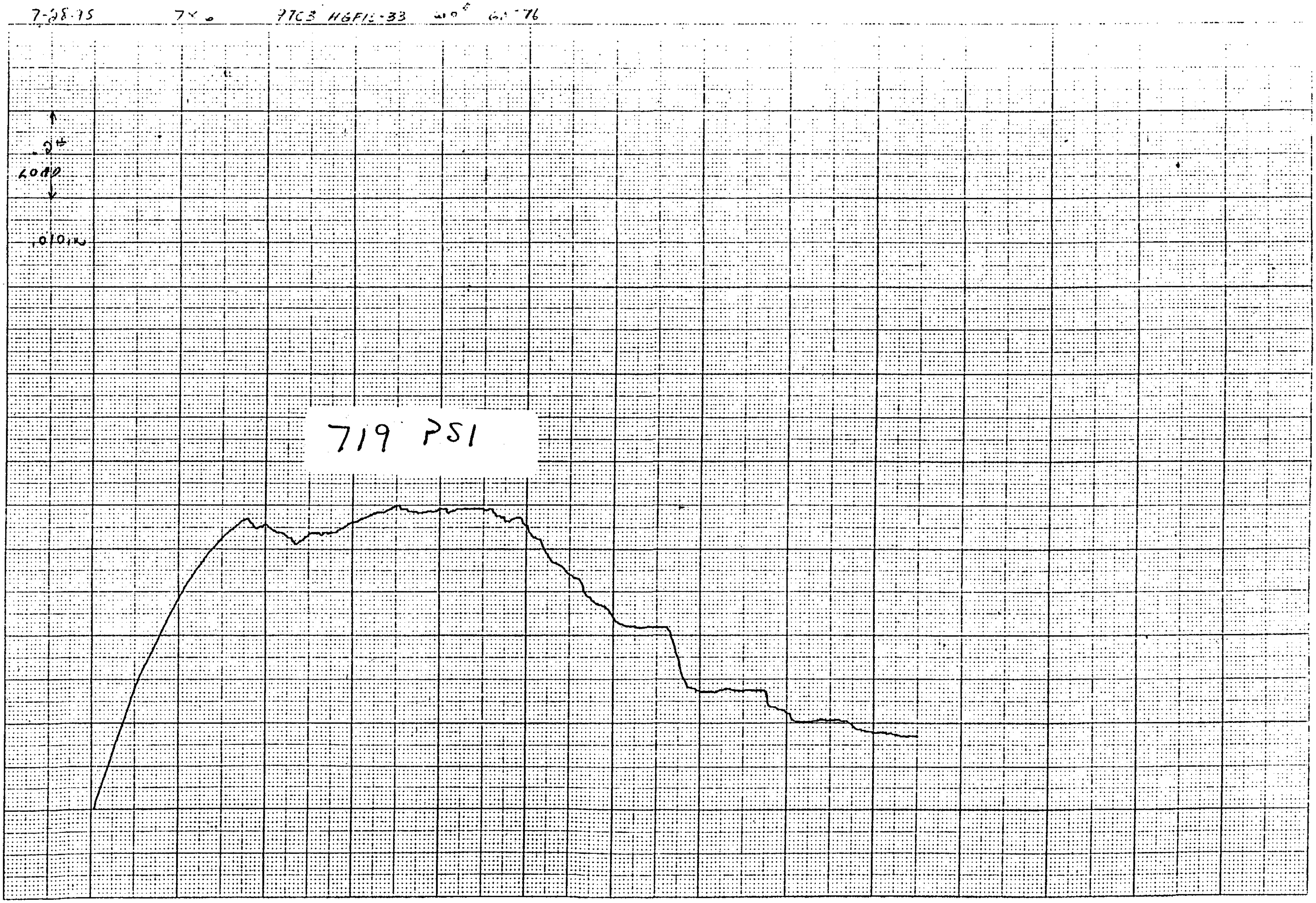

7X-7

7-27-93 7X- 9763 HGF1L-33 WO# 48276

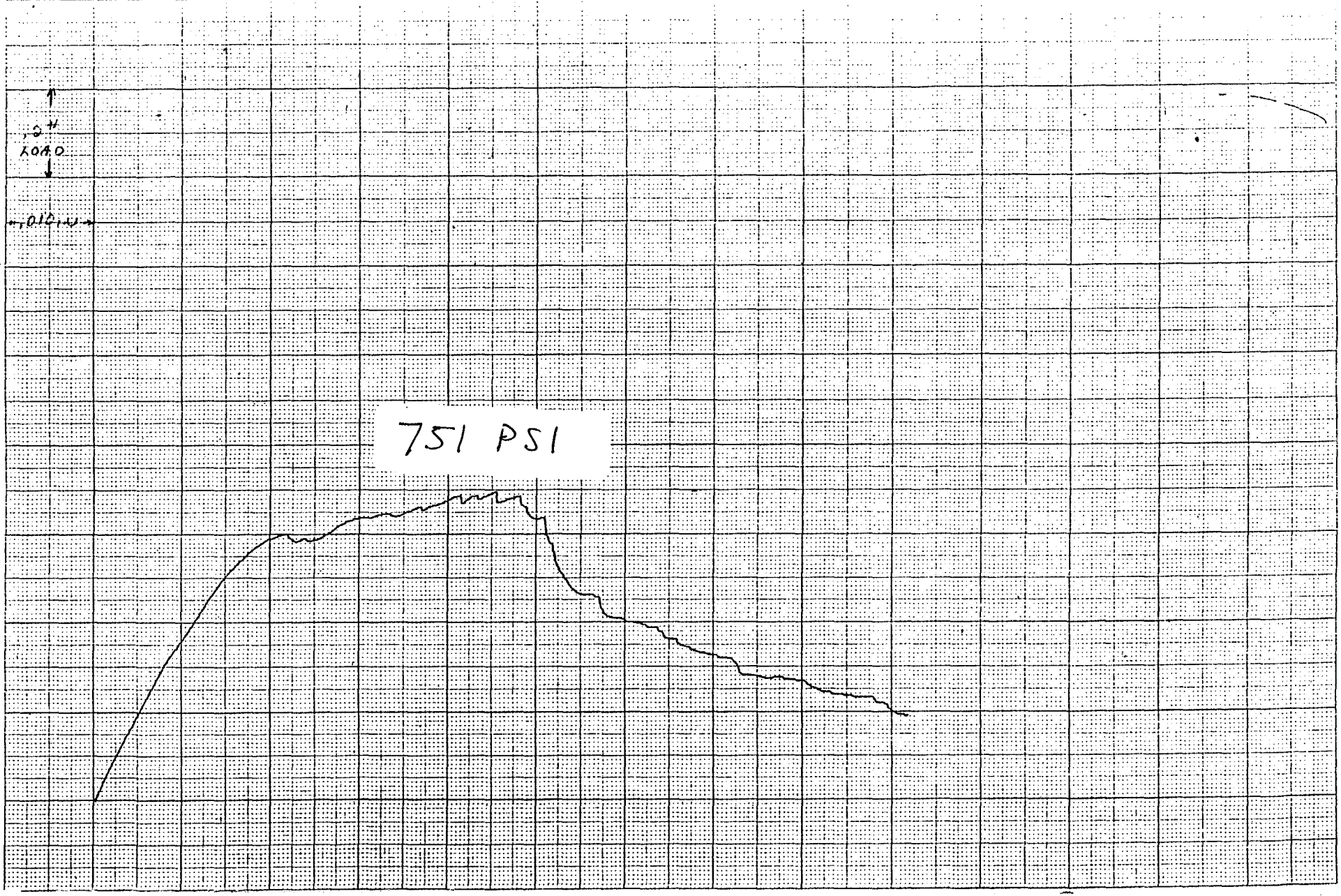

7X-8

7-28-95 7X8 9753 HGF1L-32 WO# 28076

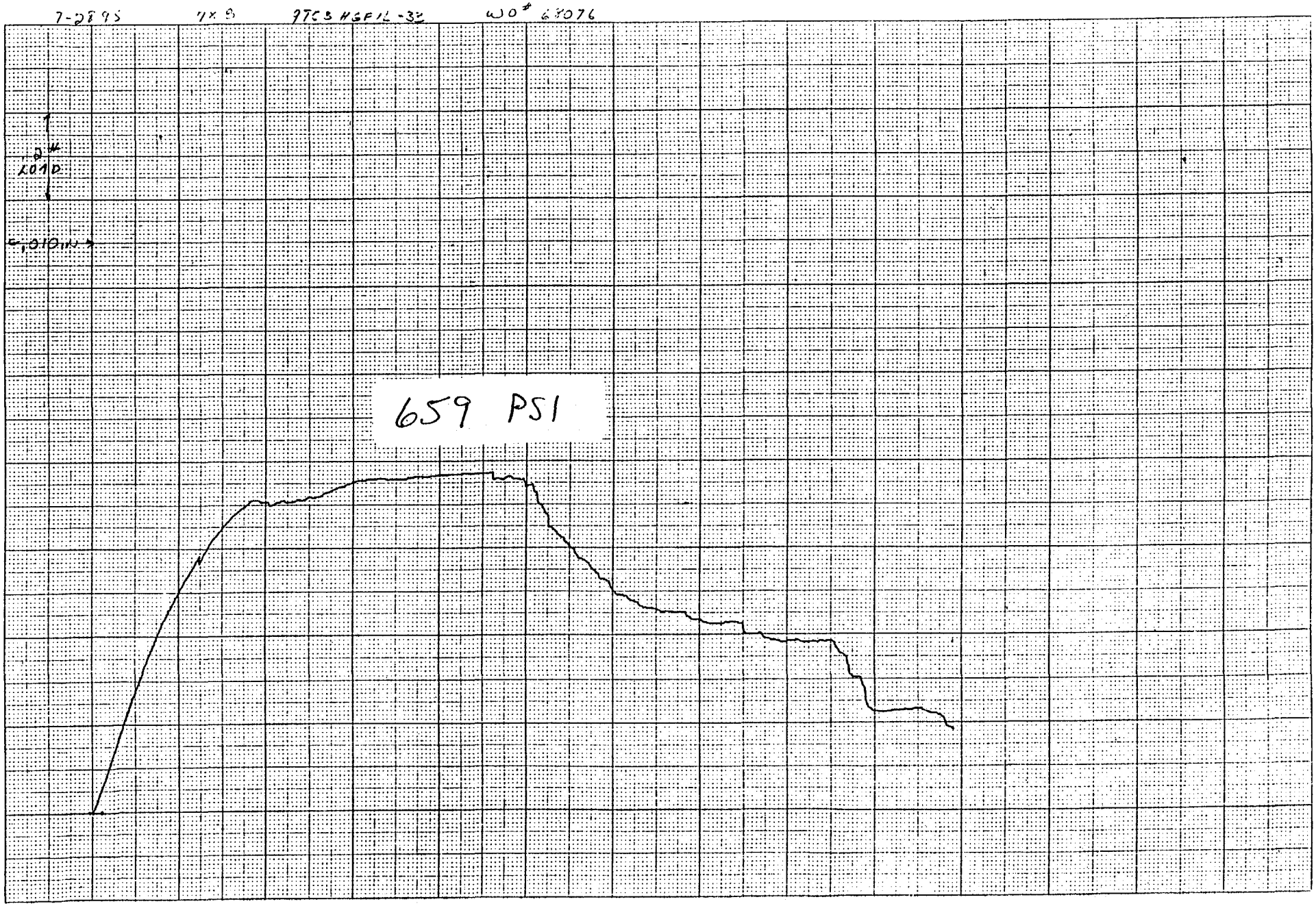

IX-1

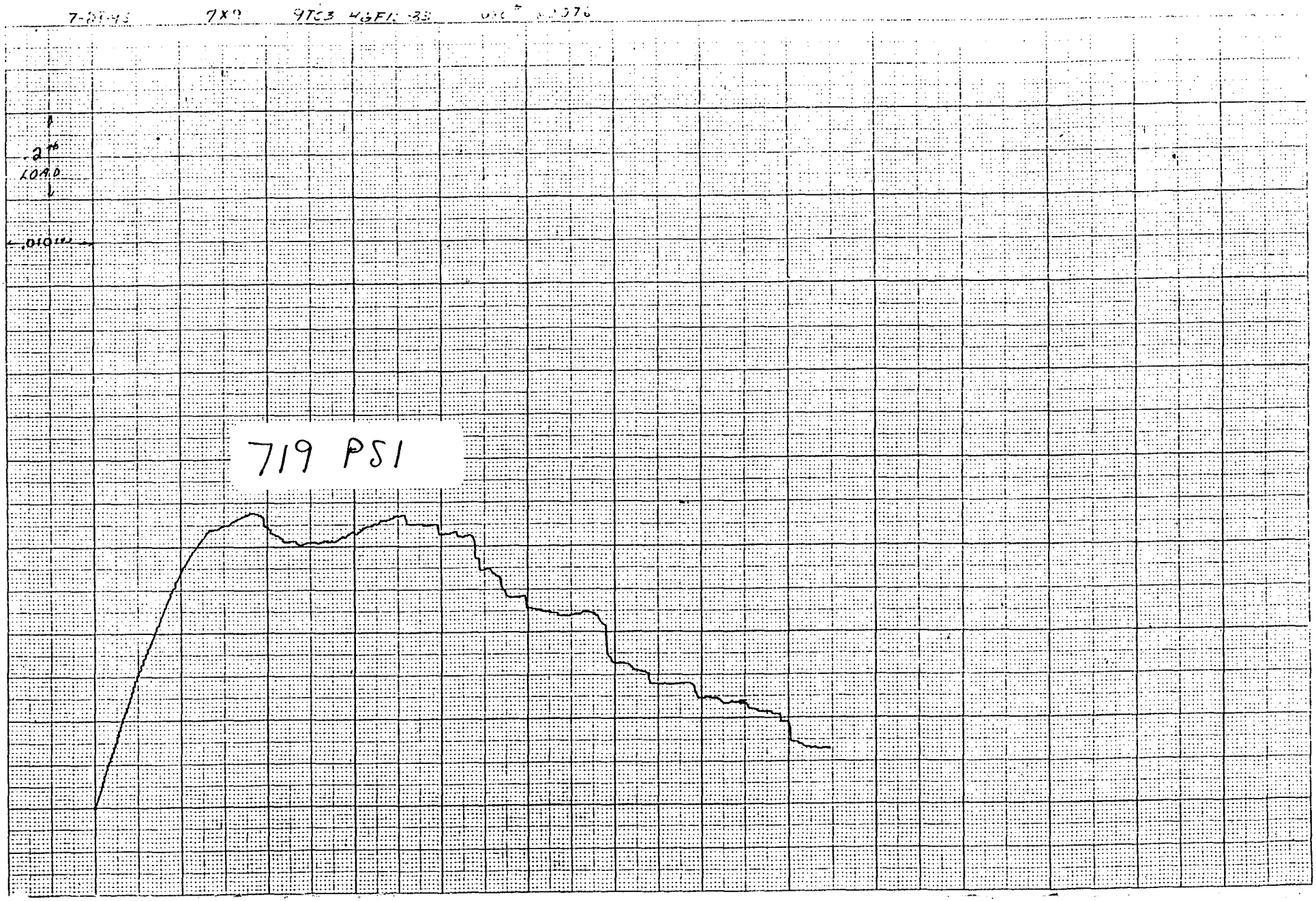

7x-10

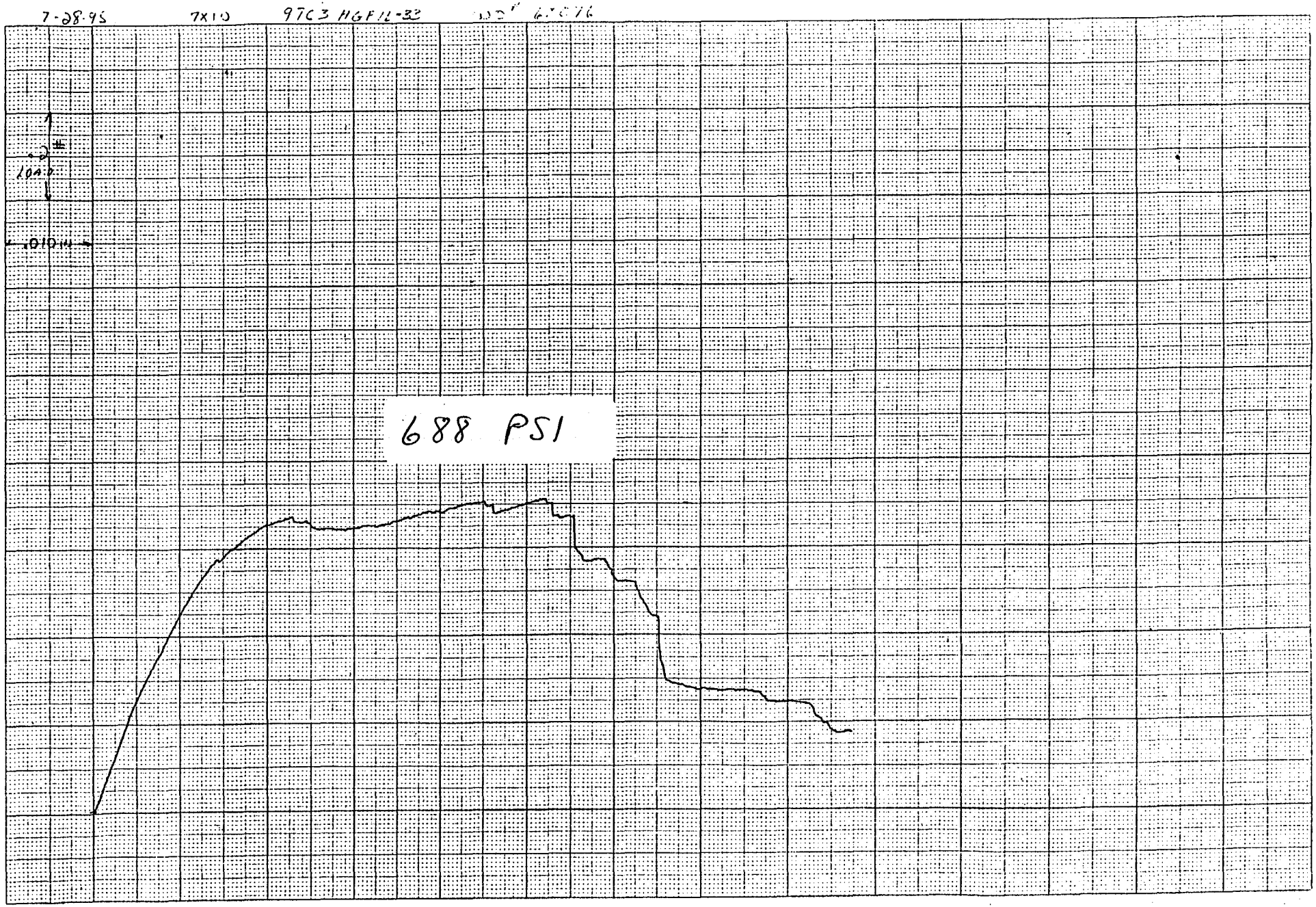

IX - 11

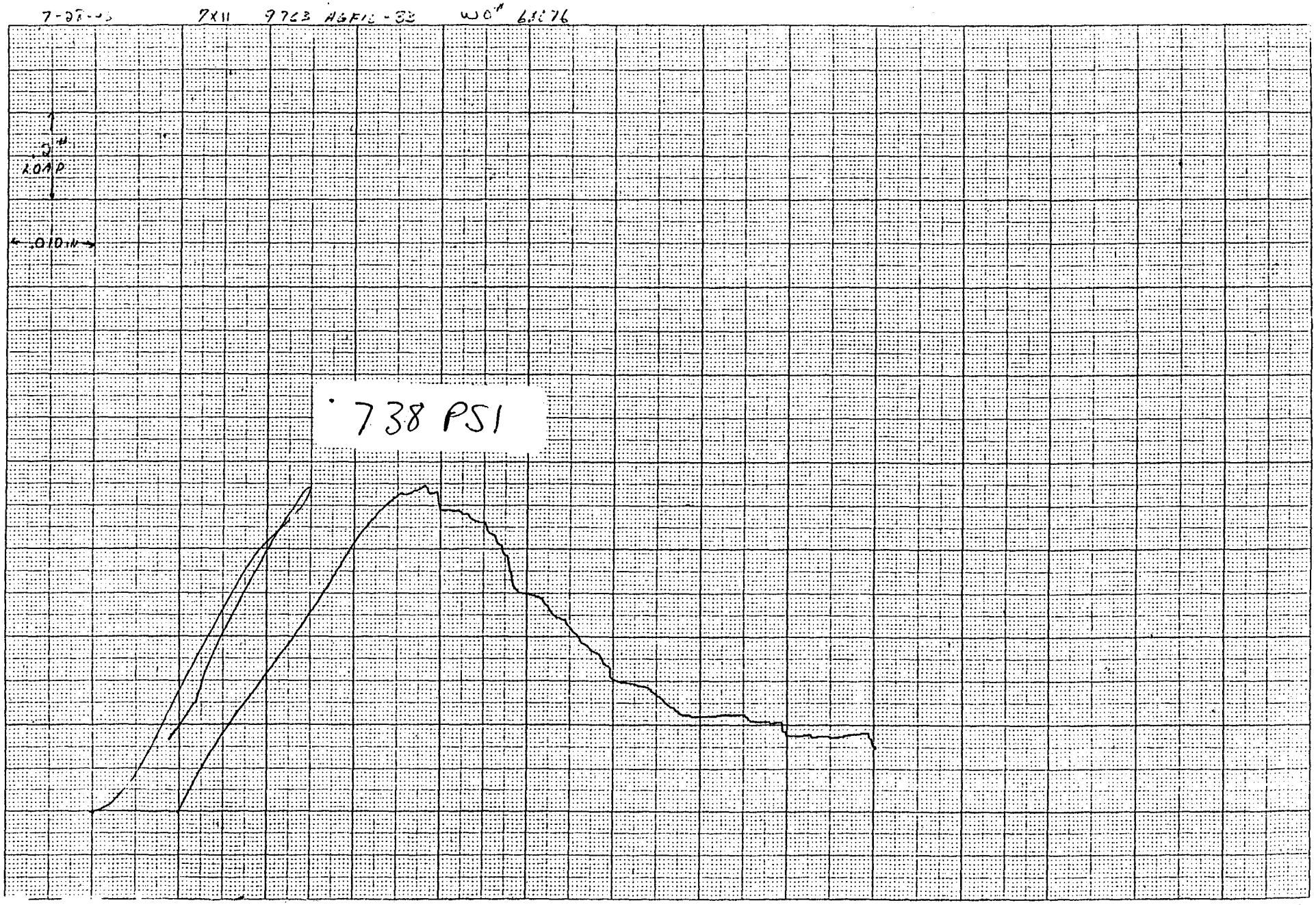

7-22-05 7x12 9763 WC# 68076

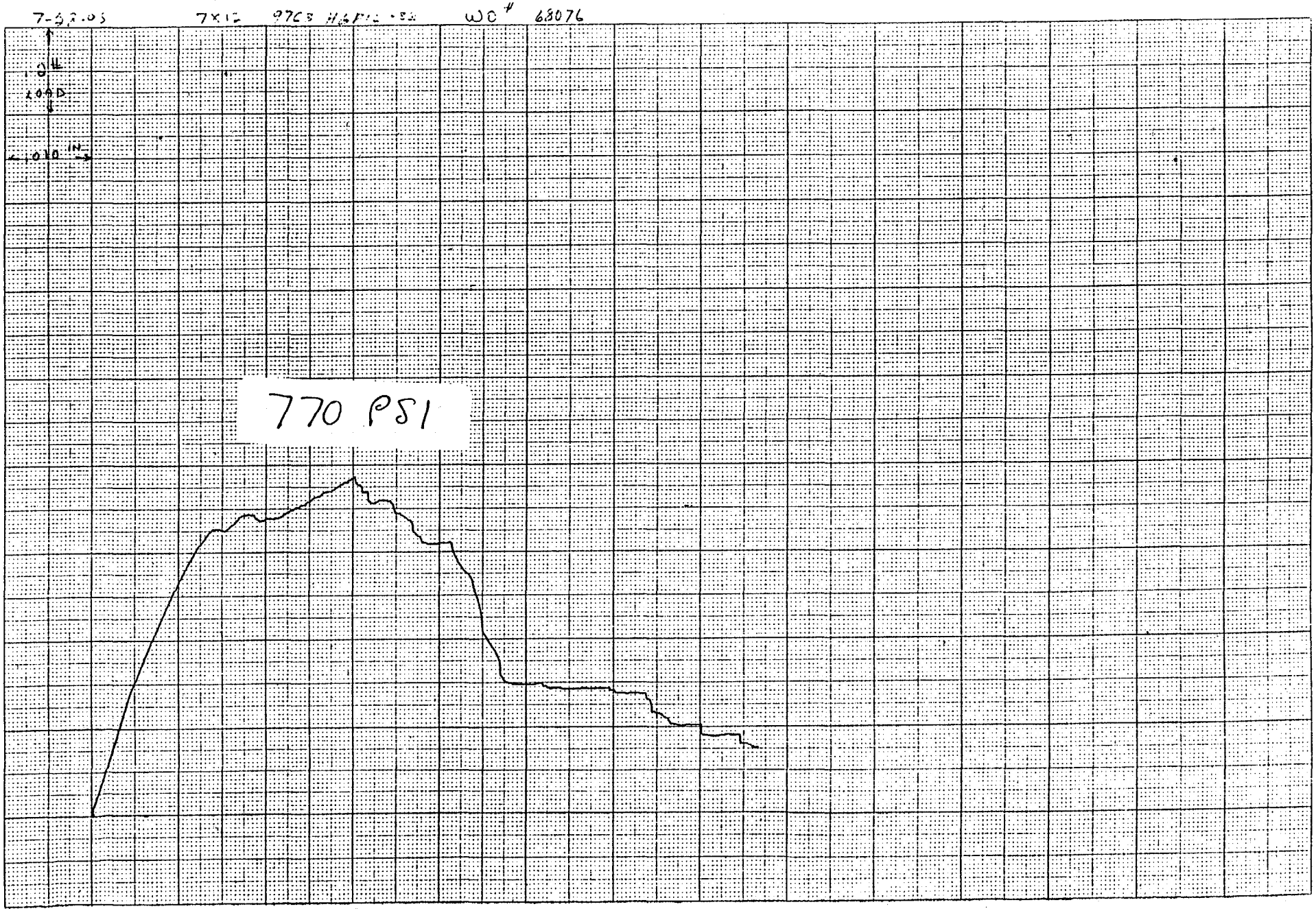

7-28-95 14- 9703 HGF11-33 WO# 68076

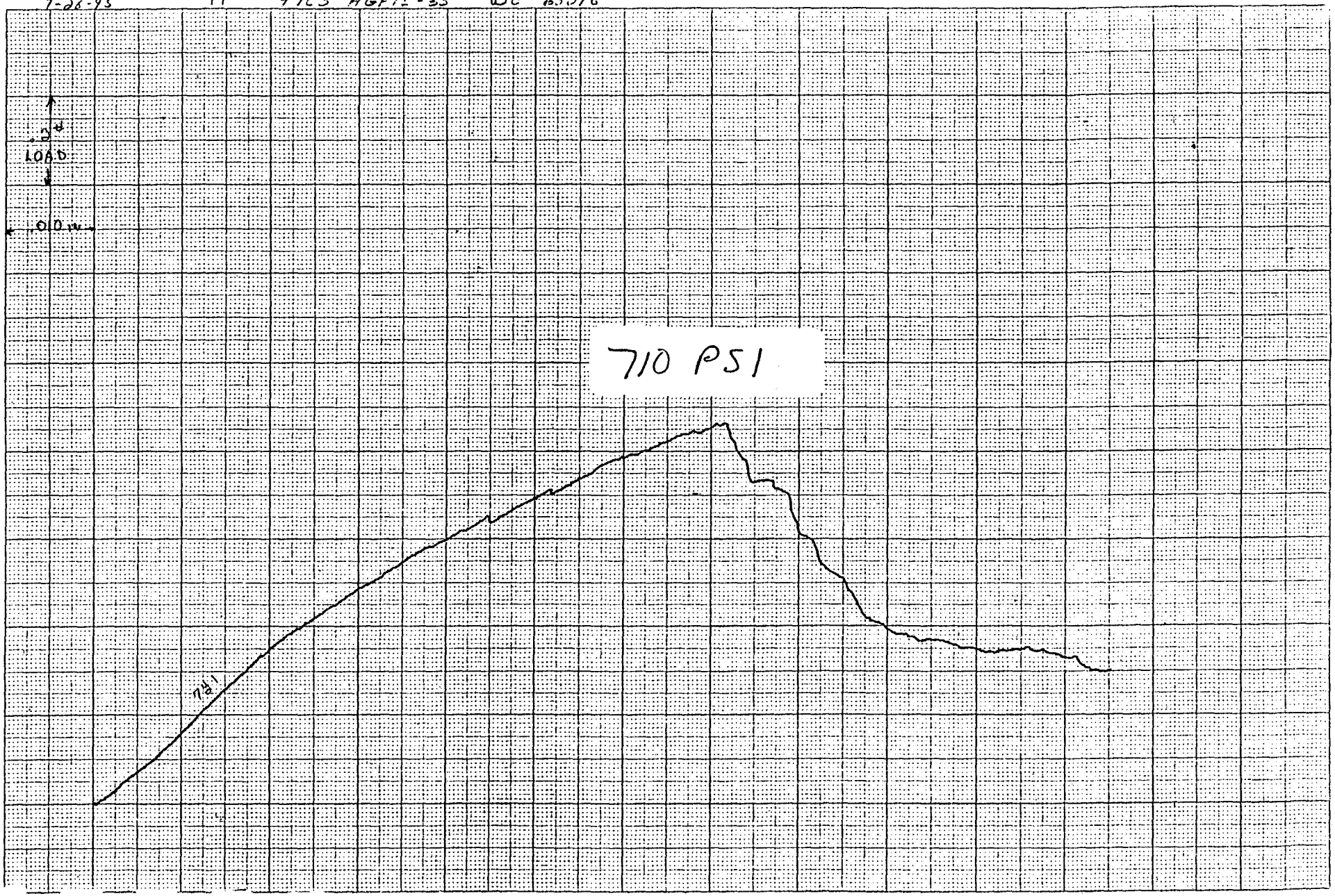

7Y-2

7-25-92 9763 HGFIL-3S

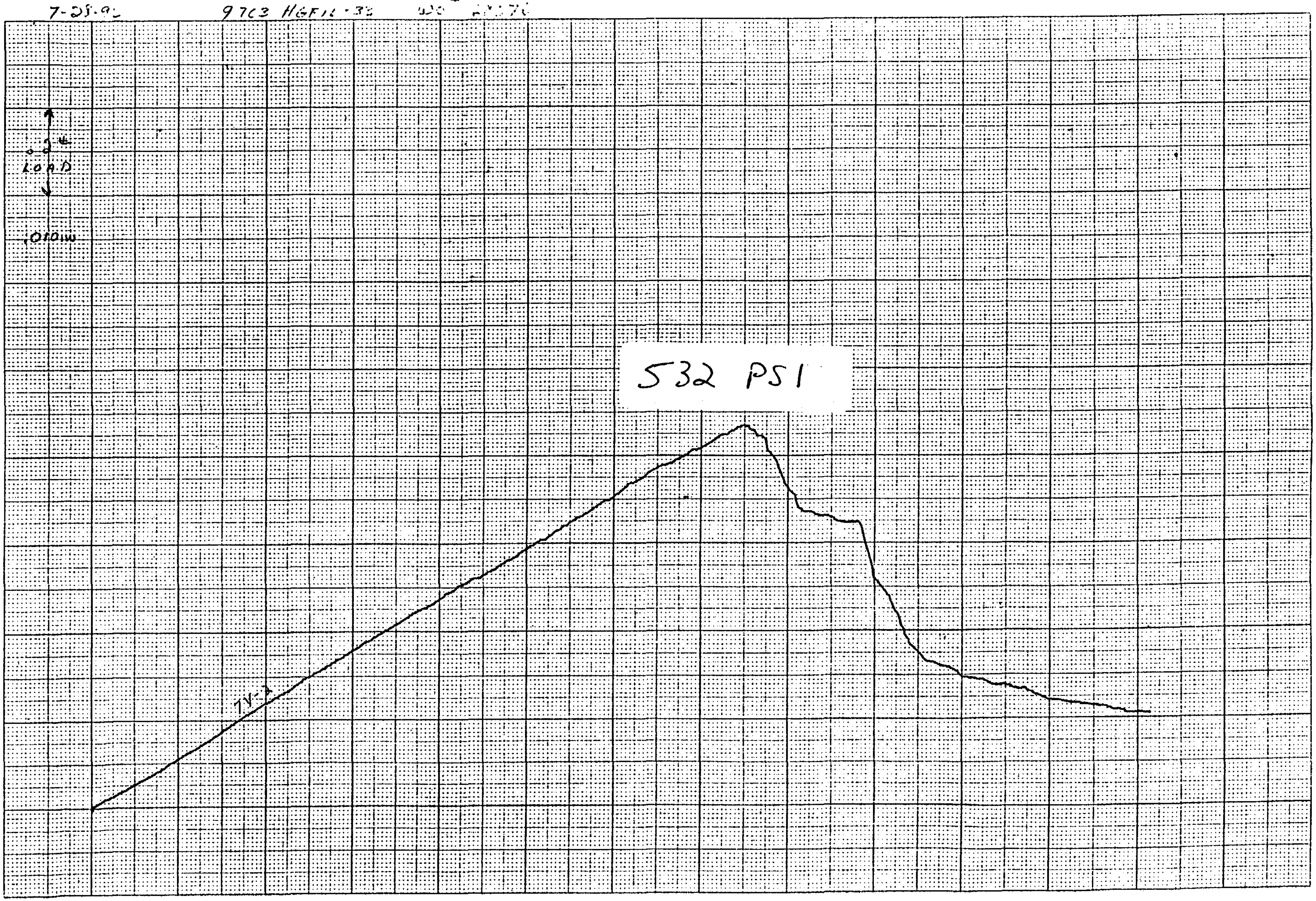

1Y-5

7-28-95 97C3116F12 -3% WO# 68076

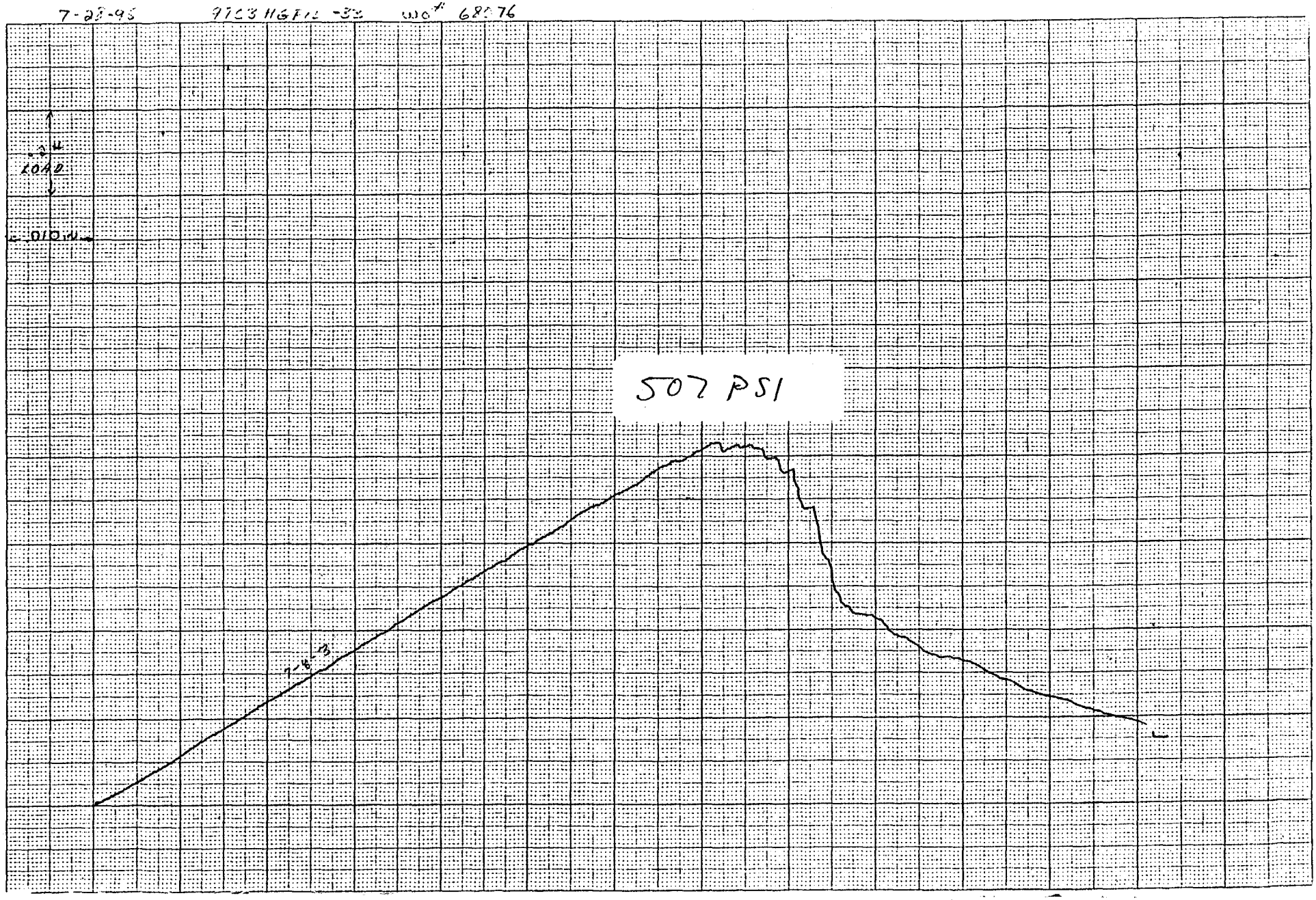

74-4

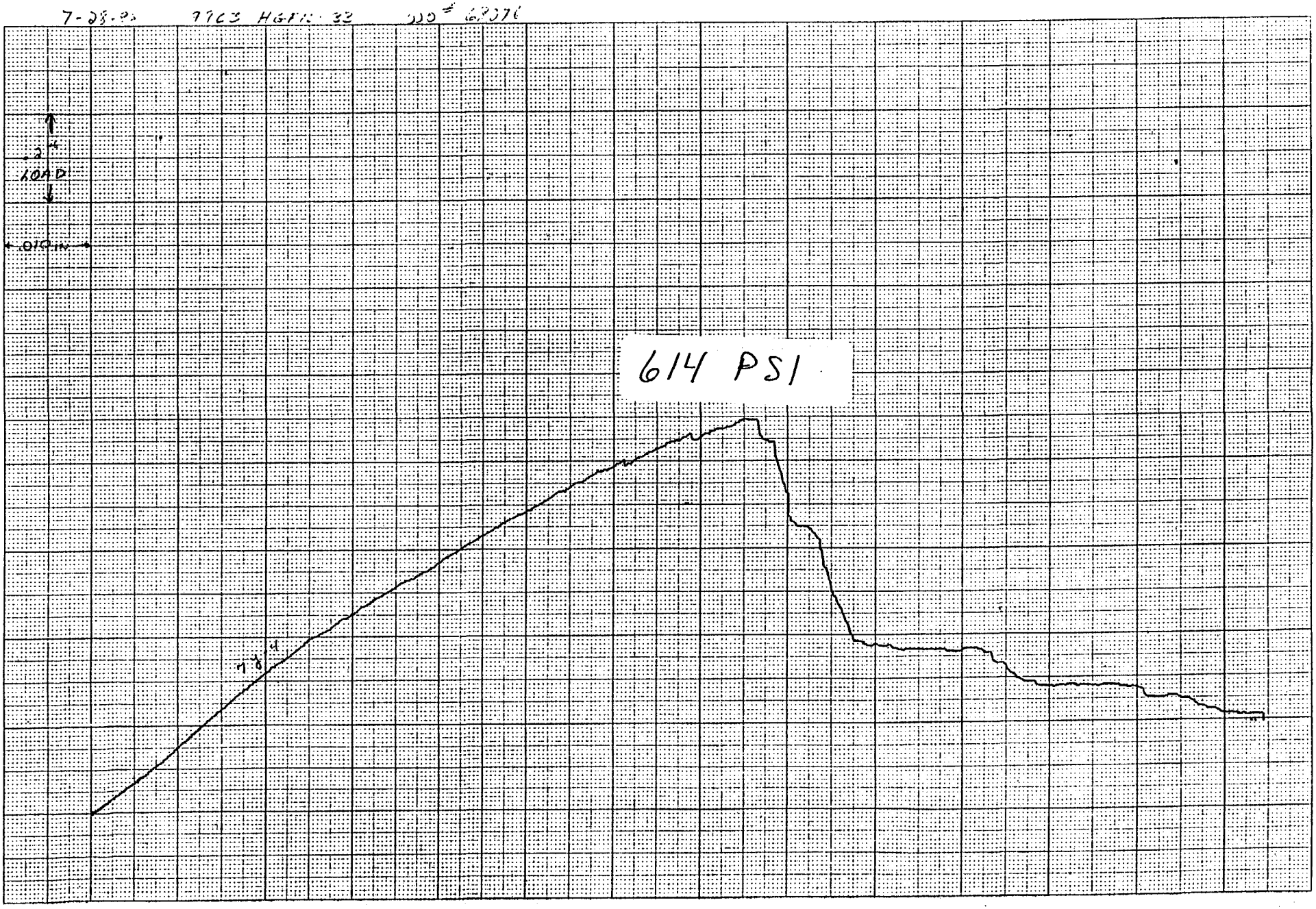

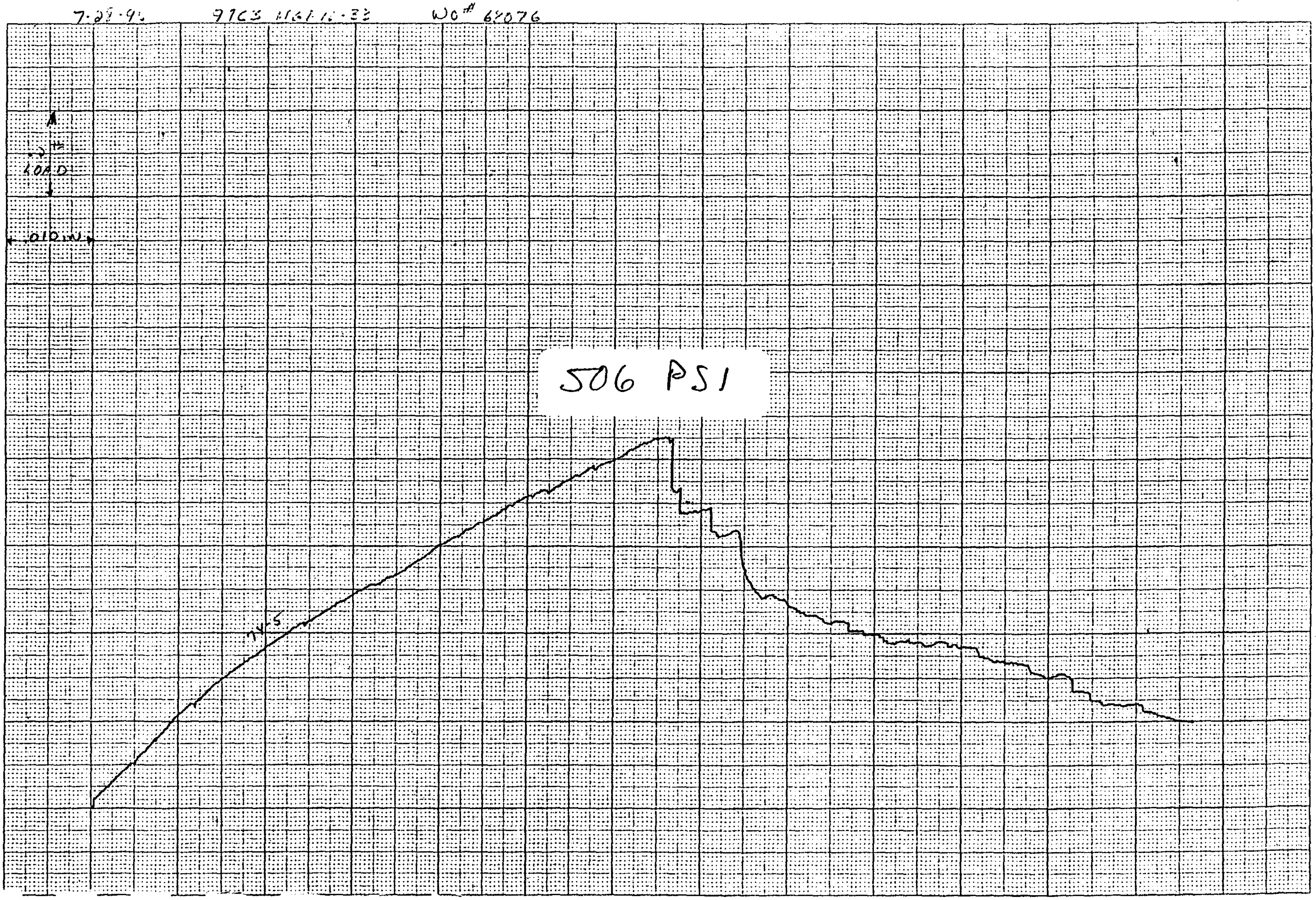
LOAD
.010 IN
506 PSI

1

7Y-6

7-28-95 7Y-6 97C3 HGFIL-33 WO# 63076

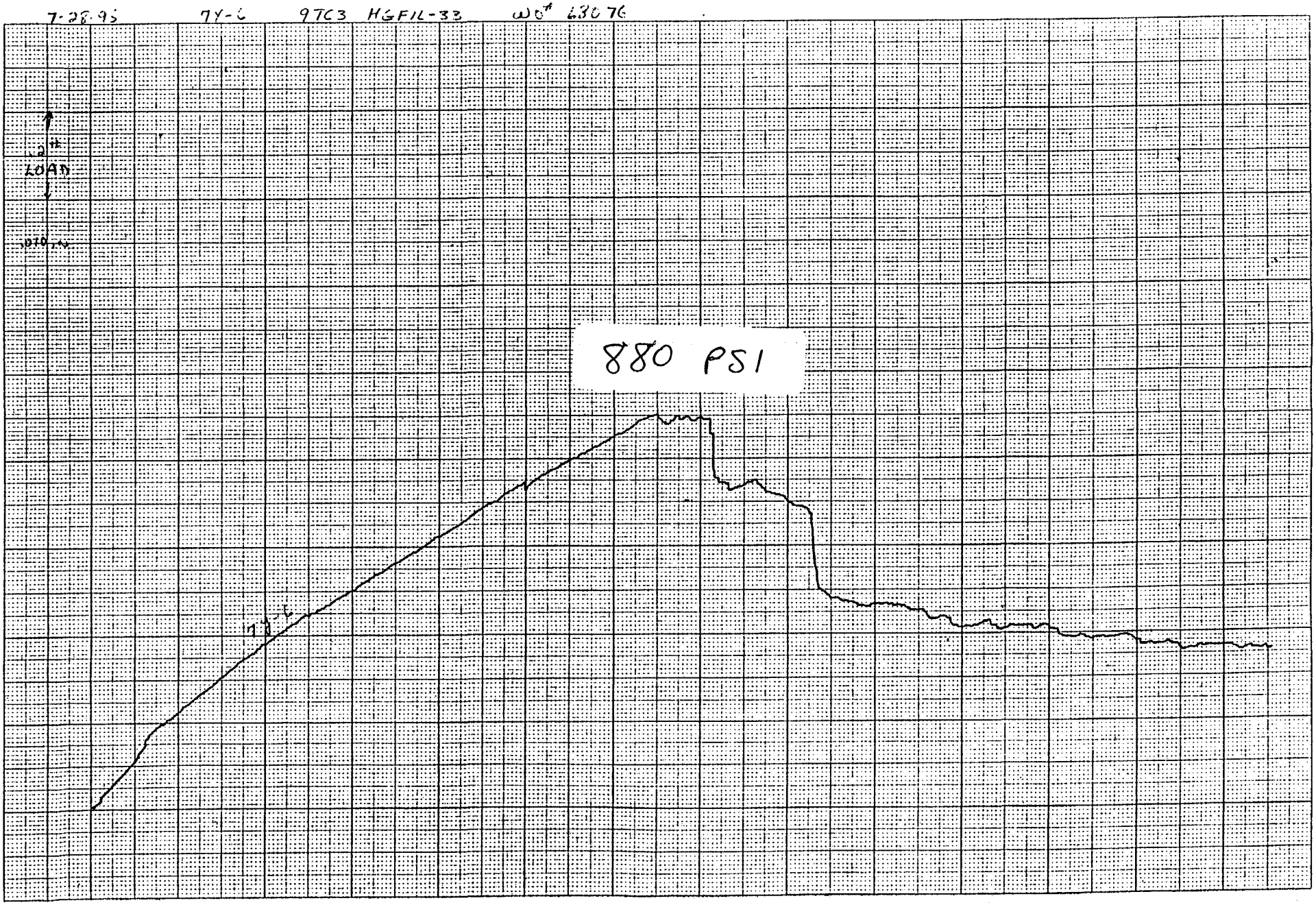

Load-Deflection Curves for CMCs fabricated from Candidate Fiber Architecture #8.

8X-1

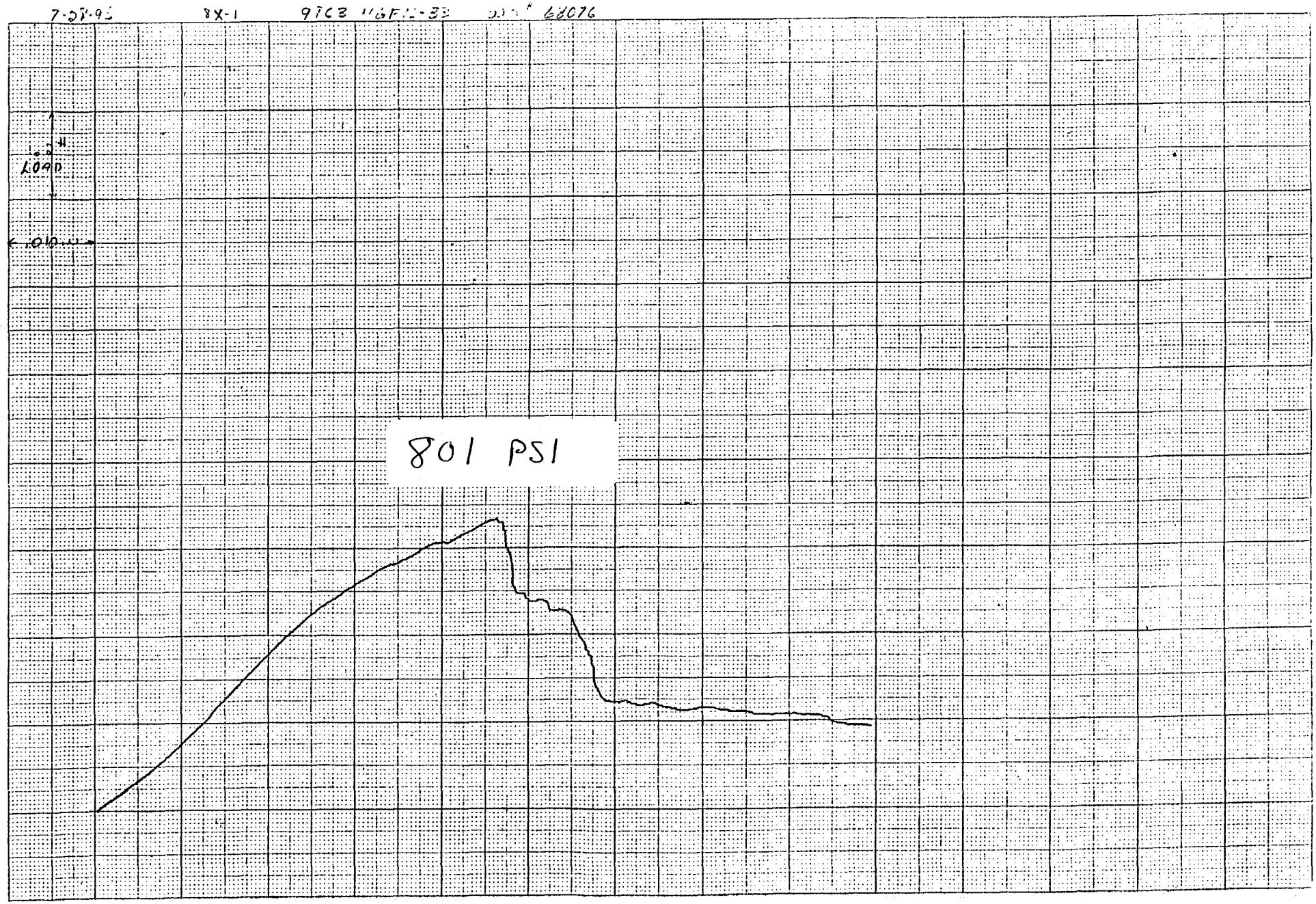

8X-2

1

7-28-95 8X-2 9703 HGP 1L-32 WO# 27370

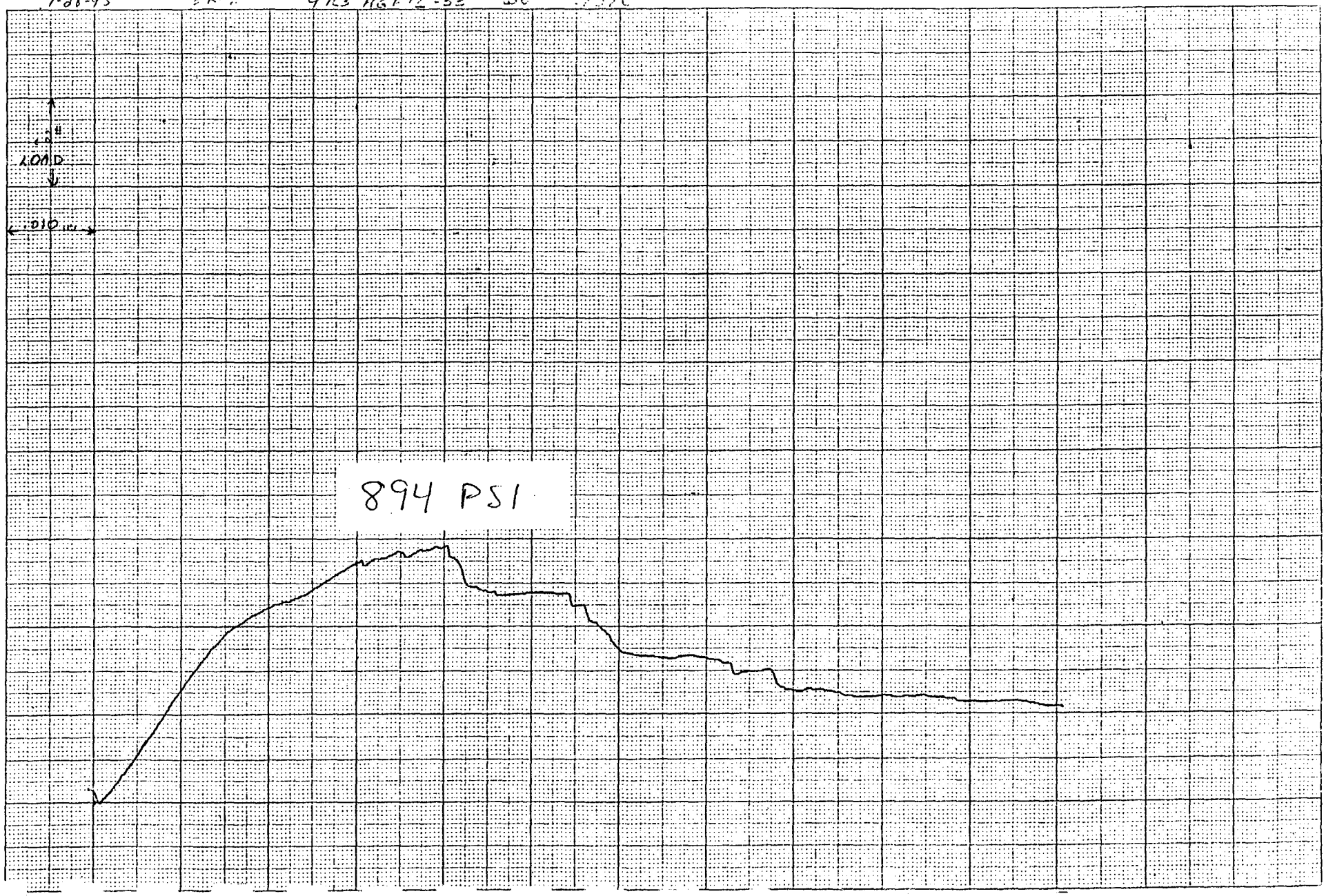

8X-5 TO 8X-10

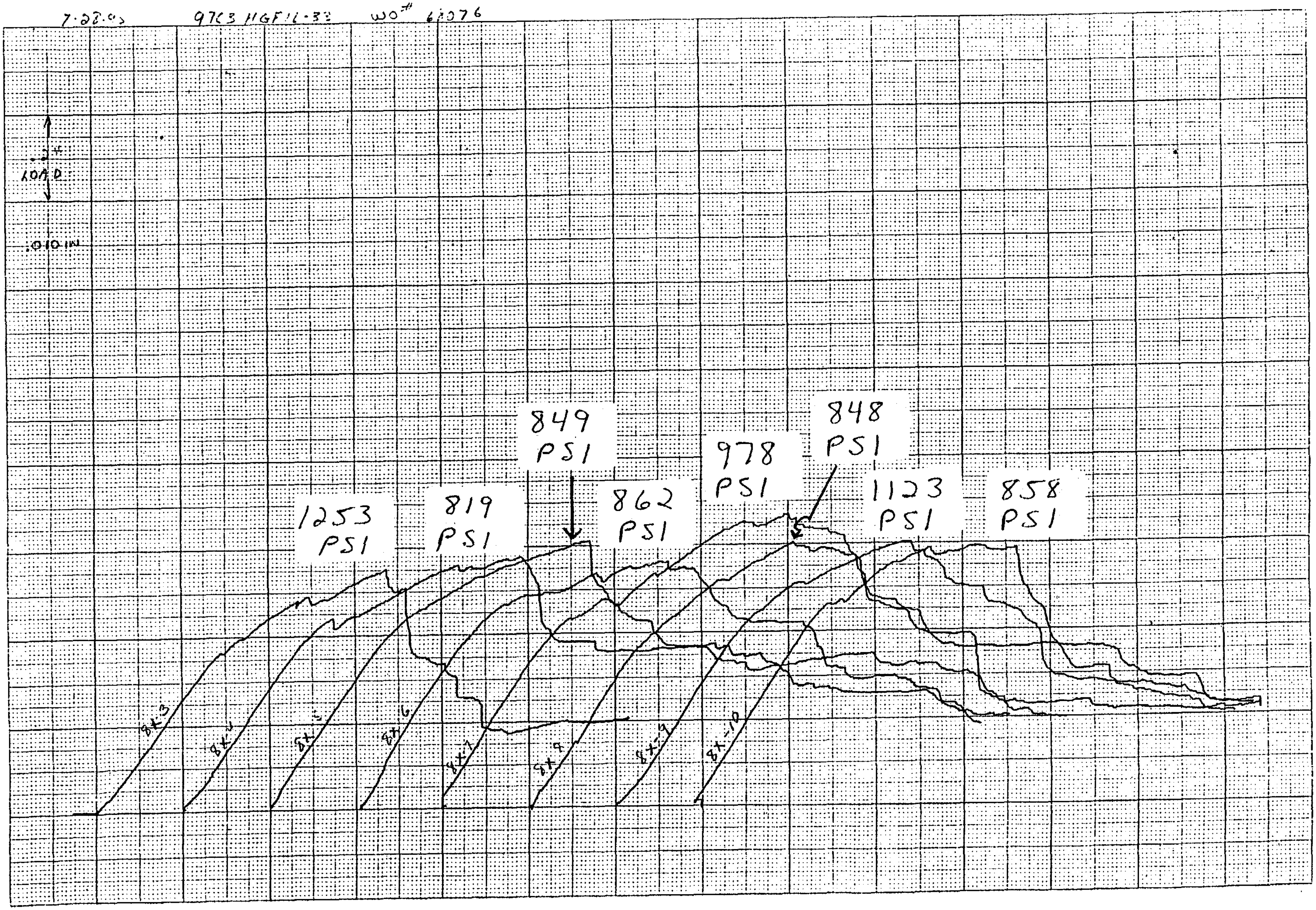

7-28-03
WO# 61076
LOAD
.010 IN
1253 PSI
819 PSI
849 PSI
862 PSI
978 PSI
848 PSI
1123 PSI
858 PSI
8X-10

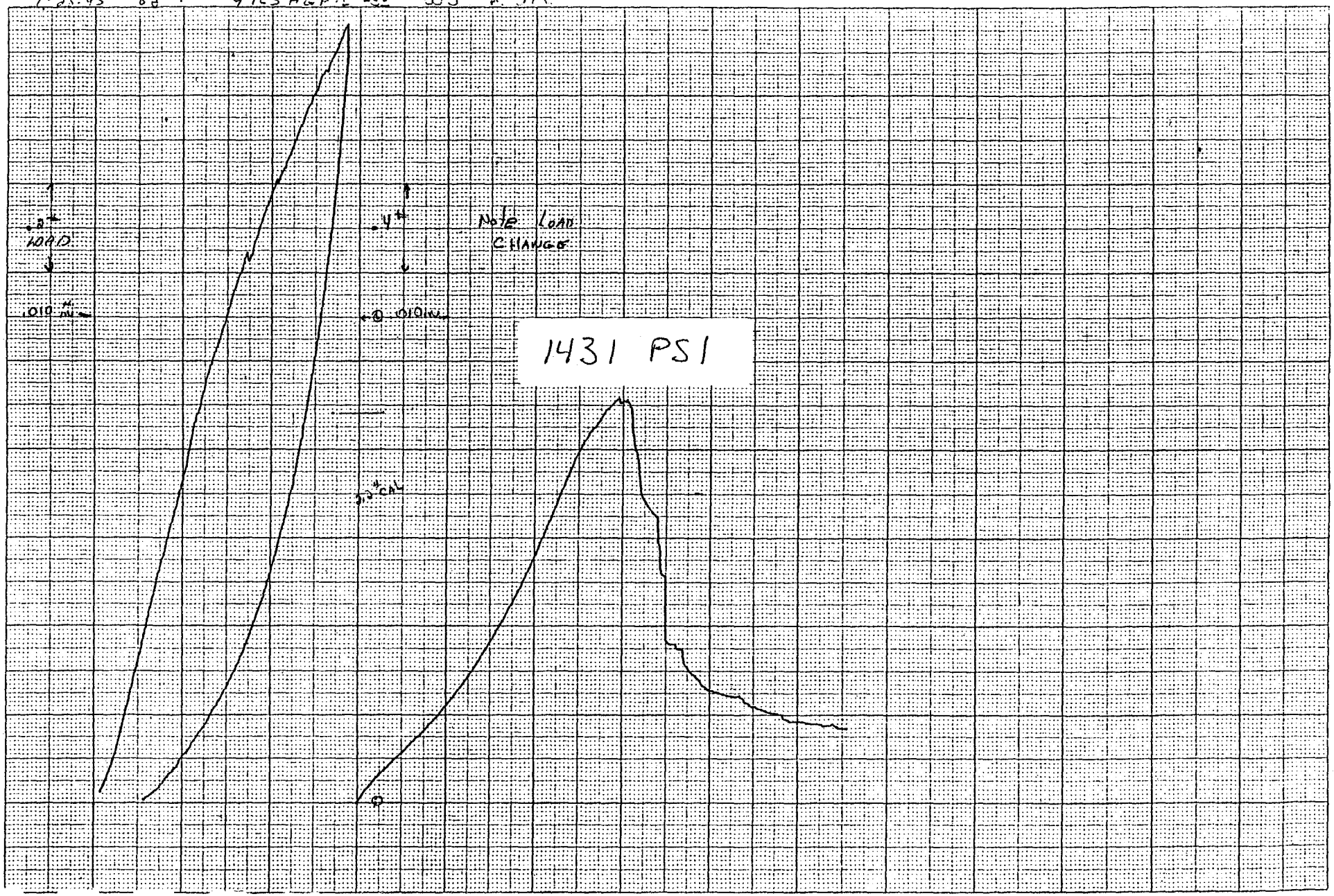
7-25-95 84-1
+a
LOAD
.010 in
+y
.010 in
Note Load
CHANGE
1431 PSI

8 1 - a

1

7-28-95 8 y-2 9763 HGFIL-3% WO# 68076

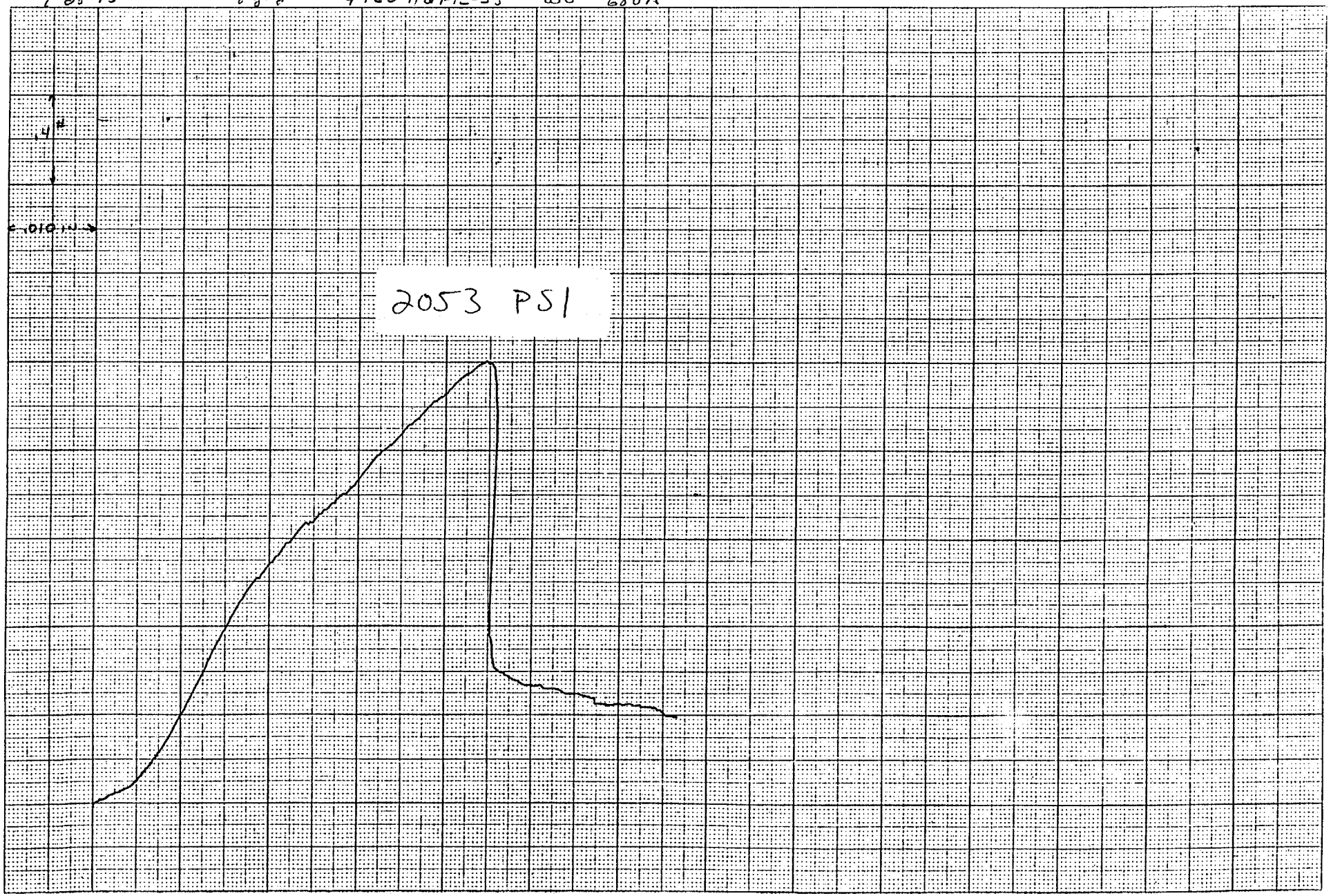

8I-3

1

7-28-92 8I-3 9703 Hill 11-33 WO# 22176

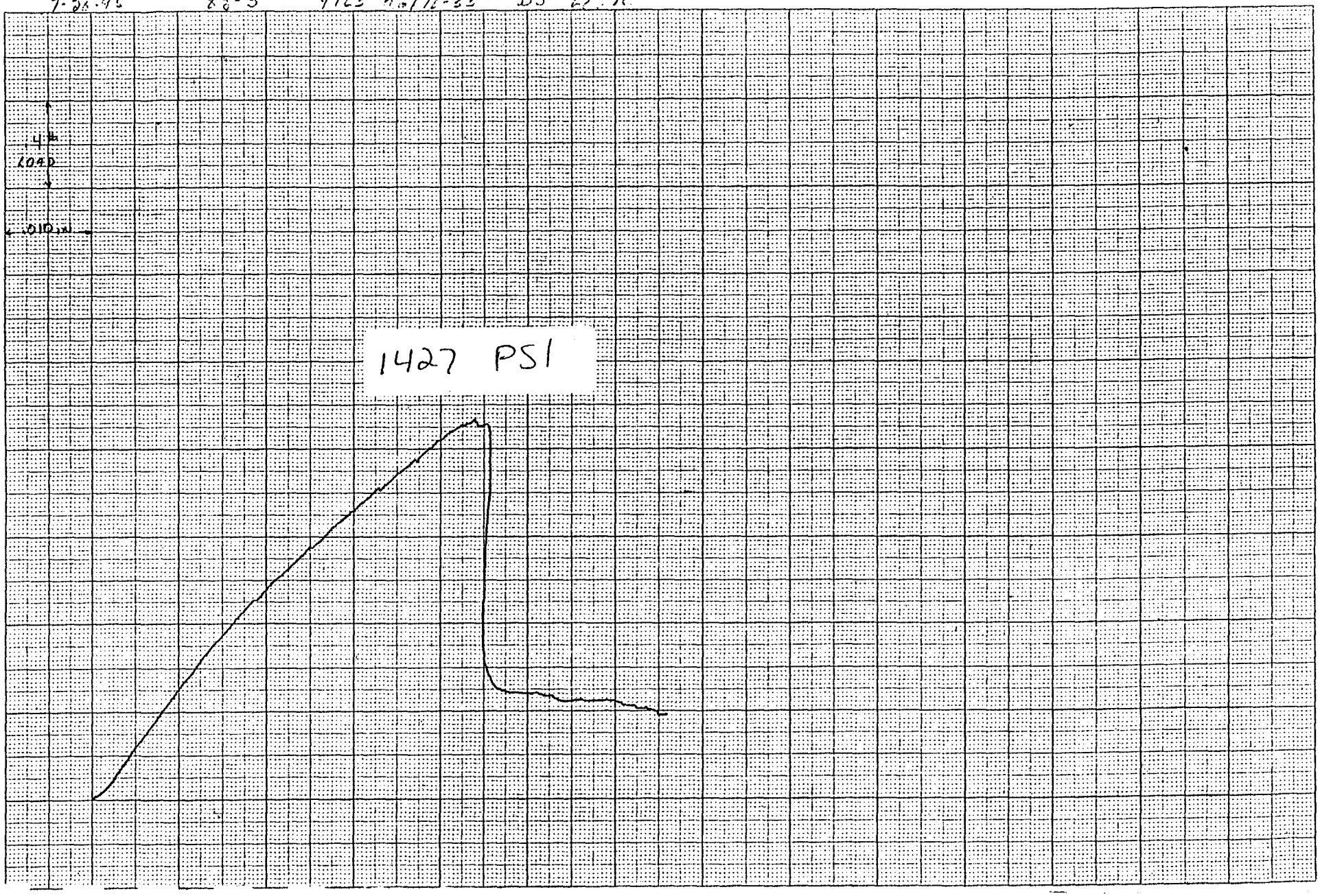

8Y-4

7-28-95 9763 MGF12-33 .010" 68076

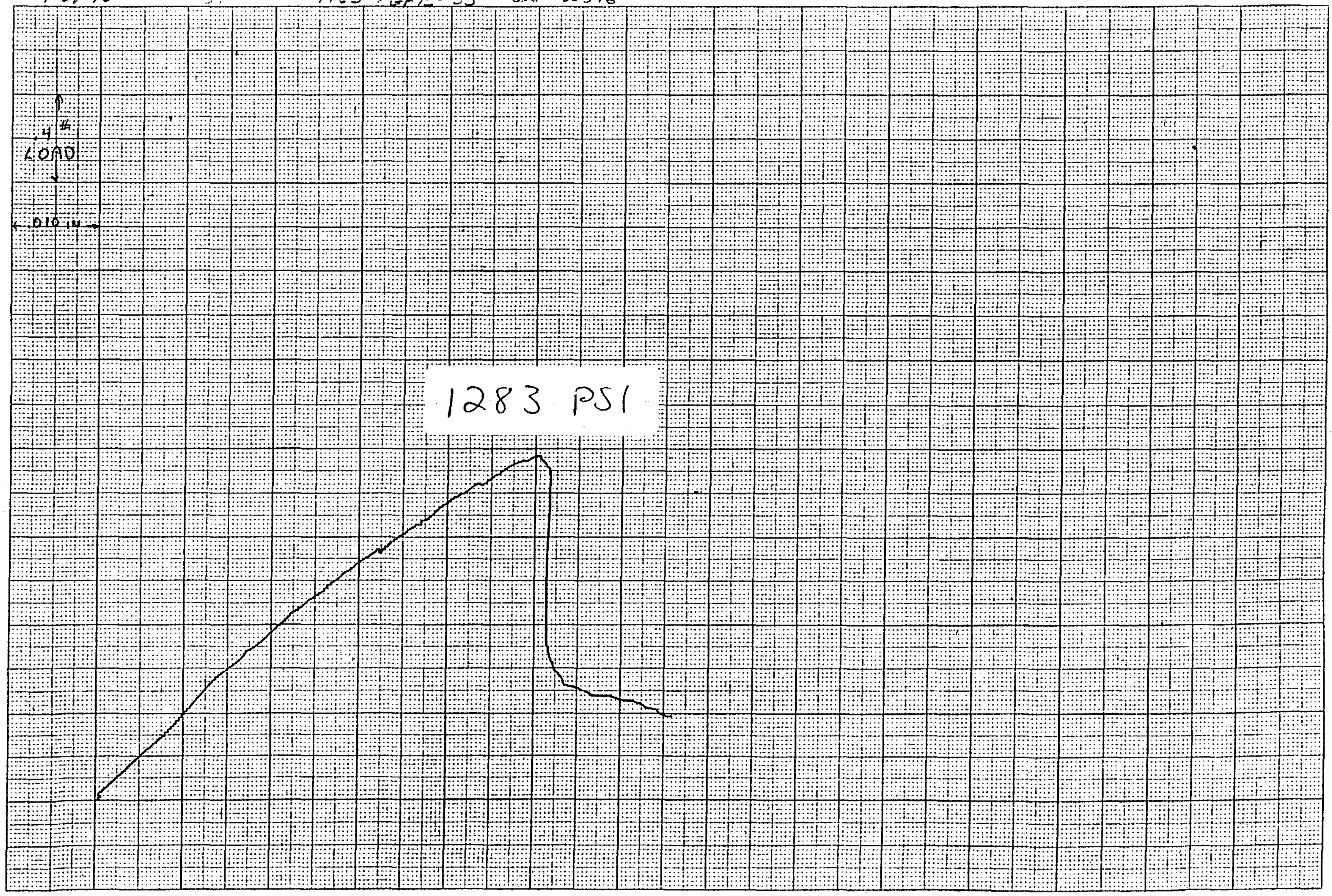

8Y-5

7-28-95 8Y-5 77C3 HGFIL-33 WO# 68076

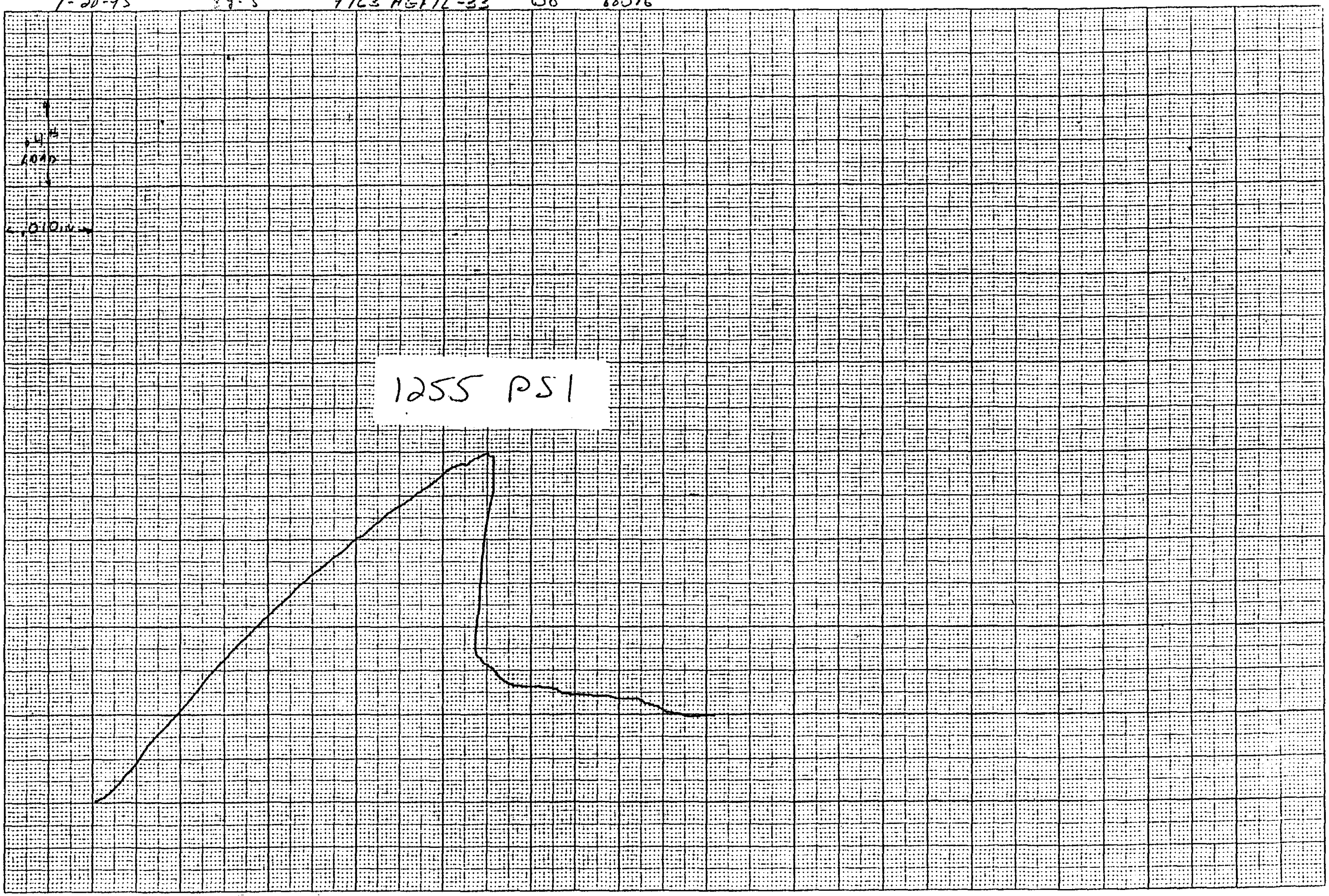

84-6

7-28-95 84-6 9TC3 HGF1L-33 WO# 68076

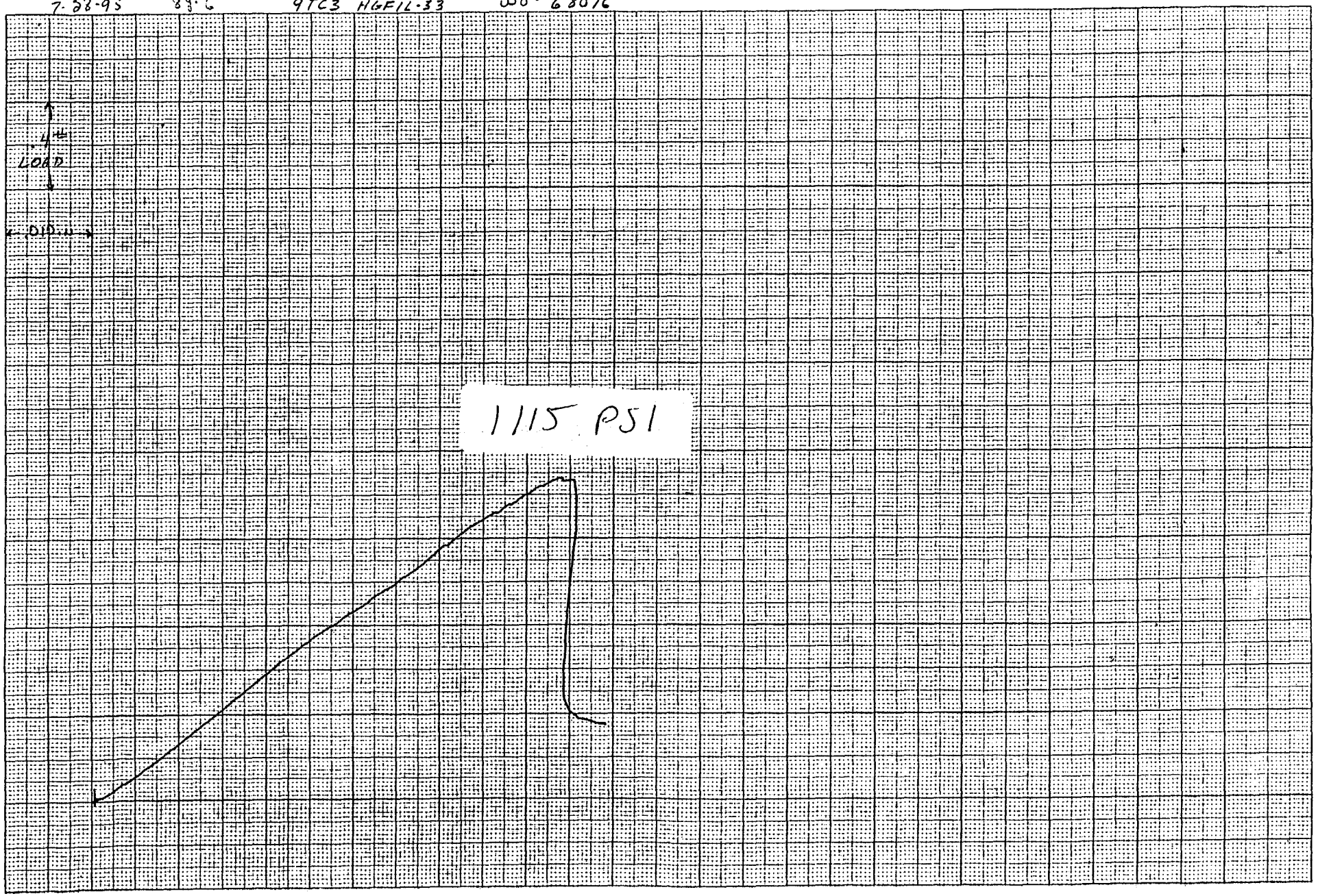

Load-Deflection Curves for CMCs fabricated from Candidate Fiber Architecture #9.

9X-1 to 9x5

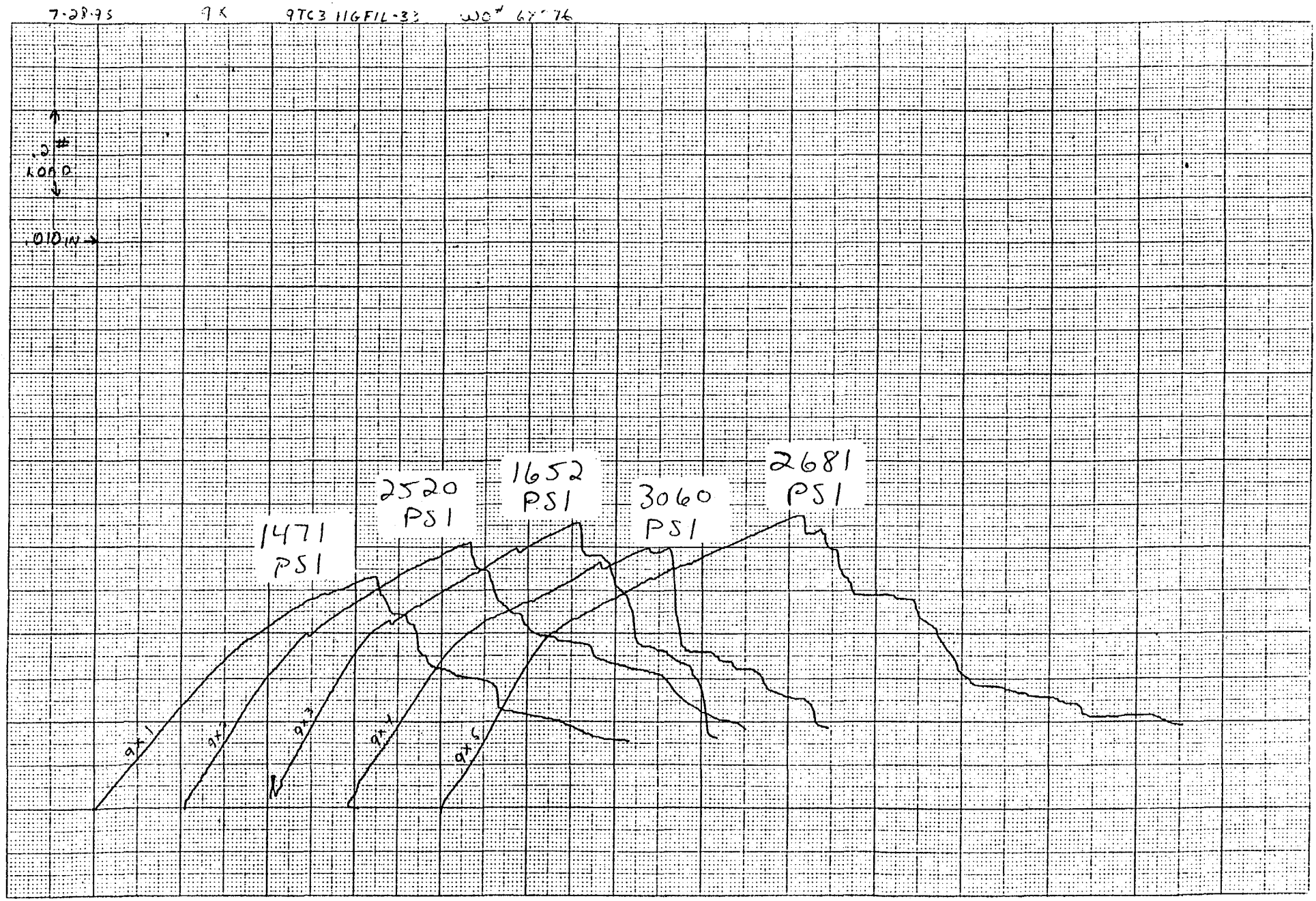
7-28-95
9X
9TC3 11GFIL-33
WO# 6X-76
.2 # LOAD
.010 IN
1471 PSI
2520 PSI
1652 PSI
3060 PSI
2681 PSI
9x-1
9x-2
9x-3
9x-4
9x-5

9X-6 10

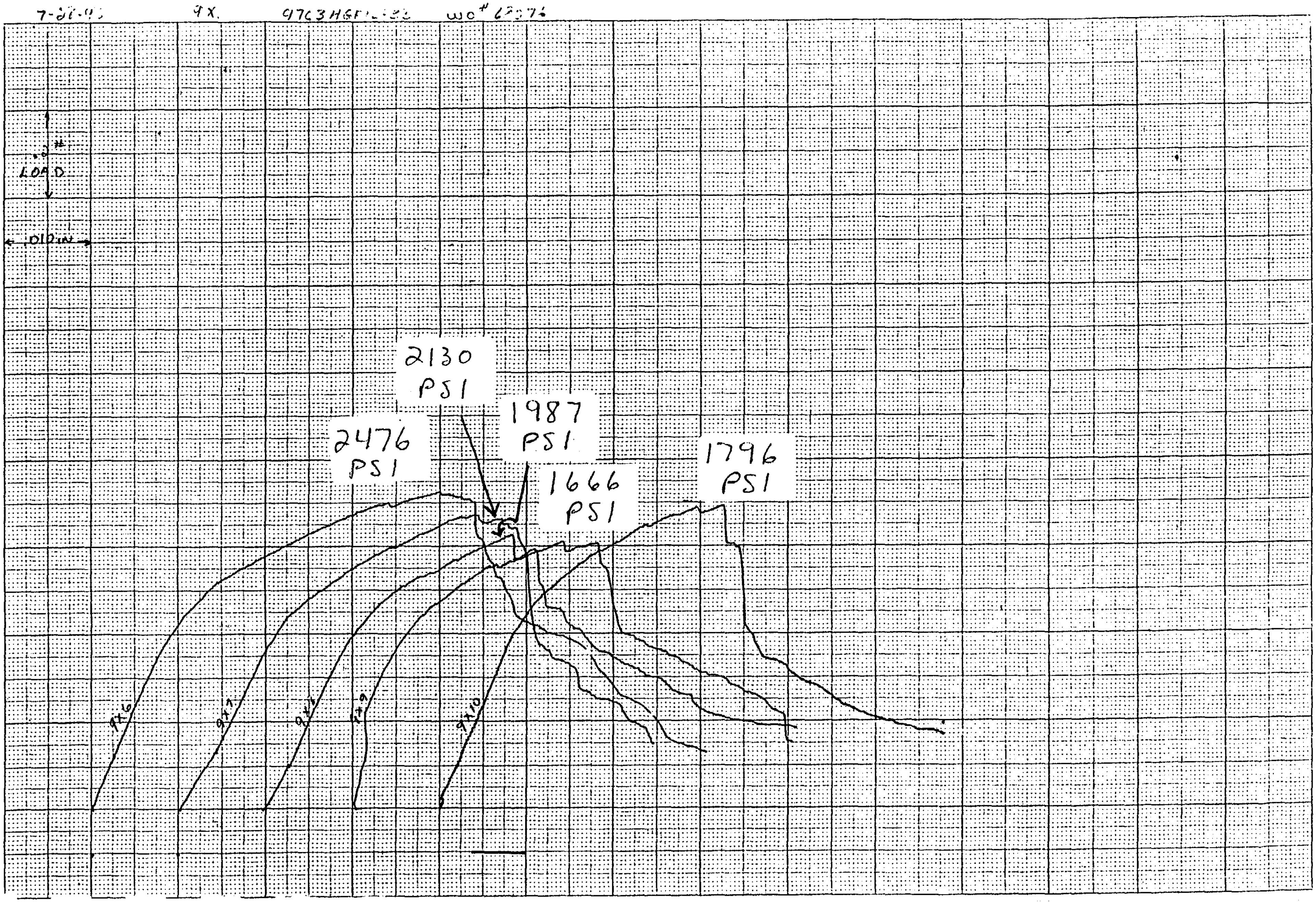
7-28-9
9X
9763HGF
WO#
LOAD
.010 IN
9x6
9x7
9x8
9x9
9x10
2476 PSI
2130 PSI
1987 PSI
1666 PSI
1796 PSI

9Y-3 to 9Y-11

7-28-95 9Y 9TC3 NGFIL-3 WO# 28376

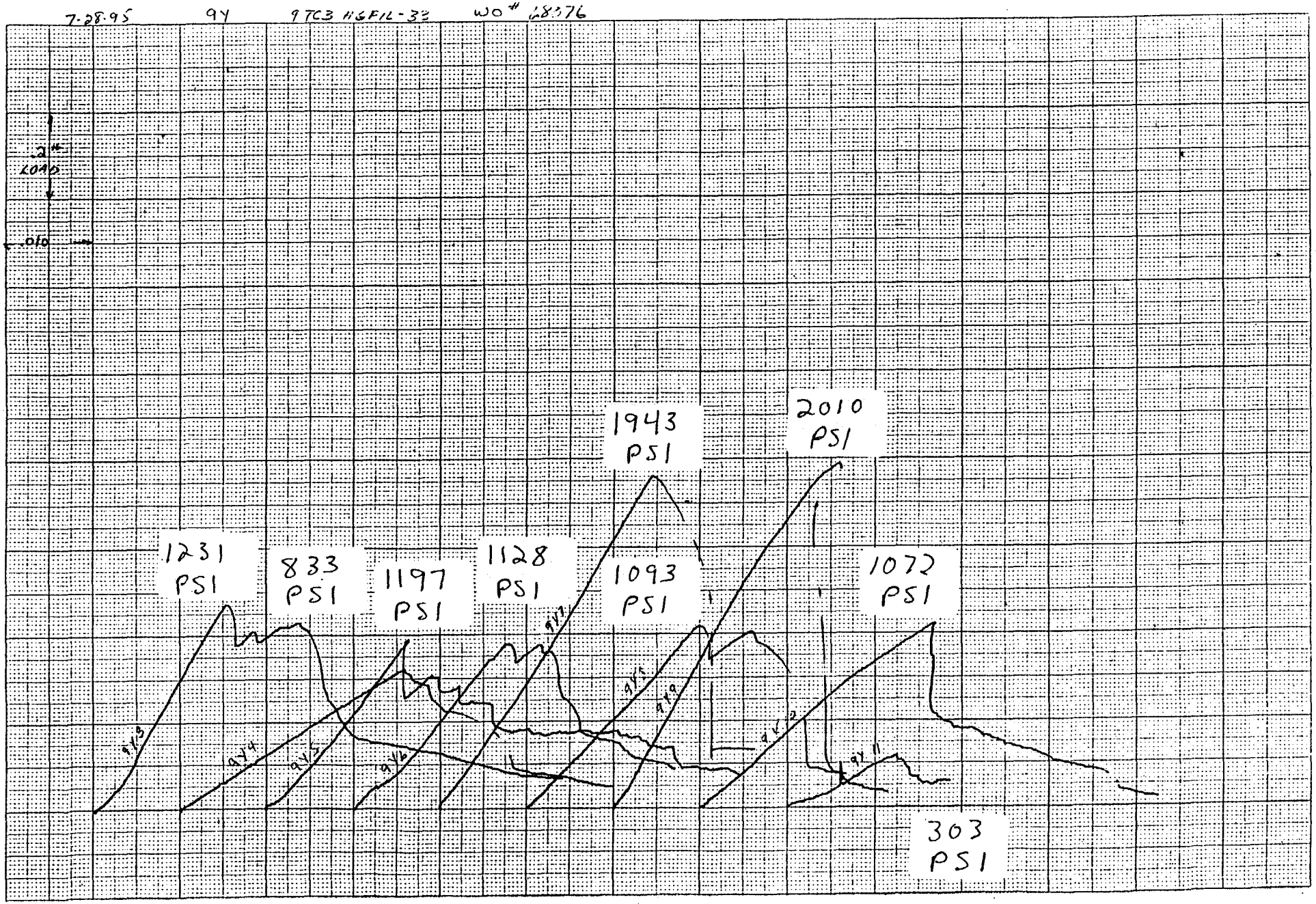

Load-Deflection Curves for CMCs fabricated from the Stuffer Modified Architectures #10-#15.

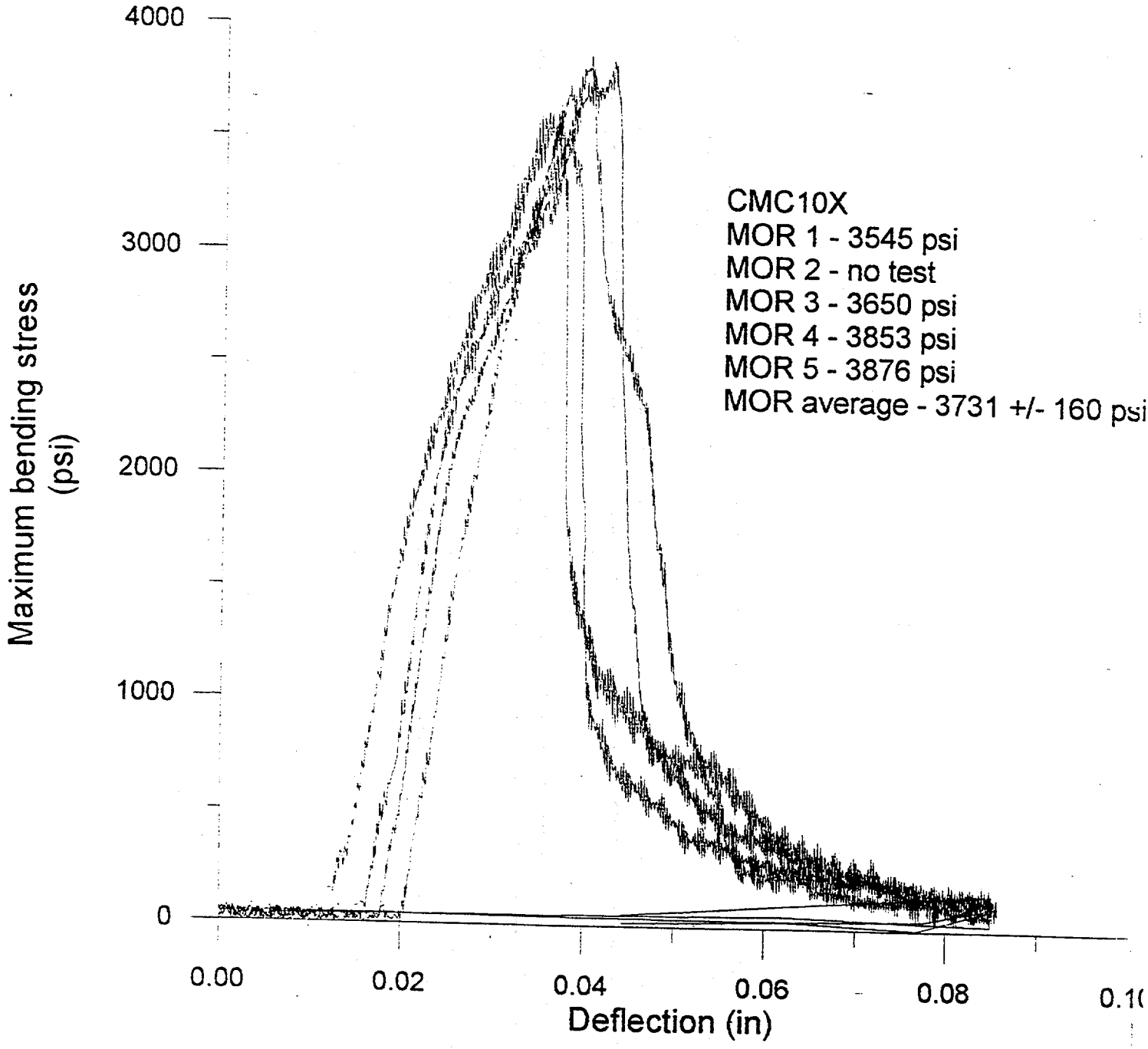
4000
3000
2000
1000
0
Maximum bending stress (psi)
0.00
0.02
0.04
0.06
0.08
Deflection (in)
CMC10X
MOR 1 - 3545 psi
MOR 2 - no test
MOR 3 - 3650 psi
MOR 4 - 3853 psi
MOR 5 - 3876 psi
MOR average - 3731 +/- 160 psi

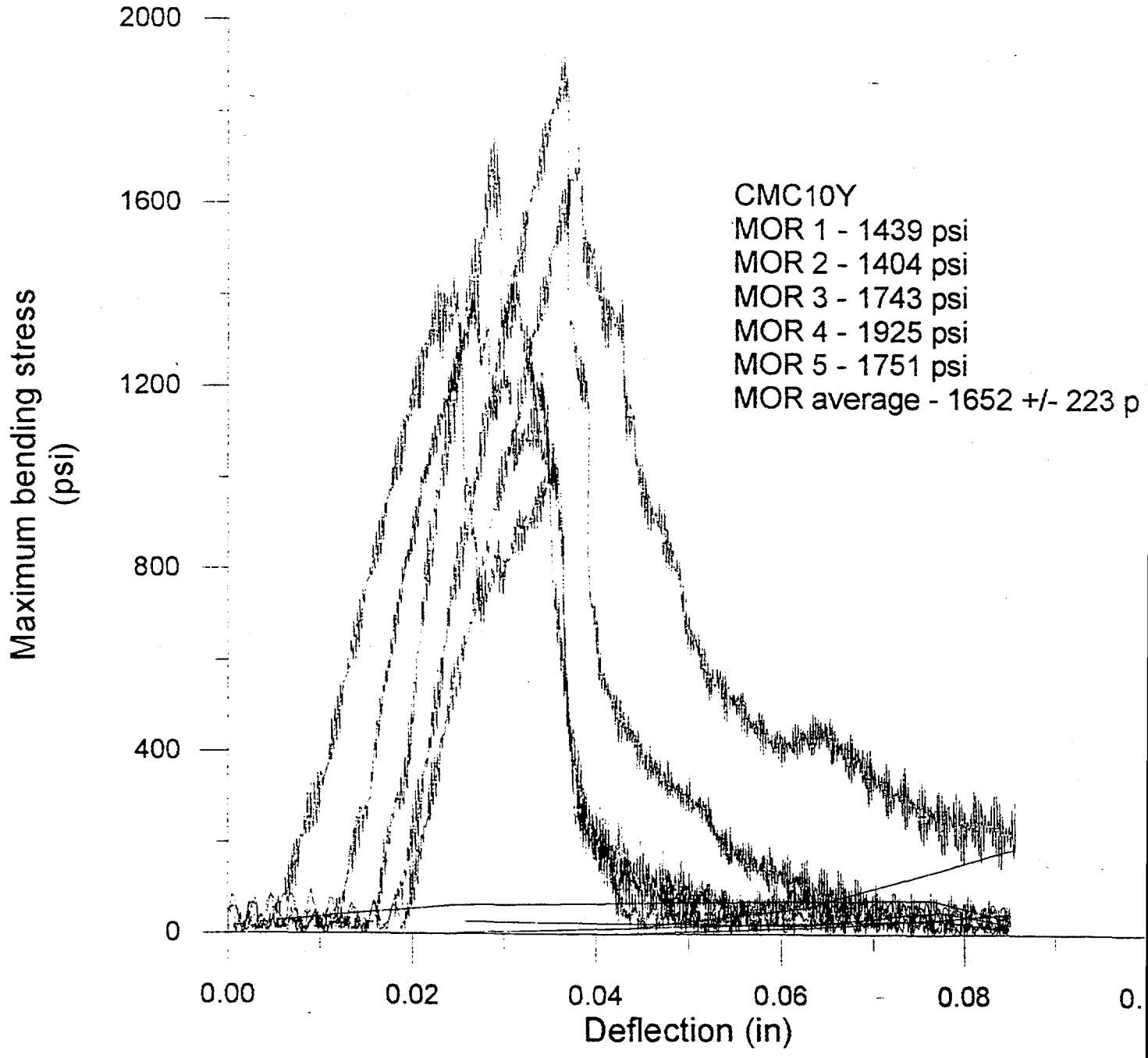
2000
1600
1200
800
400
0
Maximum bending stress (psi)
0.00
0.02
0.04
0.06
0.08
0.
Deflection (in)
CMC10Y
MOR 1 - 1439 psi
MOR 2 - 1404 psi
MOR 3 - 1743 psi
MOR 4 - 1925 psi
MOR 5 - 1751 psi
MOR average - 1652 +/- 223 p

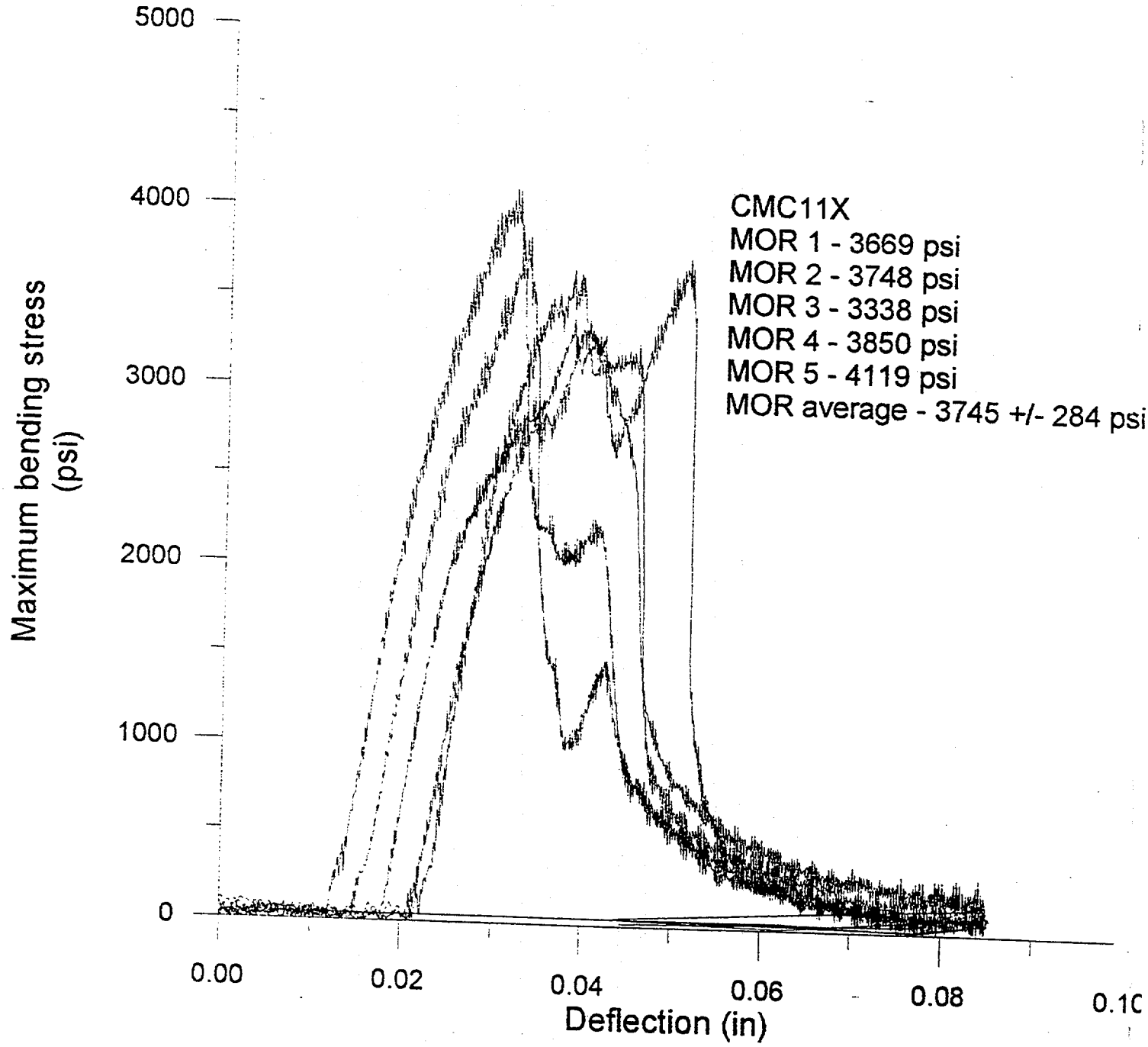
5000
4000
3000
2000
1000
0
Maximum bending stress (psi)
0.00
0.02
0.04
0.06
0.08
0.1C
Deflection (in)
CMC11X
MOR 1 - 3669 psi
MOR 2 - 3748 psi
MOR 3 - 3338 psi
MOR 4 - 3850 psi
MOR 5 - 4119 psi
MOR average - 3745 +/- 284 psi

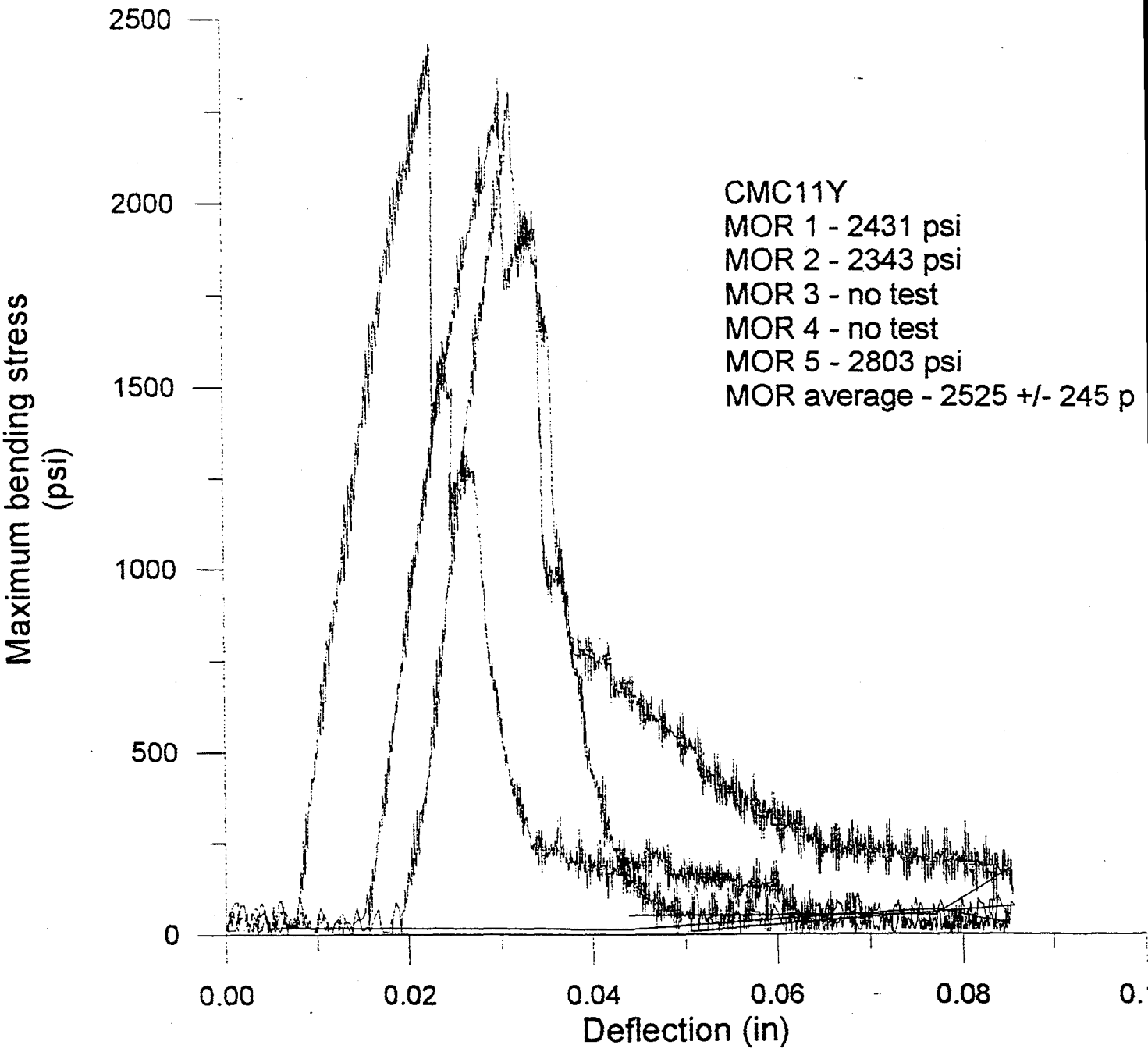
2500
2000
1500
1000
500
0
Maximum bending stress (psi)
0.00
0.02
0.04
0.06
0.08
Deflection (in)
CMC11Y
MOR 1 - 2431 psi
MOR 2 - 2343 psi
MOR 3 - no test
MOR 4 - no test
MOR 5 - 2803 psi
MOR average - 2525 +/- 245 p

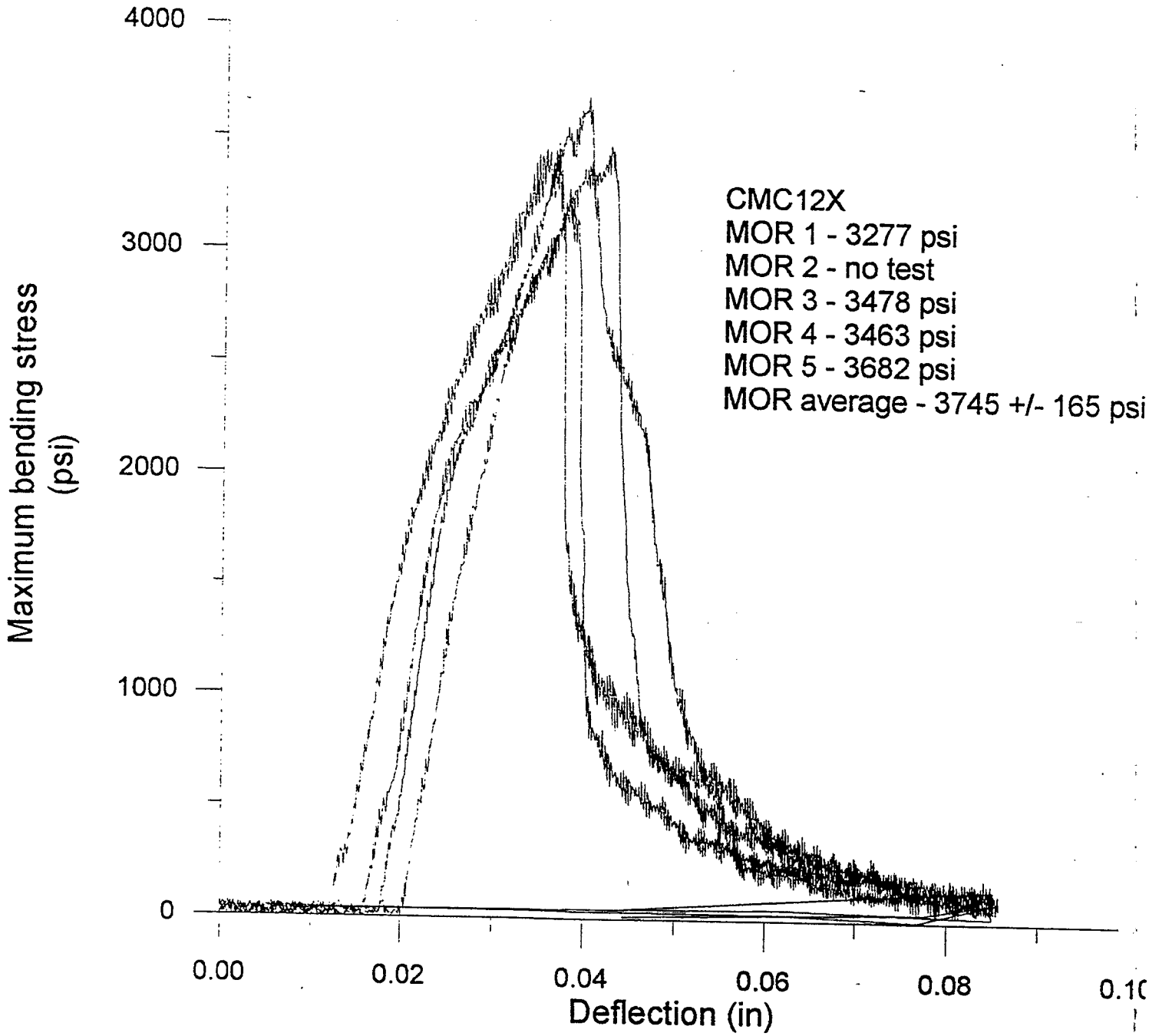
4000
3000
2000
1000
0
Maximum bending stress (psi)
0.00
0.02
0.04
0.06
0.08
0.1
Deflection (in)
CMC12X
MOR 1 - 3277 psi
MOR 2 - no test
MOR 3 - 3478 psi
MOR 4 - 3463 psi
MOR 5 - 3682 psi
MOR average - 3745 +/- 165 psi

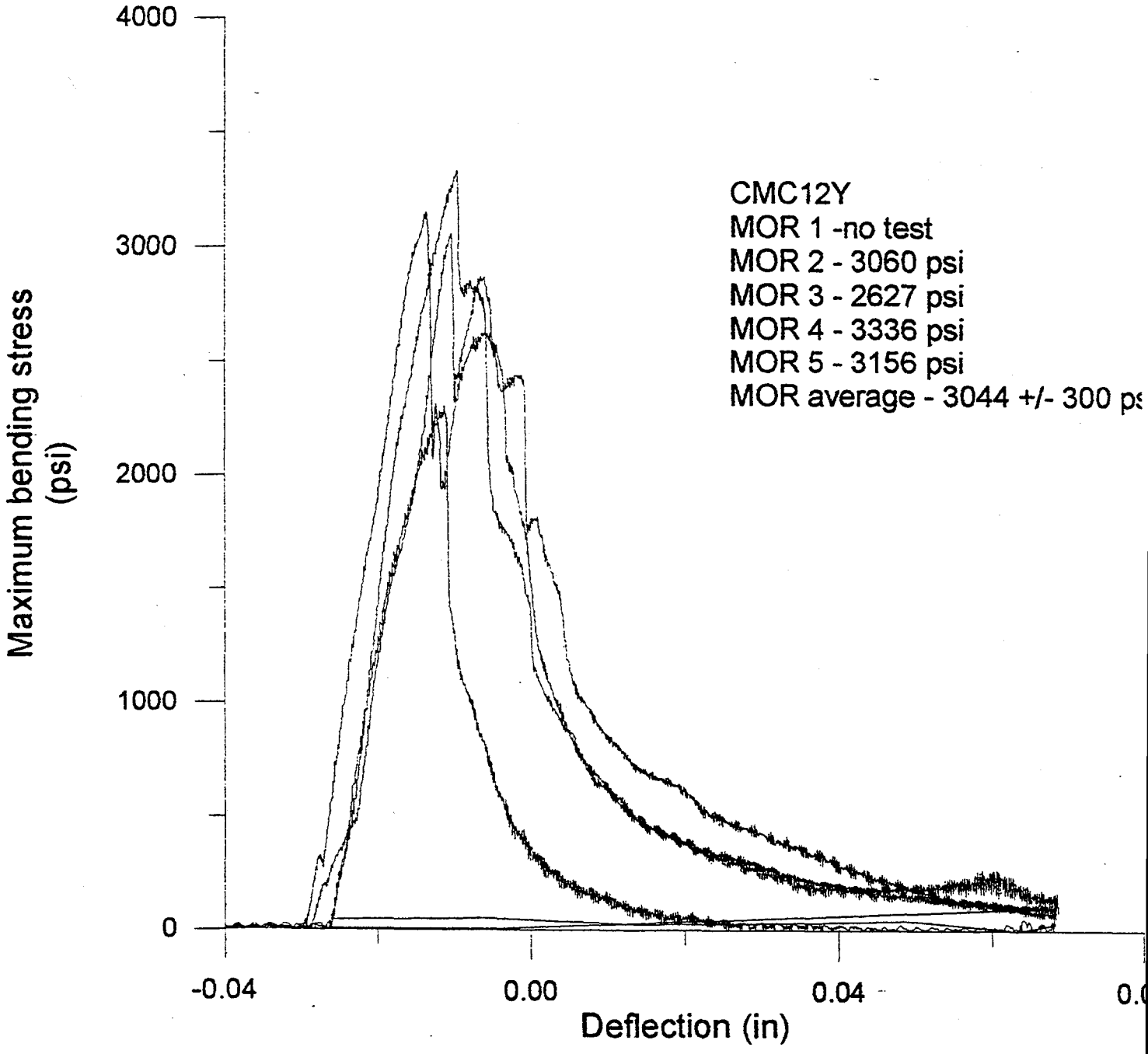
4000
3000
2000
1000
0
Maximum bending stress (psi)
-0.04
0.00
0.04
Deflection (in)
CMC12Y
MOR 1 -no test
MOR 2 - 3060 psi
MOR 3 - 2627 psi
MOR 4 - 3336 psi
MOR 5 - 3156 psi
MOR average - 3044 +/- 300 ps

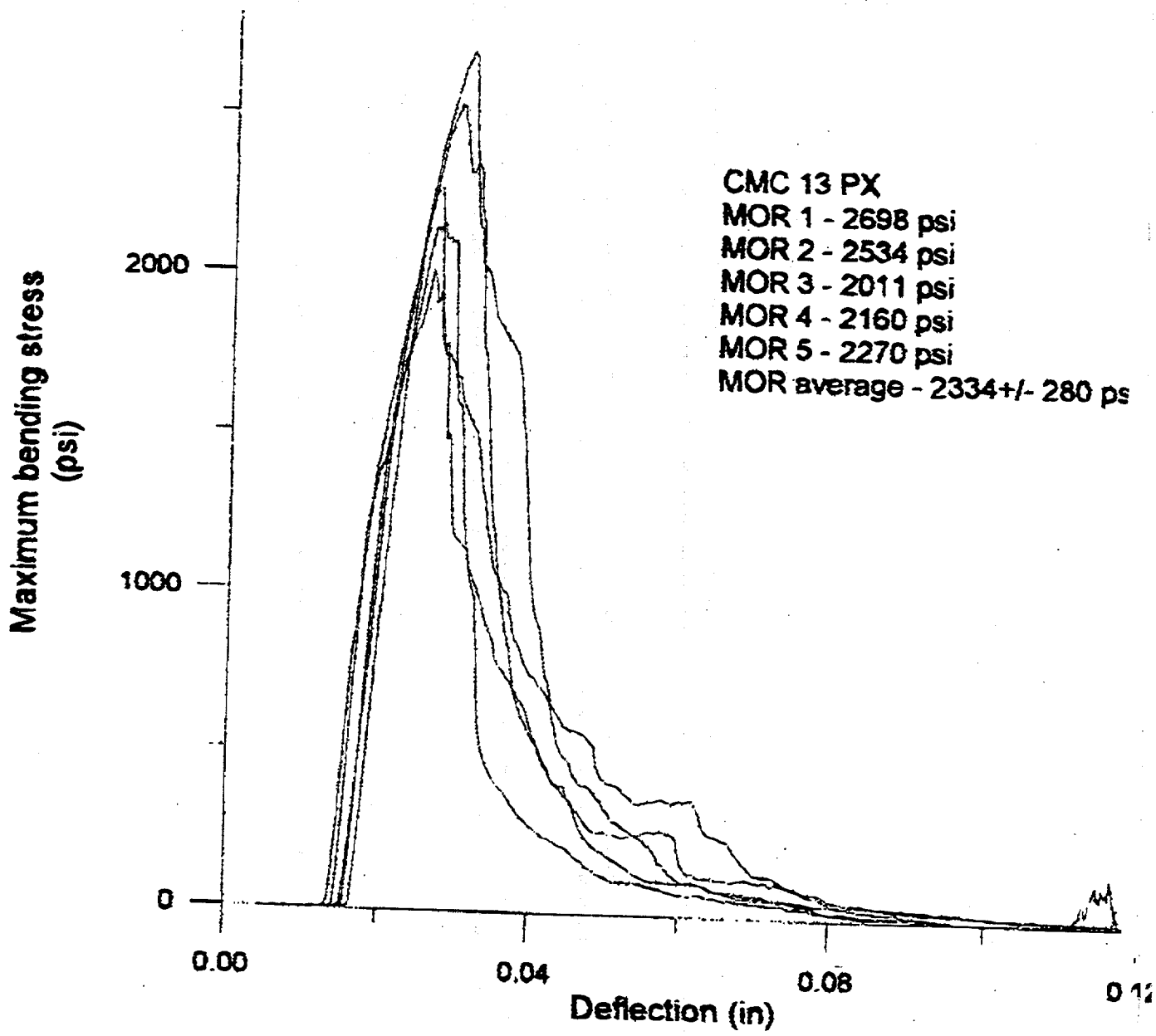
CMC 13 PX
MOR 1 - 2698 psi
MOR 2 - 2534 psi
MOR 3 - 2011 psi
MOR 4 - 2160 psi
MOR 5 - 2270 psi
MOR average - 2334+/- 280 ps
Maximum bending stress (psi)
2000
1000
0
0.00
0.04
0.08
Deflection (in)

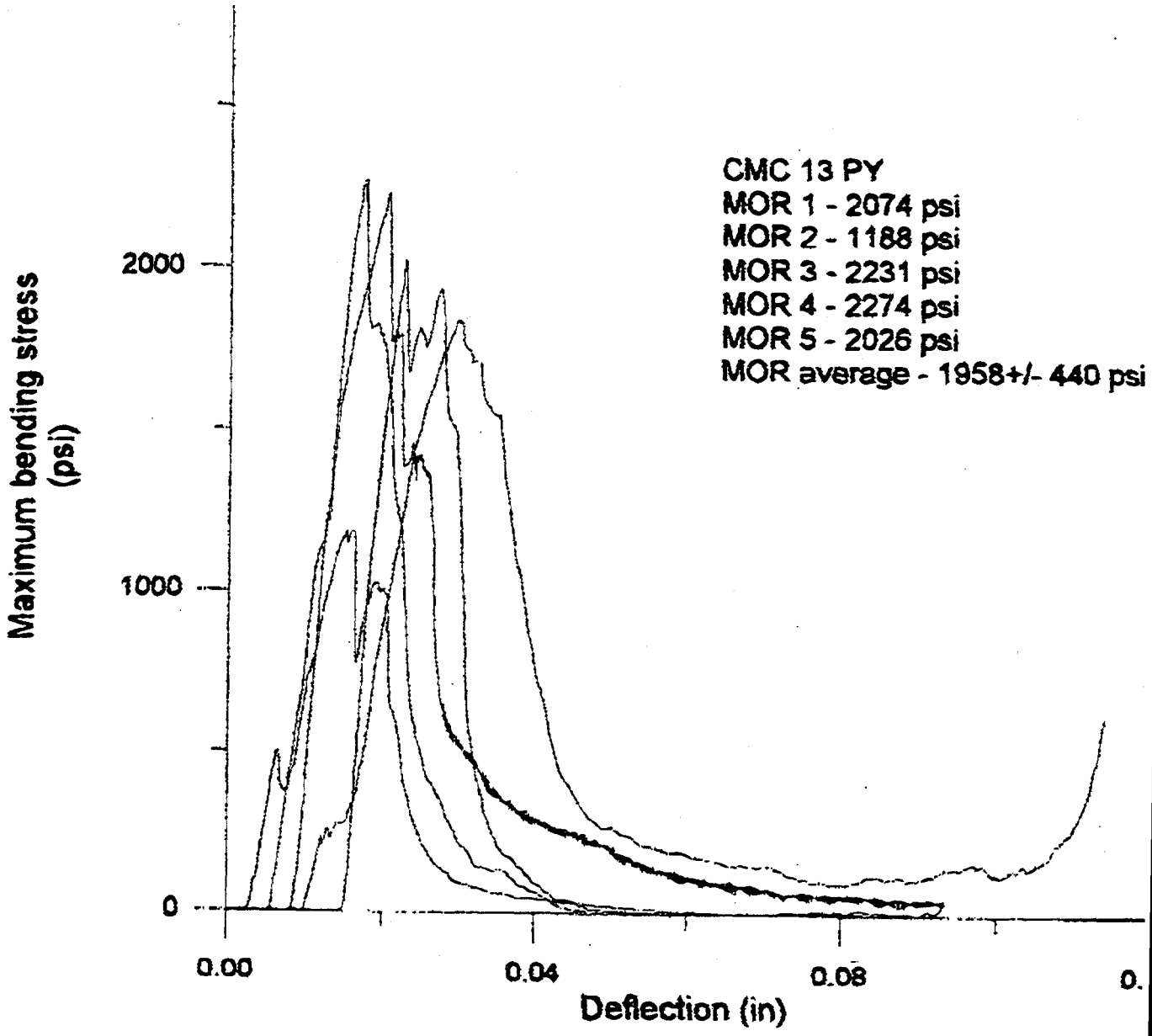
CMC 13 PY
MOR 1 - 2074 psi
MOR 2 - 1188 psi
MOR 3 - 2231 psi
MOR 4 - 2274 psi
MOR 5 - 2026 psi
MOR average - 1958+/- 440 psi
Maximum bending stress (psi)
2000
1000
0
0.00
0.04
0.08
0.
Deflection (in)

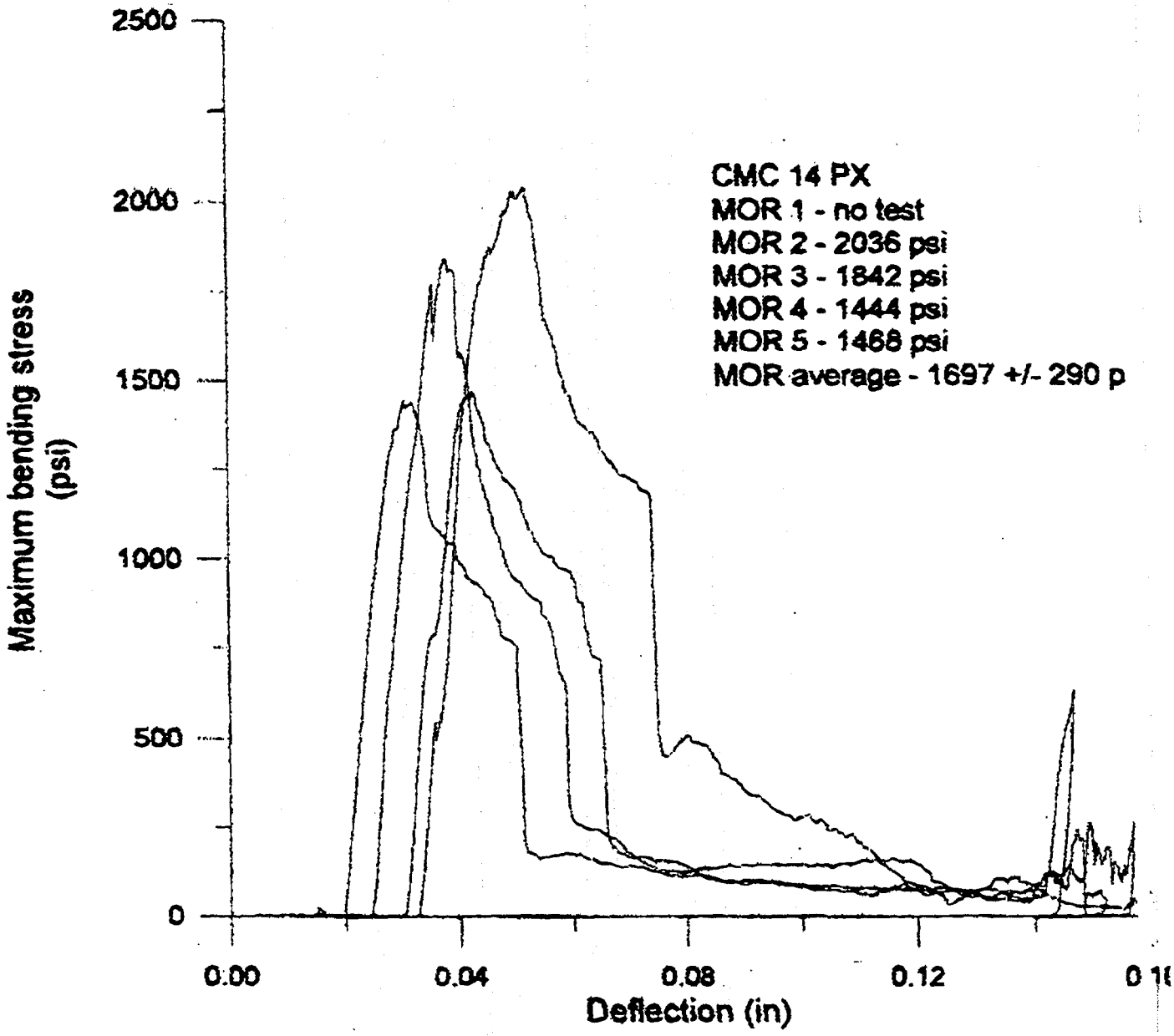
CMC 14 PX
MOR 1 - no test
MOR 2 - 2036 psi
MOR 3 - 1842 psi
MOR 4 - 1444 psi
MOR 5 - 1468 psi
MOR average - 1697 +/- 290 p
Maximum bending stress (psi)
2500
2000
1500
1000
500
0
0.00
0.04
0.08
0.12
Deflection (in)

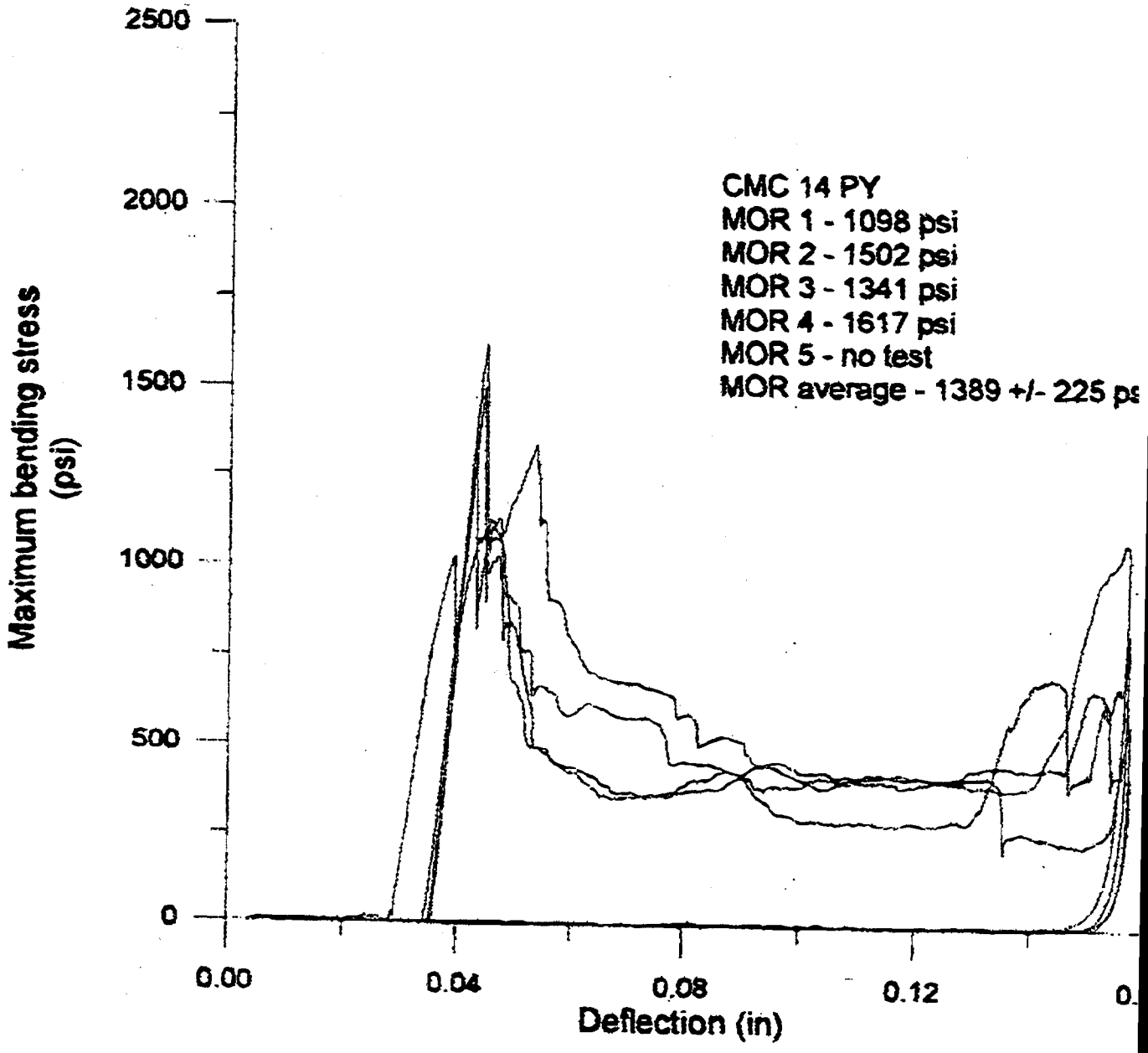
2500
2000
1500
1000
500
0
Maximum bending stress (psi)
CMC 14 PY
MOR 1 - 1098 psi
MOR 2 - 1502 psi
MOR 3 - 1341 psi
MOR 4 - 1617 psi
MOR 5 - no test
MOR average - 1389 +/- 225 ps
0.00
0.04
0.08
0.12
Deflection (in)

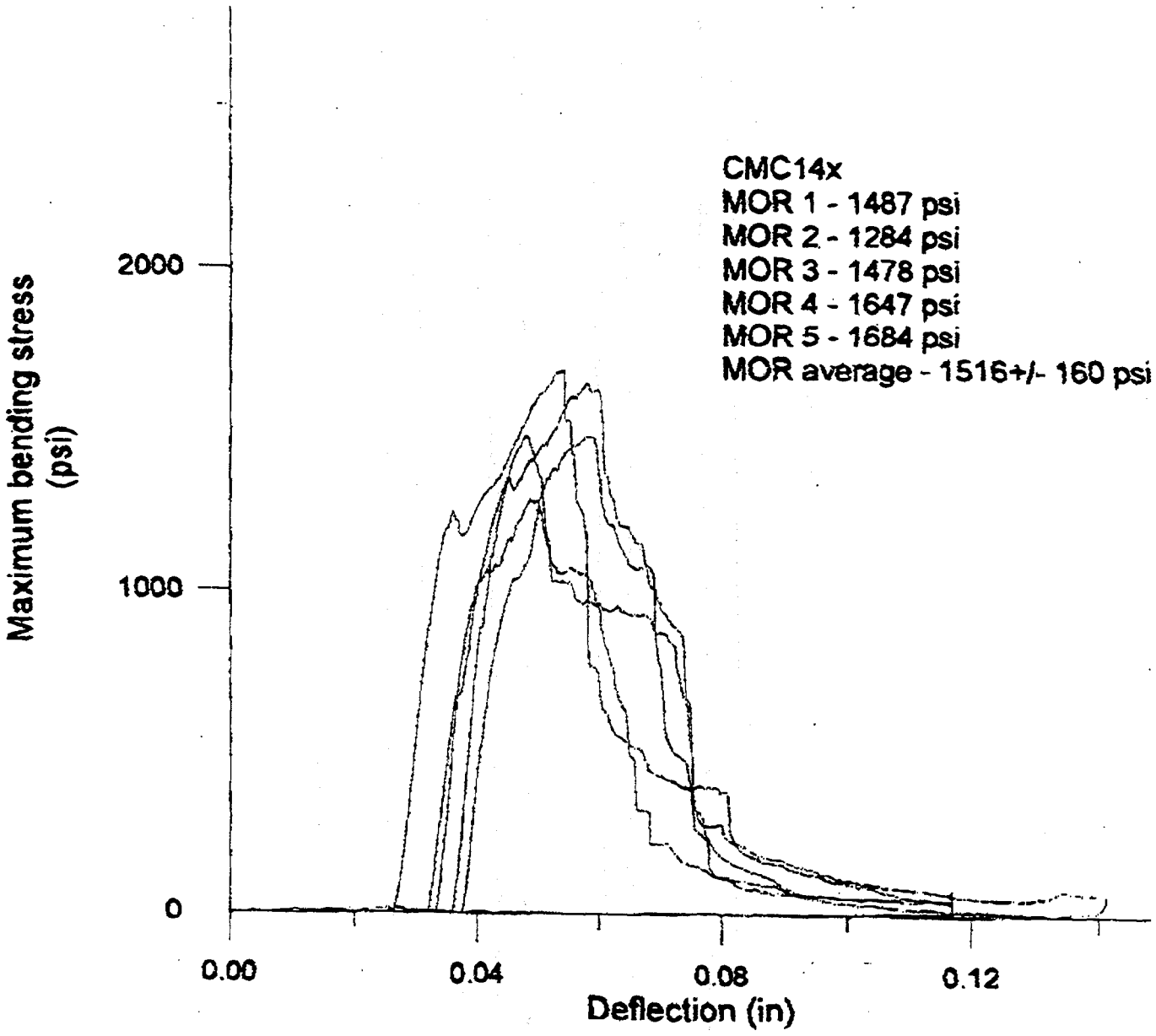
CMC14x
MOR 1 - 1487 psi
MOR 2 - 1284 psi
MOR 3 - 1478 psi
MOR 4 - 1647 psi
MOR 5 - 1684 psi
MOR average - 1516+/- 160 psi
Maximum bending stress (psi)
2000
1000
0
0.00
0.04
0.08
0.12
Deflection (in)

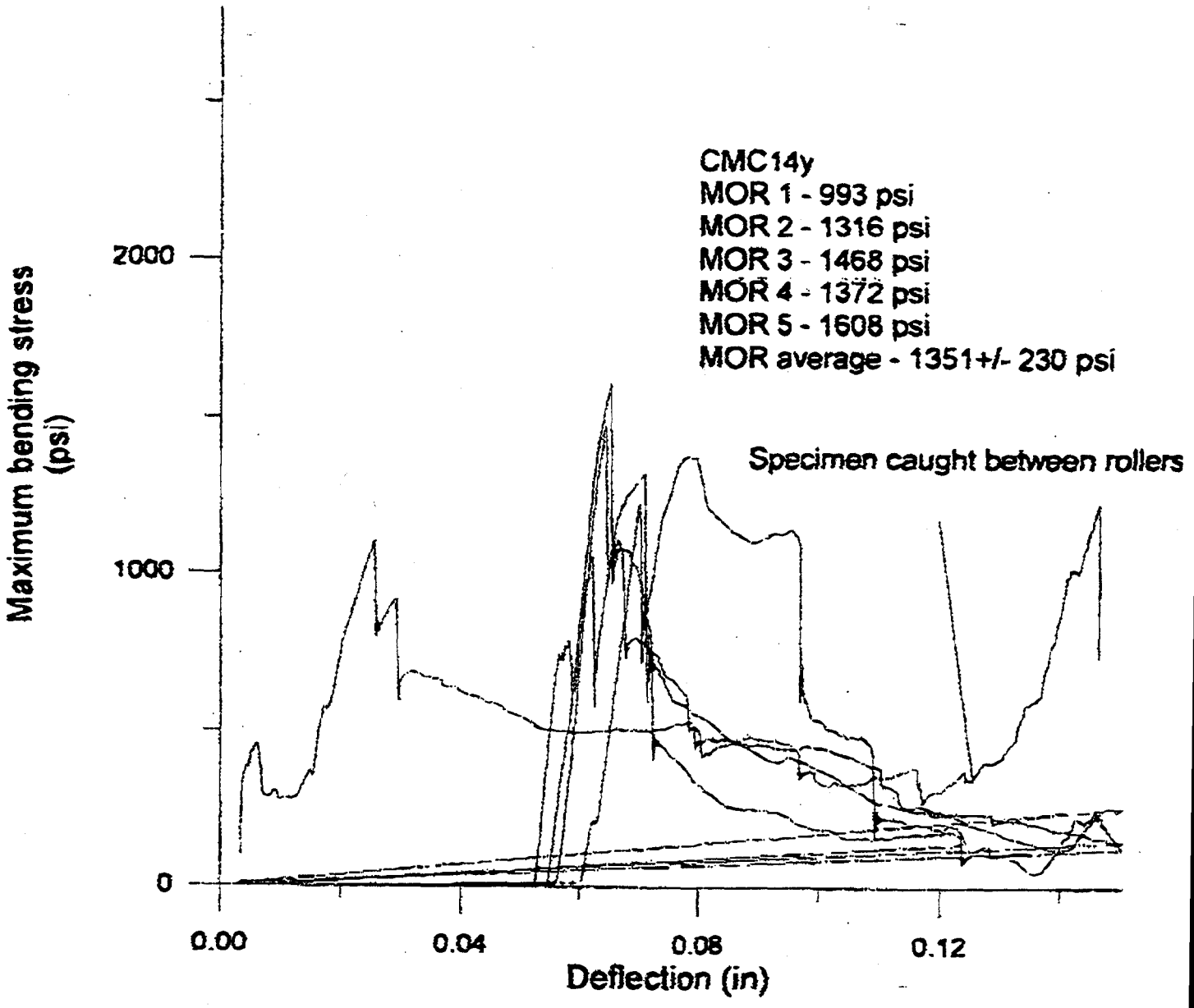
CMC14y
MOR 1 - 993 psi
MOR 2 - 1316 psi
MOR 3 - 1468 psi
MOR 4 - 1372 psi
MOR 5 - 1608 psi
MOR average - 1351+/- 230 psi
Specimen caught between rollers
Maximum bending stress (psi)
2000
1000
0
0.00
0.04
0.08
0.12
Deflection (in)

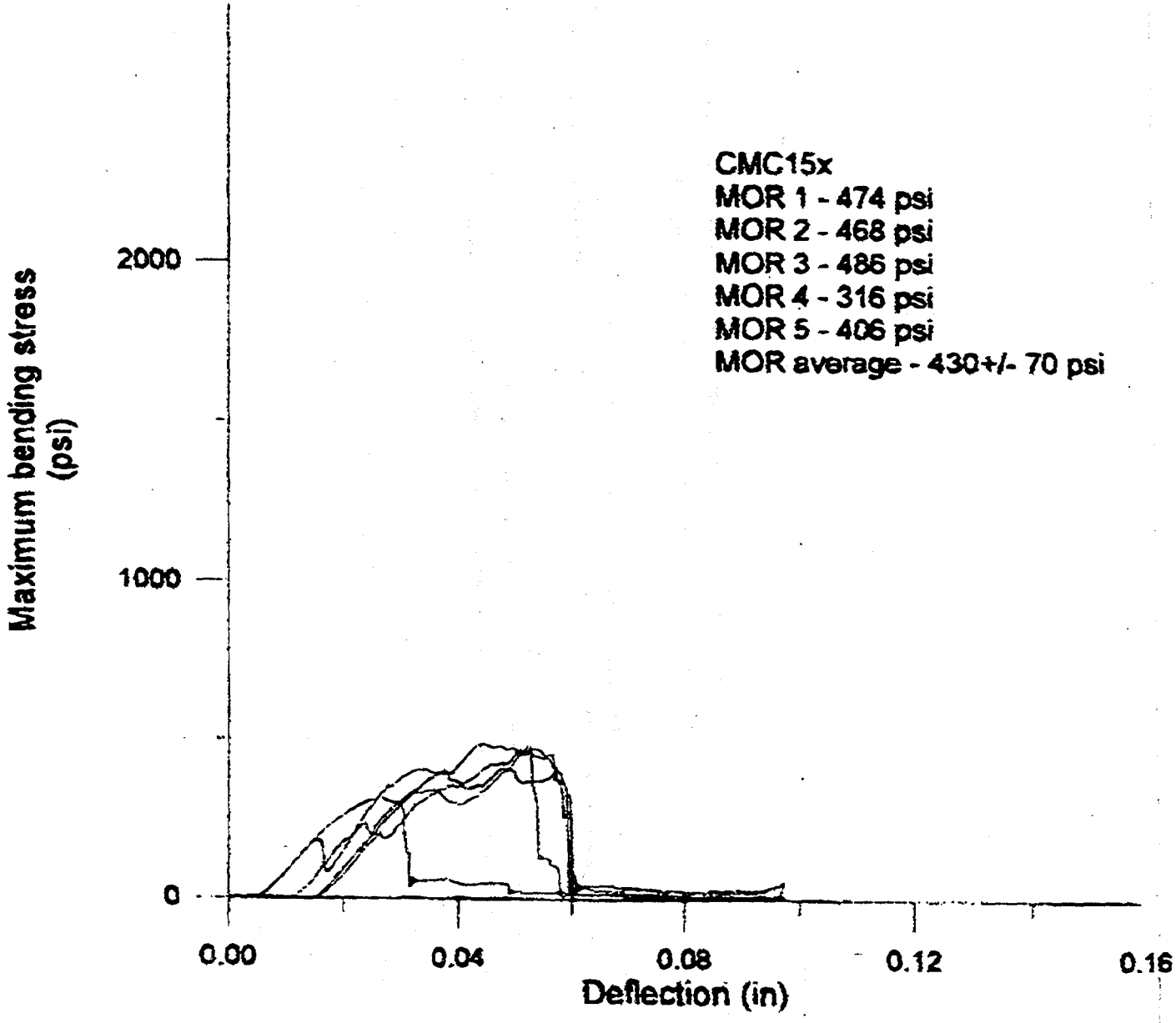
CMC15x
MOR 1 - 474 psi
MOR 2 - 468 psi
MOR 3 - 486 psi
MOR 4 - 316 psi
MOR 5 - 406 psi
MOR average - 430+/- 70 psi
Maximum bending stress (psi)
2000
1000
0
0.00
0.04
0.08
0.12
0.16
Deflection (in)

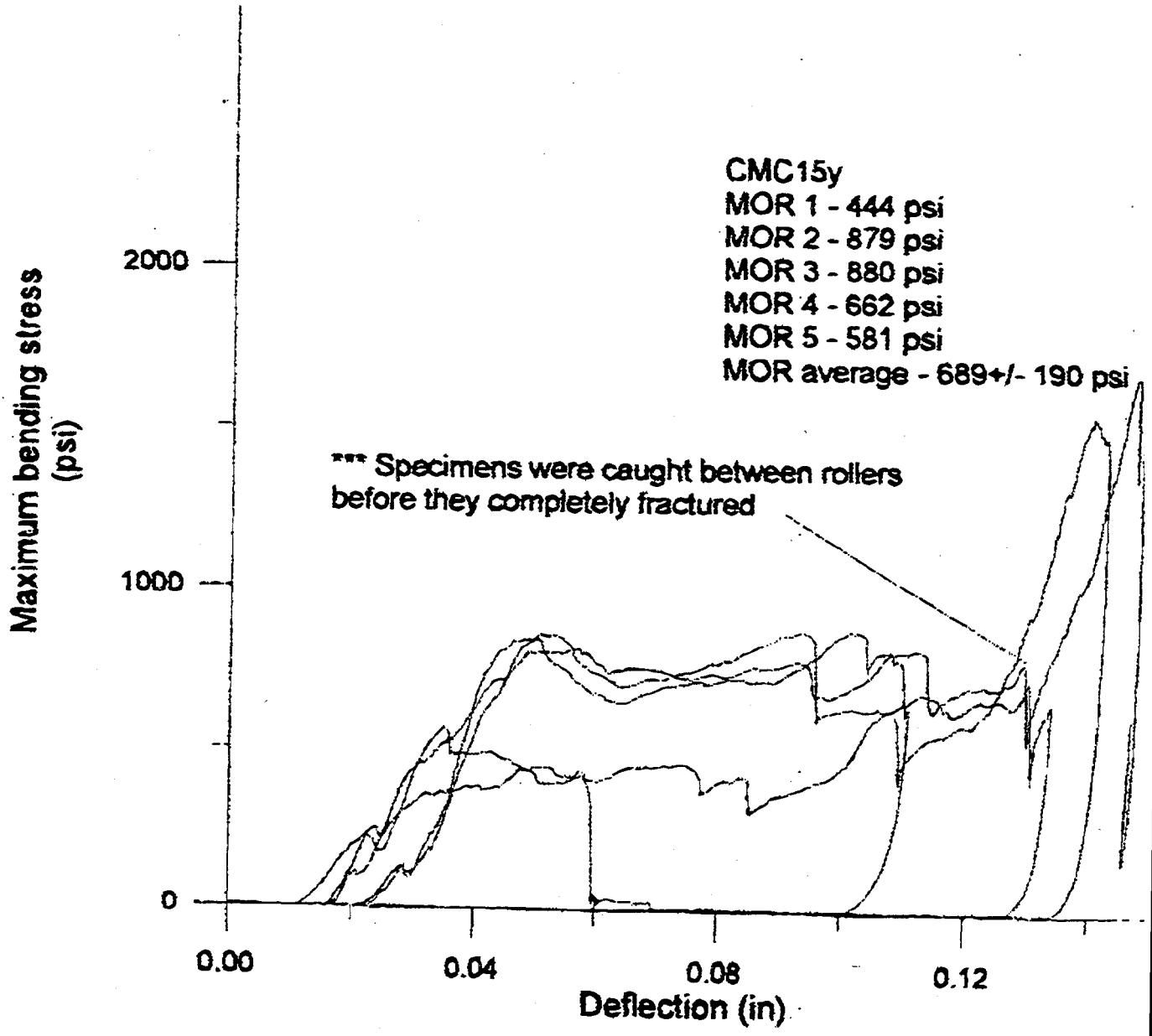
CMC15y
MOR 1 - 444 psi
MOR 2 - 879 psi
MOR 3 - 880 psi
MOR 4 - 662 psi
MOR 5 - 581 psi
MOR average - 689+/- 190 psi
*** Specimens were caught between rollers before they completely fractured
Maximum bending stress (psi)
2000
1000
0
0.00
0.04
0.08
0.12
Deflection (in)